# Machinability Study of Aluminum-Lithium Alloys for Aerospace Applications: Influences of Heat Treatments and Machining Conditions

By

LIDA RADAN

PRESENTED TO ÉCOLE DE TECHNOLOGIE SUPÉRIEURE IN PARTIAL FULFILLEMENT FOR THE DEGREE OF DOCTOR OF PHILOSOPHY
Ph.D.

MONTREAL, DECEMBER 19, 2024

ÉCOLE DE TECHNOLOGIE SUPÉRIEURE
UNIVERSITÉ DU QUÉBEC

BY THE FOLLOWING BOARD OF EXAMINERS

Mr. Victor Songmene, Thesis Supervisor
Department of Mechanical Engineering at École de technologie supérieure

Mr. Fawzy Hosny Samuel, Thesis Co-supervisor
Department of Mechanical Engineering at École de technologie supérieure

Mr. Lotfi Guizani, President of the Board of Examiners
Department of Construction Engineering at École de technologie supérieure

Mrs Elmira Moosavi, Member of the jury
Department of Mechanical Engineering at École de technologie supérieure

Mr Walid Joma, Member of the jury
Department of Mathematics and Industrial Engineering at Polytechnique Montréal

Mr. Fengfeng Xi, External independent Evaluator
Department of Aerospace Engineering at Toronto Metropolitan University

THIS THESIS WAS PRESENTED AND DEFENDED

IN THE PRESENCE OF A BOARD OF EXAMINERS AND PUBLIC

31/10/2024

AT ÉCOLE DE TECHNOLOGIE SUPÉRIEURE

## ACKNOWLEDGMENTS

Throughout the writing of this dissertation, I have received a great deal of support and assistance. I would first like to thank my supervisor and co-Supervisor, Prof. Victor Songmene and Prof. Fawzy Hosny Samuel, whose expertise were invaluable in formulating the research questions and methodology. Your insightful feedback pushed me to sharpen my thinking and brought my work to a higher level.

My appreciation also goes to Dr. Yasser Zedan and Dr. Jules Kouam, for helping me in the experimental part of the study. I could not have completed this dissertation without the support of my dear friend, Mr. Ali Tahmasebi.

I would like to extend my gratitude to Dr. Agnes M. Samuel for her meticulous editing of my articles and PhD thesis. Your careful attention to detail greatly improved the quality of my work.

I am also grateful to the Tamla Research Group (Technologie Avancée des Métaux Légers pour les Applications Automobiles) at Université du Québec à Chicoutimi (UQAC), where the castings were carried out.

In addition, I would like to thank my mother for her wise counsel and sympathetic ear. You have always been there for me.

Finally, I could not have completed this dissertation without the support of my lovely husband, Mahmoud, and my kids, Jana and Jwan, who have provided love and company during this whole journey.

**Étude d'usinabilité des alliages d'aluminium-lithium pour les applications aérospatiales: Influences des Traitements Thermiques et des Conditions d'Usinage**

Lida RADAN

## RÉSUMÉ

Cette thèse étudie l'usinabilité des alliages avancés aluminium-lithium (Al-Li, Al-Li-Cu et Al-Li-Cu-Sc), appréciés pour leur faible densité, leur haute résistance à la traction et leur résistance à la corrosion, qualités essentielles pour les applications aérospatiales. Cependant, des défis subsistent, notamment la réduction de la rugosité de surface, des forces de coupe et des émissions de fines particules métalliques. Cette étude propose une analyse détaillée des effets de la composition des alliages, des traitements thermiques et des paramètres d'usinage sur ces défis, comblant ainsi un vide dans la littérature en examinant les impacts des ajouts de scandium et de cuivre sur les alliages Al-Li, leurs traitements thermiques et leur usinabilité.

Les traitements thermiques ont été optimisés pour chaque alliage afin d'atteindre la dureté maximale. L'alliage Al-Li a atteint 97 HV avec un traitement de solution à 580 °C/1 h suivi d'un vieillissement artificiel à 150 °C/45 h, tandis que les alliages Al-Li-Cu et Al-Li-Cu-Sc ont atteint respectivement 164 HV et 182,7 HV avec un traitement de solution à 505 °C/5 h suivi d'un vieillissement à 180 °C/20 h. Des expériences de fraisage en bout ont été réalisées avec une profondeur de coupe constante (2 mm), en conditions sèches et humides, en faisant varier les avances (0,05–0,15 mm/dent) et les vitesses de coupe (200–600 m/min).

Les résultats clés montrent que l'alliage Al-Li a nécessité la plus faible force d'usinage (52,3 N), tandis que les alliages Al-Li-Cu et Al-Li-Cu-Sc ont nécessité respectivement 90 N et 67 N. Les forces de coupe ont diminué avec des vitesses de coupe plus élevées et augmenté avec des avances plus élevées pour tous les alliages. L'utilisation d'un fluide de coupe a significativement amélioré l'état de surface de l'Al-Li (de 32,2 %) et réduit les forces de coupe pour l'Al-Li-Cu-Sc (de 26,6 %), bien que son effet sur l'Al-Li-Cu ait été limité.

Les émissions de particules lors de l'usinage étaient principalement influencées par la vitesse de coupe, suivie de la dureté de l'alliage et de l'avance. L'alliage Al-Li-Cu-Sc, malgré sa haute dureté, a démontré une usinabilité supérieure grâce à une microstructure affinée par l'ajout de scandium.

Les résultats soulignent l'importance des traitements thermiques optimisés et des paramètres d'usinage pour développer des matériaux légers et résistants, adaptés aux composants aérospatiaux avec une qualité de surface et une précision d'usinage supérieures.

**Mots-clés :** Alliages à base d'Al-Li, Traitement thermique, Usinabilité, Rugosité de surface, Force de coupe, Émission de particules

**Machinability Study of Aluminum-Lithium Alloys for Aerospace Applications: Influences of Heat Treatments and Machining Conditions**

Lida RADAN

## ABSTRACT

This thesis investigates the machinability of advanced aluminum-lithium alloys (Al-Li, Al-Li-Cu, and Al-Li-Cu-Sc), prized for their low density, high tensile strength, and corrosion resistance, making them essential for aerospace applications. However, machining challenges such as reducing the surface roughness, the cutting forces and the fine metallic particles emissions remain critical concerns. This study provides a detailed analysis of how alloy composition, heat treatments, and machining parameters affect these challenges. This study thus fills a crucial gap in the literature by focusing on the effects of scandium and copper additions to Al-Li alloys and their effects on heat treatments and machinability.

Heat treatments were optimized for each alloy to achieve the highest hardness, with the Al-Li alloy reaching 97 HV under 580 °C/1 h solution treatment + 150 °C/45 h artificial aging, and the Al-Li-Cu and Al-Li-Cu-Sc alloys reaching 164 HV and 182.7 HV, respectively, under 505 °C/5 h solution treatment + 180 °C/20 h artificial aging. End milling experiments were conducted at constant depth of cut (2 mm) under both wet and dry conditions, varying feed rates (0.05–0.15 mm/th) and cutting speeds (200–600 m/min).

Key findings demonstrate that the Al-Li alloy required the lowest machining force (52.3 N), while Al-Li-Cu and Al-Li-Cu-Sc alloys required 90 N and 67 N, respectively. Cutting forces decreased with higher cutting speeds and increased with higher feed rates for all alloys. The use of cutting fluid significantly enhanced the surface finish of Al-Li (by 32.2%) and reduced cutting forces in Al-Li-Cu-Sc (by 26.6%), although it had minimal effect on Al-Li-Cu.

Particle emissions during machining were primarily influenced by cutting speed, followed by alloy hardness and feed rate. The Al-Li-Cu-Sc alloy, despite its high hardness, demonstrated superior machinability due to refined microstructure enabled by scandium additions.

The findings highlight the importance of optimized heat treatments and improving machining parameters in developing lightweight, high-strength materials for aerospace components with superior surface quality and machining precision.

**Keywords:** Al-Li based alloys, Heat treatment, Machinability, Surface roughness, Cutting force, Particle emission

**TABLE OF CONTENTS**

## LIST OF TABLES

Page

## LIST OF FIGURES

Page

## LIST OF ABREVIATIONS

| | |
|---|---|
| ANOVA | Analysis of variance |
| BUE | Built-up edge |
| ISO | International standard organizations |
| SEM | Scanning electron microscopy |
| EDS | Energy-dispersive x-ray spectroscopy |
| CNC | Computer numerical control |
| MQL | Minimum quantity lubrication |
| APS | Aerosol particle sizer |
| CPC | Condensation particle counter |
| PFZ | Precipitate free zone |
| IM-process | Ingot metallurgy process |
| PM-process | Powder metallurgy |
| DOE | Design of Experiments |

## LIST OF SYMBOLS AND UNITS OF MEAUREMENT

| | |
|---|---|
| f | Feed rate (mm/th) |
| v | Cutting speed (m/min) |
| ap | Depth of cut (mm) |
| h | Hardness (HV) |
| c | Cooling mode |
| Fx, Fy, Fz | Force components in the X, Y and Z directions (N) |
| Ra | The arithmetic average height (μm) |
| Rq | Root mean square roughness (μm) |
| Rt | The maximum height of the profile (μm) |
| Rz | Ten-point height (μm) |
| Rp | The maximum height of peaks (μm) |

# INTRODUCTION

Historically, improvements in the performance of metallic materials affected the performance of aerospace and space craft. Over time, the distinct characteristics and density of aluminum-based alloys and products have advanced alongside the evolution of the aerospace industry. Al-Li products present promising prospects for substantial enhancements in aero structural performance. Lithium, being the lightest metallic element, contributes to reducing the density and enhancing the modulus of Al-based alloys (Starke, Sanders, and Palmer 1981). The primary basis for selecting lithium as the alloying element in the development of low-density Al-based alloys stems from its dual properties of density reduction and precipitation strengthening. These alloys are lighter and have high tensile and yield strength compared to the conventional high-strength aluminum alloys. Li-containing alloys can be potential candidates for any mechanical treatments. Lithium enables the precipitation strengthening of aluminum through the uniform dispersion of coherent, spherical δ' ($Al_3Li$) precipitates (Starink et al. 1999a).

The primary difficulties encountered in machining aluminum alloys revolve around the poor quality of holes, which can potentially trigger cracks within the airframe structure, thereby compromising their reliability. Consequently, this issue may lead to the rejection of parts during the assembly phase, significantly impacting manufacturing costs (Childs 2000).

Due to their soft matrices, another problem with these alloys is the adhesion and built-up edge (BUE). The problems with the control of chips formation could be better solved by using appropriate tool materials (carbides, diamond), good tool geometry and suitable machining parameters (feed, speed) with regards to the tools selected, the machining conditions and the machining performance (cost, quality, productivity) desired (Aamir et al. 2020).

Mou et al. (2013) illustrated that the operational efficiency of components produced via milling processes is heavily influenced by factors related to surface integrity, such as spindle speed, depth of cut, feed rate, and the angle between the feed direction and rolling orientation. Furthermore, they showcased the effectiveness of liquid nitrogen in enhancing surface

integrity, by rapidly cooling the material, which minimizes thermal softening, reduces residual stresses, and prevents built-up edge formation. This cooling effect leads to a harder, smoother surface and improves chip evacuation, boosting material removal rates (Mou et al. 2013).

Although there are some studies on the machining of Al-Li alloys, optimal heat treatments and machining conditions still need to be found, especially for those containing additive element such as Cu and Sc.

In this project, the influence of heat treatments and machining conditions on machining performance of aluminum-lithium based alloys were studied. The machining was done with variable parameters involving cutting speed, feed rate and hardness. The machining was done for dry and wet conditions. The surface roughness, the cutting forces and the fine metallic particle emissions (number and mass concentrations) were studied as machining responses.

At the first stage, heat treatments were designed and applied with a trial-and-error method based on previous studies. Afterwards, the micro-hardness was measured, and microstructure was investigated to study the aging process and precipitation behaviors. Based on this evaluation, the samples with highest, lowest, and medium hardness were chosen for machining process.

The machining process was done using a 3-axis CNC milling machine under both dry and wet conditions, with cutting speed and feed rate as variants. The surface roughness of the machined parts was measured in X and Y directions using a roughness profilometer. Cutting forces were measured directly during the milling process using a table-dynamometer. Fine particles emitted during machining were measured using an Aerodynamic Particle Sizer.

**Research Objectives**

In this doctoral research study, we investigate experimentally the machinability of Aluminum-Lithium alloys for aerospace applications. This objective is divided into three specific sub-objectives:

**Objective 1:** Finding the optimized heat treatment for Al-Li alloys

To optimize the heat treatment, the samples should be prepared from three different alloys. Although there are many studies on the heat treatment of Al-Li alloys, since our alloy contains a higher percentage of lithium besides additive elements such as Cu and Sc, there is still a need to find the optimal heat treatments. The effects of heat treatment on the microstructure and strength were examined and the precipitation behavior and strengthening mechanism were investigated. Based on the achieved results, the best and most desirable result is considered for the alloy which will improve the strength and ideal condition for machining.

**Objective 2:** Establishing a Comprehensive Design of Experiments (DOE) Framework for Al-Li Alloys

To systematically evaluate the machinability of Al-Li alloys, this objective focuses on implementing a full factorial Design of Experiments (DOE) methodology. The DOE is designed to analyze the effects of key machining inputs, feed rates, cutting speeds, material properties (hardness), and the presence of cutting fluids on critical outputs including surface roughness, cutting forces, and particle emissions. By structuring the experiments using statistical software and tools, the DOE ensures that the selected machining parameters and their interactions are comprehensively studied, allowing for a precise determination of the most influential factors affecting machinability.

Prior to conducting the machining tests, the methodology ensures adherence to necessary preparatory steps. Inputs are methodically converted into outputs through a controlled process involving operations, machines, and other resources. The accuracy and reliability of the results are enhanced by minimizing the number of experimental tests while maximizing their precision (Guo and Mettas 2010; Montgomery 2017). This approach not only facilitates a clear understanding of the machining characteristics of Al-Li alloys but also establishes a framework for optimizing machining processes, particularly for alloys with unique compositions and properties.

Through this carefully structured experimental plan, the study aims to provide actionable insights into the machinability of Al-Li alloys and the optimal machining conditions required to achieve superior surface quality, reduced cutting forces, and minimized particle emissions.

**Objective 3:** Evaluation of the machining of Al-Li alloys

In alignment with the preceding two objectives, for a more comprehensive analysis of the impact of heat treatment methods on machining characteristics, it is imperative to machine the parts under meticulously controlled cutting conditions after heat treatment. This phase aims to concentrate on assessing the effects of hardness, cutting speed, feed rate, and cooling mode on surface roughness, cutting force, and chip formation during milling of these aluminum lithium alloys across various heat treatment conditions. Such an approach would facilitate a more precise delineation of the machinability of the alloy.

**Thesis Outline**

The thesis is comprised of six chapters, alongside the introduction which encompasses the thesis statement and objectives. It is structured in a manuscript style format. Chapter 1 focuses on conducting a literature review concerning heat treatment, machining, and machinability of Al-Li based alloys. Chapter 2 delineates the experimental procedure, encompassing devices and equipment, workpiece materials, and cutting tools employed to achieve the stated objectives. Chapter 3 is dedicated to the results and discussions on heat treatment of the alloys. Chapter 4 presents the results and discussion on surface roughness. Chapter 5 discusses the results related to the cutting force. Finally, Chapter 6 covers the results and discussion of particle emissions. The thesis ends with additional section, wherein the recommendations are outlined.

# CHAPITRE 1

# LITERATURE REVIEW

## 1.1 Introduction

Aluminum alloys are categorized into two primary groups: cast alloys and wrought alloys. This classification is dependent on phase solubility that the thermal treatment method directly influences. The treatment methods which have effects are solution heat treatment, quenching, and aging hardening.

## 1.2 Aluminum Alloys Nomenclature

Wrought alloys are denoted by four-digit numbers according to the following classification (Committee 1990):

- 1xxx: Controlled unalloyed (pure) compositions.
- 2xxx: Alloys primarily containing copper as the main alloying element, although magnesium and other elements may also be specified.
- 3xxx: Alloys with manganese as the primary alloying element.
- 4xxx: Alloys containing silicon as the main alloying element.
- 5xxx: Alloys with magnesium as the principal alloying element.
- 6xxx: Alloys containing magnesium and silicon as primary alloying elements.
- 7xxx: Alloys primarily consisting of zinc as the main alloying element, with additional elements such as copper, magnesium, chromium, and zirconium possibly specified.
- 8xxx: Alloys composed of tin and some lithium.
- 9xxx: Reserved for future use.

Al-Li alloys fall under the category of group 8xxx. Specific alphanumeric characters and digits are appended to aluminum alloys based on the mechanical and heat treatment methods applied to them (Garza Elizondo 2010).

## 1.3 Aluminum-Lithium Alloys

In recent years, the aerospace manufacturers have more tendency to use Al-Li alloys in order to improve performance and fuel efficiency (Starke, Sanders, and Palmer 1981). Lithium is the lighter metal with much lower density (540 kg/$m^3$) compared aluminum (2700 kg/$m^3$) (De Jong 1984; Prasad, Gokhale, and Rao 2003). High strength and low density are the Al-Li alloy point of difference from Al alloys (De Jong 1984; McDonald 2009). By adding more Lithium to aluminum alloys composition, higher modulus and excellent cryogenic toughness could be achieved (Prasad, Gokhale, and Rao 2003; Joshi 2005). The main rationale behind selecting lithium as the alloying element stems from its combined features of reducing density and strengthening through precipitation (Starink et al. 1999a).

### 1.3.1 Technical Reasons for Alloying Aluminum Alloys with Li Additions

- 1 wt pct Li addition provides approximately 3 pct decrease in density.
- 1 wt pct Li addition provides approximately 6 pct increase in young's elastic modulus.
- Li additions enable the formation of potent hardening precipitates.
- Li additions impart higher fatigue crack growth resistance (De Jong 1984).

### 1.3.2 Fabrication Techniques of Al-Li Alloys

There are some different methods to produce Al-Li alloy such as ingot metallurgy process (IM-process) as a low-cost method, powder metallurgy (PM-process) to produce Al-Li alloys with

different composition and microstructure. And a third method, which is a kind of PM-process, is melt-spinning or splat-cooling process (De Jong 1984).

### 1.3.3 Commercial Al-Li Alloys

The commercial Al-Li alloys in the market are listed as below (Prasad, Gokhale, and Rao 2003):

- Weldalite 049 (composition(wt%): Cu5.4, Li1.3, Ag0.4, Mg0.4, Zr0.14, bal.Al)
- Alloy 2090 (composition(wt%): Cu2.7, Li2.2, Zr0.12, bal.Al)
- Alloy 2091 (composition(wt%): Cu2.1, Li2.0, Zr0.10, bal.Al)
- Alloy 8090 (composition(wt%): Cu1.3, Li2.54, Mg0.95, Zr0.12, bal.Al) (Joshi 2005)
- Alloy 1420 (composition (wt%): Li2.0, Mg5.0, Zr0.1, Si0.15, Fe0.15, bal.Al)
- Alloy 1421 (composition (wt%): Li2.1, Mg5.2, Si0.1, Fe0.15, bal.Al)
- Alloy 1460 (composition (wt%): Cu3.0, Li2.0, Si0.15, Fe0.1, bal.Al)
- Alloy 1441(composition(wt%): Cu1.75, Li2.0, Mg0.9, Zr0.1, Si0.1, Fe0.1, bal.Al)

### 1.3.4 Short Comings of Old Al-Li Products and Their Solution

- High mechanical property anisotropy
- Deviation of cracks
- Reduced fracture toughness
- Formation of microcracks during manufacturing
- Inadequate corrosion resistance
- Deterioration of toughness following simulated thermal exposure (Rioja and Liu 2012)

The issue of crack deviation in the crack path of third-generation Al-Li 2199 (C47A) was resolved through a reduction in mechanical property anisotropy achieved via composition optimization and control of crystallographic texture, grain size and shape, cold deformation, and the amount and type of precipitates. In contrast to the highly tortuous crack path and crack

deviation observed in the second-generation 8090-T86 alloy, the crack in the third generation is straight and perpendicular to the stress axis. Furthermore, in third-generation Al-Li alloy 2199, fracture toughness was significantly enhanced through composition optimization, thermal-mechanical processing (TMP), and control of precipitate microstructure (Rioja and Liu 2012).

### 1.3.5 Application of Al-Li Alloys

Throughout history, advancements in metallic materials have had a direct and significant impact on the performance of aerospace and spacecraft. Due to their unique characteristics, Al-Li alloys have emerged as key players in the aerospace industry, particularly in military and space applications, owing to their lightweight nature which greatly influences efficiency, fuel consumption, and aircraft payload.

The excellent fatigue resistance of Al-Li alloys makes them suitable for various components of commercial aircraft, including lower wing surfaces, leading and trailing edges, access covers, and seat skins. Moreover, they find widespread use in the center fuselage, control surfaces, and main wing box of military aircraft. These alloys are highly favored for cryogenic applications such as liquid oxygen and hydrogen fuel tanks, as well as the tankage of booster systems. Additionally, they are considered a viable alternative to aluminum alloys for specific applications in helicopters, rockets, and satellite systems (Joshi 2005; Prasad, Gokhale, and Rao 2003).

Al-Li alloys offer significant enhancements in aerostructural performance through density reduction, increased stiffness, improved fracture toughness, resistance to fatigue crack growth, and enhanced corrosion resistance. However, previous generations of Al-Li alloys, such as 2090-T81 plate, 8090-T86 plate, and 2091-T84 sheet, exhibited mechanical property anisotropy in both in-plane and through-thickness directions. These alloys were associated with undesirable design and manufacturing characteristics, including crack deviation, microcracking during cold hole expansion, low short-transverse fracture toughness, poor

corrosion resistance, and inadequate thermal stability. The durability (e.g., corrosion and fatigue resistance) and damage tolerance (e.g., residual strength and fatigue crack growth) properties often dictate the size of aircraft components, with their significance varying depending on the specific aircraft component and its position (Rioja and Liu 2012). The application of Al-Li alloys in commercial aircraft is depicted in Figure (1.1).

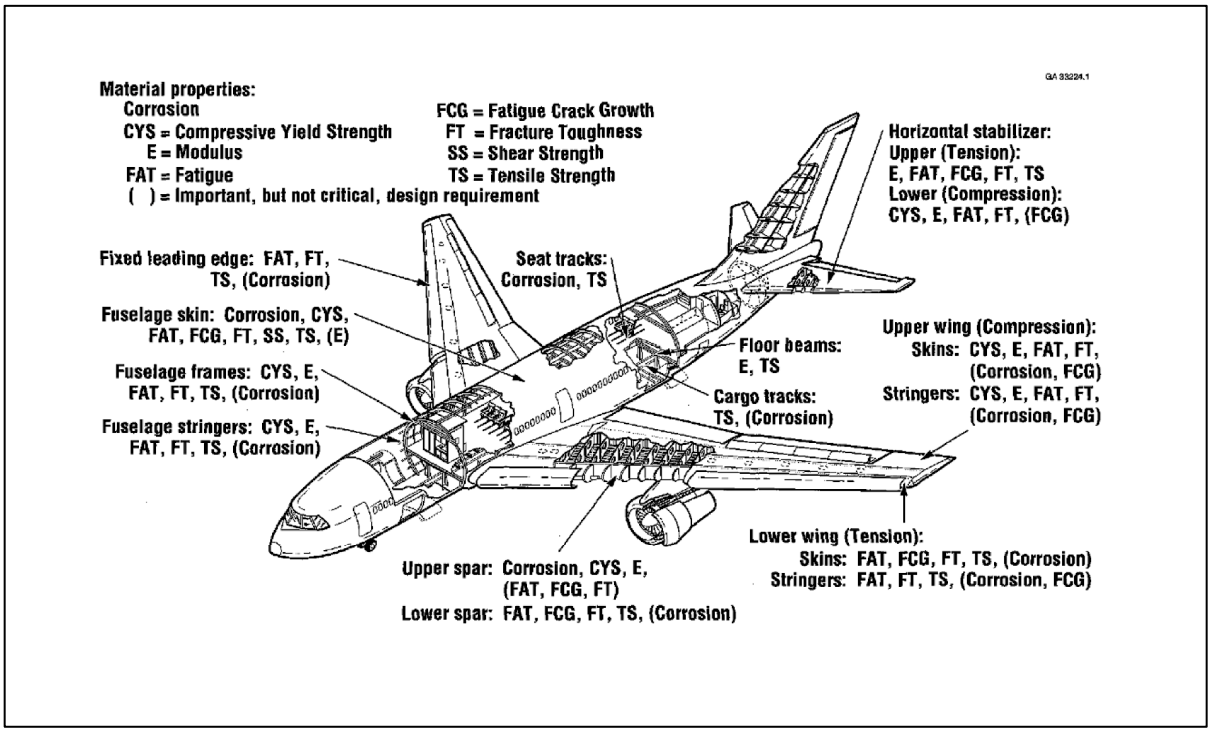


Figure 1.1 Al-Li alloy applications in a commercial aircraft
Taken from Rioja and Liu (2012)

The fundamental mechanisms utilized to strengthen Al-Li alloys for structural purposes include precipitation strengthening, solution strengthening, and strengthening through grain and sub-grain refinement, as well as strengthening via dislocations. The first two mechanisms are significantly influenced by the alloy composition and heat treatment and are typically applied in a metastable state. Conversely, the latter two mechanisms primarily rely on thermo-mechanical processing methods (Starink et al. 1999a).

### 1.3.6 Background Information that Led to Improvements in Al-Li-X Alloys

Anisotropy in mechanical properties is a critical consideration in the widespread application of aluminum alloys within aerospace contexts. Early Al-Li alloys, which incorporated zirconium (Zr) as a grain refiner, exhibited elongated pancake-shaped grains with a distinct crystallographic texture (Bull and Lloyd 1986). In these alloys, Zirconium formed coherent $Al_3Zr$ dispersoids during ingot preheat, impeding recrystallization during typical ingot breakdown and subsequent processing stages. The presence of shearable precipitates, precipitate-free zones, and strain localization resulted in significant in-plane anisotropy in tensile, fatigue, and fracture properties, potentially leading to delamination at both ambient and cryogenic temperatures. Delamination occurrences were associated with periodic shifts from high to low relative grain misorientations (Palmer et al. 1986).

Studies by Palmer et al. demonstrated that thermomechanical processing led to the development of a fine recrystallized grain structure in Al-Li-X alloys, exhibiting nearly isotropic tensile properties in an unstretched, peak-aged condition. Rioja discussed the intricate relationship between processing parameters, alloy composition, texture, and properties of aerospace aluminum alloys. Notably, the presence of the "Brass" texture component in unrecrystallized plates resulted in mechanical property anisotropy both in-plane and through thickness. This anisotropy could be mitigated by reducing the intensity of crystallographic texture, achieved through recrystallization during solution heat treatment or by intermediate steps during wrought alloy processing. Strategies included reducing deformation, replacing coherent dispersoids with semi-coherent or incoherent dispersoids through composition control and thermomechanical processing (Palmer et al. 1986; Rioja, Giummarra, and Cheong 2008).

Moreover, it was observed that the influence of texture on properties varied for different tempers in 2XXX alloys. The "Goss" texture could enhance the strength-toughness relationship in recrystallized fuselage sheets in the T3 temper, while the "Brass" texture improved fatigue

crack growth resistance of plate products in the T3 temper for lower wing applications (Starke Jr 2014).

Another study demonstrated that the strength of Al-Li alloys could be augmented through magnesium or copper additions. More recently, these additions have been incorporated into the development of quaternary Al-Li-Mg-Cu alloys. Additionally, the presence of these additional alloying elements was expected to influence the precipitation of δ' itself (Gregson and Flower 1984). Figure 1.2 illustrates the chronological development and early usage of lithium in aluminum.

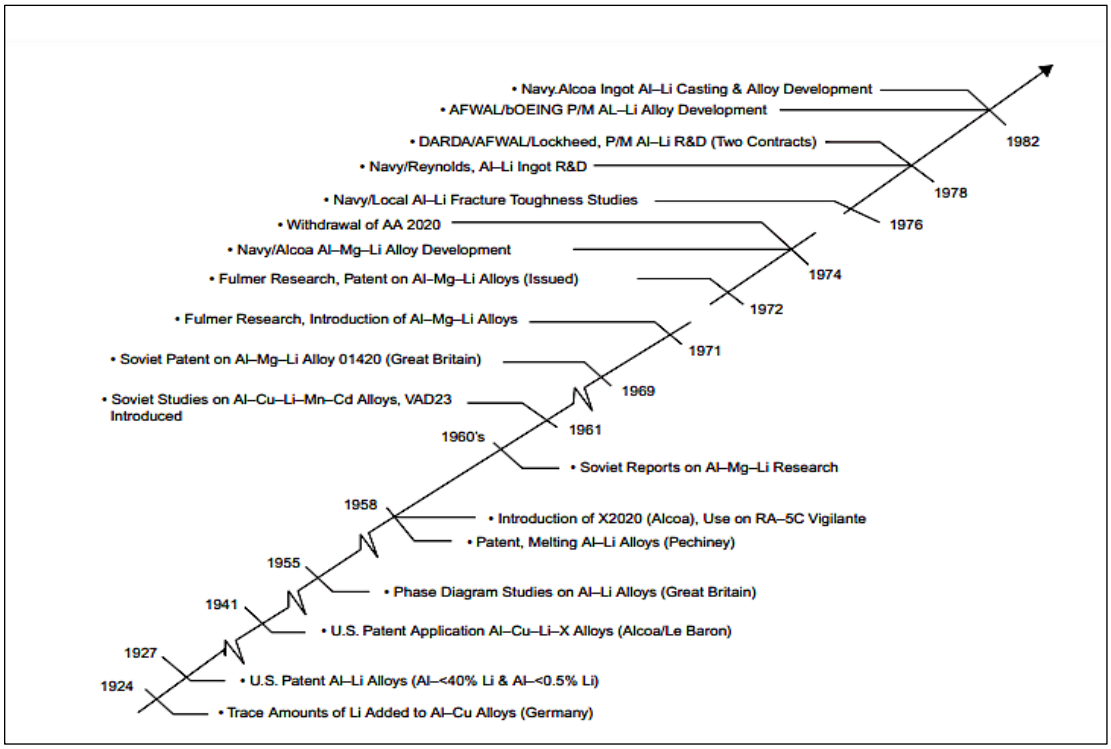


Figure 1.2 Chronological early development and use of lithium in aluminum
Taken from Starke Jr (2014)

### 1.3.7 Development of Al-Li Alloys

I.N. Fridlyander et al. (Fridlyander et al. 1992) discovered the hardening effect in a group of alloys within the Al-Li-Mg system. This groundbreaking work, dating back to 1965, led to the

development of alloy 01420, which contains 2% Li, 5.5% Mg, and 0.1% Zr. This alloy, patented in several countries, is approximately 10-12% lighter than 2024. They asserted that the alloy exhibited high corrosion resistance, good weldability, a high elastic modulus, and static strength. Additionally, they developed a modification of 01420 containing scandium. Scandium, known for its superior ability to prevent recrystallization compared to Zr, Cr, and Mn, contributes to the formation of a fine sub-grain structure in wrought products. It provides additional strengthening by forming stable $Al_3Sc$ dispersoids. Scandium has higher atomic solubility than Zr in aluminum, approximately 1.7 times greater by weight. It also boasts similar solubility by weight compared to Zr (0.25 vs. 0.28 wt%). Among the available alloys with the lowest density suitable for commercial use is alloy 01420.

In the annals of aluminum metallurgy history, the development and exploration of Al-Li alloys, which commenced in the late 1970s and 1980s, stands out as one of the most significant single alloy development programs. This initiative involved the participation of hundreds of scientists and engineers. During the 1970s, the value of the Al-Li alloys market soared, with a particular focus on weight reduction to minimize landing weight fees. Extensive research was conducted to identify the feature with the greatest impact on weight savings. Surveys indicated that the most advantageous change was a reduction in density, with lithium identified as the lightest element capable of achieving significant density reduction in aluminum. Ekvall et al. (Ekvall, Rhodes, and Wald 1982), concerned about the competition between nonmetallic composites and aluminum alloys for aerospace materials, spurred aluminum companies to invest heavily in the development of low-density alloys. They believed that a substantial advancement in aluminum metallurgy was essential to maintain competitiveness. Detailed design studies forecasted that Aluminum-Lithium alloys meeting predefined alloy development targets could achieve weight savings ranging from 8 to 15% through a combination of density reduction and stiffness enhancement. The primary objective of most Al-Li development studies was to leverage insights from previous aluminum metallurgy research. These insights included minimizing iron and silicon content to the economically feasible minimum for high toughness and ductility. Given that large Mn-rich dispersoids may compromise ductility by nucleating voids, zirconium was employed instead of manganese to form $Al_3Zr$ dispersoids for grain

refinement. Additionally, since cadmium appeared to exacerbate intergranular fracture in alloy 2020, it was omitted as an element for nucleating strengthening precipitates. These research endeavors culminated in the emergence of the "second generation" of aluminum-lithium alloys (Starke Jr 2014).

### 1.3.8 Understanding the Precipitate Structure in Al-Li-X Alloys

Prior to machining the alloys, it's imperative to optimize their characteristics to enhance machining behaviors and properties. Al-Li alloys with varying element compositions exhibit distinct sensitivities to heat treatment strengthening. Moreover, the dominant precipitates at different stages of heat treatment vary. Consequently, the strengthening mechanism and optimal heat treatment processes for specific Al-Li alloys also differ.

To optimize alloying additions and thermal-mechanical processing (TMP), understanding the influence of chemical composition and microstructure is essential. Ashton et al. explored the impact of iron content on the fracture toughness of aluminum-lithium alloys, particularly in 2090-T8 (Ashton, Thompson, and Gayle 1986). Depending on the presence of other alloying elements, lithium can form the coherent $Al_3Li$ (δ′) phase, which serves as a primary strengthening phase during aging. Copper additions can lead to the formation of either $Al_2Cu$ (θ′) or $Al_2CuLi$ (T1), with T1 being the major strengthening phase depending on the Cu:Li ratio. Zirconium additions result in the formation of the coherent $Al_3Zr$ phase, effective in preventing recrystallization but contributing to a strong deformation texture. In AlMgLi alloys, phases such as $Al_2MgLi$ and δ′ may form, while in complex Al-Li alloys containing copper, $Al_2CuMg$ (S′) can form, potentially suppressing the formation of $Al_2Cu$. The precipitation process during aging can be intricate, with multiple phases forming in competition with each other. Figure (1.3) illustrates schematically the precipitate phases that form in AlLiX alloys (Starke Jr 2014).

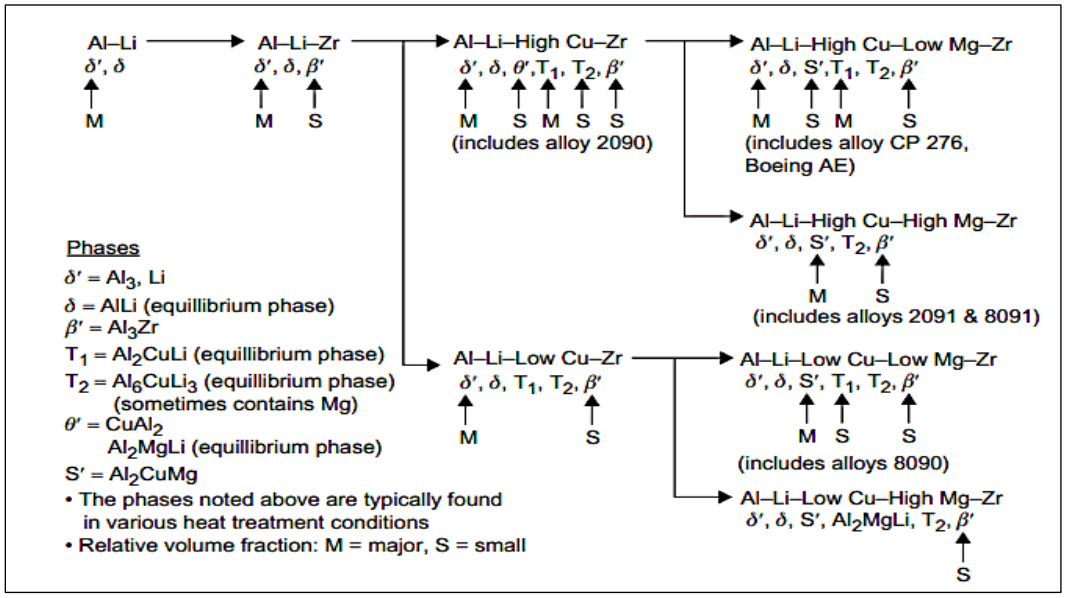


Figure 1.3 Schematic of the precipitate phase that form in Al-Li-X alloys
Taken from Starke Jr (2014)

### 1.3.9 Heat Treatment of Al-Li Alloy

In age-hardened Al–Cu–Li alloys, the T1($Al_2CuLi$), δ′($Al_3Li$), and θ′($Al_2Cu$) phases play crucial roles as strengthening precipitates. Compared to other alloys, the AA2050 alloy, a third-generation Al-Cu-Li alloy, exhibits a higher Cu/Li mass ratio, potentially suppressing the formation of the coherent δ′ phase. Consequently, significant precipitation strengthening occurs during aging treatment, leading to an optimal balance of strength and ductility in the alloy.

Research by Xie et al. indicates that elevating the aging temperature notably enhances aging kinetics, resulting in the precipitation of larger T1 phases and a subsequent decrease in number density. Double aging serves to homogenize the size and distribution of precipitated phases, thereby reducing micro-deformation disparities. Pre-deformation increases the number of nucleation sites for the T1 phase, significantly reducing average size and increasing number density.

The study findings reveal that material hardness increases with aging time, with the rate of increase influenced by aging temperature, single/double aging approaches, and pre-deformation. Single aging commences either post-solid solution quenching or after pre-deformation, while double aging initiates after 120 °C/4 h pre-aging. Higher aging temperatures expedite the aging hardening process. Notably, SA160 and DA160 exhibit slow aging processes, failing to reach peak-aging at 24 hours, unlike DA190, which approaches peak-aging within the same timeframe. Upon pre-deformation application, the aging process accelerates significantly, with P7SA160 and P7DA160 reaching peak-aging at 24 hours, the latter exhibiting a faster hardening process. P7DA190 peaks at approximately 4 hours, experiencing minimal hardness changes during over-aging stages, slightly lower than the 160 °C sample at 24 hours. Additionally, pre-deformation introduction eliminates softening phenomena during double aging in the final aging stage (Xie et al. 2022).

Table 1.1 Sample names under different experimental conditions

Taken from Xie, Liang et al. (2022)

| Sample name | Pre-deformation (%) | Pre-aging temperature(°C)/time(h) | Final-aging temperature(°C)/time(h) |
|---|---|---|---|
| SA160 | - | - | 160/4, 8, 16, 24 |
| DA160 | - | 120/4 | 160/4, 8, 16, 24 |
| DA190 | - | 120/4 | 190/4, 8, 16, 24 |
| P7SA160 | 7 | - | 160/4, 8, 16, 24 |
| P7DA160 | 7 | 120/4 | 160/4, 8, 16, 24 |
| P7DA190 | 7 | 120/4 | 190/4, 8, 16, 24 |

Various heat treatment processes can yield different types, sizes, distributions, and number densities of the precipitated phase in 2195 Al–Li alloy. Wu et al. explored the microstructure evolution and associated mechanical properties of Al–2Cu–2Li during aging within the temperature range of 150–225 °C. The findings indicated that the growth of T1 was controlled by the diffusion rate of Cu along the dislocation. For a high Li content, some δ′ phases were present and underwent significant coarsening with increasing aging temperature. The δ′ phase

exhibited the lowest thermal stability, and its gradual dissolution led to a notable reduction in material strength as the temperature rose (Wu, Zhang, et al. 2021).

Tao et al. examined the precipitation dynamics of Al–4Cu–1Li within the temperature range of 100–175 °C. Their investigations indicated that at constant aging durations, the microstructural transition progressed from the Guinier-Preston (GP) zone and θ′ phases to the T1 and θ′ phases as the aging temperature rose. Consequently, there was a gradual enhancement in material strength accompanied by a reduction in elongation (Tao et al. 2018).

Lin et al. investigated the microstructure and tensile properties of the Al-2.58Cu-1.64Li alloy under T6, T8 single aging, and T8 double aging conditions. Their findings indicated that T8 double aging led to a significant enhancement in tensile properties, primarily attributed to the abundance of fine T1 and δ′ phases, along with the presence of discontinuous Cu-rich intergranular phases (Lin, Wei, and Zheng 2018).

In another study conducted by Duan et al. (Duan, Matsuda, et al. 2021), the microstructures and mechanical properties of a novel cast Al–Cu–Li alloy during heat treatment were examined. The results revealed that most of the secondary phases along grain boundaries in the as-cast state dissolved into the Al matrix after homogenization and solution treatment. However, the Cu-rich phases slightly re-segregated on grain boundaries after aging. A relatively favorable balance of strength and ductility was achieved after natural aging. The investigation also unveiled a complex precipitate distribution in this cast alloy after natural aging. Compared to similar alloys with pre-introduced dislocations before aging, the density of T1($Al_2CuLi$) phases decreased while the size increased.

The improvement in performance was attributed to the low volume fraction of δ′ phase, medium density of needle-shaped precipitates, and a relatively narrow precipitate-free zone with varying widths near the grain boundary.

In the optical microscopy (OM) and scanning electron microscopy (SEM) images of the initial as-cast alloy, the microstructure revealed distinct and wide grain boundaries, suggesting significant segregation of elements and secondary phases during solidification.

To mitigate this segregation and facilitate the dissolution of alloying elements into the matrix, a two-stage homogenization and solution treatment process was implemented. The OM and SEM images of the as-quenched alloy are depicted in Figure 1.4. A comparison with the as-cast alloy reveals relatively cleaner grain boundaries, with only minimal secondary phases remaining.

Subsequently, the samples underwent natural aging, and similar analyses were conducted. In the optical microstructure (Figure 1.4c), an increase in the number of fine black spots and lines along the grain boundaries indicates a slight re-precipitation of secondary phases after aging. These findings were corroborated by the SEM image (Figure 1.4f), where the white areas exhibited a slight increase compared to the as-quenched state (Duan, Matsuda, et al. 2021).

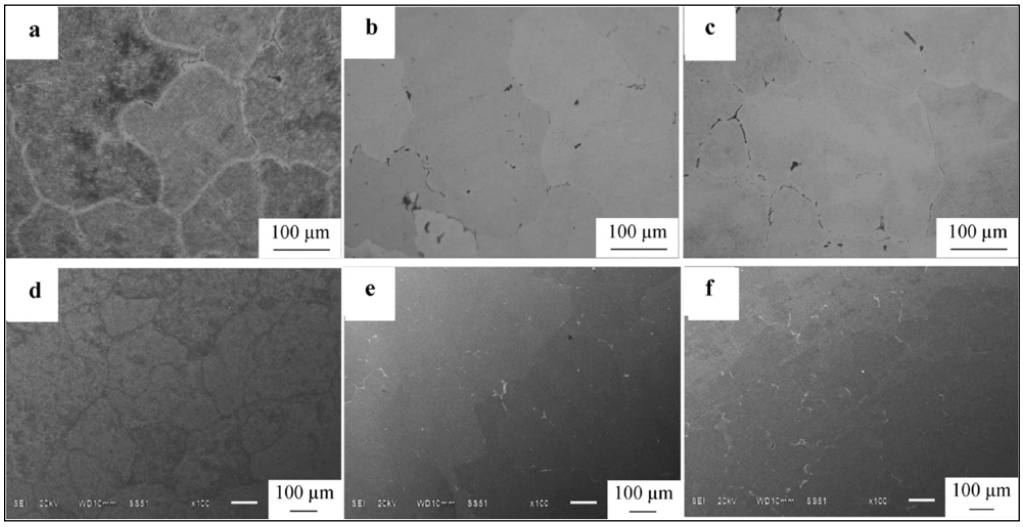


Figure 1.4 a, b, c) OM images and d-f SEM images of different stages during heat treatment: a, d) as-cast alloy; b, e) as-quenched alloy; c, f) after aging
Taken from Duan, Matsuda et al. (2021)

Figure 1.5 depicts a progressive increase in hardness over aging time until peak aging is achieved. The peak hardness, measured at 136 HV, is reached after 24 hours of aging. Moreover, samples in the peak-aged condition can undergo further hardening, reaching up to 144 HV, during subsequent 6-month natural aging (Duan, Matsuda, et al. 2021). Wang and Starink (Wang and Starink 2005) observed significant softening in the initial stages of artificial

aging in 2198 and 2196 alloys. This softening is primarily attributed to the dissolution of solute clusters, particularly Cu-rich clusters. Additionally, their research suggests that the rapid increase in hardness is directly associated with the precipitation of numerous precipitates, such as T1, θ', and δ' ($Al_3Li$), with their coarsening during over-aging contributing to a decline in hardness.

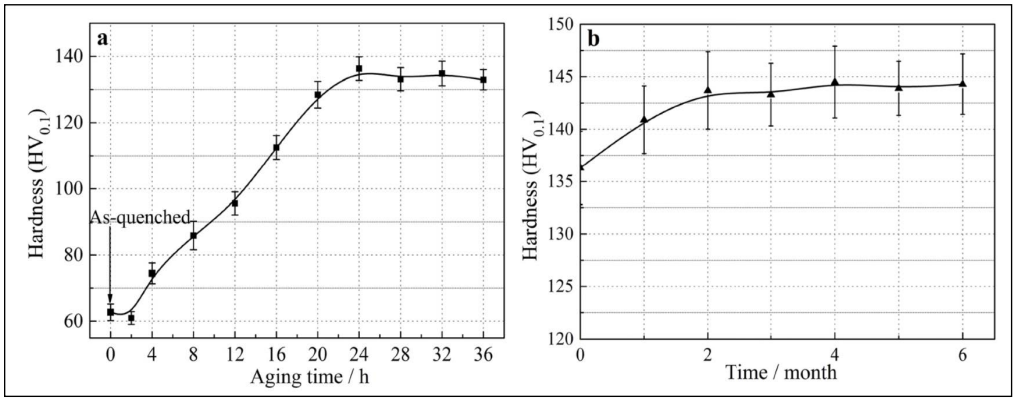


Figure 1.5 Hardness evolution of studied alloy: a) artificial aging at 175 °C and b) natural aging of artificial peak aged alloy

Taken from Duan, Matsuda et al. (2021)

### 1.3.10 The Effect of Alloying- Scandium

Sc addition also increased the precipitation nucleation efficiency and promoted the uniform precipitation of the η′ phase of 7055 alloy during aging. Compared with pure 7055 alloy, a hardness, tensile strength, ductility, and thermal stability of the 7055 alloy with Sc is improved. This improvement was attributed to the finer size, higher density, more uniformly distributed η′ phase, less η phase, and finer Al grains of 7055 alloy with Sc (Teng et al. 2018).

Ma et al. investigated the impact of a minor addition of Sc on the microstructure, age hardening behavior, tensile properties, and fracture morphology of the 1460 alloy. They observed that increasing the Sc content from 0.11 wt% to 0.22 wt% resulted in grain refinement in the as-cast alloy but also led to the coarsening of Cu-rich particles. The alloy containing 0.11 wt% Sc exhibited improved mechanical properties and age hardening effects. The grains in the samples

with 0 wt% Sc and 0.11 wt% Sc were columnar dendritic and cellular dendritic, as depicted in Figure 1.6, whereas the grains in the alloy with 0.22 wt% Sc were entirely non-dendritic, with an estimated grain size of approximately 80 μm (Ma et al. 2014).

Previous investigations on alloy 8090 demonstrated that higher Sc concentrations (0.43 wt% and 0.84 wt%) could reduce the grain size to 30 μm and eliminate dendrites (Huang et al. 2021).

In alloy 1460, the addition of 0.22 wt% Sc was also observed to effectively refine the grains. Therefore, the addition of Sc to the Al–3%Cu alloy suggests that Sc is effective in grain refinement and dendrite elimination by enhancing constitutional supercooling (Liu et al. 2019).

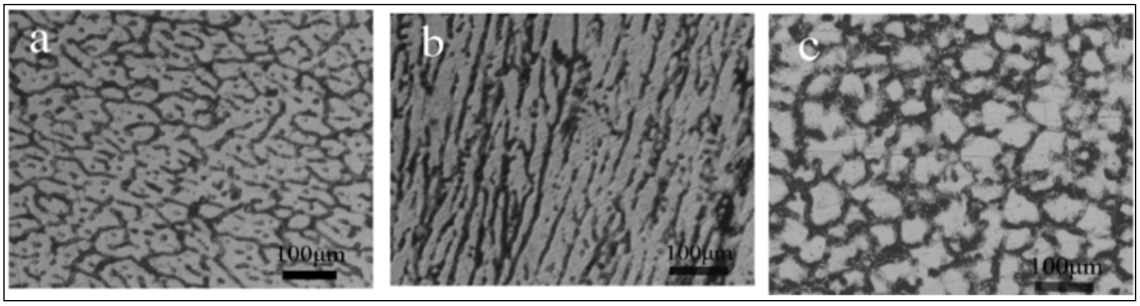


Figure 1.6 Optical micrographs of as-cast alloys with (a) 0.11 wt% Sc, (b) 0 wt% Sc, (c) 0.22 wt% Sc

Taken from Ma, Desheng et al. (2014)

Figure 1.7 displays the optical micrographs of T6 peak-aged (540 °C/ 1 h + water quenched + 190 °C/10 h) alloys. In Figures 1.7(a) and (c), the alloys containing 0.11 wt% Sc and 0.22 wt% Sc show no signs of recrystallization, while the Sc-free alloy (depicted in Figure 1.7b) has fully recrystallized, with a grain size of 100 μm, much larger than that in the Sc-containing alloys. Therefore, the addition of Sc is effective in inhibiting recrystallization in alloy 1460.

Age-hardening curves of alloys with 0.11 wt% Sc, 0 wt% Sc, and 0.22 wt% Sc after aging at 190 °C are presented in Figure 1.8. All three alloys exhibit a hardness peak. The hardness of the alloy with 0.11 wt% Sc is higher than that of the Sc-free alloy, possibly due to the presence of un-recrystallized grains and the precipitation of several $Al_3$(Sc, Zr). However, increasing the Sc content did not result in higher hardness; it appears that the optimal addition of Sc to

alloy 1460 is 0.11 wt%, considering that the alloy with 0.22 wt% Sc exhibited lower hardness (Ma et al. 2014).

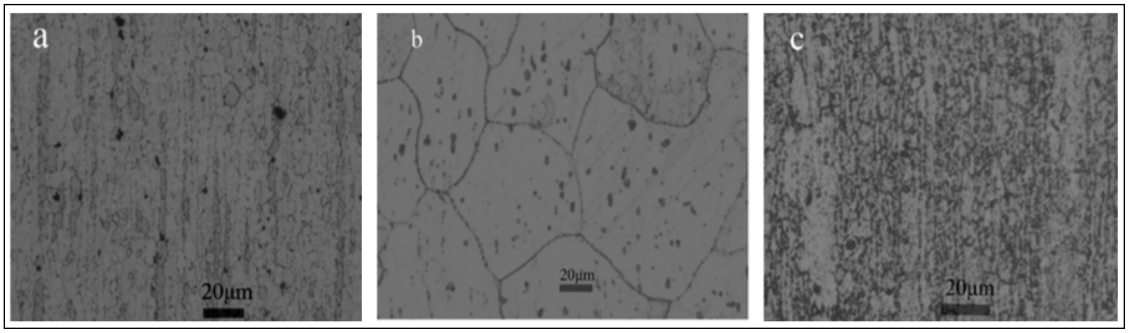


Figure 1.7 Optical micrographs T6 peak aged alloys (a) alloy 4 with 0.11 wt% Sc; (b) alloy 5 with 0 wt% Sc; (c) alloy 6 with 0.22 wt% Sc
Taken from Ma, Desheng et al. (2014)

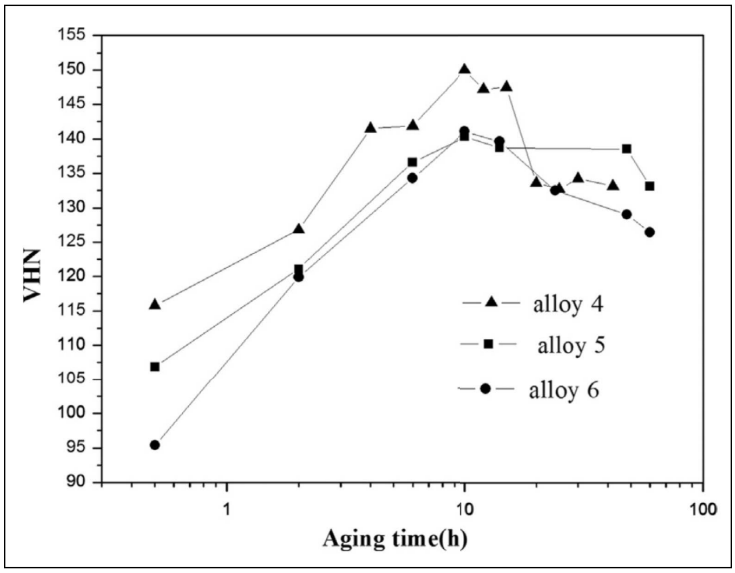


Figure 1.8 Hardening curve for alloys 4-6 aged at 190 °C for various time
Taken from Ma, Desheng et al. (2014)

## 1.4 Machining and Machinability

Machining, a manufacturing technique, involves shaping a workpiece by removing excess material from a larger piece. This method is often referred to as subtractive manufacturing since it involves the removal of material to create a part.

Machinability, on the other hand, refers to the ease, cost, and quality of the metal cutting process. It encompasses the interactions between the workpiece, cutting tool (including its material and geometry), and cutting medium (whether wet or dry) during various removal processes such as turning, drilling, and milling. Different cutting parameters like cutting speed, feed rate, and depth of cut further influence machinability. Key factors affecting workpiece properties and machinability include alloy chemistry and additives, as well as the morphology, size, and volume fraction of constituent phases, among others (Li, Wan, et al. 2012).

Milling is a machining process that involves the removal of material from a workpiece using a rotating cutter (see Figure 1.9). In the context of aluminum alloys, milling is a widely employed method due to the material's prevalence in various industries, and it is chosen to study the aluminum-lithium (Al-Li) alloys, due to its precision and adaptability in controlling cutting parameters. This process allows for precise manipulation of feed rate, depth of cut, and tool geometry, enabling detailed analysis of how Al-Li alloys respond under varying machining conditions. In aerospace, milling is essential to achieve the required surface finish and tight tolerances, minimizing machining-induced surface defects like microcracks and residual stresses, which could impact performance and durability. Milling also enables testing of various conditions (e.g., dry vs. wet milling, different cutting speeds) to optimize the machining. Al-Li alloys are widely used in structural components such as fuselages, wings, and interior parts due to their high stiffness and low weight, which require intricate milling operations for specific shapes and lightweight designs (Li, Wan, et al. 2012).

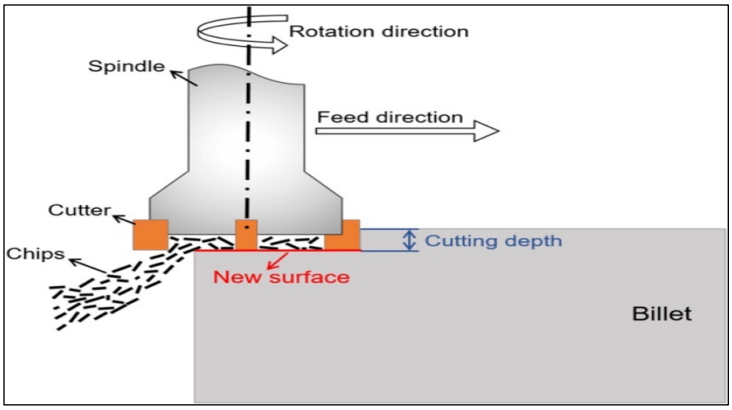


Figure 1.9 Schematic of the milling process
Taken from Wu, Chengpeng et al. (2023)

In milling operations, material removal is facilitated by the relative motion between the workpiece and the cutting tool, where essential parameters such as cutting speed, feed rate, and depth of cut dictate the efficiency of the process. Cutting speed represents the surface speed of the workpiece in relation to the cutting tool, while feed rate denotes the relative velocity at which the tool advances against the workpiece, and depth of cut signifies the volume of material removed within a specified timeframe. Optimal material removal hinges upon the judicious selection of these parameters (Li, Wang, et al. 2012). Process variables, observable during machining, encompass factors like cutting force and chip formation zone temperature, while effect variables, measurable post-machining, include workpiece characteristics such as surface roughness, tool wear, and machine tool conditions (Toenshoff and Denkena 2013).

Force, roughness (surface quality) and particle emissions are crucial machinability criteria for evaluating the performance of milling processes. Cutting forces, exerted on the cutting tool during milling, are monitored to assess tool performance and machining stability. Surface finish, characterized by roughness measurements like Ra or Rz, indicates the quality of the machined surface. While cooling mode and particle emissions are not direct machining outputs, they are important factors that can indirectly impact machining performance and surface quality (Childs 2000).

### 1.4.1 Cutting Force

Monitoring and controlling cutting forces in milling are essential for improving the machining process. Excessive cutting forces can lead to tool wear, poor surface finish, and reduced dimensional accuracy of machined parts. By effectively understanding and managing cutting forces, manufacturers can achieve higher productivity, lower production costs, and improved part quality. The mechanical properties of the workpiece material, such as hardness, ductility, and toughness, significantly influence cutting forces. Additionally, parameters such as cutting speed, feed rate, and depth of cut directly affect cutting forces, with higher speeds and feed rates generally resulting in increased cutting forces. The depth of cut plays a crucial role, as deeper cuts require higher forces to remove material (Stephenson and Agapiou 2018). The design and material of the cutting tool, including the number of flutes, rake angle, and tool coating, also influence cutting forces. Proper selection of tool geometry and material can help minimize cutting forces and prolong tool life. Furthermore, utilizing cutting lubricants can markedly influence both the contact length and cutting forces, effectively decreasing seizure and substantially diminishing the forces involved at low cutting speeds (Trent and Wright 2000).

### 1.4.2 Surface Roughness

Surface roughness refers to the microscopic irregularities in the surface texture of a material, quantifying deviations from an ideal smooth surface. High surface roughness can increase friction, wear, and fatigue, reducing the efficiency and lifespan of machined components, making it essential to control within specified tolerances to meet quality standards (Duan, Li, et al. 2021). Factors influencing surface roughness include material properties, cutting parameters (e.g., cutting speed, feed rate, depth of cut), tool geometry, cutting fluid, and the machining environment (Patel, Batish, and Bhattacharya 2009). While cutting speed and feed rate significantly affect surface roughness, the depth of cut has a less pronounced impact (Sogorovic and Knezevic 2019). At medium speed and low feed, the surface roughness is maximum, but at higher speed, the achieved roughness is average. By increasing the speed and

feed, roughness increases as well (Pattnaik et al. 2018). Achieving excellent surface quality relies on selecting appropriate cutting parameters and control strategies (Xiuli et al. 2010). Surface roughness is measured using instruments like profilometers, which provide quantitative measurements of parameters such as average roughness (Ra), root mean square roughness (Rq), and maximum peak-to-valley height (Rz) (Jiang et al. 2020).

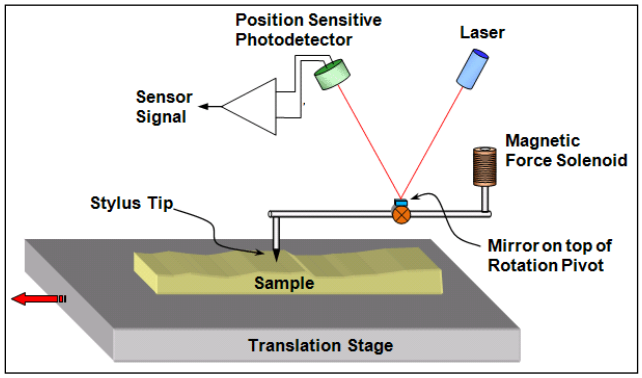


Figure 1.10 Basic elements of a stylus profilometer

Taken from Lee and Cho (2012)

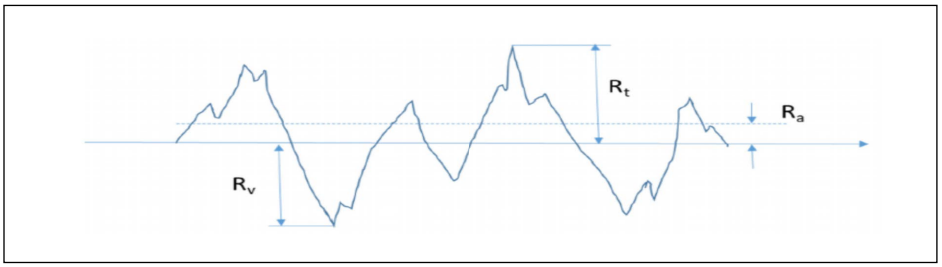


Figure 1.11 A schematic profile of surface roughness and its parameters

Taken from Wu, Kanz, et al. (2021)

### 1.4.3 Metallic Particles Emission During Machining

Despite its numerous advantages, machining poses hazards for both operators and the environment due to the generation of aerosols in liquid or solid forms during most machining processes. The chip formation process and sources of metallic particle emission during

machining (shearing, deformations and frictions) is illustrated in Figure 1.12. Machining is a technique employed for shaping metallic and non-metallic materials. Particle emission refers to the release of various-sized solid particles into the air during machining. These particles range in size from a few nanometers (ultrafine particles, <100 nm) to several hundred micrometers (larger debris, >100 µm), depending on the process and materials involved. Larger, heavier particles (>50 µm) tend to settle quickly, whereas fine dust particles (PM10, <10 µm, and PM2.5, <2.5 µm) remain airborne, posing significant respiratory risks. Ultrafine particles (<1 µm) are especially concerning as they can penetrate deep into the respiratory system. This distinction is critical, as fine and ultrafine dust emissions are more hazardous for operators due to inhalation risks and their potential combustibility, particularly in aluminum machining environments (Djebara, Jomaa, et al. 2013). Therefore, understanding the conditions governing dust production during machining is imperative (Zaghbani, Songmene, and Khettabi 2009). Increasing cutting speed during turning and milling of nearly all brittle materials results in a higher intensity of particle formation. The quantity and particle size of machining dust are influenced by cutting parameters, tool material, workpiece material, and tool geometry. Additionally, lubrication directly affects the quantity and size of the produced particles. Figure 1.13 illustrates a diagram of all factors contributing to dust emission (Songmene and Olufayo 2020).

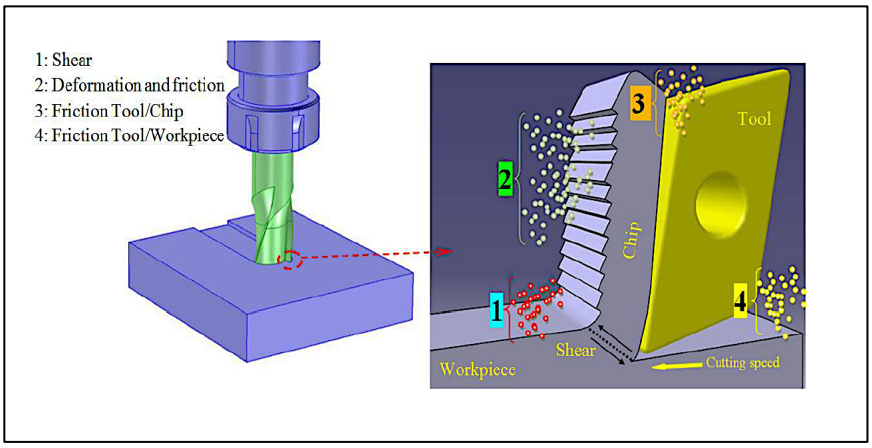


Figure 1.12 Schematic of the chip formation process

Taken from (Songmene et al. 2015)

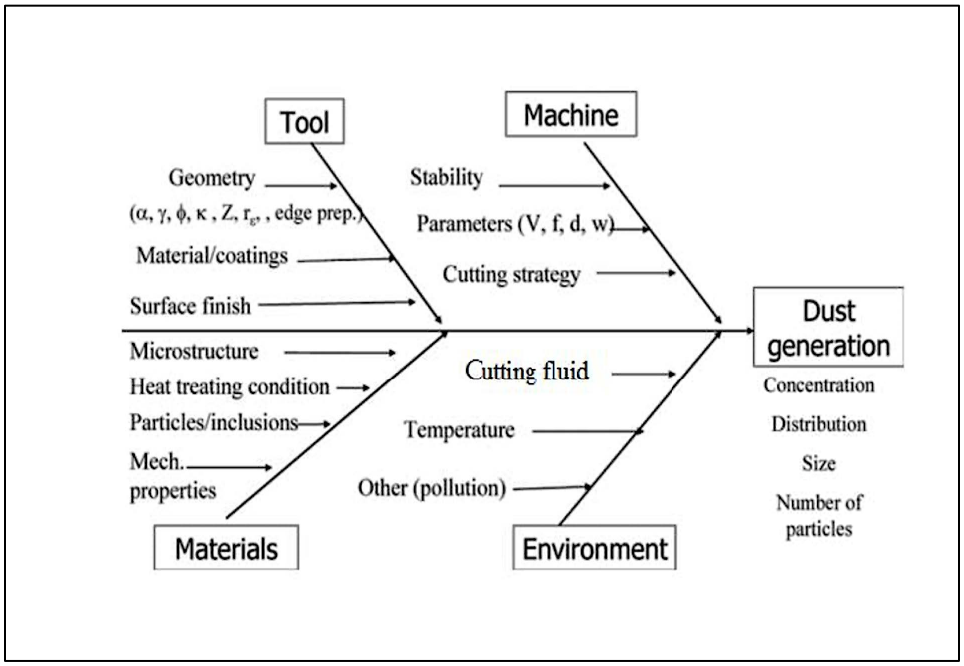


Figure 1.13 Cause and effects diagram of dust emission
Taken from Songmene and Olufayo (2020)

Dasch et al. (Dasch et al. 2005) demonstrated that the quantity of mist and dust generated during machining increases with the cutting speed, feed rate, and depth of cut. Increasing the cutting feed results in a rise in particle mass concentration, while it decreases with the cutting speed. The presence of cutting fluid contributes to generating particles with submicron size, supported by the observation that wet milling produces 3 to 5 times more particles compared to dry milling.

In dry milling, generated dust can be mitigated by increasing the cutting speed due to material softening in the chip formation zone, which does not facilitate particle separation from the chips. Wet milling generates more particles in the submicron size range than dry milling. Additionally, in wet milling, the cutting speed and feed per tooth do not significantly influence nanoparticle mass concentrations, whereas cutting speed has a notable impact on nanoparticle mass concentration in dry milling (Zaghbani, Songmene, and Khettabi 2009).

### 1.4.4 Cutting Fluid in Machining

Cutting fluids are important in machining, especially in metal cutting operations where heat generation is significant. Proper selection and application of these elements are vital for optimizing machining because they help control heat, reduce friction, and enhance overall machining performance, leading to increased productivity and improved quality part (Lee and Cho 2012).

The primary function of coolant is to dissipate heat generated during machining to prevent overheating of the cutting tool and workpiece. Various cooling modes are employed in machining, including flood, mist, and air cooling. Proper cooling mode prevents thermal damage to the tool and workpiece, reduces tool wear, and improves machining accuracy and surface finish (Wu, Kanz, et al. 2021).

Cutting fluids serve multiple purposes in machining. Using cutting fluids helps reduce friction and heat generation at the cutting interface, leading to improved tool life, better surface finish, and increased machining efficiency. Different types of cutting fluids are available, such as water-based, oil-based, and synthetic fluids (Zaghbani, Songmene, and Khettabi 2009).

## 1.5 Machining of Aluminum and Aluminum-Lithium Alloys

The recent rise in the utilization of aluminum alloys in manufacturing is attributed to their unique blend of lightweight properties and robust strength, yet they face challenges such as built-up edge (BUE) formation and rake surface layering, negatively impacting surface finish and tool longevity during machining (Pattnaik et al. 2018). However, careful selection of cutting parameters like speed, feed rate, and cutting tool material can mitigate these effects, emphasizing the critical role of surface integrity and tool longevity in workpiece performance (Santos et al. 2016). Heat treatments can enhance hardness and reduce BUE, especially in heat-sensitive aluminum alloys, while particle emission levels peak at critical cutting speeds influenced primarily by workpiece material rather than machining processes, suggesting a consistent critical speed across different operations (Tash et al. 2006; Khettabi et al. 2011).

Additionally, heat treatment significantly impacts mechanical properties and particle emission quantity, with the condition of the workpiece material affecting emitted particle levels at critical speeds (Songmene et al. 2011).

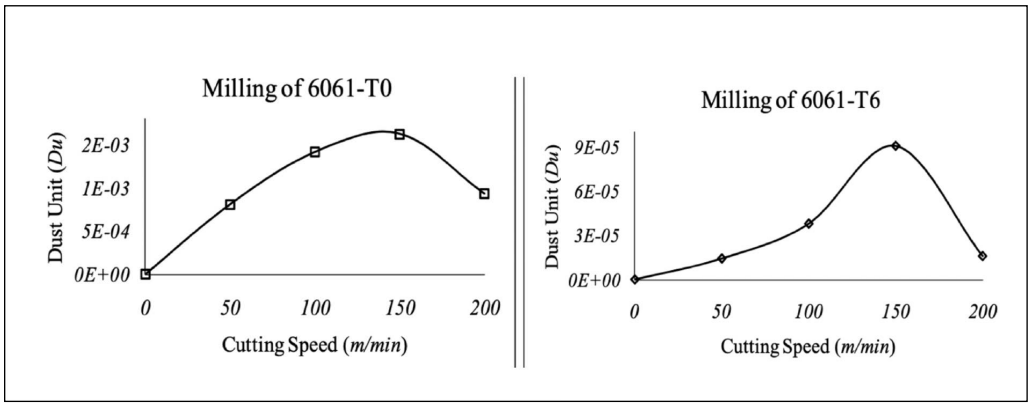


Figure 1.14 Experimental (Du) during milling of aluminum alloy 6061-T6 and T0
Taken from Songmene, Khettabi et al. (2011)

Tash et al. (Tash et al. 2006) investigated the drilling performance of heat-treated 356 and 319 alloys, revealing that higher magnesium (Mg) content increases cutting force due to the formation of a greater volume fraction of Mg-intermetallic or precipitates in high Mg-content 319 alloys compared to lower Mg content variants. Conversely, low copper (Cu) content in 356 alloy resulted in elevated cutting force compared to 319 alloys with similar hardness levels, attributed to enhanced homogeneity of the alloy matrix hardness in 319 alloys facilitated by Cu- and Mg-intermetallic, where hardening occurs through cooperative precipitation of $Al_2Cu$ and $Mg_2Si$ phase particles. Cooling and quenching rates minimally influenced cutting force and moment, while heat treatments elevating hardness levels concurrently reduced built-up-edge (BUE) occurrence.

Furthermore, hardness significantly impacted 319 alloy machinability, with both cutting force and moment rising with increasing hardness while BUE formation decreased (Tash et al. 2007). Gonçalves et al. found that increasing copper content within Al-Si-Mg-Cu aluminum alloy enhanced precipitation hardening by stabilizing hardening phases such as $Al_5Cu_2Mg_8Si_6$ and

$Al_2Cu$, resulting in higher overall hardness levels in 6351 aluminum alloy samples with higher copper content (Gonçalves and da Silva 2015).

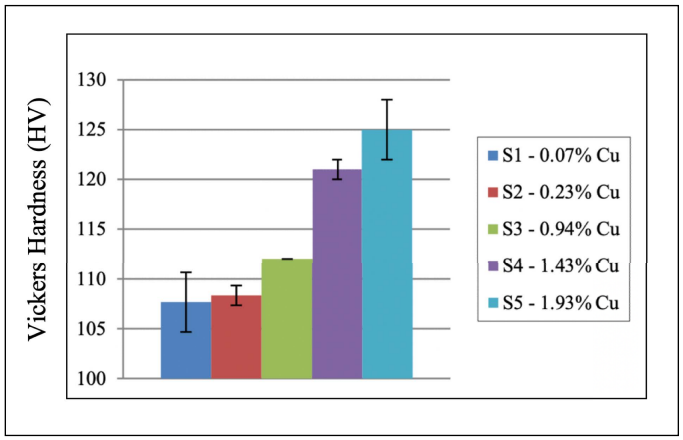


Figure 1.15 Vickers Hardness of 6351 aluminum alloy samples
Taken from Gonçalves and Bacci da Silva (2015)

In their study, Zedan et al. (Zedan and Alkahtani 2013) investigated the machining of heat-treated (T6) Al–10.8Si cast alloys and observed a detrimental effect on drill longevity with increased levels of copper (Cu) and/or magnesium (Mg) within the alloy due to the formation of significant quantities of coarse block-like $Al_2Cu$ phases. Contrary to expectations, higher strength and hardness levels of the aluminum alloy led to rougher surface finishes, as demonstrated in Figure 1.16. Particularly, the sample containing 1.43% copper, exhibiting intermediate hardness and mechanical strength, yielded the highest roughness values across all cutting speeds examined (Gonçalves and da Silva 2015).

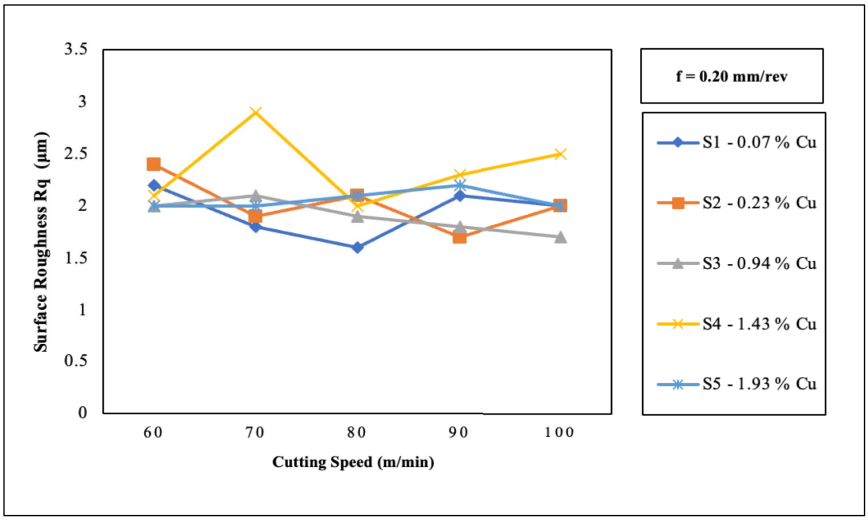


Figure 1.16 Surface Roughness Rq versus Cutting Speed

Taken from Gonçalves and Bacci da Silva (2015)

With the feed rate increase, the Rq roughness showed a significant increase (Figure 1.17) (Carvalho et al. 2021). In this scenario, the specimen containing 1.93% exhibited elevated hardness and mechanical strength but lower ductility, leading to the poorest surface finish across all tested feed rates.

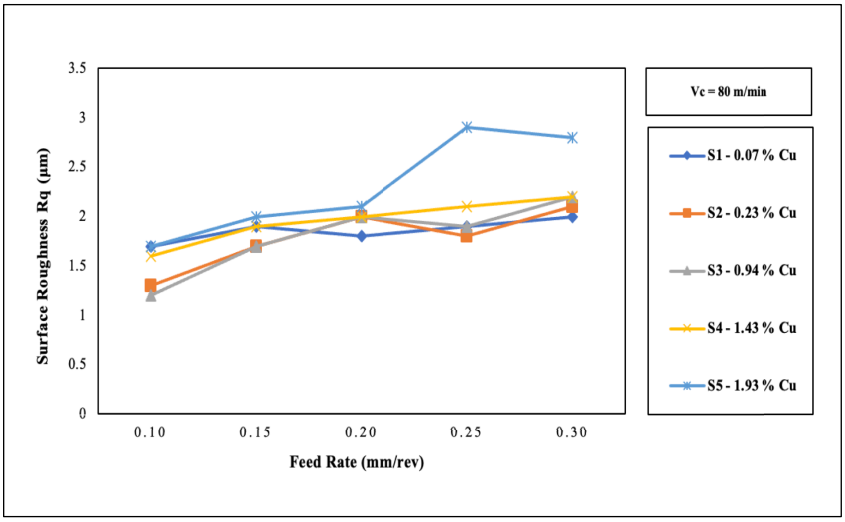


Figure 1.17 Surface roughness Rq versus Feed Rate

Taken from Gonçalves and Bacci da Silva (2015)

Achieving optimal machinability in Al-Li alloys also has proven challenging. Various studies address these issues by exploring different machining techniques, tool materials, and cutting parameters. Bagali et al. (Bagali, JS, and Nayak 2023) used the Taguchi method to determine that adjusting feed rates and cutting speeds significantly improves surface finish for Al-Li alloys, emphasizing the sensitivity of these alloys to precise machining adjustments. Wang et al. (Wang, Zhang, and Li 2022) found that ultrasonic-assisted end milling could reduce cutting forces, enhancing both surface integrity and tool longevity, which is particularly useful in high-speed aerospace machining. Tamura et al. (Tamura, Morii, and Matsumura 2024) highlighted the importance of optimized cutting speeds and feed rates to mitigate chip formation issues and reduce heat, both of which are crucial in maintaining the alloy's structural integrity during machining.

Studies like Marakini et al. (Marakini et al. 2024) have shown that using PVD-coated carbide tools improves the machining of Al-Li alloys by reducing tool wear and achieving a smoother surface finish. Research by Yue et al. (Yue et al. 2020) which employed particle swarm optimization for thin-wall workpieces, demonstrated that precise parameter optimization can reduce deformation and improve surface accuracy, directly benefiting aerospace components that require tight tolerances for Al-Li alloys machining.. Moradi (Moradi 2014) optimized pocket milling parameters for Al-Li alloy skins, finding that balanced speeds and feeds can reduce built-up edge formation, enhancing surface accuracy in thin-walled aerospace components. This study employs a multi-level experimental methodology to investigate the effects of high feed rates and cooling modes, expanding on findings by Yue et al. (Yue et al. 2020) who showed that optimized parameters reduced deformation in thin-wall structures, thereby improving the durability and precision of critical aerospace components.

The current research study builds on existing research in Al-Li alloy machinability, which has traditionally focused on moderate lithium content and advancements in cutting parameters and tool technologies. By investigating high-lithium, scandium-enhanced Al-Li alloys, this study aims to provide new insights into machinability and material performance. The addition of scandium, an effective but costly alloying element, sets this research apart from previous studies that primarily use copper and magnesium as secondary elements. Scandium, combined

with high lithium content, is expected to reduce tool wear and improve surface quality by refining the grain structure, achieving an optimal balance between strength and machinability.

This study fills a crucial gap in the literature by focusing on the effects of scandium and copper additions to Al-Li alloys. Through this unique alloy composition, it aims to reveal a high-performance material that not only reduces weight but also enhances machinability, potentially establishing new standards for aerospace-grade Al-Li alloys. These insights are critical for advancing the efficient manufacturing of lightweight, durable aerospace components.

## 1.6 Conclusions

This chapter has explored the development, classification, and specific properties of aluminum alloys, with a particular focus on aluminum-lithium (Al-Li) alloys.

Aluminum alloys are broadly categorized into cast and wrought alloys, distinguished by their phase solubility and thermal treatment methods such as solution heat treatment, quenching, and aging hardening. The development of Al-Li alloys has been significant, particularly for the aerospace industry due to their high strength-to-weight ratio and excellent fatigue resistance. Early generations of Al-Li alloys aimed at reducing density and improving mechanical properties, but they faced challenges such as mechanical property anisotropy, crack deviation, and low fracture toughness. Innovations in alloy composition and thermal-mechanical processing have led to enhanced properties and greater applicability in modern aerospace applications. These improvements have been driven by a deeper understanding of the precipitate structures, the influence of alloying elements, and advanced heat treatment processes, making Al-Li alloys a critical material in achieving performance and efficiency gains in aerospace technology.

The findings highlight that the addition of copper and scandium significantly enhances mechanical properties, particularly hardness, while optimized heat treatments could further improve machinability. Despite these advancements, critical gaps remain in the literature. Most studies on Al-Li alloys focus on moderate lithium content with traditional additives like copper

and magnesium, leaving scandium-enhanced alloys with higher lithium content largely underexplored. Additionally, limited research exists on particle emissions during machining of high-lithium Al-Li alloys, particularly regarding environmental impact and operator safety. To bridge these gaps, challenges can be mitigated by carefully selecting machining parameters and tool materials. Understanding these factors is crucial for improving machining performance and enhancing component quality.

# CHAPITRE 2

# METHODOLOGY AND EXPERIMENTAL PROCEDURE

## 2.1 Introduction

The aim of this chapter is to outline and elucidate the experimental procedures utilized in this research. In the first step of this study, the effects of heat treatment on the microstructure and strength (micro- hardness) of aluminum–lithium (Al-Li) base alloy containing copper (Cu) and scandium (Sc) were investigated, with a view to enhancing the alloy performance for aerospace applications. The heat treatment conditions were investigated to understand the precipitation behavior and the mechanisms involved in strengthening. Experiments in machining were carried out to examine the effects of chosen heat treatments, the introduction of Cu and Sc to the Al-Li base alloy, and machining parameters (cutting speed, feed rate and cooling mode) on machinability. These experiments encompassed the measurement of different machinability criteria, such as cutting forces, surface roughness, and particle emission.

## 2.2 Alloys and Casting Procedure

The Al-Li alloy was received as an Al-4 wt.% Li master alloy. Alloying elements were introduced in the form of pure Cu, Al-2 wt.% Sc master alloy, and commercially pure Al (99.5%) to achieve the compositions of the Al-Li, Al-Li-Cu, and Al-Li-Cu-Sc alloys, as presented in Table 2.1. The castings were performed at the Université du Québec à Chicoutimi (UQAC), within the Tamla Research Group (technologie avancée des métaux légers pour les applications automobiles) by Mohamed et al. (Salem Mohamed 2018).

Prior to casting, the melting temperature was maintained at 750 ± 5 °C, and the melts were degassed for approximately 15–20 minutes using a rotary graphite impeller rotating at ~130 rpm with pure dry argon. This step ensured the removal of oxides, inclusions, and hydrogen. The melt was then carefully skimmed to remove surface oxide layers. To ascertain the exact

chemical composition of each alloy, three samples for chemical analysis were collected at the beginning, middle, and end of the casting process. These samples were poured into preheated graphite molds at 600 °C to approximate equilibrium solidification conditions. During this process, a K-type thermocouple (chromel–alumel) was inserted into the center of the mold to record temperature–time data, which provided insights into the reactions occurring during solidification and facilitated microstructural examination Abdelaziz et al. (Abdelaziz et al. 2020).

The process for preparing ingot castings of the three alloys is illustrated in Figure 2.1.

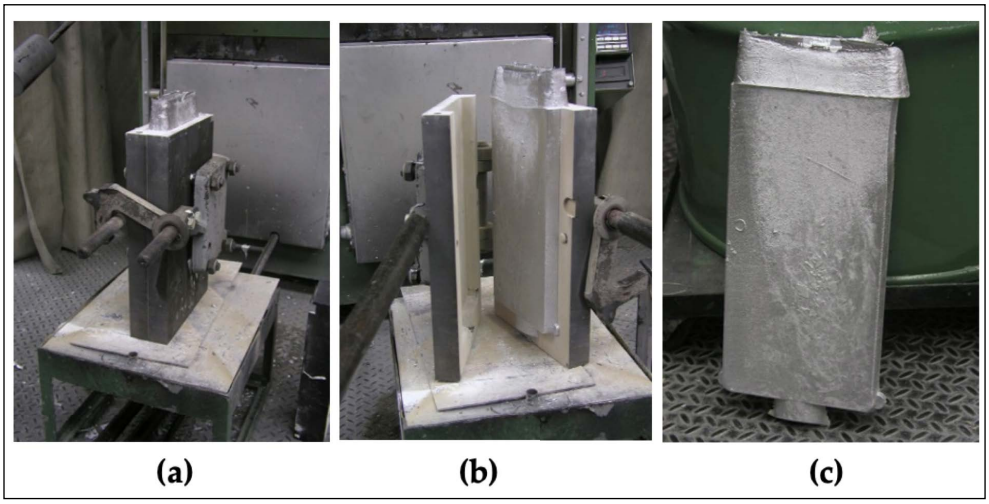


Figure 2.1 Casting of ingots of alloys used in the present study: (a) metallic mold with casting; (b) open mold showing casting inside; (c) actual casting

Table 2.1 Chemical compositions of the Al-Li alloys used in this study

| Element (wt.%) | Si | Mg | Cr | Mn | Fe | Cu | Zn | Ni | Ti | V | Li | Zr | Sc |
|---|---|---|---|---|---|---|---|---|---|---|---|---|---|
| Al-Li | 0.58 | <0.003 | <0.003 | 0.027 | 0.28 | 0.23 | 0.040 | 0.010 | 0.052 | 0.012 | 1.9 | 0.3 | <0.010 |
| Al-Li-Cu | 0.18 | <0.003 | <0.003 | 0.012 | 0.099 | 2.9 | 0.039 | 0.007 | 0.090 | 0.010 | 3.0 | 0.3 | <0.010 |
| Al-Li-Cu-Sc | 0.17 | <0.003 | <0.003 | 0.011 | 0.10 | 2.6 | 0.039 | 0.007 | 0.067 | 0.010 | 2.9 | 0.3 | 0.185 |

## 2.3 Sample Preparation and Heat-Treatment

Different heat treatment schedules were designed to study the effect of the corresponding treatments on the microstructural features and micro-hardness of the three alloys. Samples (10 mm × 15 mm × 20 mm) sectioned from the casting ingot for each alloy were divided into three sets: for Al-Li alloy, one set was kept in the as-cast condition, while the second set was solution heat-treated at 580 °C/1h, then quenched in warm water, and kept at −10 °C until testing. The third set was solution heat treated as before, quenched in warm water, followed by artificial aging at 130 °C and 150 °C for 1 h, 2.5 h, 5 h, 10 h, 15 h, 25 h, 35 h, and 45 h at each temperature. For the Al-Li-Cu and Al-Li-Cu-Sc alloys, one set was kept in the as-cast condition, the second set was solution heat-treated at 505 °C/5 h, then quenched in warm water, and kept at −10 °C until testing. The third set was solution heat treated as before, quenched in warm water, followed by artificial aging at 160 °C, 180 °C, and 200 °C for 5 h, 10 h, 15 h, 20 h, 25 h, and 30 h at each temperature. A summary of the heat treatment procedures is provided in Table 2.2.

Table 2.2 Heat treatments applied to the used Al-Li alloys

| Alloy | Solution Heat Treatment Temp (°C)/Time (h) | Aging Temp (°C) | Aging Time (h) |
|---|---|---|---|
| Al-Li | 580 °C/1 h | 130, 150 | 1, 2.5, 5, 10, 15, 25, 35, 45 |
| Al-Li-Cu | 505 °C/5 h | 180 | 5, 10, 15, 20, 25, 30 |
| Al-Li-Cu-Sc | 505 °C/5 h | 200 | 5, 10, 15, 20, 25, 30 |

In all, 58 samples were used. The solution and aging heat treatments were carried out in a Thermolyne Electric Furnace (Thermo Fisher Scientific, Waltham, MA, USA). Samples were mounted in bakelite using a Struers CitoPress-5 (Struers Limited, Mississigauga, ON, Canada) (force of 300 bars; heating time of 3 min, cooling time of 2 min). After being ground with standard SiC abrasive papers, the samples were mechanically polished in a sequence of 3 μm, 1 μm, and 0.5 μm diamond and subsequently electropolished in a Colloidal Silica-0.06 micron-

blue solution using a Buehler VibroMetTM 2 Vibratory Polisher (Buehler, Lake Bluff, IL, USA) for a duration of 24 h (see Figure 2.2 and 2.3).

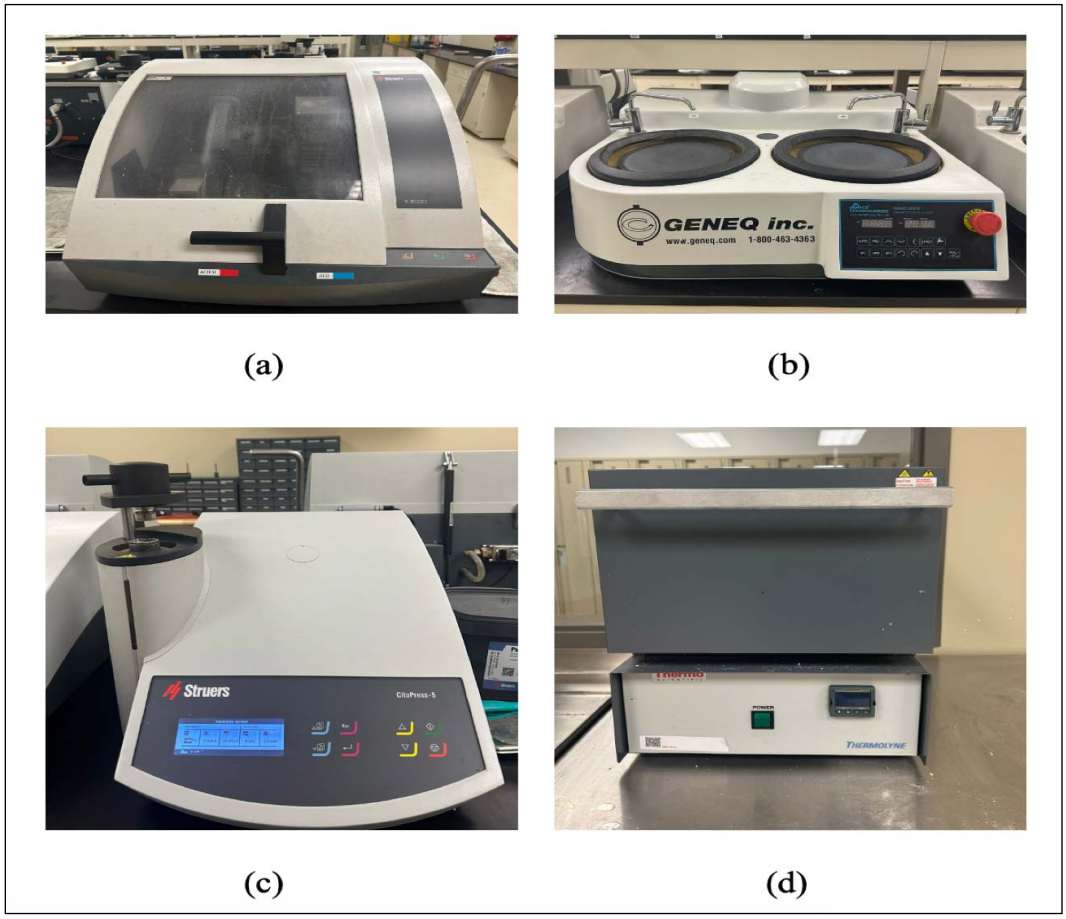


Figure 2.2 (a) Struers Labotom-5 manual cutter, (b) Thermo Fisher Scientific F48015-60 furnace, (c) Struers CitoPress-5 automatic mounting press, and (d) Pace Technologies Nano 2000T grinder – polisher

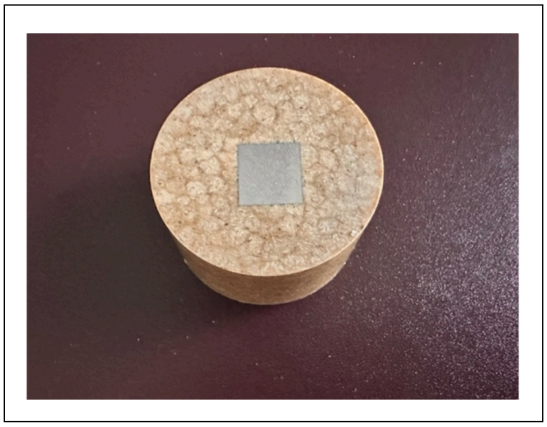

Figure 2.3 Prepared sample

## 2.4 Material Characterization

This study employs a multi-level full factorial design of experiment methodology to explore the impact of different factors on the machining of three alloys: Al-Li, Al-Li-Cu, and Al-Li-Cu-Sc. In the context of designing experiments for machining of aluminum alloys, a full factorial design may be preferred over fractional or composite designs. When working with a particular aluminum alloy that might not have been extensively studied, the full factorial approach provides a robust analysis across all conditions. This makes it especially useful when exploring a material with unknown sensitivities to the machining parameters. Furthermore, it provides high accuracy and allows for the investigation of all possible interactions between factors involved in the machining process. Since machining is a complex process where factors often influence each other, capturing these interactions is crucial for a comprehensive understanding.

The alloys underwent a specified heat treatment as per the experimental design. The machining experiments were carried out in both dry and wet milling conditions.

Tables 2.3, 2.4, 2.5 outline the experimental factors for machining and their associated levels. Qualitative factors encompassed workpiece materials and cooling mode, while the other factors were treated as quantitative variables.

Table 2.3 Design 1: Experimental variables and their levels for Al-Li alloy (54 tests)

| | Minimum Level | Intermediate Level | Maximum Level |
|---|---|---|---|
| A: Cutting Speed (m/min) | 200 | 400 | 600 |
| B: Feed Rate (mm/th) | 0.05 | 0.10 | 0.15 |
| C: Hardness (HV) | 56 | 76.5 | 97 |
| D: Cooling Mode | Dry | | Wet |
| E: Depth of Cut (mm) | 2 | | |

Table 2.4 Design 2: Experimental variables and their levels for Al-Li-Cu alloy (54 tests)

| | Minimum Level | Intermediate Level | Maximum Level |
|---|---|---|---|
| A: Cutting Speed (m/min) | 200 | 400 | 600 |
| B: Feed Rate (mm/th) | 0.05 | 0.10 | 0.15 |
| C: Hardness (HV) | 129 | 146.7 | 164 |
| D: Cooling Mode | Dry | | Wet |
| E: Depth of Cut (mm) | 2 | | |

Table 2.5 Design 3: Experimental variables and their levels for Al-Li-Cu-Sc alloy (54 tests)

| | Minimum Level | Intermediate Level | Maximum Level |
|---|---|---|---|
| A: Cutting Speed (m/min) | 200 | 400 | 600 |
| B: Feed Rate (mm/th) | 0.05 | 0.10 | 0.15 |
| C: Hardness (HV) | 144.6 | 163.4 | 182.7 |
| D: Cooling Mode | Dry | | Wet |
| E: Depth of Cut (mm) | 2 | | |

The milling operation was performed on a block with dimensions of 103 mm in length, 41 mm in width, and 33 mm in depth. The investigation encompassed 18 distinct conditions, derived through a Cartesian combination of three key variables: material type, heat treatment variations, and dry or wet machining environments, yielding 18 unique combinations (3×3×2 = 18). Each condition was subjected to nine different tool paths, determined by adjusting cutting speed and feed rate parameters, resulting in 9 unique tool paths per condition, as illustrated in Figure 2.4. Each test width was 10 mm corresponding to the full tool immersion ( 10 mm diameter). Thus, a total of 162 experiments were carried out. Tables 2.6 outline the parameters for the nine tool paths, repeated for each of the 18 conditions. Cutting speed and

feed rate settings were determined based on the recommendations provided by the tool manufacturer, detailed in Table 2.7.

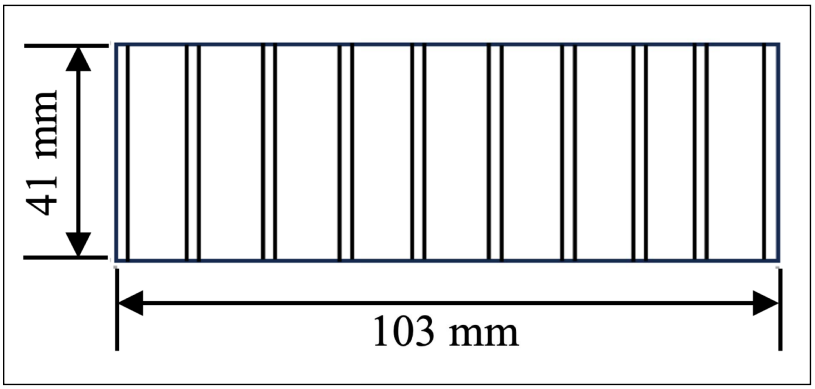


Figure 2.4 The tests layout during the experiments

Table 2.6 Cutting Parameters of Each Condition

| Test (Tool Path) | Feed Rate (mm/tooth) | Cutting speed (m/min) |
|---|---|---|
| 1 | 0.05 | 200 |
| 2 | 0.1 | 200 |
| 3 | 0.15 | 200 |
| 4 | 0.05 | 400 |
| 5 | 0.1 | 400 |
| 6 | 0.15 | 400 |
| 7 | 0.05 | 600 |
| 8 | 0.1 | 600 |
| 9 | 0.15 | 600 |

Table 2.7 Cutting speed and feed rate recommended by the tool manufacturer

Adapted from (Solutions 2024)

| Material | Cutting speed (m/min) | Tool immersion | Tool diameter | | | | |
|---|---|---|---|---|---|---|---|
| | | | 4 mm | 6 mm | 8 mm | 10 mm | 12 mm |
| Aluminium alloys 6061-T6/T651 | | | Feed rate (mm /tooth) | | | | |
| | 426.72 | 100% Full slotting | 0.0254 | 0.0508 | 0.0508 | 0.0762 | 0.01016 |
| 7075-T6<br><br>2024 T4/T6<br>2014 | 518.16 – 609.6 | 25-40% immersion | 0.0635 | 0.1016 | 0.127 | 0.1524 | 0.2032 |

### 2.4.1 Characterization

#### 1.1.1 Hardness Measurement

The microhardness of samples was assessed using a Future-Tech FM-1 micro-hardness tester (Figure 2.5). The machine allows for the adjustment of load based on the sample material, ranging from 10 grams to 1 kilogram. A uniform load of 100 grams (0.9807 N) was applied to all samples during measurement. Measurements were taken at seven distinct points for each sample, and the microhardness value was established by computing the average of these measurements.

Following the machine operation, an indentation was left on the sample surface. The hardness of the sample at a specific point was determined by inserting the average value of the diagonals of this quadrilateral into Equation 2.1:

$$HV = 0.1891 \frac{F}{d^2} \quad (2.1)$$

Here, HV represents microhardness, F is the force in Newtons, and d is the average value of the diagonals in millimeters.

Figure 2.5 Future-Tech FM-1 microhardness tester

### 2.4.2 SEM Characterization

The microstructure of the samples was examined through SEM imaging. Scanning electron microscopic (SEM) analysis was carried out employing a Hitachi SU-8230 FE-SEM (Hitachi High-Tech Corporation, Ibaraki, Japan) equipped with a Bruker Quantax Flat Quad EDS detector (Bruker AXS LLC, Madison, WI, USA) (see Figure 2.6).


Figure 2.6 Hitachi SU-8230 FE-SEM

### 2.4.3 X-Ray

X-ray diffraction (XRD) analysis was used to investigate phase evolution in the heat-treated and reference samples. The XRD experiments were carried out using a PANalytical X-ray diffraction machine model X'Pert Pro (Malvern Panalytical Ltd., Malvern, United Kingdom) (Figure 2.7), using CuKα anode material, K-alpha 1 (Å): 1.54060, with step size (◦2θ): n0.0170 and scan step time (s): 99.7000. The data obtained were analyzed by means of the associated X'Pert High Score software.


Figure 2.7 PANalytical X-ray diffraction machine

### 2.4.4 DSC Investigation

Differential scanning calorimetry (DSC) analyses were performed using a DSC2500 Discovery series machine (TA Instruments, New Castle, DE, USA) (see Figure 2.8), with a scanning rate of 10 °C/min under argon atmosphere. Samples of approximately 9 mg were mechanically cut into squares of 1.9 mm × 1.9 mm × 1.2 mm size from the as-cast ingots and then solution treated. Alloy conditions for DSC analyses were as follows: Al-Li (solution treated at 580 °C for 1 h); Al-Li-Cu and Al-Li-Cu-Sc alloys (solution treated at 505 °C for 5 h). The samples were put into the alumina pan of the DSC machine; DSC runs were initiated at 40 °C and completed at 400 °C to examine the kinetics of phase transitions.

Figure 2.8 DSC2500 Discovery series machine

## 2.5 Machining Procedure

All 162 experiments were carried out under dry and wet milling conditions, employing a 3-axis CNC machine-tool with specific attributes, including a power output of 50 kW, a rotational speed of 28000 rpm, and a torque of 50 Nm (Figure 2.9).

Milling operations were executed utilizing uncoated carbide end mills featuring a three-flute design (z = 3) and a diameter of 10 mm. Figure 2.10 of the cutting tool used in the experiment. To maintain consistency in test conditions, the tools were changed after every nine tool paths, resulting in the use of a total of eighteen unique tools during the experiments.


Figure 2.9 HURON K2X10 CNC milling machine

| | |
|---|---|
| Cutter Diameter: | 0.3750" (3/8) |
| Length of Cut: | 0.5000" (1/2) |
| Shank Diameter: | 0.3750" (3/8) |
| Overall Length: | 2.0000" (2) |
| Flutes: | 3 |

Figure 2.10 Cutting tool (3 Flute, Square - 40° Helix, Variable Pitch)
Adapted from (Solutions 2024)

### 2.5.1 Cutting Force Measurement

Accurate measurement and analysis of cutting forces are essential for optimizing machining processes, predicting tool wear, and enhancing overall machining efficiency.

In this study, three cutting force components (Fx, Fy, and Fz) were measured using a three-axis dynamometer (Kistler, model 9255-B), which was mounted in the milling machine and

connected to a data acquisition and analysis. A sampling frequency of 12 kHz was used to achieve the cutting force signals.

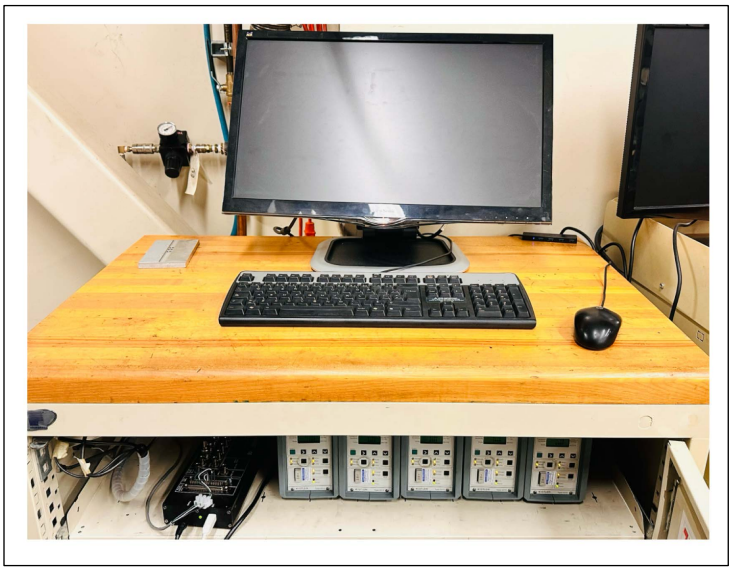

Figure 2.11 Cutting force measurement: Acquisition and analysis unit

### 2.5.2 Surface Roughness

Surface roughness measurements are essential for quality control, ensuring that machined components meet specified standards and functional requirements. The choice of measurement method depends on factors such as material properties, surface finish requirements, and the level of precision needed. In this investigation, the Mitutoyo SJ-410 surface roughness tester, as depicted in Figure 2.12, was utilized to assess the surface roughness of the machined surfaces. It operates based on a stylus profilometer principle to measure the surface roughness of machined surfaces. The instrument is equipped with a stylus or probe, which is a very fine-tipped, diamond stylus.

The stylus is brought into contact with the surface of the material being measured, traverses the surface, following the contours and irregularities of the material. As the stylus moves along the surface, it experiences vertical displacement due to the variations in the surface topography

and measures the vertical movements of the stylus as it traces the surface. Then processed by the instrument's internal software. The software calculates various roughness parameters such as Ra, Rz, and Rq. Each toolpath was assessed in two segments, and the average of the two measurements was considered as the ultimate roughness value for that sample.

Figure 2.12 Mitutoyo SJ-410 surface roughness tester used for surface roughness measurement

### 2.5.3 Particle Emission

The emission of metallic particles during machining was monitored using an Aerosol Particle Sizer (APS). Additionally, a laser photometer was utilized to gauge particle concentration. The APS was employed to measure particle size distribution within the aerodynamic size range of 0.5 to 20 µm. Subsequently, particles are sorted based on their ability to traverse an electric field and are quantified using a Condensation Particle Counter (CPC) (Khettabi, Songmene, and Masounave 2010). Figure 2.13 illustrates the Aerosol Particle Sizer (APS) and the Condensation Particle Counter (CPC).

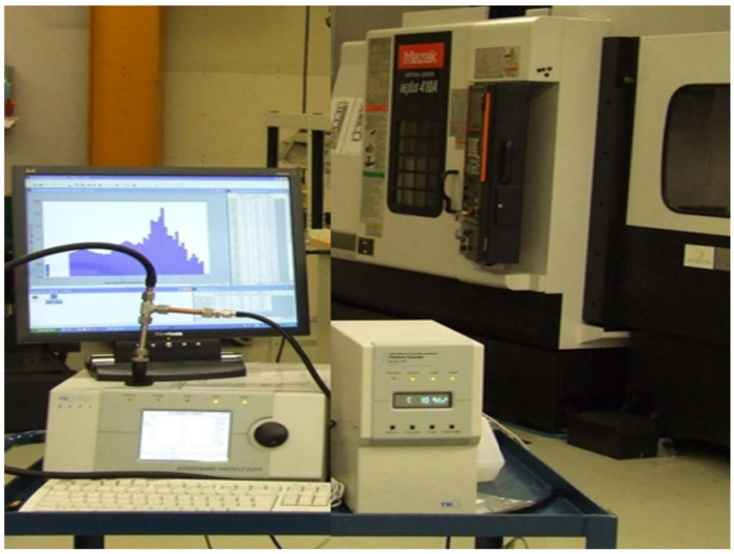

Figure 2.13 Aerosol Particle Sizer (APS)

## 2.6 Validation of Results

To ensure the reliability and consistency of findings in both the heat treatment and machining phases, several validation methods were employed. The optimized heat treatment parameters for each alloy were validated through repeatability testing.

The machining outcomes were compared with findings from existing studies on Al-Li alloy machinability. To assess the significance of variations in machining parameters, statistical Analysis of Variance (ANOVA) were applied.

# CHAPITRE 3

# RESULTS AND DISCUSSION OF HEAT TREATMENT

At the outset of this chapter, it is important to highlight the dissemination of findings from the heat treatment segment of our study. This segment has yielded significant contributions to the scientific community through both published and presented work.

In 2023, a peer-reviewed journal article titled "Investigating the Effect of Heat Treatment on the Microstructure and Hardness of Aluminum-Lithium Alloys" was published, showcasing the influence of heat treatment processes on the structural and mechanical properties of these advanced materials.

Additionally, a poster presentation was delivered at the 2022 aluminium Research Centre (REGAL) student Day conference, titled "Investigating the Effect of Heat Treatment on the Microstructure and Strength of Aluminum-Lithium Alloys for Aerospace Applications." This presentation focused on the application-driven aspect of the study, particularly how tailored heat treatment protocols could enhance the strength and performance of aluminum-lithium alloys in high-demand aerospace environments.

## 3.1 Introduction

Aluminum is the most common material used in the aerospace industry because of its ease of availability, recyclability, and low density. Adding lithium (Li) to aluminum (Al) as a lighter element creates great possibilities to enhance the overall performance of aircrafts (Rioja and Liu 2012; Dursun and Soutis 2014; Pérez-Landazábal et al. 2000). Furthermore, addition of elements and optimizing the precipitates are the main reasons for the excellent mechanical properties of Al-Li alloys. The properties and performance of Al-Li alloys are influenced by a range of microstructural characteristics, including the size and shape of the grains, the formation of different phases at different places (Li, Liu, et al. 2015).

To enhance the strength of Al-Li alloys for structural purposes, several approaches are resorted to, including precipitation strengthening, solution strengthening, grain and sub-grain strengthening, and strengthening by dislocations (Starink et al. 1999b).

The aim of this chapter is to explore how the addition of scandium (Sc) and lithium (Li), along with various heat treatment conditions, impacts the microhardness of the Al-Li base alloy. Additionally, it seeks to identify the highest and lowest hardness attained across all heat treatment conditions applied to the studied alloys. To accomplish this goal, three aluminum alloys Al-Li, Al-Li-Cu, and Al-Li-Cu-Sc were subjected to heat treatment and characterization. Aging was carried out at temperatures of 130 °C and 150 °C for aging times of 1 h, 2.5 h, 5 h, 10 h, 15 h, 25 h, 35 h and 45 h at each temperature for Al-Li alloy and at 160 °C, 180 °C, and 200 °C for aging times of 5 h, 10 h, 15 h, 20 h, 25 h and 30 h at each temperature for Al-Li-Cu and Al-Li-Cu-Sc alloys. This analysis offers valuable insights into the microstructural changes and elemental composition of the alloys under different conditions.

Based on the literature review, it becomes evident that heat treatment has the potential to significantly enhance the mechanical properties of Al-Li based alloys. To date, despite the considerable research efforts dedicated to the heat treatment of Al-Li alloys, since the Al-Li-Cu and Al-Li-Cu-Sc alloys used in our study (synthesized from Al-4 wt% Li master alloy) contain a high percentage of Li in addition to Sc and Cu, there is a definite need to find the appropriate heat treatments and investigate the precipitation strengthening behavior of these Al-Li based alloys. The present investigation aims to perform a series of heat treatment processes on these Al-Li based alloys and study the influence of heat treatment process parameters on the Vicker's hardness and its microstructure.

In the subsequent analysis, the machinability of the identified conditions (the highest, medium, and lowest hardness) will be investigated.

## 3.2 Effect of the Heat Treatments on Microhardness

Figure 3.1 shows the development of hardness as a function of the natural aging time. The Al-Li alloy exhibits an increase in hardness with increase in aging time. Solution treatment for 1 h at 580 °C followed by artificial aging at 150 °C causes a change in hardness from 44.7 HV to its peak value of 97.2 HV after 45 h in Al-Li alloys. The primary cause of the increase in hardness observed in the Al-Li alloy was the formation of the δ' phase. The Al-Li-Cu and Al-Li-Cu-Sc alloys also show an increase in hardness with increase in aging time. For all heat treatment conditions, addition of Cu and Sc resulted in the highest peak-hardness. The strengthening effect of solution and aging treatments is the main reason for the change in hardness. Artificial aging at 180 °C for 20 h in Al-Li-Cu and Al-Li-Cu-Sc alloys led to peak-hardness values of 163.6 HV and 182.6 HV, respectively. Results of hardness values obtained for all three alloys are presented in Appendices A-C, respectively, at the end of the article.

Based on the binary Al-Li alloy diagram, the precipitation heat treatment process to enhance the strength and hardness of the material involves heating the Al-Li alloy to a temperature range of 130-200 °C, which facilitates the formation of precipitates. However, aging above 160 °C coarsens the precipitates; this has a negative effect on strength of the alloy. The δ' phase that forms during the heat treatment process is the strengthening phase in Al-Li alloys and it plays a significant role in enhancing the alloy strength and stiffness.

The actual degree of strengthening contributed by δ' is a function of the volume fraction and the size distribution of the particles. When Al-Li alloys are heat-treated, the alloying elements (such as Li) diffuse through the aluminum matrix and combine to form the delta prime precipitates. While these precipitates are very small (typically less than 100 nm in size), they have a significant strengthening effect on the alloy. The precipitates act as obstacles to dislocation motion, making it more difficult for dislocations to move through the crystal lattice (Mahalingam et al. 1987).

Both Al-Li-Cu and Al-Li-Cu-Sc alloys show a similar behavior and higher hardness because of the presence of Cu and hence the presence of copper aluminide phases such as T1, θ'. In addition, the precipitation of a large number of phases such as T1, θ', and δ', directly contributes

to the rapid rise in hardness. Utilizing elevated temperatures can speed up the diffusion path of solute atoms. However, this acceleration might induce untimely growth of the strengthening phases, ultimately resulting in a decline in the nucleation density of precipitates. Consequently, such an outcome would have a detrimental impact on the hardness, or strength of the alloy.

In the course of solution treatment, the secondary phases in the alloy dissolve into the matrix, leading to the creation of a supersaturated solid solution. During the aging process, the nature of precipitates within the alloy undergoes transformations and changes which influence the alloy's characteristics. These variations in the precipitates ultimately contribute to the alterations observed in the hardness of the alloy (Deschamps et al. 2013; Chen et al. 2020).

In addition to the named precipitates, the Al-Li-Cu-Sc alloy containing Sc exhibited the highest hardness values. This was ascribed to the presence of AlSc precipitates, which, having a very small size (10-100 nm), creates a high density of obstacles for dislocations to move through. Furthermore, the addition of Sc to aluminum alloys promotes the formation of a high density of fine, uniformly distributed precipitates within the grains which further contribute to the strengthening (Kolobnev 2002; Suresh et al. 2018).

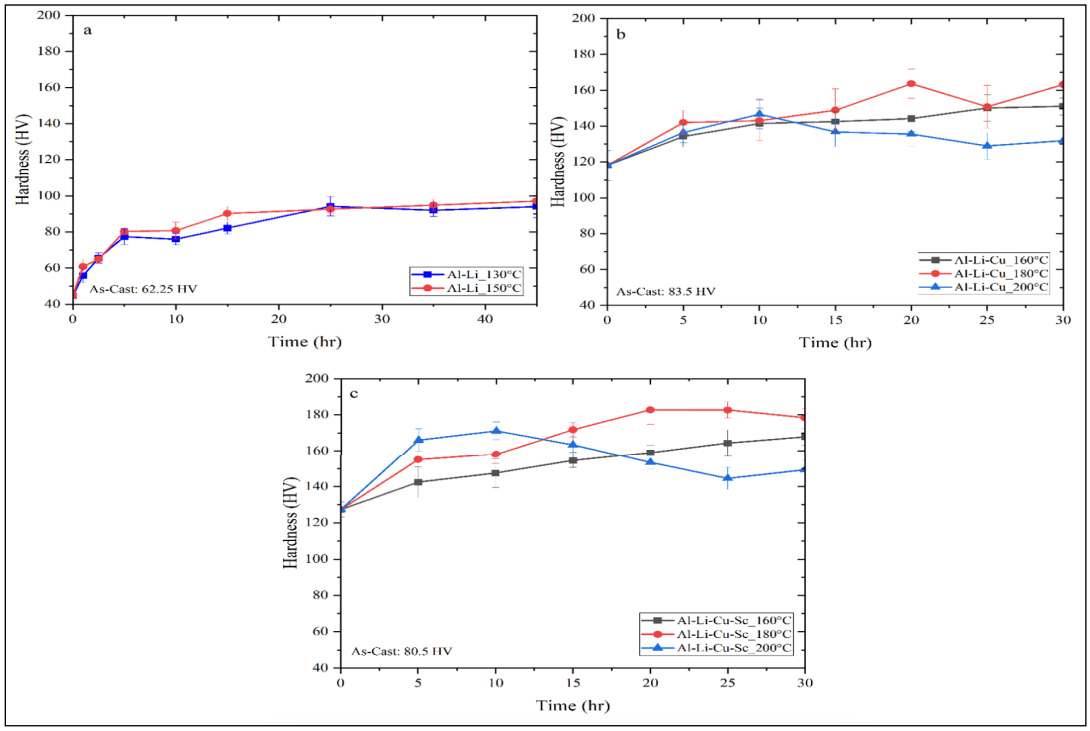


Figure 3.1 Variation in Vickers hardness values with aging time in samples of (a) Al-Li, (b) Al-Li-Cu, and (c) Al-Li-Cu-Sc alloys subjected to different heat treatment temperatures

## 3.3 SEM Characterization

SEM images of aluminum lithium alloys can provide a detailed view of the micro-structure of the material, including the distribution and morphology of precipitates. The precipitates present in Al-Li alloys are typically small and can range in shape from spherical to elongated or needle-like.

Figures 3.2, 3.3 and 3.4 display various SEM micrographs of the three alloys studied. Figure 3.2(a) depict Al-Li alloy after aging in lower magnification which shows δ (AlLi) precipitates that mainly precipitates in grain boundaries and α-Al in matrix with homogenous microstructure. In figure 3.2(b), $Al_3Zr$ precipitates could be seen that they are mostly dispersed in grain boundaries and form as discontinuous networks or clusters. They act as effective barriers to dislocation movement, impeding plastic deformation and enhancing the alloy's strength. Overall, the $Al_3Zr$ precipitates in grain boundaries of aluminum lithium alloys

contribute to strengthening the material and promoting a fine-grained microstructure. These effects result in improved mechanical properties and increased performance in various applications (Liu et al. 2021). The bull's-eye structure that shows spherical structure could be seen in Figure 3.2(c). The presence of spherical β′ facilitates the initiation of nucleation sites for δ′ leading to the formation of a distinctive pattern known as the bull's-eye structure (Prasad, Prasad, and Gokhale 2014).

Comparing Figures 3.2(a), 3.3(a), and 3.4(a) shows that adding Cu to the Al-Li alloy changes the size of the grain in the microstructure. Copper atoms tend to segregate to grain boundaries in aluminum alloys and act as a grain refiner in aluminum lithium alloys, but in figure 3.3(a) the grains grow unexpectedly. The presence of copper at the grain boundaries may hinder grain boundary mobility and promote grain growth. This can lead to larger grain sizes compared to the pure aluminum lithium alloy. The grain size is reduced by adding Sc to the alloy (see Figure 3.4(a)). In addition to that, the presence of Cu and Sc to the Al-Li alloy causes the precipitates to distribute within the matrix rather than being precipitated at the grain boundaries. During the aging treatment, the alloy forms several precipitates, namely T1 ($Al_2CuLi$), θ′ ($Al_2Cu$), β′($Al_3Zr$) and δ′ ($Al_3Li$) phases. Among these, the T1 phase is the one that impedes dislocation movement effectively, attributed to its non-shearing properties.

The higher magnification images presented in Figures 3.3(b) and 3.4(b) show that the shapes of the precipitates are changed after adding Cu and Sc to the Al-Li alloy. Tiny spherical precipitates are visible in the microstructure of the Al-Li-Cu-Sc alloy as may be seen in Figure 3.4(b). It seems that the larger plate-like phases precipitate at the grain boundaries, whereas the smaller ones appear within the grains. Incorporating Sc into the alloy increases the density of precipitates and encourages a more uniform dispersion of these particles. Additionally, it is widely acknowledged that Sc significantly improves the mechanical properties of aluminum alloys by facilitating the formation of the $Al_3Sc$ phase through precipitation (Figure 3.4(c)). The dispersion of particles of $Al_3Sc$ enhances the strength, substantially reinforces the substructure, and hinders the process of recrystallization (Suresh et al. 2018).

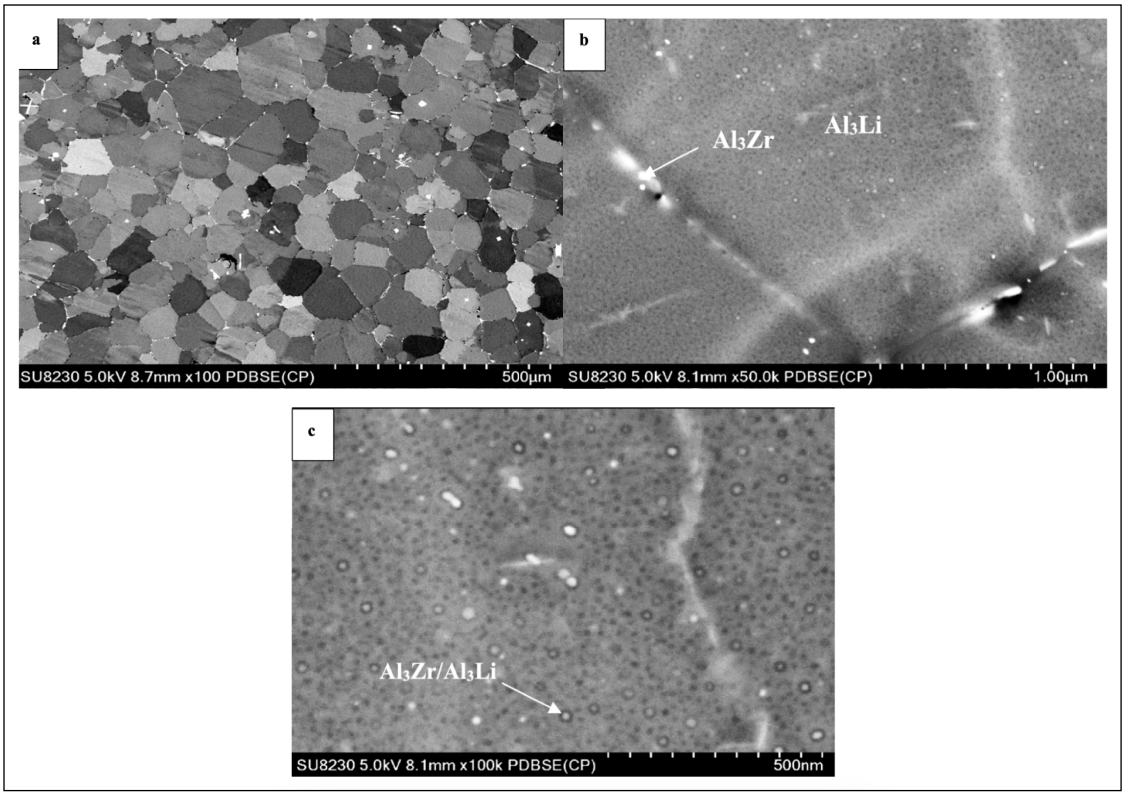


Figure 3.2 SEM micrographs of after aging treatment of Al-Li alloy with different magnifications

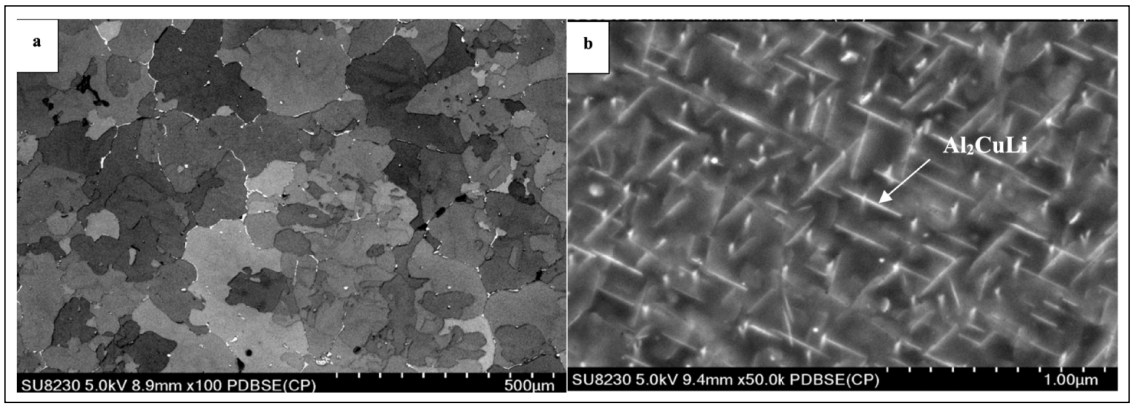


Figure 3.3 SEM micrographs of after aging treatment of Al-Li-Cu alloy with different magnifications

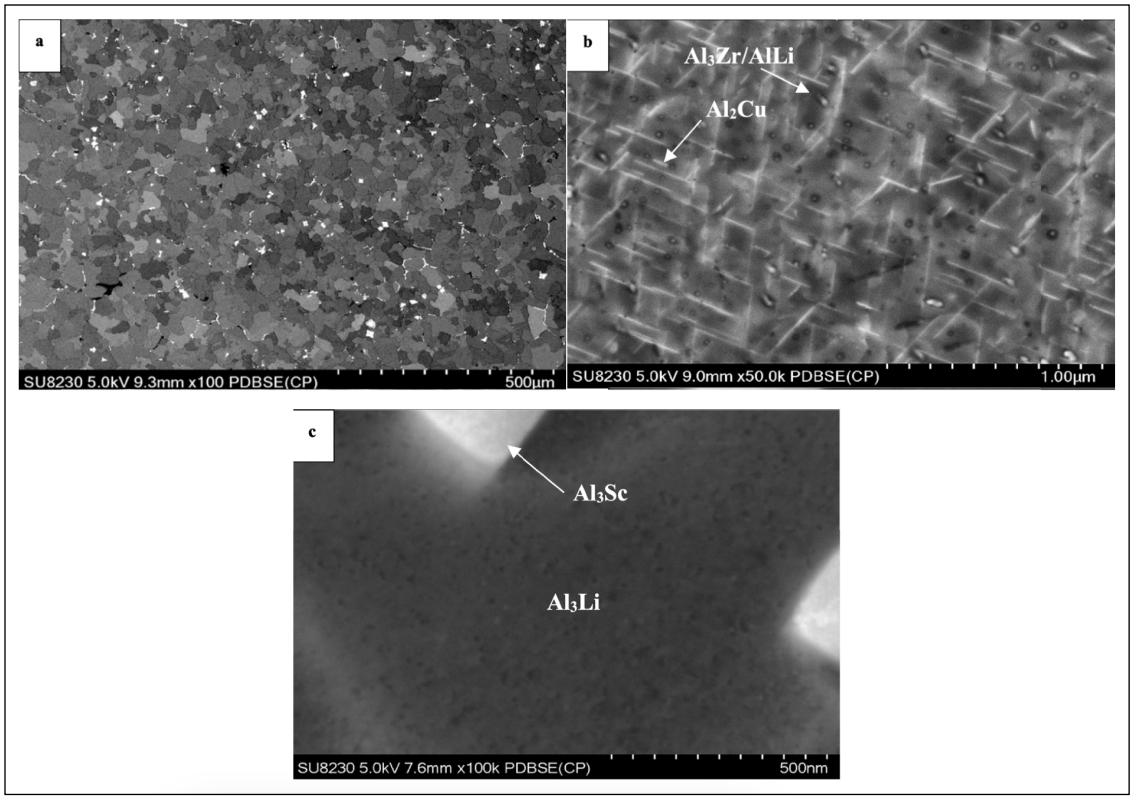


Figure 3.4 SEM micrographs of after aging treatment of Al-Li-Cu-Sc alloy with different magnifications

Scandium (Sc) exhibits low solubility in aluminum and serves as a potent structure modifier in Al-Li alloys. It also displays an anti-recrystallization effect (Žist et al. 2022).

According to the studies conducted by Norman et al. (Norman, Prangnell, and McEwen 1998) and Hyde et al. (Hyde, Norman, and Prangnell 2001), it has been suggested that primary $Al_3$(Sc,Zr) particles possess a quasi-cubic morphology, while their two-dimensional shape appears to be rectangular. The SEM micrograph in Figure 3.5(a) reveals a triangular-shaped $Al_3$(Sc, Zr) particle. The distribution of alloying elements is heterogeneous. The particle exhibits a layered structure, where each layer has a distinct composition. Some layers are enriched in Sc or Zr but depleted in Al, while other layers are enriched in Al but depleted in Sc and Zr. A diagrammatic representation of the layered structure of the rectangular particle is provided in Figure 3.5(b).

The formation of the layered structure in these particles follows a specific sequence of reactions. Initially, central oxides act as nucleation sites for the $Al_3Zr$ phase, making it the first phase to form. Subsequently, the first layer of aluminum (Al) is formed through the reaction $Al_3Zr$ + liquid → Al. Following this, $Al_3Sc$ is formed on the Al layer via the reaction liquid → α-Al + $Al_3Sc$. The close orientation relationship and small lattice mismatch between Al and $Al_3Sc$ facilitate the easy nucleation of $Al_3Sc$ on Al. As a result, alternating eutectic reactions occur between $Al_3Sc$ on Al and Al on $Al_3Sc$, leading to the formation of a multi-layered $Al_3$(Sc,Zr) phase particle. Consequently, the multi-layer structure consisting of $Al_3Zr$ + α-Al + $Al_3Sc$ + α-Al + $Al_3Sc$ + ... is developed (Hyde, Norman, and Prangnell 2001; Li, Wiessner, et al. 2015; Murray, Peruzzi, and Abriata 1992; Murray 1998).

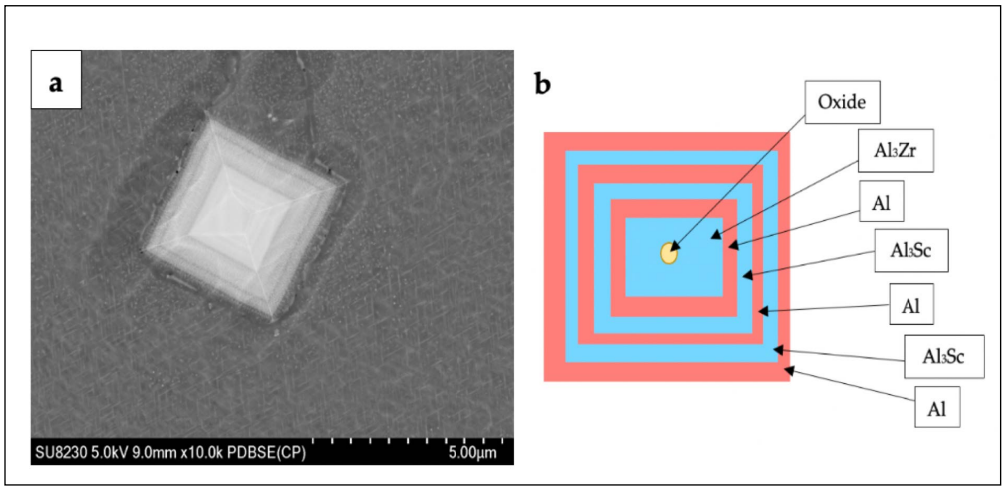


Figure 3.5 (a) SEM image of the morphology of an $Al_3$(Sc,Zr) particle; (b) Diagrammatic sketch of the structure of the layered particle

## 3.4 X-Ray Diffraction (XRD) Analysis

Since the atomic number of lithium is low, EDS cannot be used to detect the distribution of Li and its constituent phases. Therefore, to evaluate the influence of heat treatment on the phase types in the alloys investigated, the X-Ray diffraction (XRD) technique was used. Figure 3.6 presents a synopsis of the diffraction peaks observed for the as-cast, solution heat-treated and aged samples of Al-Li, Al-Li-Cu and Al-Li-Cu-Sc alloys as an example.

In the Al-Li alloys, based on the XRD phase analysis and detection results, it was observed (Figure 3.6(a)) that the predominant Li-containing alloy phases present in the Al-Li alloy were α-Al, AlLi and $Al_3Li$ phases. Furthermore, it was found that these phases remained unchanged even after subjecting the alloy to heat treatment. In the as-cast alloy, α-Al and AlLi phases were the main peaks. Most intermetallic phases that dissolved into the Al matrix cause the decline of the diffraction peaks of the secondary phases after solution heat treatment. The δ(AlLi) phase disappeared after aging (SHT + 150 °C /45 h) and the δ′($Al_3Li$) phase was precipitated and appear.

As may be seen from Figure 3.6(b), while different secondary phases were observed in the as-cast alloy, α-Al and $Al_3Li$ phases were the main peaks noted. In the context of previous studies (Nikitin, Osintsev, and Betsofen 2010), other phases such as $Al_2Cu$, AlLi and $Al_6CuLi_3$ should also exist in the as-cast alloy, but no visible peaks of these phases were discerned in the present sample, possibly because of their relatively small amounts. According to Noble and Bray (Noble and Bray 1998), the intermetallic phase δ'-Al3Li is present in all the as-cast alloys due to the de-composition of the α-Al supersaturated solid solution during the solidification process.

The obvious decline of the diffraction peaks of the secondary phases after solution heat treatment is the most significant aspect, which indicates that most intermetallic phases have dissolved into the Al matrix. Following the solution treatment, the AlLi phase disappeared, and a few $Al_2Cu$ phase particles were generated. Subsequently, during the aging process (SHT + 200 °C /20 h), precipitation of the T1, θ', and δ' ($Al_3Li$) phases was observed.

It was observed that the predominant phases in Al-Li-Cu-Sc alloy were α-Al, $Al_3Li$, θ′ and T1 phases. In the as-cast alloy, α-Al, δ(AlLi) and T1 phases were the main peaks. The δ(AlLi) intermetallic phase dissolved into the Al matrix after solution heat treatment. The δ(AlLi) phase disappeared after aging (SHT + 180 °C /20 h), and the T1, θ′ and δ′ ($Al_3Li$) phases were seen to precipitate. In Al-Li-Cu-Sc alloy, other phases which contain Sc are expected to exist in all conditions, but no visible peaks of these phases were detected in the present sample, possibly because of their relatively small amounts in the alloy.

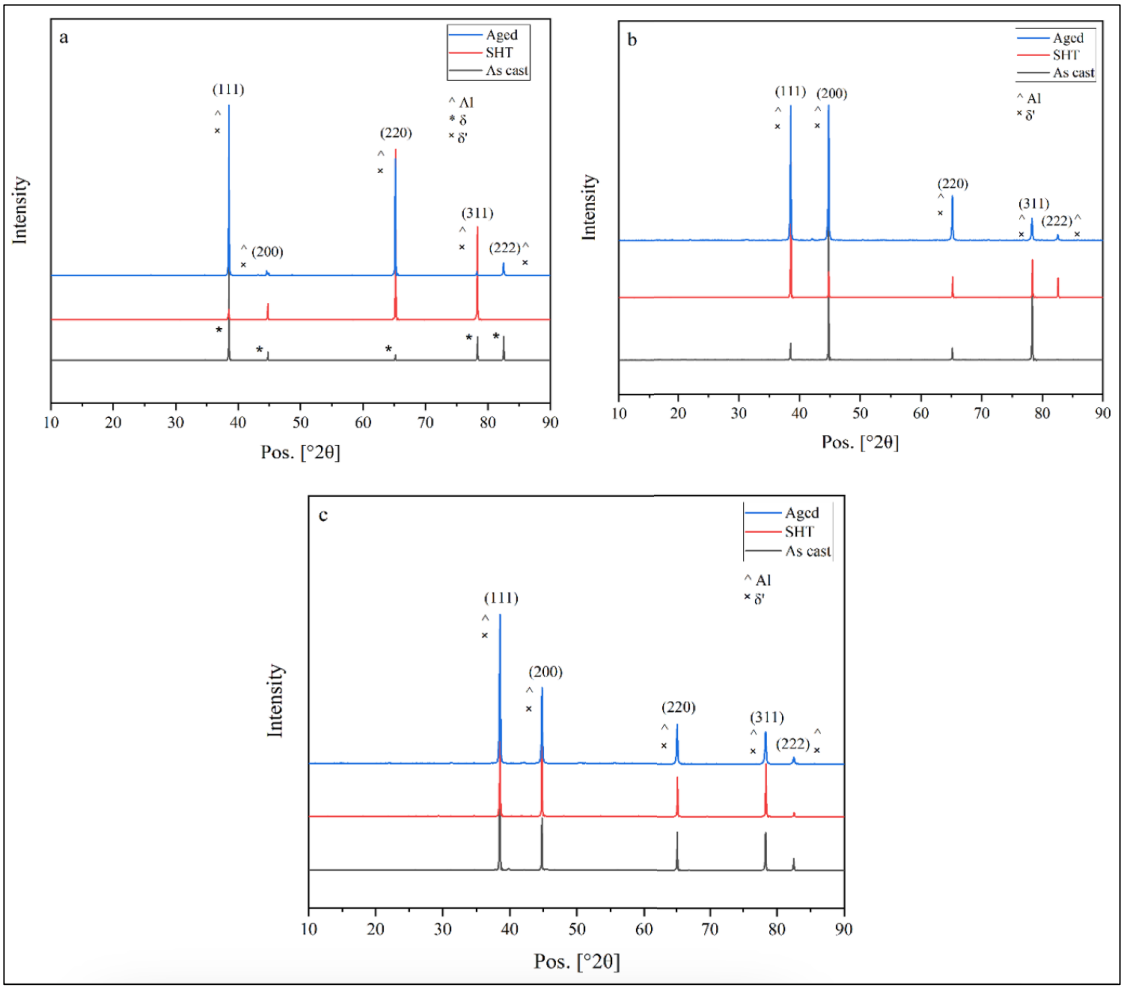


Figure 3.6 XRD patterns of: (a) Al-Li alloy for different conditions of as-cast, solution heat treated (580 °C /1 h) and aged (SHT + 150 °C /45 h); (b, c) Al-Li-Cu and Al-Li-Cu-Sc for different conditions of As-cast, solution heat treated (505 °C/5 h) and aged (SHT + 180 °C/20 h)

## 3.5 DSC Investigation

The thermal behavior and phase transformations in an alloy are influenced by various factors, including the alloy composition, heat treatment, and the presence of impurities. Figure 3.7 illustrates the DSC curves acquired for the as-quenched samples of the studied alloys, Al-Li, Al-Li-Cu and Al-Li-Cu-Sc, at a heating rate of 10 °C min-1.

For Al-Li alloys, a commonly observed exothermic peak occurs during the precipitation of the strengthening phase, which is usually Li-rich. The peak associated with this phase precipitation can typically be found in the temperature range of 100-250 °C, depending on the specific alloy composition. After solution treatment, upon cooling or during the early stages of aging, the formation of Guinier-Preston (GP) zones occurs. As aging progresses, the GP zones grow and transform into more coherent and strengthening precipitates of δ'($Al_3Li$). The formation of δ' precipitates occurs through a nucleation and growth process, leading to the clustering of Li atoms. The temperature range for δ' precipitate formation typically occurs in the range of 180-250 °C (Wang and Shenoy 1998; Klobes et al. 2022; Noble and Trowsdale 1995).

In Figure 3.7(a), the exothermic peak A appears to correspond to the formation of GP zones, while the small endothermic peak A' around ~150 °C likely indicates the dissolution of GP zones. The presence of peak B at approximately 250 °C can be attributed to the formation of the δ' phase.

Aging in Al-Li-Cu alloys typically involves the formation of GP zones, which are clusters of Cu atoms within the aluminum matrix. The copper aluminide precipitates are usually $Al_2CuLi$ intermetallic compound. The exact temperature range in which this precipitate forms is typically within 120 °C-250 °C. Further aging at higher temperatures leads to the transformation of copper aluminide precipitates into a more stable phase θ' ($Al_2Cu$). The $Al_2CuLi$ (T1) precipitates are usually $Al_2CuLi$ intermetallic compounds with a refined and ordered structure. The temperature range for this precipitate formation typically occurs in the range of 160 °C - 250 °C. In some Al-Li-Cu alloys, the aging process can also lead to the formation of δ' precipitate (Wang and Shenoy 1998; Klobes et al. 2022; Noble and Trowsdale 1995; YUAN et al. 2007).

In Figure 3.7(b), the DSC curve for the Al-Li-Cu alloy exhibits an exothermic peak at 100 °C (Peak A) that represents the formation of GP zones. The dissolution of GP zones is observed in the second peak, peak B. The exothermic reaction corresponding to peak C is attributed to the precipitation and growth of θ', T1, and δ' phase precipitates. After solution treatment, during the early stages of aging, the formation of GP zones occurs. As aging progresses, the GP zones

undergo a transformation and grow into coherent and strengthening θ'($Al_2Cu$) precipitates. The presence of Sc influences the precipitation process and can affect the size, distribution, and stability of the θ' precipitates.

In Al-Li-Cu-Sc alloys, the addition of Sc promotes the formation of $Al_3Sc$ precipitates. The formation of the $Al_3Sc$ phase in Al-Li-Cu-Sc alloys generally occurs at temperatures ranging from approximately 300 °C to 400 °C (Klobes et al. 2022; Noble and Trowsdale 1995; YUAN et al. 2007; Wu et al. 2014). Figure 3.7(c) is the DSC curve for a quenched Al-Li-Cu-Sc alloy specimen. The formation of GP zones is indicated by the exothermic peak A. Additionally, a small endothermic peak A' occurring around ~125 °C is observed, likely associated with the dissolution of the GP zones. The formation of the δ' phase can be attributed to peak B at approximately 260 °C. The exothermic reaction corresponding to peak C is ascribed to the precipitation and growth of θ' and T1 phases. The last peak D, at ~370 °C is expected to correspond to the formation of $Al_3Sc$ precipitates.

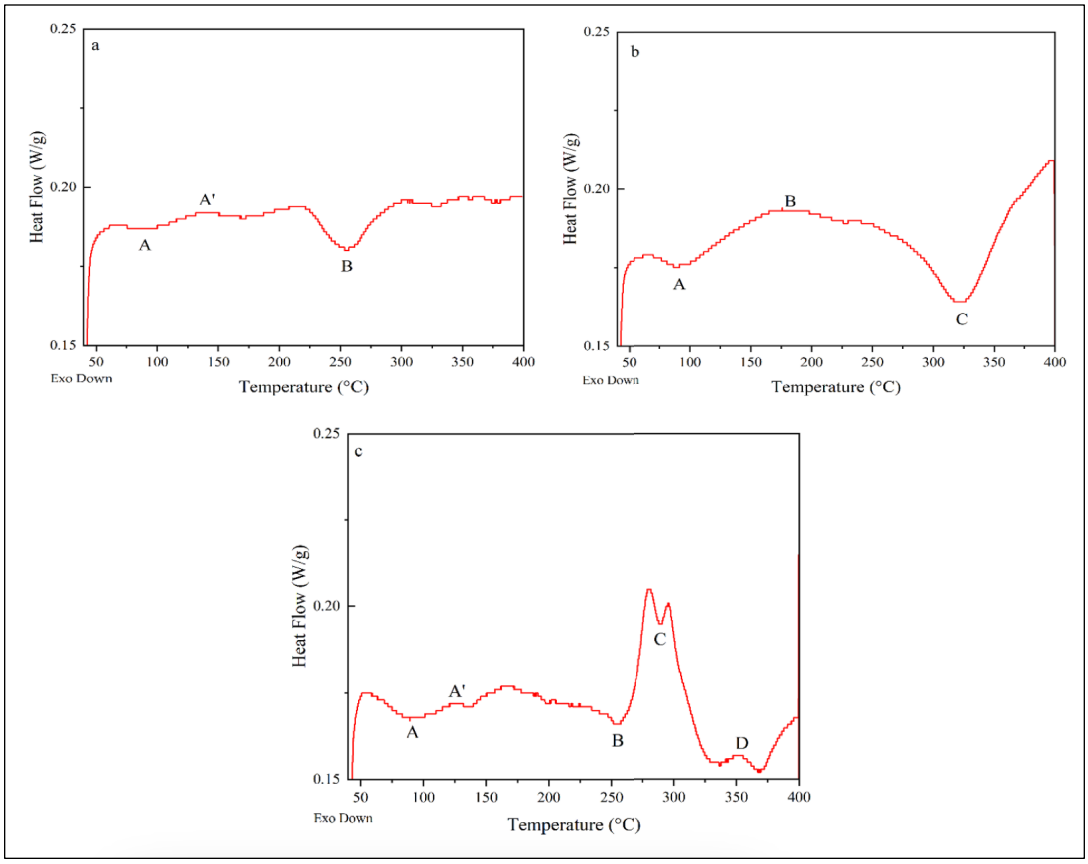


Figure 3.7 The DSC analysis was performed on the as-quenched (solutionized) samples of all compositions and obtained at 10 °C/min. (a) DSC heating curve of the Solutionized Al-Li alloy; (b) DSC heating curve of the Solutionized Al-Li-Cu alloy; (c) DSC heating curve of the Solutionized Al-Li-Cu-Sc alloy

## 3.6 Conclusion

This study focused on the heat treatment of Al-Li, Al-Li-Cu, and Al-Li-Cu-Sc alloys to investigate their microstructure and microhardness under different heat treatment processes. A detailed examination of the alloy samples was carried out to analyze the influence of these processes. Based on the findings from SEM, XRD and DSC analyses, as well as micro-hardness measurements, the following conclusions were drawn.

The main strengthening phase in Al-Li alloy is the δ' ($Al_3Li$) phase, while in Al-Li-Cu and Al-Li-Cu-Sc alloys the main strengthening phases are the δ' ($Al_3Li$) phase, the T1 ($Al_2CuLi$) phase, and the θ' ($Al_2Cu$) phase. The dispersion of small spherical particles of $Al_3Sc$ in Al-Li-Cu-Sc alloy enhances the strength, substantially reinforces the substructure, and hinders the process of recrystallization.

Cu and Sc addition slightly refine the grain size and produce additional Cu-rich secondary phases. The precipitation and evolution of precipitates during the aging process can further strengthen the alloy. The number density of Cu-rich precipitates (mainly T1) increased with the Cu addition during aging. The results obtained from this study could thus provide experimental data and a reference for further investigations that could possibly promote the development and applications of Al-Li alloys with 2-3 wt. % Li content beside Cu and Sc addition.

The strength of the Al-Li-Cu and Al-Li-Cu-Sc alloys increases rapidly with aging time and reaches a maximum, and then decreases slowly. The hardness of these two alloys exhibits an initial increase followed by a slight decrease during the aging process.

The optimal heat treatment process is determined to be as follows:

- 580 °C/1 h solution heat treatment + 150 °C/45 h artificial aging for Al-Li alloy.
- 505 °C/5 h solution treatment + 180 °C/20 h artificial aging for Al-Li-Cu and Al-Li-Cu-Sc alloys.

Under these conditions, the maximum hardness of the heat-treated Al-Li, Al-Li-Cu and Al-Li-Cu-Sc alloys are, respectively, 97.2 HV, 163.6 HV and 182.6 HV.

The results obtained from this study could thus provide experimental data and a reference for further investigations, that could possibly promote the development and applications of Al-Li alloys containing 2-3 wt. % Li, and Cu and Sc additions.

# CHAPITRE 4

# RESULTS AND DISCUSSION OF SURFACE ROUGHNESS

Key findings from machining part of the study have been disseminated through a poster presentation at the REGAL Conference in 2023, titled "Machinability Study of Aluminum-Lithium Alloys for Aerospace Applications: Influences of Heat Treatments and Machining Conditions." This presentation highlighted the relationship between machining conditions, alloy properties.

Additionally, a journal paper on the machinability of Al-Li alloys is currently under preparation.

## 4.1 Introduction

Efficient material removal and the production of high-quality machined components relies on the adjustment of machining processes. In this chapter, our investigation aims to comprehend the complex relationship among different factors that affect the machinability of alloys. We specifically examine how mechanical properties resulting from heat treatment, cutting parameters such as feed rate and cutting speed, and machining conditions like wet and dry, influence crucial machinability standards. Our primary focus is on assessing surface roughness as a key indicator of machinability (Benardos and Vosniakos 2003).

This chapter involves conducting individual statistical analyses for each alloy. This method allows us to thoroughly understand how different factors affect machinability outcomes. By examining the relationships between mechanical properties, cutting parameters, machining conditions, and machinability criteria, we seek to offer valuable insights for improving machining processes to improve efficiency and performance.

## 4.2 Importance of Surface Roughness Analysis and Methods Used

Surface roughness is critical in determining the quality and functionality of mechanical components, impacting properties such as corrosion resistance, wear, tensile strength, and fatigue life. Achieving the desired surface finish is challenging due to the complexity of its formation, influenced by machining variables (e.g., cutting speed, feed rate, depth of cut), machining conditions (e.g., tool material, geometry, cooling methods), and workpiece characteristics (e.g., material composition, heat treatments). Conservative process parameters are often used to mitigate roughness issues, but this approach may not ensure optimal surface finish or efficiency. Understanding the interplay of these factors allows manufacturers to refine machining strategies, enhancing product performance and efficiency (Bhushan, Kumar, and Das 2010; Zhang et al. 2015).

Surface roughness measurements are collected using instruments such as profilometers or surface roughness testers. These measurements are typically taken at multiple locations on the machined surface to capture variability. The collected data is organized and prepared for analysis. Statistical methods to analyze and interpret data related to surface roughness measurements obtained during machining operations.

**ANOVA**: ANOVA is a statistical method used to evaluate differences in surface roughness across varying machining conditions or materials. It determines whether these differences are statistically significant by analyzing variance. Key metrics include:

p-value indicates the probability of observing the test statistic under the null hypothesis. A p-value below the chosen significance level (e.g., 0.05) suggests significant differences between group means, warranting rejection of the null hypothesis. A high p-value suggests no significant differences.

$R^2$ (coefficient of determination) represents the proportion of variability in the response variable explained by the independent variables. Higher $R^2$ values indicate a better model fit, with values ranging from 0 (no variability explained) to 1 (all variability explained). These

metrics help identify impactful input variables and their effect on surface roughness, often visualized through comparative diagrams.

Three separate diagrams are utilized to explore and contrast the most impactful input variables affecting the output:

**Pareto Chart:** A Pareto chart is a graphical tool that prioritizes factors by arranging them in descending order of frequency or impact. It features vertical bars to represent each factor's significance and a cumulative percentage line to highlight their combined contribution. By identifying the "vital few" factors with the greatest impact, Pareto charts help focus improvement efforts effectively.

**Main Effect Plot:** A main effect plot graphically illustrates the impact of different factors on a response variable in factorial experiments. It shows the average response at each level of a factor, isolating its influence from other factors. These plots help identify which factors significantly affect the response and reveal the direction and magnitude of their effects.

**Interaction Plot:** An interaction plot visualizes how two or more factors in a factorial experiment jointly affect a response variable. It highlights interactions where the combined effects of factors differ from the sum of their individual effects. By displaying responses across factor combinations, the plot helps researchers detect and understand complex relationships between variables (Sadiq et al. 2019; 'Machining and Mechanical Finishing' 2018).

### 4.2.1 Arithmetic Average Roughness (Ra) of Machined Al-Li, Al-Li-Cu and Al-Li-Cu-Sc Alloys

The statistical analysis of Al-Li alloy's surface roughness data, shown in Table 1 and summarized in the ANOVA table (Table II.1), reveals essential insights into the effect of machining parameters. The high R-squared value of 86.74% suggests that cutting speed, feed rate, and cooling mode explain most of the variability in surface roughness (Ra), validating the model's reliability. Notably, all three factors show statistically significant p-values ($p = 0$), with significant interaction effects for feed rate with cutting speed ($p = 0.0001$) and hardness with

cooling mode (p = 0.0005). These results set a clear foundation for interpreting individual factors and interactions.

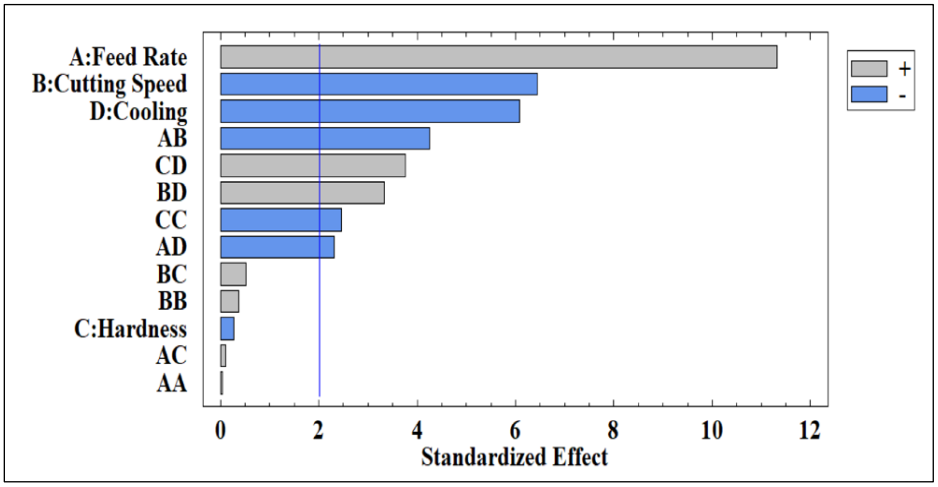


Figure 4.1 Pareto chart of Ra for Al-Li alloy

The Pareto chart (Figure 4.1) and main effect plot (Figure 4.2-a) highlight feed rate as the primary influence on Ra. Specifically, increasing feed rate from 0.05 mm/th to 0.15 mm/th corresponds to a substantial rise in Ra from 0.44 µm to 1.07 µm. This pattern aligns with well-documented findings, where elevated feed rates increase surface roughness due to amplified tool deflection, vibration, and tool wear (Kiswanto, Zariatin, and Ko 2014; Vakondios et al. 2012). Such mechanical instabilities impact surface finish, as observed by (Kuttolamadom, Hamzehlouia, and Mears 2010) in aluminum alloys, where Ra significantly increased under higher feed rates.

This outcome suggests that for the Al-Li alloy, controlling feed rate is crucial to maintain surface integrity, as elevated feed rates could compromise the alloy's surface by inducing inconsistencies. This sensitivity might be particularly relevant in Al-Li alloy due to its inherent material characteristics, including high strength and lightweight properties, which can lead to greater susceptibility to surface vibrations and tool deflection. As expected from literature,

achieving a fine surface finish in Al-Li would thus benefit from conservative feed rates, balancing efficiency and quality.

Cutting speed, the second most impactful variable, also influences Ra significantly. As shown in Figure 4.2-b, increasing cutting speed reduces Ra by promoting faster material removal and limiting tool-workpiece interaction time, thereby producing smoother surfaces. This pattern is in line with results from (Pham et al. 2020; Sequeira et al. 2012), who observed similar trends in aluminum alloys. By shortening interaction time, increased cutting speeds reduce the potential for tool marks and localized heat buildup, a phenomenon beneficial to the machinability of high-strength materials like Al-Li alloy.

The observed reduction in Ra at higher speeds is consistent with literature, which emphasizes that increasing speed limits friction-induced damage on softer, heat-sensitive alloys like Al-Li. Moreover, in high-strength applications where fatigue resistance is vital, this smoother finish aids in enhancing the alloy's performance, as smoother surfaces reduce stress concentrations and improve resistance to crack initiation under cyclic loading. Therefore, as suggested by the results and literature, optimizing cutting speed emerges as a favorable strategy to enhance Al-Li alloy machinability.

Interestingly, hardness shows minimal impact on Ra, as indicated by a negligible 0.01 μm variation across a hardness range of 56 to 97 Hv. This finding diverges from the typical influence of hardness on surface roughness, where higher hardness often correlates with increased Ra due to enhanced resistance to cutting. (Sadiq et al. 2019; Kumar et al. 2020) observed significant hardness effects on Ra in other alloys, attributing this to material rigidity and the tool's ability to penetrate harder materials.

For Al-Li alloy, however, it seems that its distinct high strength-to-weight ratio, alongside specific microstructural properties, diminishes the expected hardness influence on Ra. This could stem from Al-Li's intrinsic characteristics, such as a stable microstructure that resists deformation during cutting. As seen in literature, alloys with high fatigue and tensile strengths, such as Al-Li, may show resilience to minor variations in hardness, suggesting that the surface integrity of Al-Li is relatively unaffected by hardness alone. This finding supports the concept

that machining practices for Al-Li alloy can potentially prioritize parameters like feed rate and cutting speed over hardness control to optimize surface finish.

The application of wet cooling significantly improved surface roughness, reducing Ra by minimizing temperature-related deformations and thermal expansion during machining (Figure 4.2-d). This result aligns with findings from (Tosun and Huseyinoglu 2010; Özsoy and Ozsoy 2019), where cooling strategies, particularly Minimal Quantity Lubrication (MQL), reduced Ra in aluminum alloys. By decreasing tool wear and heat accumulation, wet cooling mitigates common machining challenges, enhancing surface consistency and dimensional accuracy.

For Al-Li alloy, which is prone to thermal damage due to its heat sensitivity, wet cooling is particularly advantageous. Literature suggests that cooling fluid stabilizes tool temperature and minimizes thermal expansion, which is critical for alloys like Al-Li that are susceptible to thermal softening. Therefore, wet cooling could be strategically adopted in Al-Li alloy machining, especially at lower speeds, to control heat build-up and prevent surface roughness deterioration.

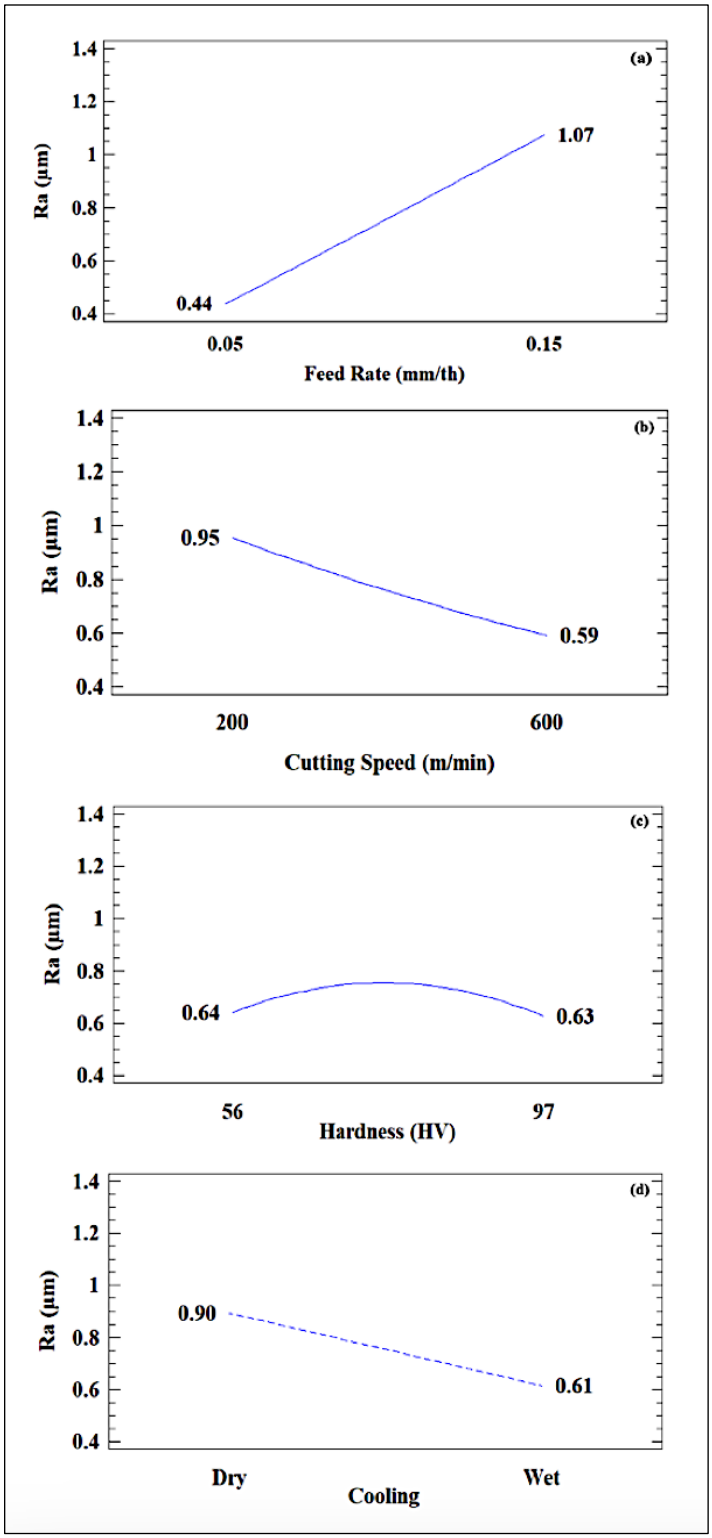


Figure 4.2 Main effects plot for Ra in machined Al-Li alloy

As surface roughness profiles show (Figure 4.3) under the same cooling condition and hardness, in lowest feed rate (0.05 mm/th) and highest cutting speed (600 m/min), the surface roughness is low, and the signals are very close to each other (Figure 4.3-a). But in Figure 4.3-b, in highest feed rate (0.15 mm/th) and lowest cutting speed (200 m/min), the surface roughness is increased significantly with a relatively maximum height of 6 µm.

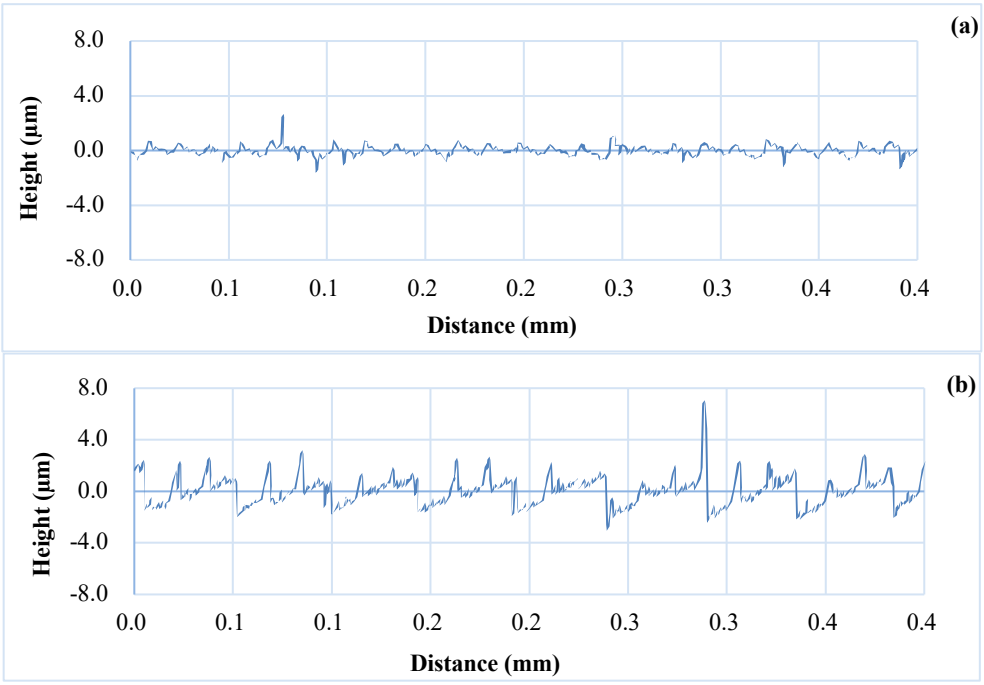


Figure 4.3 The surface roughness profile under similar cooling conditions when using:

a) feed rate: 0.05 mm/th, cutting speed: 600 m/min,
b) feed rate: 0.15 mm/th, cutting speed: 600 m/min

The interactions between cutting speed and feed rate, as well as hardness and cooling mode, reveal significant implications. For instance, Figure 4.4 shows that reducing feed rate while increasing cutting speed optimally enhances surface finish, a pattern consistent with the literature. Such interactions highlight the synergy between cutting speed's reduction of thermal effects and feed rate's minimization of mechanical impact, leading to improved Ra. This suggests that using a balanced combination of higher speeds with lower feed rates can optimize

surface quality, a finding corroborated by similar patterns observed in aluminum alloy machining (Pham et al. 2020).

Furthermore, the interaction between hardness and cooling mode (Figure 4.4-b) reveals that at lower hardness levels, wet cooling improves surface roughness significantly, but this effect diminishes at higher hardness values. This pattern could stem from the interaction of thermal effects on softer materials, where wet cooling reduces thermal stresses, while harder materials maintain a more stable microstructure regardless of cooling. Literature suggests that the effectiveness of wet cooling on Ra varies with material hardness, as softer materials benefit more from thermal control due to their propensity for thermal expansion (Jiang et al. 2010).

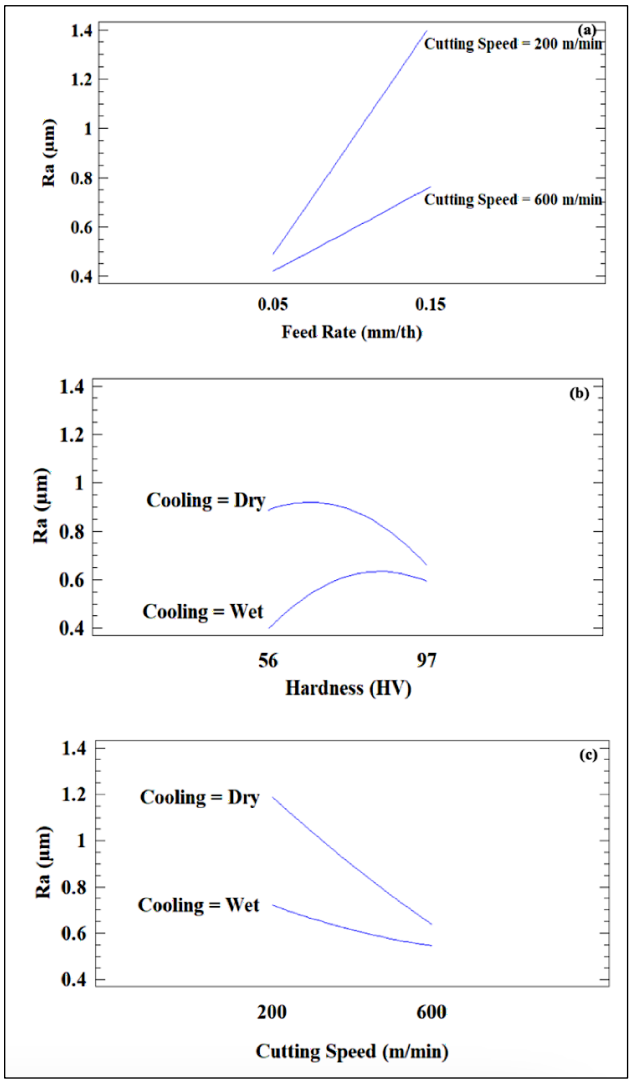


Figure 4.4 Interaction plot for Ra in machining of Al-Li alloy

The 3D surface plots depicted in Figure 4.5 illustrate the interactive impacts of cutting parameters (cutting speed and feed rate), machining conditions (cooling mode), and the material property of the workpiece (hardness).

Figures 4.5-a to 4.5-d reveal that optimal surface roughness, irrespective of the workpiece hardness and cooling mode, is attained at lower feed rates and higher cutting speeds.

In this study, wet machining exhibited a beneficial effect on the surface quality of Al-Li, regardless of the workpiece hardness. Among all the plots in Figure 4.5, the highest surface roughness is observed in the workpieces subjected to machining under the dry cooling mode condition (Figures 4.5-a and 4.5-c).

Furthermore, as it could be seen, hardness didn’t have significant effect on the surface roughness by comparing Figures 4.5-a and 4.5-c with Figures 4.5-b and 4.5-d.

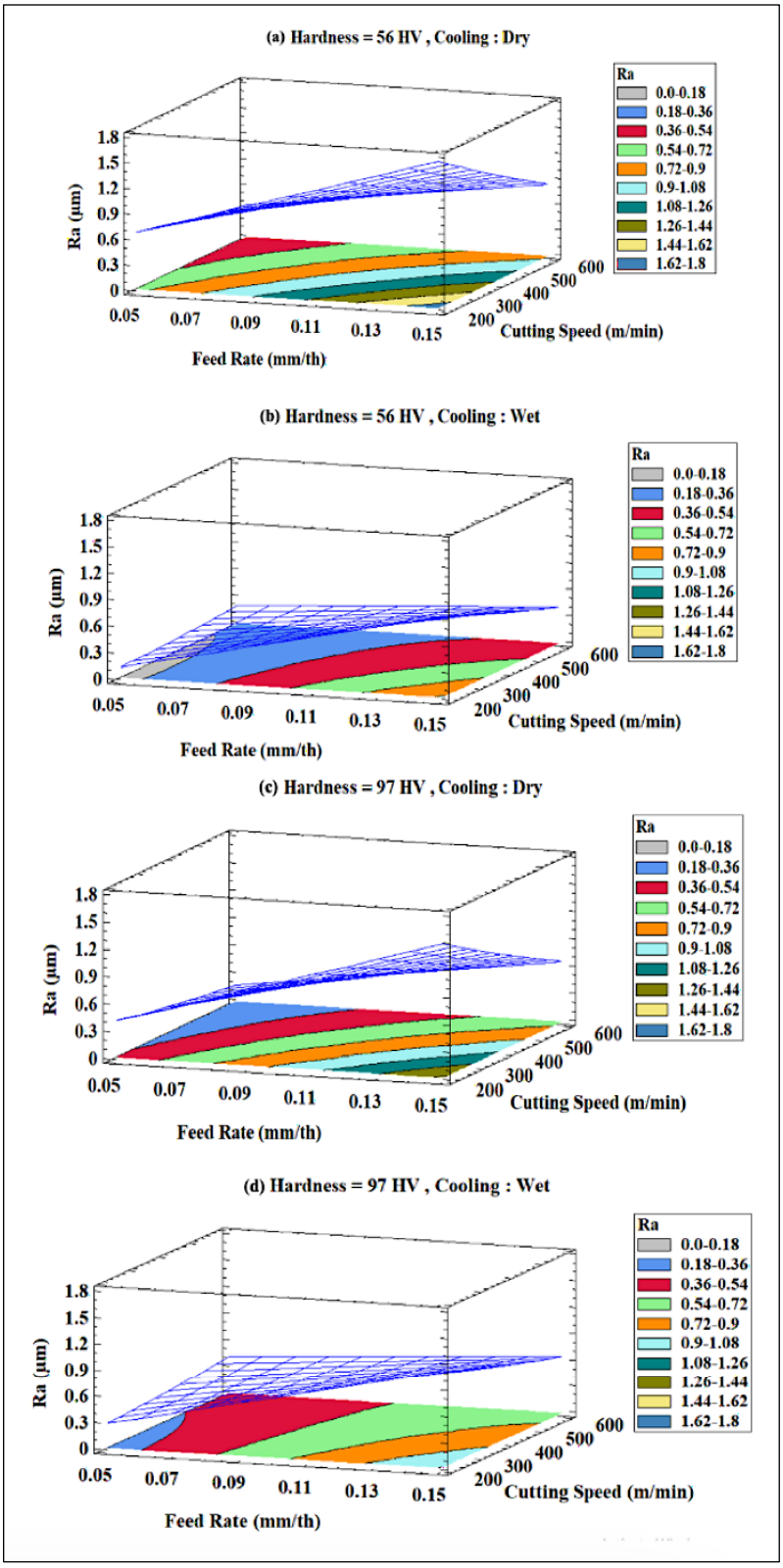


Figure 4.5 Surface plots of Ra in different Hardness and cooling mode for Al-Li alloy

The surface roughness results for the Al-Li-Cu alloy are outlined in Table 5. Much like the Al-Li alloy, this alloy exhibits considerable sensitivity to variations, reflected in an R-squared value of approximately 80.71%. Through our experimental analysis, as depicted in the ANOVA table (Table II.3), we observed that the p-values for feed rate, hardness, and cutting speed are all statistically significant, with values of zero, 0.006, and 0.0095 respectively, indicating their notable influence on surface roughness. Furthermore, the interaction between hardness-cooling mode and cutting speed-cooling mode yielded p-values of 0.0079 and 0.175 respectively, surpassing the 95% confidence threshold, thereby confirming their statistical significance. However, the impact of cooling mode on roughness was found to be negligible, with a p-value of 0.1811.

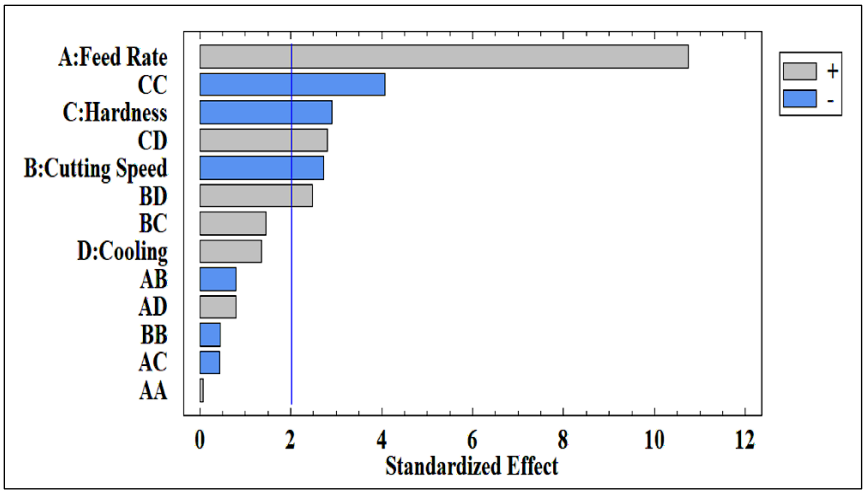


Figure 4.6 Pareto chart of Ra for Al-Li-Cu alloy

As depicted in Figure 4.6, feed rate is the most significant factor influencing Ra. Increasing feed rate from 0.05 to 0.15 mm/th results in a notable roughness increase of 0.8 µm. This finding aligns with (Özsoy 2019; Sadiq et al. 2019), who demonstrated that higher feed rates lead to increased roughness due to enhanced tool wear and vibration. In Al-Li-Cu, as with other

aluminum alloys, controlling feed rate is crucial to maintaining surface finish quality since high rates amplify surface irregularities caused by deflection and vibration.

Higher cutting speeds correlate with reduced surface roughness, as Ra decreases from 1.19 μm at 200 m/min to 0.98 μm at 600 m/min (Figure 4.7-b). Studies such as Perez et al. and Songmene et al. (Perez et al. 2018; Songmene et al. 2011) support this trend, attributing the improvement to reduced thermal damage and better chip formation at elevated speeds. Faster cutting speeds limit tool-material interaction time, thereby decreasing friction and thermal effects, which is particularly beneficial for high-strength Al-Li-Cu alloy. This suggests that, similar to other aluminum alloys, optimized cutting speed can significantly improve the alloy's surface finish by mitigating surface deformation and tool wear.

Higher hardness correlates with smoother surfaces, likely due to the alloy's stable microstructure, which reduces plastic deformation during machining (Figure 4.7-c). Matras and Singh et al. (Matras 2019; Singh et al. 2019) found that increased hardness in aluminum alloys generally yields a finer surface texture due to decreased deformation and more stable cutting. For Al-Li-Cu, a stable microstructure allows harder materials to resist machining-induced imperfections, resulting in better surface quality. This characteristic suggests that hardness could be advantageous in maintaining surface quality during machining, especially in alloys where minimal deformation is critical.

The study indicates that cooling mode does not significantly influence Ra in Al-Li-Cu alloy (Figure 4.7-d). Although literature generally supports cooling's effectiveness in reducing surface roughness (Wang et al. 2015; Biermann and Heilmann 2010), our findings show negligible improvement with wet cooling. This discrepancy may stem from the specific thermal properties of Al-Li-Cu, which may respond less to cooling interventions. Unlike Al-Li, where cooling mitigates heat build-up effectively, Al-Li-Cu's material properties might reduce coolant penetration or alter thermal response, underscoring that material-specific analyses are essential.

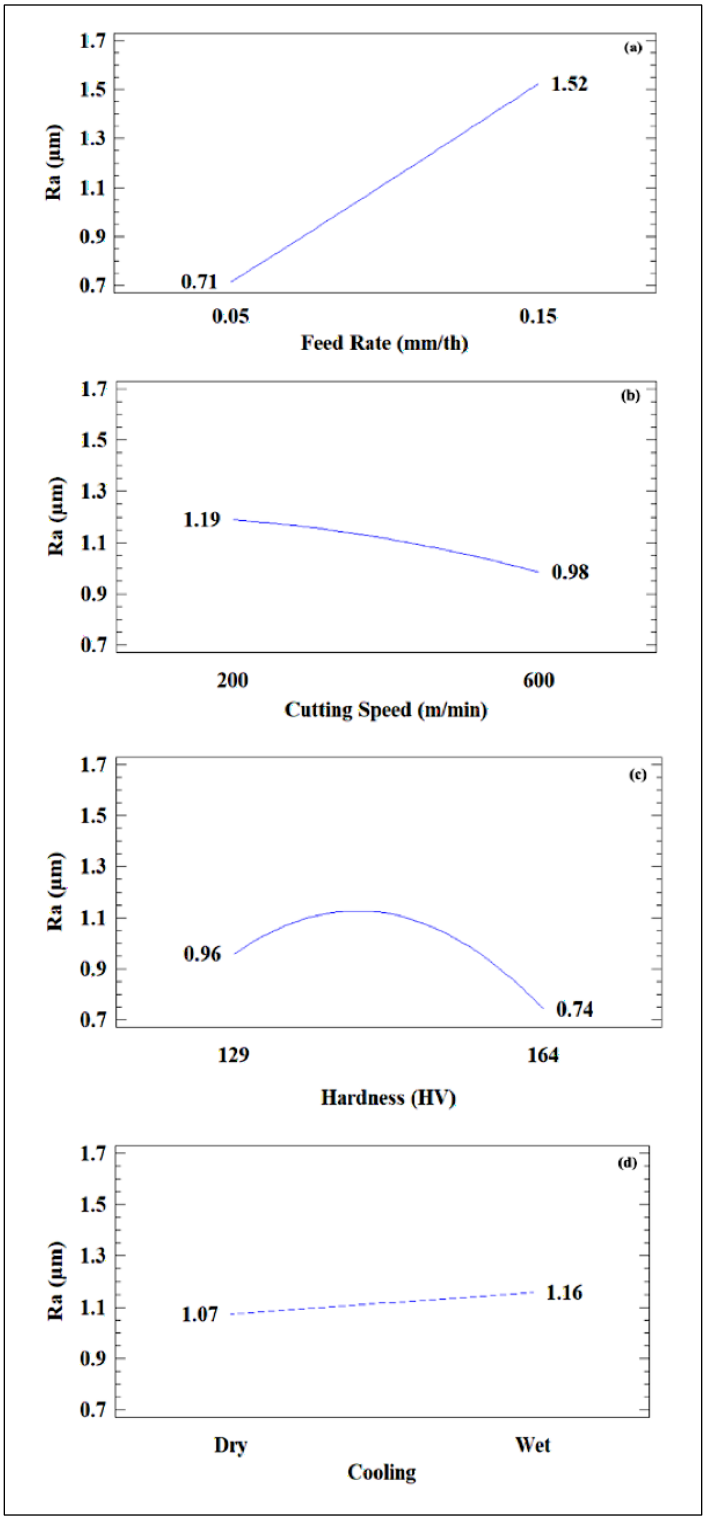


Figure 4.7 Main effects plot for Ra in machining of Al-Li-Cu alloy

As illustrated in Figure 4.8, maintaining consistent feed rate, and cutting speed, the shift from dry cooling (Figure 4.8-a) to wet cooling (Figure 4.8-b) did not result in significant changes in surface roughness. Both profiles exhibit systematic cycles, with Figure 4.8-a (dry condition) showing a maximum height of approximately 1 µm, and Figure 4.12-b (wet condition) showing a maximum height of approximately 2 µm. As shown in the main effect plot (Figure 4.8-d), although the effect of wet cooling is not significant, it does cause a small increase in surface roughness.

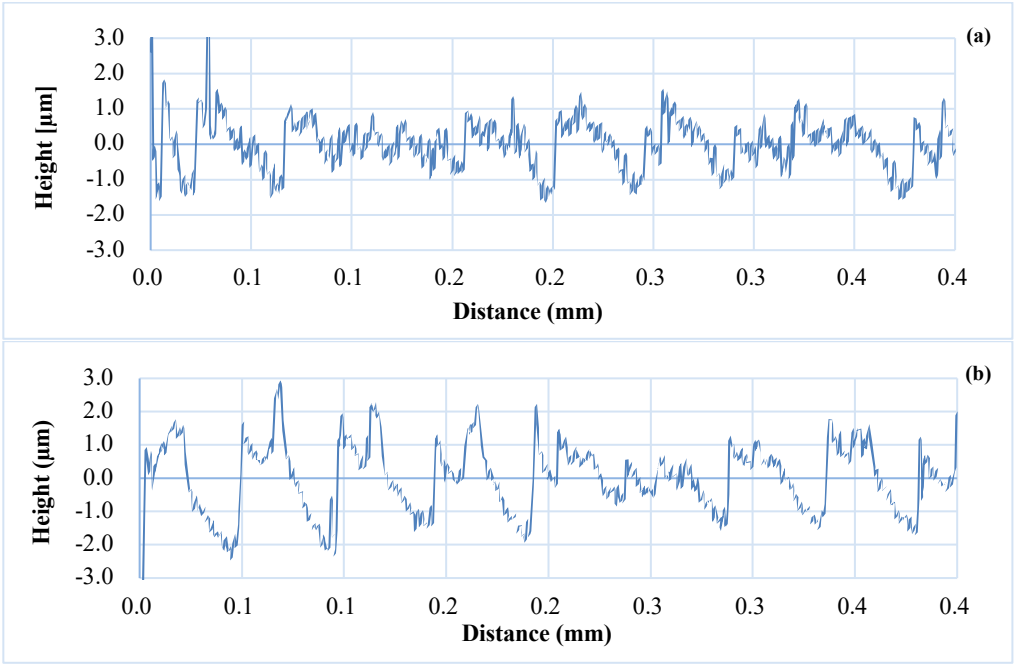


Figure 4.8 The surface roughness profile under:
a) feed rate: 0.15 mm/th, cutting speed: 400 m/min, Dry condition,
b) feed rate: 0.15 mm/th, cutting speed: 400 m/min, Wet condition

The interactions between hardness-cooling mode and cutting speed-cooling mode, while significant, reveal nuanced effects. At lower hardness levels, wet cooling slightly improves Ra, but at higher hardness levels, the effect diminishes (Figure 4.9-a). Literature suggests that softer materials benefit more from cooling due to their susceptibility to thermal expansion (Singh, Singh, and Chattopadhyay 2020). This interaction indicates that while cooling's impact

is generally minor, it may help reduce surface roughness in specific conditions, especially with lower hardness.

Additionally, the interaction between cutting speed and cooling mode suggests that dry conditions may yield better results at higher speeds, as seen in Figure 4.9-b. Lower speeds benefit from wet cooling's thermal reduction effects, which aligns with the expectation that cooling is more beneficial in low-speed, heat-sensitive machining operations.

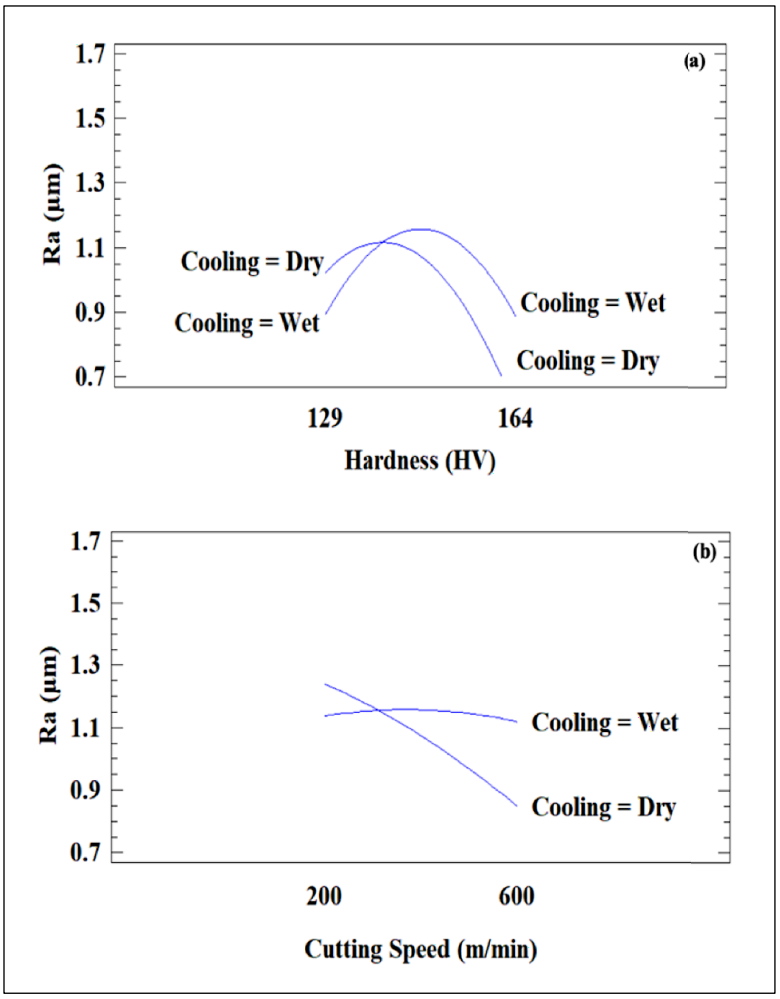


Figure 4.9 Interaction plot for Ra in machining of Al-Li-Cu alloy

3D surface plots (Figures 4.10-a to 4.10-d) illustrate that optimal Ra is achieved at higher speeds and feed rates, with minimal effect from cooling mode. Specifically, dry machining provides better results at higher hardness levels, supporting the idea that thermal stability in harder materials lessens the cooling effect. However, softer materials display slightly improved Ra under wet conditions, reinforcing the role of material properties in cooling response.

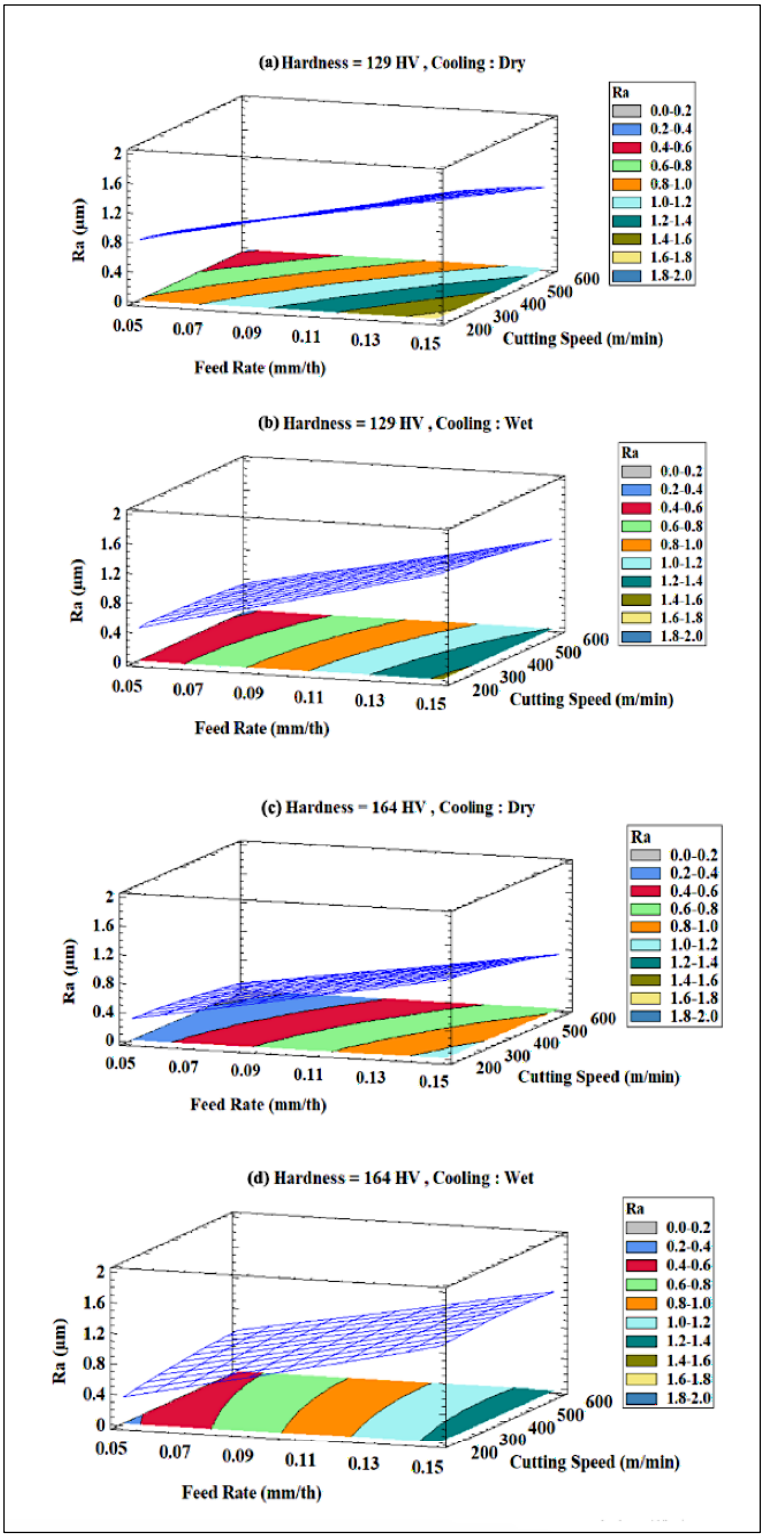


Figure 4.10 Surface plots of Ra in different Hardness and cooling mode for Al-Li-Cu alloy

The machining process of the Al-Li-Cu-Sc alloy demonstrates a notable sensitivity to variations in cutting parameters. Specifically, the developed model effectively accounts for 80.13% of the observed variability in Ra, indicating a clear correlation between the selected cutting parameters and the resulting surface roughness.

Five effects exhibit P-values less than 0.05, indicating their significant departure from zero. The ANOVA table for the statistical analysis of the Al-Li-Cu-Sc alloy is provided in Table II.5.

In the Pareto chart (Figure 4.11), which illustrates all independent variables and their interactions, it is apparent that only the cutting speed fails to exceed the threshold indicated by the blue line. This finding underscores the limited confidence level associated with cutting speed and its minimal impact on Ra during the machining process of this alloy.

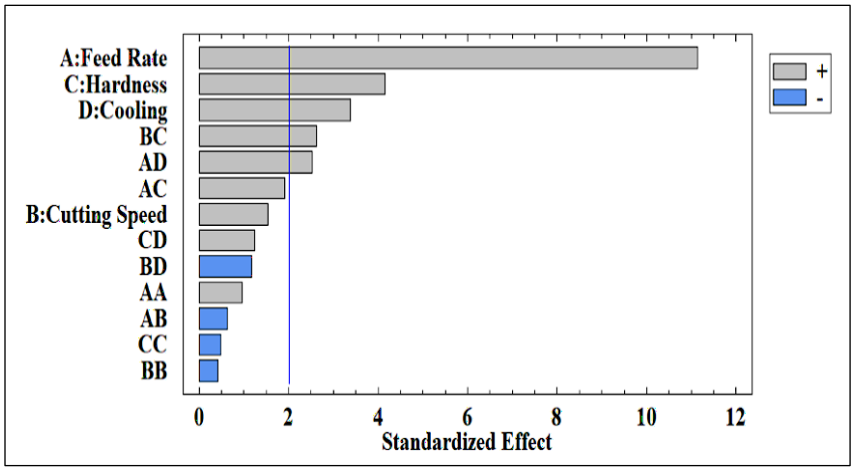


Figure 4.11 Pareto chart of Ra for Al-Li-Cu-Sc alloy machining

As seen in the main effect plot (Figure 4.12-a), Ra increases from 0.54 µm at low feed rates to 1.32 µm at high feed rates, underscoring feed rate's substantial effect on surface roughness. This aligns with studies by Venkatesan et al. and Akkurt et al. (Venkatesan et al. 2014; Akkurt et al. 2004), who found that higher feed rates in aluminum alloys lead to rougher surfaces due to increased tool wear and vibration. For Al-Li-Cu-Sc, controlling feed rate is essential to

maintaining surface quality, particularly since the alloy's strength from Scandium increases sensitivity to mechanical stresses during machining.

The refined microstructure of the Al-Li-Cu-Sc alloy, characterized by uniformly dispersed Al3Sc precipitates, plays a critical role in its machining behavior (Figure 3.4-c). These fine precipitates enhance material hardness and reduce deformation, leading to minimal variation in surface roughness (Ra) across cutting speeds. Unlike typical aluminum alloys, where higher cutting speeds often improve Ra, the stability observed in the Al-Li-Cu-Sc alloy (Figure 4.12-b) can be directly attributed to its microstructural reinforcement, ensuring consistent machining performance (Perez et al. 2018; Karkalos et al. 2021).

Increasing hardness slightly raises Ra by 0.29 μm, a result supported by studies showing that harder materials generally yield rougher surfaces due to increased tool wear (Songmene et al. 2011; Tash et al. 2006). For Al-Li-Cu-Sc, the enhanced microstructure from Scandium's presence likely amplifies resistance to cutting deformation, resulting in more stable yet rougher surfaces at higher hardness levels (Figure 4.12-c).

Contrary to other alloys, wet cooling increased Ra for Al-Li-Cu-Sc alloy, possibly due to thermal shocks from rapid cooling that introduce micro-cracks on the surface (Figure 4.12-d). Studies like Biermann and Heilmann (Biermann and Heilmann 2010) show wet cooling usually improves Ra by minimizing thermal distortion; however, Scandium's impact on the alloy's thermal properties may make it more susceptible to micro-cracking under rapid cooling conditions, emphasizing the need for controlled cooling when machining this alloy.

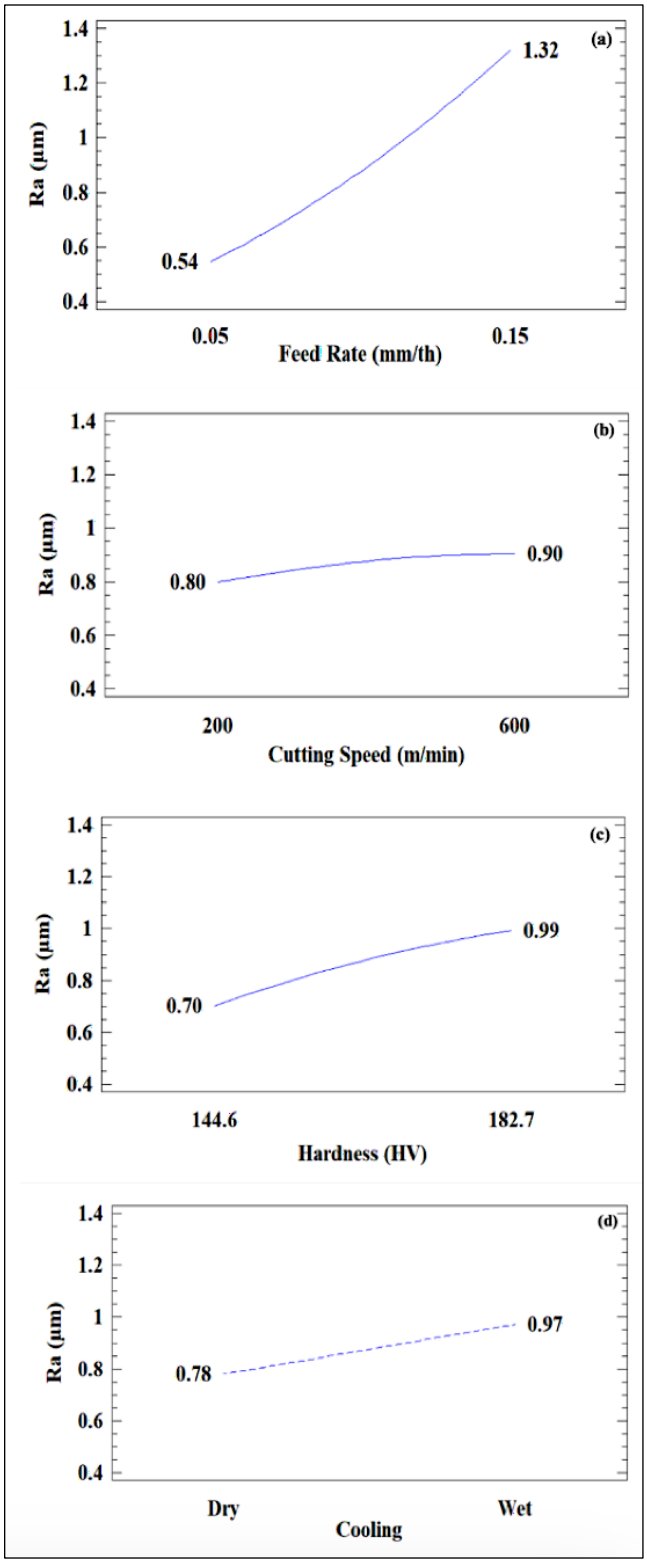


Figure 4.12 Main effects plot for Ra in machining of Al-Li-Cu-Sc alloy

As depicted in Figure 4.13 under the same cutting speed condition, increase in hardness cause increase in surface roughness and the higher surface roughness was obtained by increasing hardness (Figure 4.13-b).

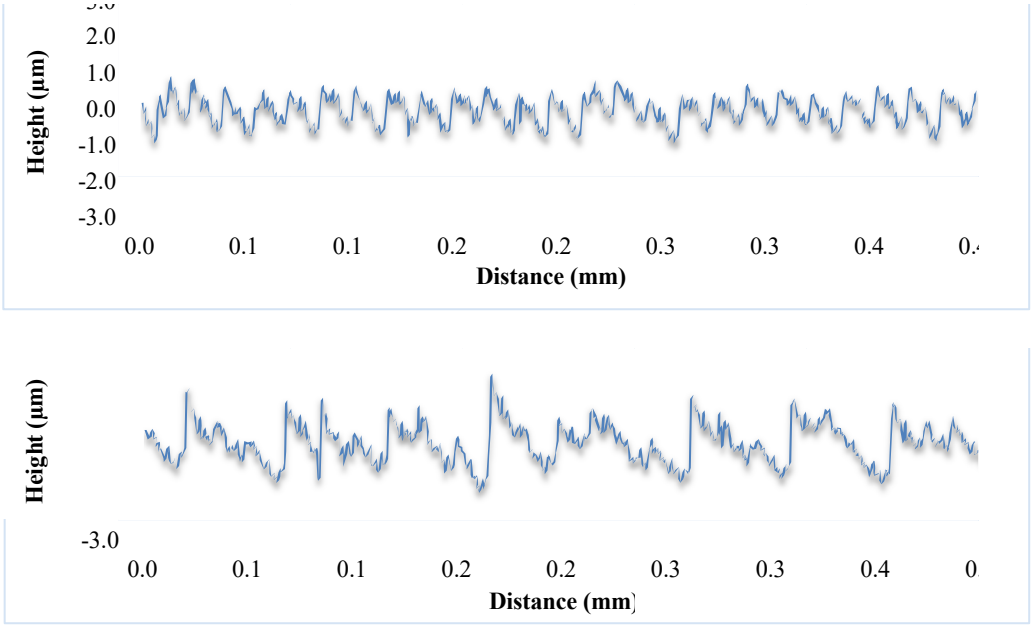


a) Feed rate: 0.05 mm/th, Hardness: 144.6 HV,
b) Feed rate: 0.05 mm/th, Hardness: 182.7 HV

The interactions between hardness and cooling mode, as well as cutting speed and hardness, significantly affect Ra. For example, harder materials machined under dry conditions show improved surface quality, likely because Scandium-enhanced hardness resists plastic deformation, reducing cooling's effect (Figure 4.14). Additionally, at lower feed rates, Ra remains stable regardless of cooling, while at higher feed rates, wet cooling slightly increases Ra (Figure 4.14). This suggests that cooling might be beneficial primarily at low feed rates where thermal impacts are minimal.

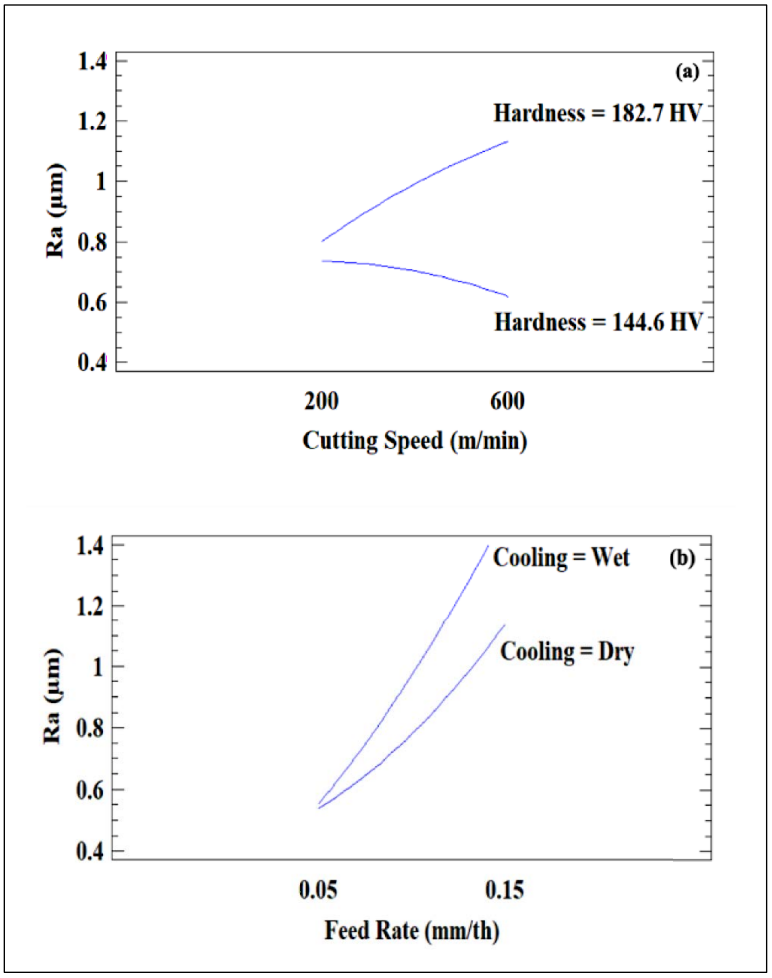


Figure 4.14 Interaction plot for Ra in machining of Al-Li-Cu-Sc

The 3D surface plots (Figure 4.15) indicate that feed rate and hardness are the most influential factors on Ra. Under high feed rates and wet cooling, harder materials yield rougher surfaces, highlighting the alloy's increased sensitivity to thermal and mechanical effects from higher feed rates. Optimal Ra (0.3 µm) is achieved at low feed rates and high speeds for softer materials, suggesting that careful control of these parameters enhances surface finish in Al-Li-Cu-Sc alloy.

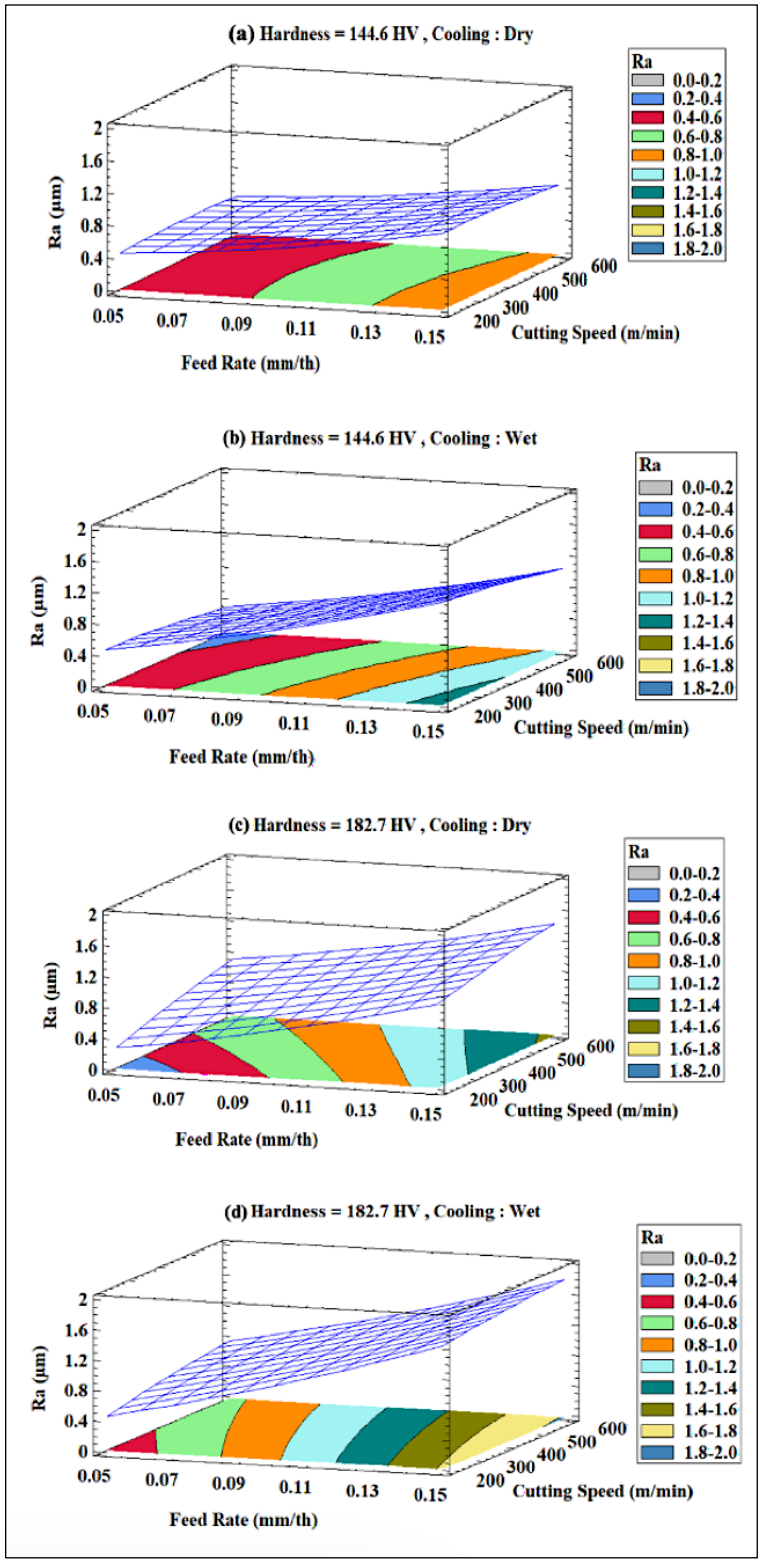


Figure 4.15 3D Surface plots of Ra in different Hardness and cooling mode for Al-Li-Cu-Sc

### 4.2.2 Total Height of the Profile (Rt) of Machined Al-Li, Al-Li-Cu and Al-Li-Cu-Sc Alloys

In order to validate the Pareto chart depicting the Ra factor of our alloy's surface roughness, we expanded our inquiry to encompass the analysis of Rt outcomes. The Pareto chart (Figure 4.6) illustrates both the adverse and favorable impacts of various factors on Rt, mirroring the trends observed for Ra.

In the statistical analysis of Al-Li surface roughness data presented in Table 2, the ANOVA results in Table II.2 show an R-squared value of 82.58 %, indicating a strong responsiveness of the analytical model to changes in process parameters. The p-values for cutting speed, feed rate, and cooling mode are all zero, while the p-values for the interactions between hardness and cooling mode, feed rate and cutting speed, and cutting speed and cooling mode are 0.0001, 0.0011, and 0.0066, respectively.

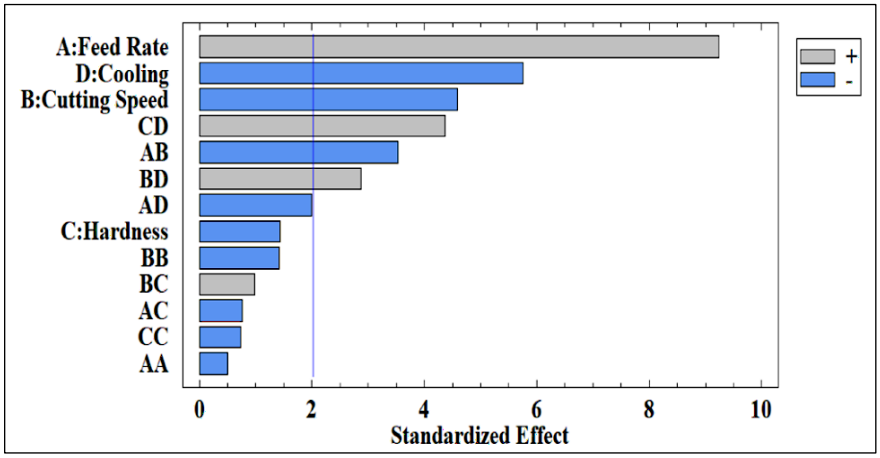


Figure 4.16 Pareto chart of Rt for Al-Li alloy

The Pareto chart in Figure 4.16 highlights that feed rate has the most significant impact on surface roughness. This is further corroborated by the main effect plot in Figure 4.17-a, where the Ra value increases from 6.77 µm at the lowest feed rate (0.05 mm/th) to nearly 9.09 µm at the highest feed rate (0.15 mm/th).

Following feed rate, cooling mode and cutting speed are identified as the primary factors affecting Ra in the machining of Al-Li alloy. The study indicates that hardness does not significantly influence surface roughness, as shown in Figure 4.17-c, where varying hardness values from 56 HV to 97 HV result in only a 0.36 µm change in surface roughness. If the machining technique was effective in minimizing vibrations, tool deflection, and other factors affecting surface finish, the increase in hardness may not have had a significant impact. And another possible reason behind this result may be because of high strength-to-weight ratio and excellent fatigue resistance of Aluminum-lithium alloy that may have overshadowed the influence of hardness on surface roughness during machining.

The results also demonstrate that using wet cooling conditions and a high flow of cutting fluid during machining of Al-Li alloy improves surface quality, reducing roughness. This beneficial effect is depicted in Figure 4.17-d.

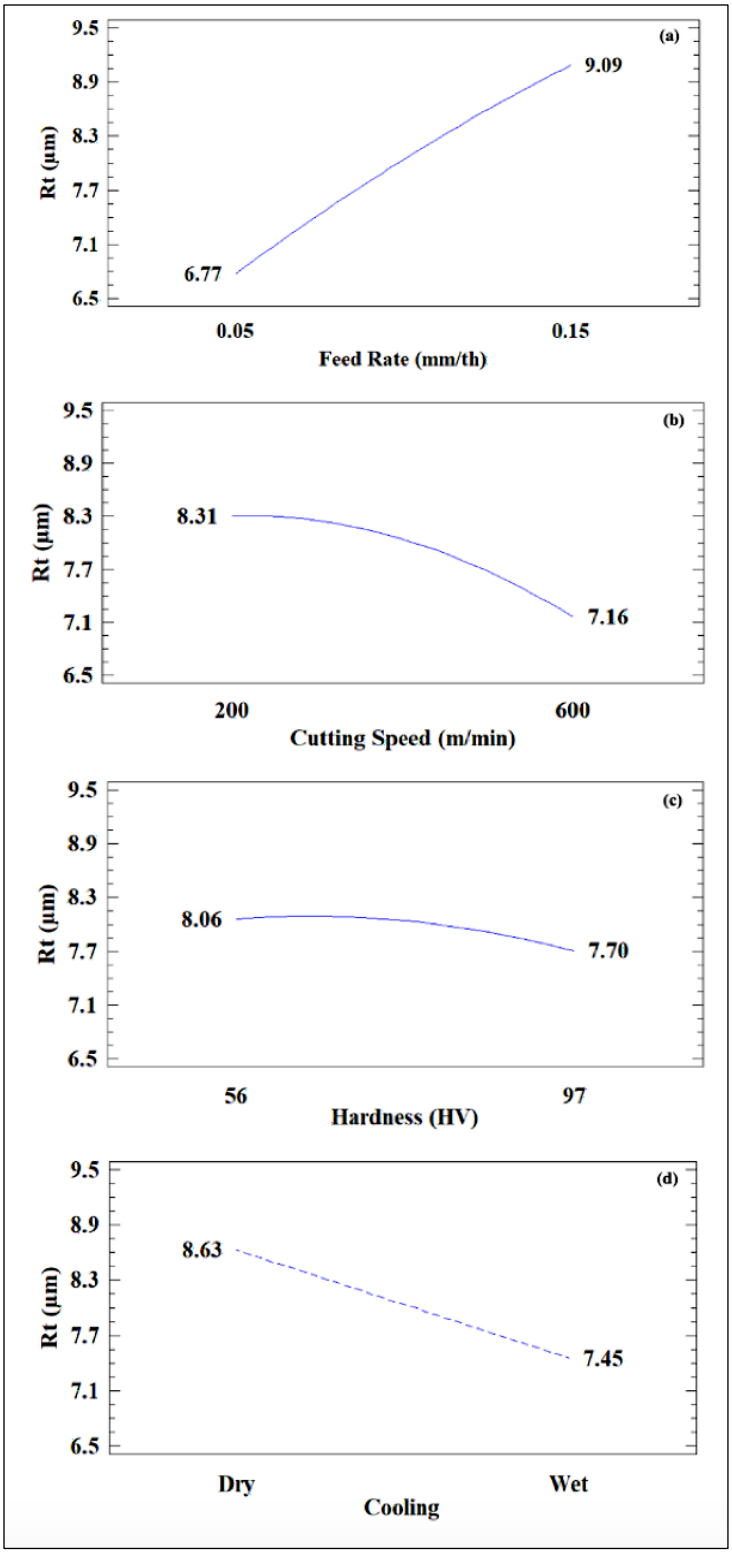


Figure 4.17 Main effects plot for Rt in machined Al-Li alloy

After feed rate, cooling mode, and cutting speed, the interactions between hardness and cooling mode, feed rate and cutting speed, and cutting speed and cooling mode significantly affect Rt (Figure 4.18). At lower hardness levels, wet cooling improves surface roughness, but this effect diminishes at higher hardness due to factors like reduced thermal conductivity and increased tool wear. Additionally, at high feed rates, lower cutting speeds result in rougher surfaces, while increasing cutting speed improves roughness. Wet machining shows the greatest benefit at low cutting speeds, where it reduces roughness more effectively than dry machining, especially for Al-Li alloys.

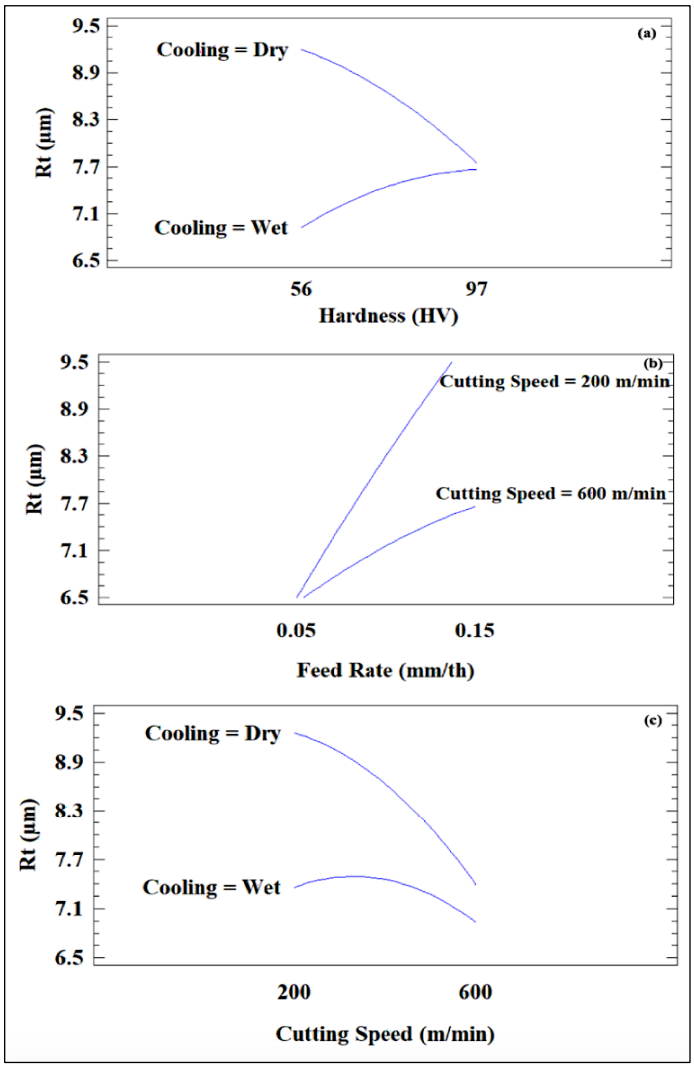


Figure 4.18 Interaction plot for Rt in machining of Al-Li alloy

The 3D surface plots in Figure 4.19 illustrate the interactive effects of cutting parameters (cutting speed and feed rate), machining conditions (cooling mode), and the workpiece's material property (hardness). Figures 4.19-a to 4.19-d demonstrate that optimal surface roughness, regardless of workpiece hardness, is achieved at lower feed rates and higher cutting speeds.

The study shows that wet machining improves the surface quality of Al-Li, as evident when comparing Figure 4.19-a with Figure 4.19-b and Figure 4.19-c with Figure 4.19-d. This beneficial effect is consistent across different hardness levels of the workpiece.

Among all the plots in Figure 4.19, the highest surface roughness is observed in workpieces machined under dry conditions with the lowest hardness of 56 HV, as shown in Figure 4.19-a.

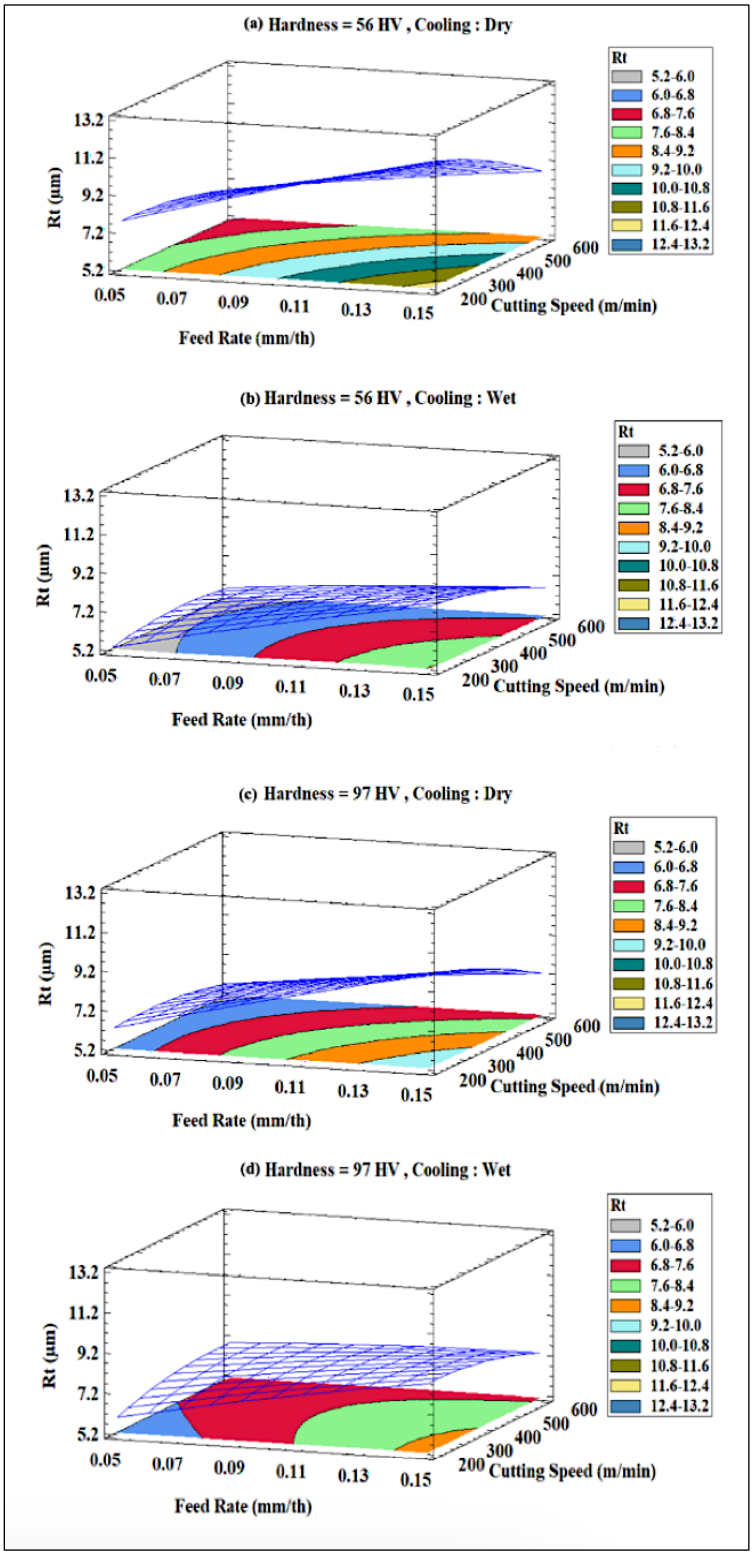


Figure 4.19 Surface plots of Rt in different Hardness and cooling mode for Al-Li alloy

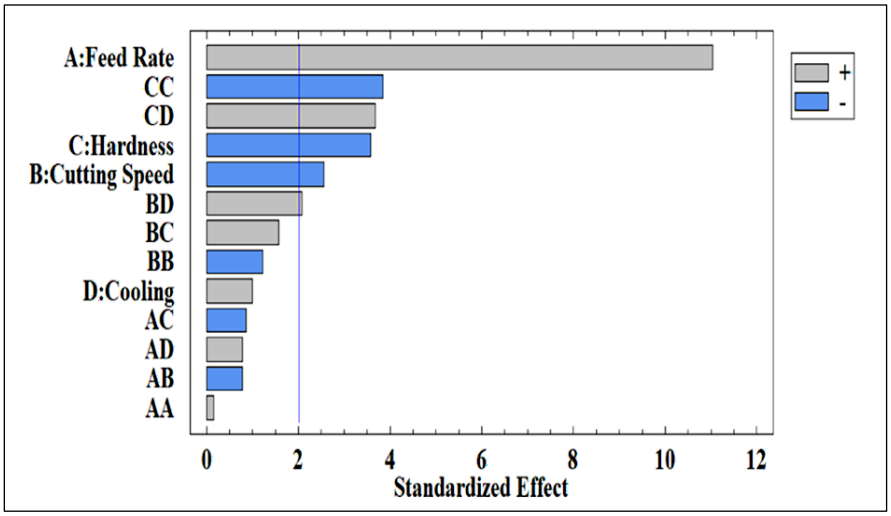


Figure 4.20 Pareto chart of Rt for Al-Li-Cu alloy

The Pareto chart (Figure 4.20) shows that feed rate, hardness, and cutting speed significantly impact surface roughness (Rt) for the Al-Li-Cu alloy, with an R-squared of 81.87%. Feed rate notably increases roughness, while higher cutting speed and hardness improve surface finish, likely due to the alloy's stable microstructure that minimizes deformation (Figures 4.21-a to 4.21-c). Cooling mode's effect on Rt is minimal, as shown in both the Pareto and main effect plots (Figure 4.21-d).

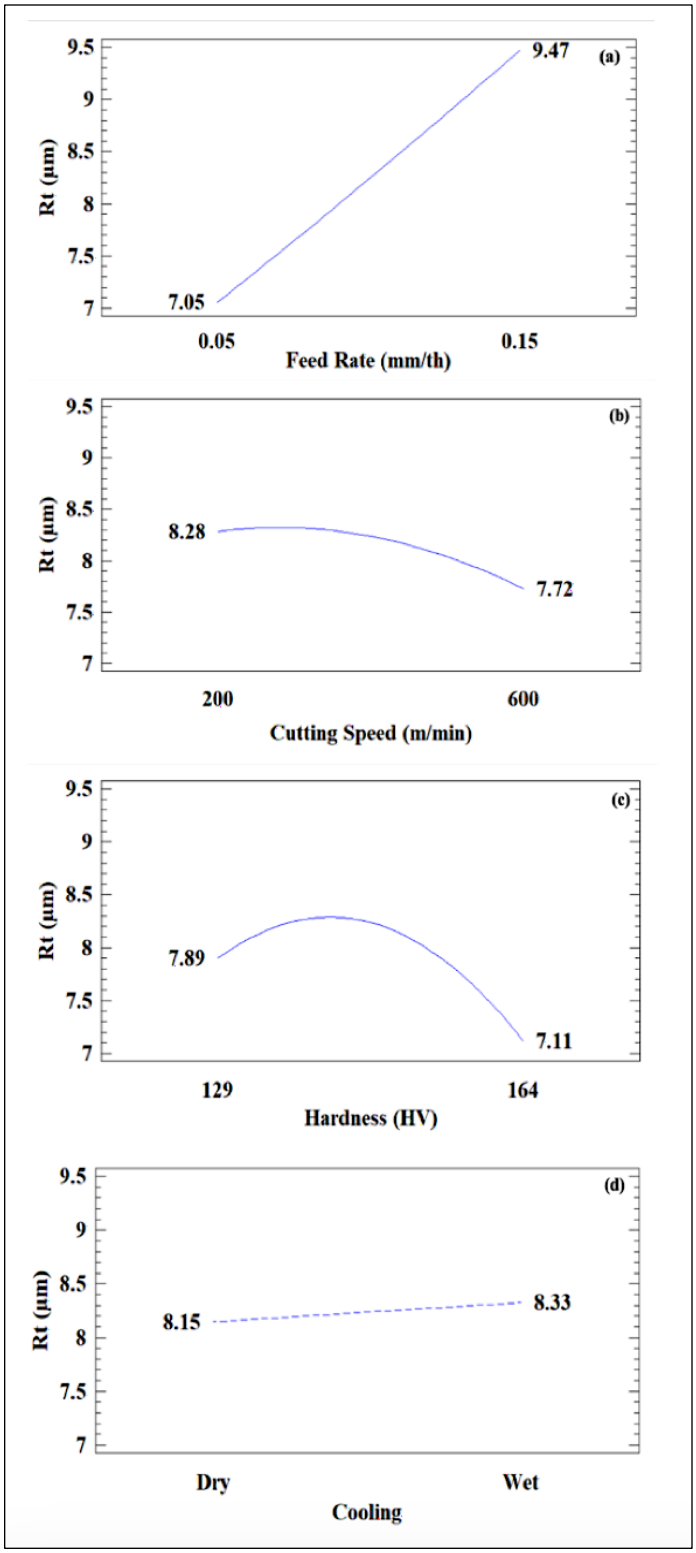


Figure 4.21 Main effects plot for Rt in machining of Al-Li-Cu alloy

The interaction plots (Figure 4.22) reveal that dry conditions yield better surface quality at high hardness levels, with cooling mode being more effective at lower hardness levels. At lower cutting speeds, cooling mode has a negligible impact, but at higher speeds, dry conditions further enhance surface finish by efficiently managing heat.

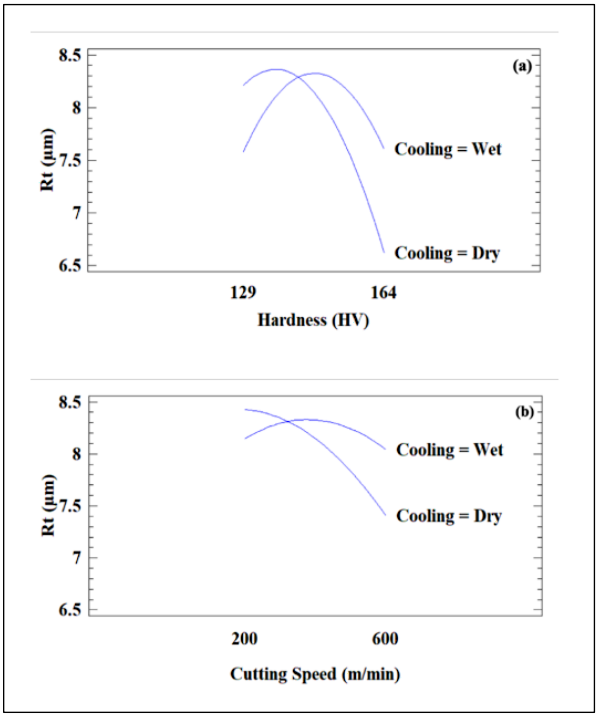


Figure 4.22 Interaction plot for Rt in machining of Al-Li-Cu alloy

The 3D surface plots (Figure 4.23) confirm that under dry conditions, harder materials have reduced Rt compared to softer ones, with little difference observed in wet conditions.

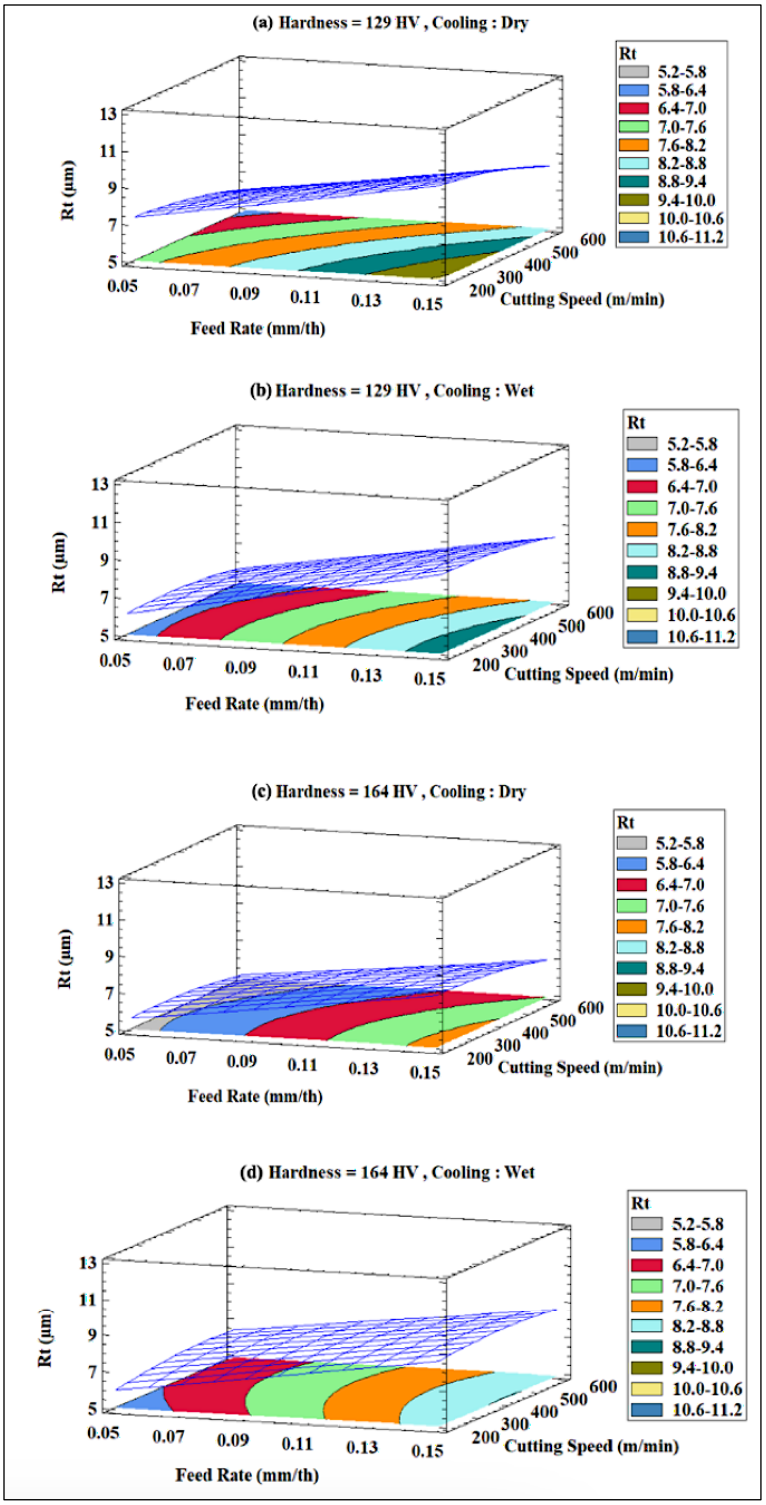


Figure 4.23 3D Surface plots of Rt in different Hardness and cooling mode for Al-Li-Cu alloy

As depicted in Figure 4.24, the Pareto chart shows both negative and positive impacts of various factors on Rt, aligning with the patterns observed for Ra.

The machining process of the Al-Li-Cu-Sc alloy demonstrates significant sensitivity to variations in cutting parameters. The developed model accounts for 80.13% of the observed variability in Ra, indicating a strong correlation between the selected cutting parameters and the resulting surface roughness.

Four effects exhibit p-values less than 0.05, highlighting their significant influence. The ANOVA table of Rt for the statistical analysis of the Al-Li-Cu-Sc alloy is presented in Table II.6.

In the Pareto chart (Figure 4.24), which illustrates all independent variables and their interactions, only cutting speed does not exceed the threshold indicated by the blue line. This finding underscores the limited confidence level associated with cutting speed and its minimal impact on Rt during the machining process of this alloy.

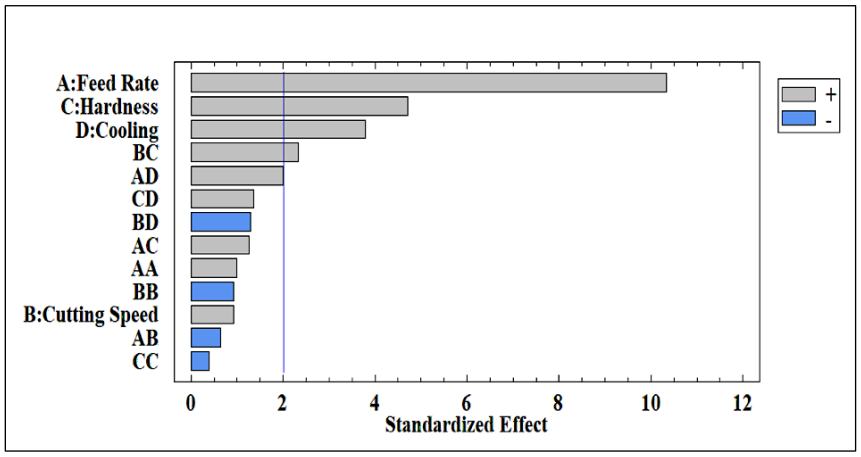


Figure 4.24 Pareto chart of Rt for Al-Li-Cu-Sc alloy

According to the Pareto chart (Figure 4.24) and the main effect plots (Figure 4.25), variations in feed rate have the most substantial impact on Rt in the machining of Al-Li-Cu-Sc alloy. The main effect plot shows a significant increase in roughness from 6.72 µm at low feed rates to nearly 9.13 µm at high feed rates, highlighting the notable influence of feed rate on surface roughness (Figure 4.25-a).

In contrast to the behavior observed in other alloys where cutting speed positively impacts surface roughness, cutting speed does not affect surface quality for this alloy (Figure 4.25-b).

An increase in hardness results in a roughness increment of approximately 1.1µm when comparing the hardest and softest variants of this alloy (Figure 4.25-c). Additionally, the findings indicate that wet cooling mode unexpectedly has a detrimental effect on surface roughness, leading to an increase in roughness from 7.36 µm to 8.09 µm (Figure 4.25-d).

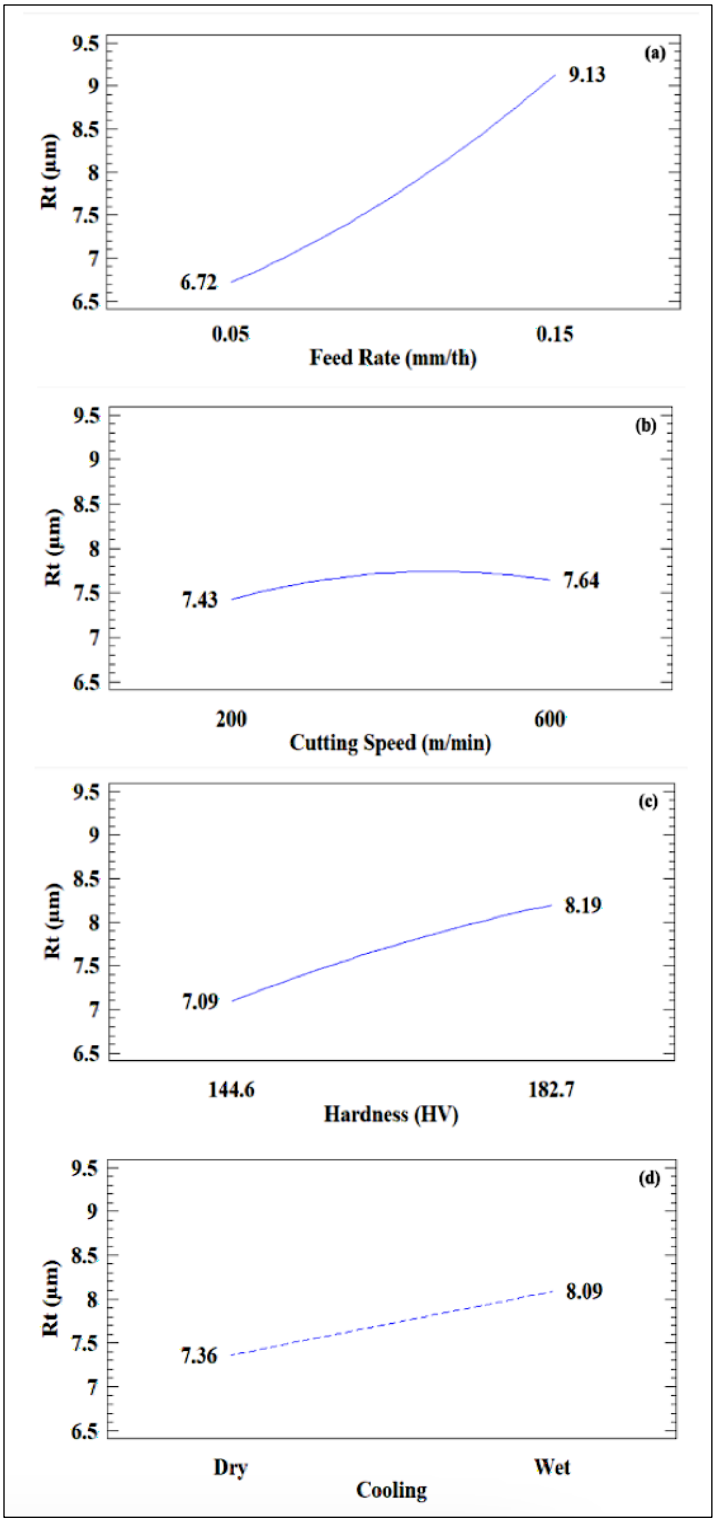


Figure 4.25 Main effects plot for Rt in machined Al-Li-Cu-Sc alloy

While cutting speed alone does not significantly impact roughness, its interaction with hardness notably affects surface quality (Figure 4.26). For the softest block (144.6 HV), higher cutting speed (600 m/min) reduces roughness to 6.65 µm, while for the hardest block (182.7 HV), the same speed increases roughness to 8.42 µm. At the lowest cutting speed (200 m/min), roughness values for both hardness levels are similar, around 7.15–7.6 µm. Thus, higher cutting speeds improve surface quality for softer materials but increase roughness for harder ones.

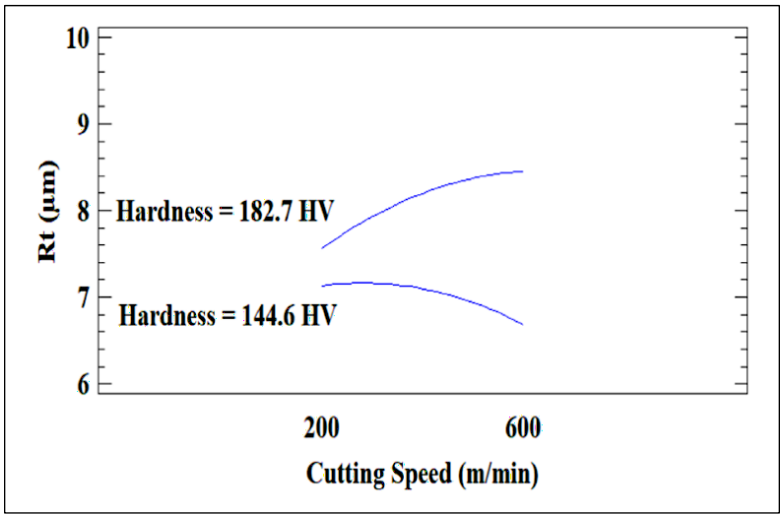


Figure 4.26 Interaction plot for Rt in machining of Al-Li-Cu-Sc alloy

As depicted in Figures 4.27-a and 4.27-c, under the same cooling mode (dry), increasing hardness leads to an increase in surface roughness. This change is insignificant at the lowest cutting speed (200 m/min) but becomes significant at the highest cutting speed (600 m/min). This phenomenon is also evident when comparing Figures 4.27-b and 4.27-d and is further supported by the main effect plot in Figure 4.27-c.

Another insight from the 3D plots is that changing the cooling mode from dry to wet increases surface roughness. This increase is particularly noticeable at higher feed rates, as shown in Figures 4.27-a and 4.27-b, and Figures 4.27-c and 4.27-d. This effect is more significant under these conditions.

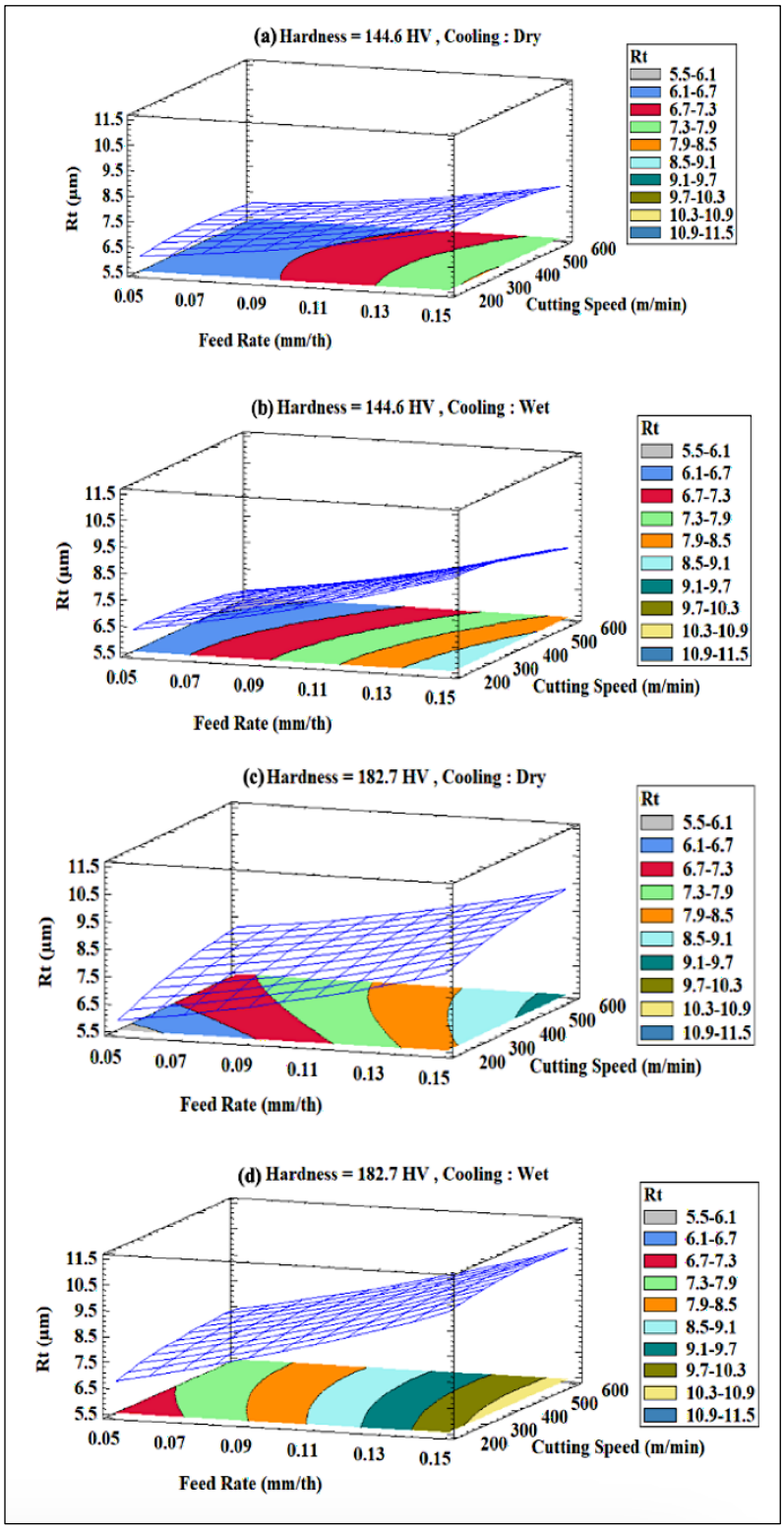


Figure 4.27 3D Surface plots of Rt in different Hardness and cooling mode for Al-Li-Cu-Sc

## 4.3 Effect of Material and it's Hardness on Surface Roughness and Machinability:

### 4.3.1 Al-Li Alloy

By eliminating insignificant variables and concentrating exclusively on significant factors influencing surface roughness (Ra), it becomes feasible to establish a mathematical correlation among them. Equation 4.1 shows the regression equation, with f representing the feed rate ($0.05 < f < 0.15$), v indicating the cutting speed ($200 < v < 600$), h denoting the hardness (56 HV, 76.5 HV and 97 HV), and c representing the cooling mode (-1 and +1).

$$R_a = 0.8254 + 15.8364 \times f - 0.0013 \times v - 0.8202 \times c - 0.0146 \times f \times v - 2.5966 \times f \times c + 0.0009 \times v \times c - 0.1201 \times h^2 + 0.2121 \times h \times c, \; R^2 = 86.74\% \qquad (4.1)$$

To evaluate the effect of feed rate and cutting speed on surface roughness, the cooling mode was kept constant (dry) in the equation above. Surface roughness was then assessed for Al-Li alloy at three levels of hardness: high, medium, and low.

By examining the main effect plots of the Al-Li alloy across different hardness levels, it is evident that surface roughness increases with higher feed rates and decreases with higher cutting speeds in all three cases. Additionally, the best surface roughness among the three hardness levels is achieved with the lowest feed rate (0.05 mm/th) and the highest cutting speed (600 m/min) for the Al-Li alloy with the highest hardness (see Figure 4.28). Figure 4.31 – 4.33 also show the same result.

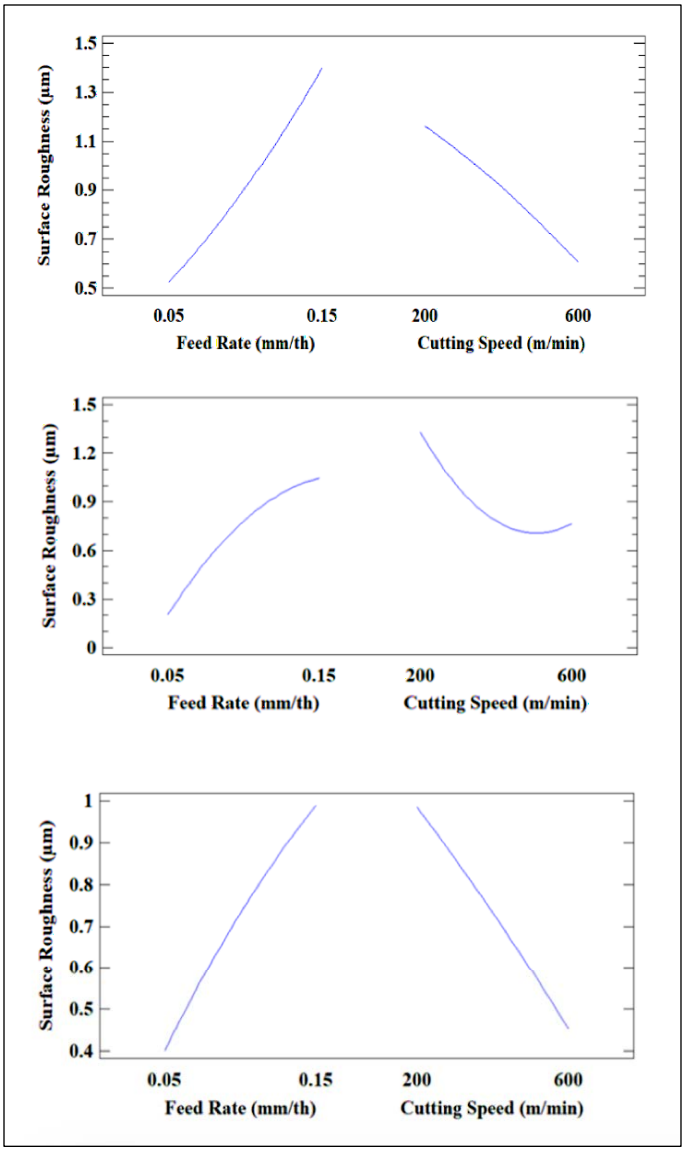


Figure 4.28 Main effects plot for surface response of Al-Li Alloy for (a) lowest hardness, (b) medium hardness and (c) maximum hardness in dry condition

### 4.3.2 Al-Li-Cu Alloy

Based on the Pareto chart (Figure 4.8), the predominant factors influencing Ra are feed rate, hardness, cutting speed, and the interaction between cooling mode-hardness and cutting speed-cooling mode. By focusing on these variables and disregarding the influence of others, the model shows highly significant variables, with an R-squared value of 81.88.

The regression equation representing Ra is provided in Equation 4.2, where feed rate (0.05 < f < 0.15), v indicating the cutting speed (200 < v < 600), h denoting the hardness (129 HV, 146.7 HV and 164 HV), and c representing the cooling mode (-1 and +1).

$$R_a = 0.8557 + 8.1802 \times f - 0.0016 \times v + 0.5449 \times h + 0.0009 \times v \times c - 0.2663h^2 + 0.2111 \times h \times c \quad , R^2 = 81.88\ \%. \tag{4.2}$$

To evaluate the effect of feed rate and cutting speed on surface roughness, the cooling mode was kept constant (dry) in the equation above. Surface roughness was then assessed for Al-Li-Cu alloy at three levels of hardness: high, medium, and low.

By examining the main effect plots of the Al-Li-Cu alloy across different hardness levels, surface roughness increases with higher feed rates and decreases with higher cutting speeds in all three cases. Moreover, the optimal (lowest) surface roughness among the three hardness levels is achieved with the lowest feed rate (0.05 mm/th) and the highest cutting speed (600 m/min) for the Al-Li-Cu alloy with the highest hardness (see Figure 4.29). Figures 4.31 to 4.33 also demonstrate the same result.

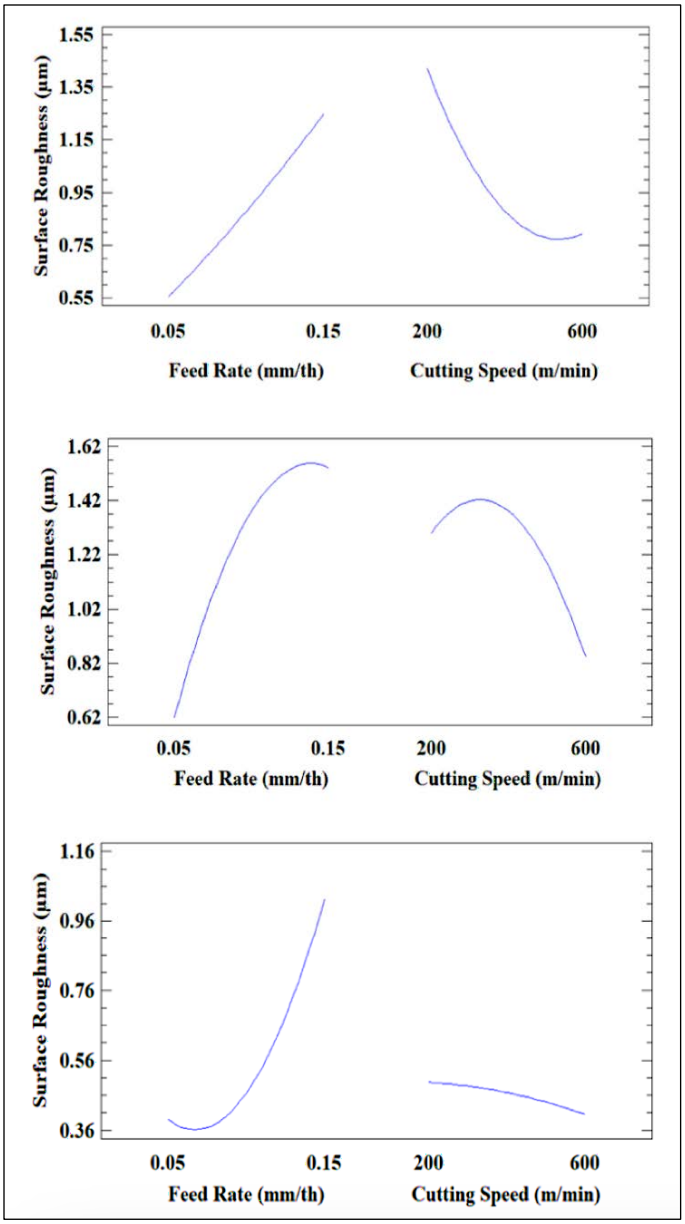


Figure 4.29 Main effects plot for surface response of Al-Li-Cu Alloy for (a) lowest hardness, (b) medium hardness and (c) maximum hardness in dry condition

### 4.3.3 Al-Li-Cu-Sc Alloy

When considering only the influence of feed rate (f), hardness (h), cooling mode (c), and the interaction between cutting speed (v) and hardness, as well as between feed rate (f) and cooling mode (c), the model remains significantly effective in explaining the variation in roughness,

as evidenced by an R-squared value of 80.13%. Equation 4.3 precisely outlines the relationship between the input variables and the resulting surface roughness, denoted as Ra. where feed rate ($0.05 < f < 0.15$), v indicating the cutting speed ($200 < v < 600$), h denoting the hardness (144.6 HV, 163.4 HV and 182.7 HV), and c representing the cooling mode (-1 and +1).

$$R_a = 0.641707 - 4.3509 \times f - 0.2581 \times h - 0.1702 \times c + 3.5253 \times f \times c + 0.0005 \times v \times h, \quad R^2 = 80.13\% \tag{4.3}$$

To evaluate the effect of feed rate and cutting speed on surface roughness, the cooling mode was kept constant (dry) in the equation above. Surface roughness was then assessed for Al-Li-Cu-Sc alloy at three levels of hardness: high, medium, and low.

By examining the main effect plots of the Al-Li-Cu-Sc alloy across different hardness levels, surface roughness increases with higher feed rates. But just in lowest hardness the surface roughness is decreases with increase in cutting speeds. At higher speeds, especially with harder alloys, there is a tendency for material to adhere to the cutting edge of the tool, forming a built-up edge (BUE). This BUE can affect the tool's cutting action and result in a rougher surface.

Here the optimal surface roughness among the three hardness levels is achieved with the lowest feed rate (0.05 mm/th) and the lowest cutting speed (200 m/min) for the Al-Li-Cu-Sc alloy with the medium hardness (see Figure 4.30). and a low hardness alloy (with lowest feed rate and cutting speed) surface roughness is also close to the medium hardness one. Figures 4.31 to 4.33 also demonstrate the same result.

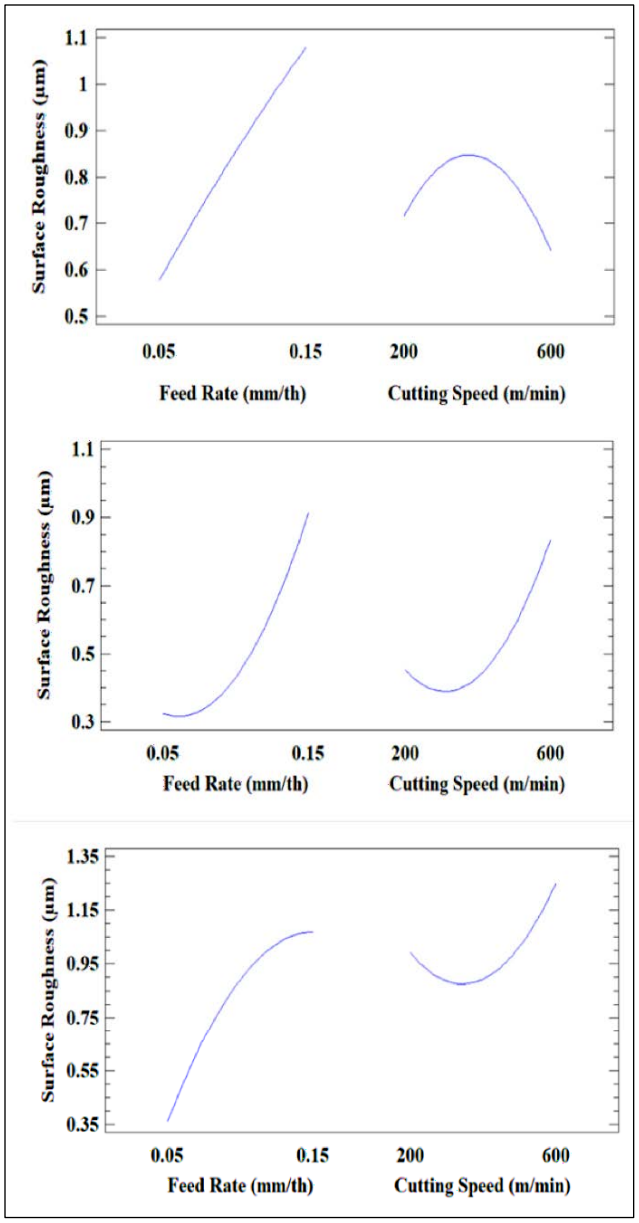


Figure 4.30 Main effects plot for surface response of Al-Li-Cu-Sc Alloy for (a) lowest hardness, (b) medium hardness and (c) maximum hardness in dry condition

## 4.4 Summary of Surface Roughness Statistical Analysis for Al-Li, Al-Li-Cu and Al-Li-Cu-Sc alloys

Figures 4.31 to 4.34 illustrating the behavior and performance of Al-Li, Al-Li-Cu, and Al-Li-Cu-Sc alloys under various conditions of cutting speed, feed rate, and cooling mode. These figures present detailed statistical analyses of surface roughness for these alloys.

Figure 4.31 illustrates the behavior of the three alloys at a low cutting speed of 200 m/min under different cooling conditions and feed rates. Under dry cooling with a feed rate of 0.05 mm/th (Figure 4.31-a), Al-Li alloy exhibits moderate roughness, Al-Li-Cu alloy shows higher roughness, while Al-Li-Cu-Sc alloy demonstrates the lowest roughness. When wet cooling is applied at the same feed rate (Figure 4.31-b), the roughness of Al-Li alloy decreases, while Al-Li-Cu remains high, and Al-Li-Cu-Sc exhibits moderate roughness. For a higher feed rate of 0.15 mm/th under dry cooling (Figure 4.31-c), Al-Li alloy shows the highest roughness, Al-Li-Cu alloy still maintains high roughness, and Al-Li-Cu-Sc alloy presents lower roughness. Wet cooling at this higher feed rate (Figure 4.31-d) results in moderate roughness for Al-Li, high roughness for Al-Li-Cu, and moderate roughness for Al-Li-Cu-Sc.

H1, H2, H3 and H4 are different heat treatments which are described in table 4.1

Table 4.1 Description of different heat treatments

| Alloy | Heat Treatment | | Hardness (HV) |
|---|---|---|---|
| Al-Li | 580 °C/1 h + 130 °C /1 h | H1 | 56 |
| Al-Li | 580 °C/1 h + 150 °C / 45 h | H2 | 97 |
| Al-Li-Cu | 505 °C/5 h + 200 °C / 25 h | H3 | 129 |
| Al-Li-Cu | 505 °C/5 h + 180 °C / 20 h | H4 | 164 |
| Al-Li-Cu-Sc | 505 °C/5 h + 200 °C / 25 h | H5 | 144.6 |
| Al-Li-Cu-Sc | 505 °C/5 h + 180 °C / 20 h | H6 | 182.7 |

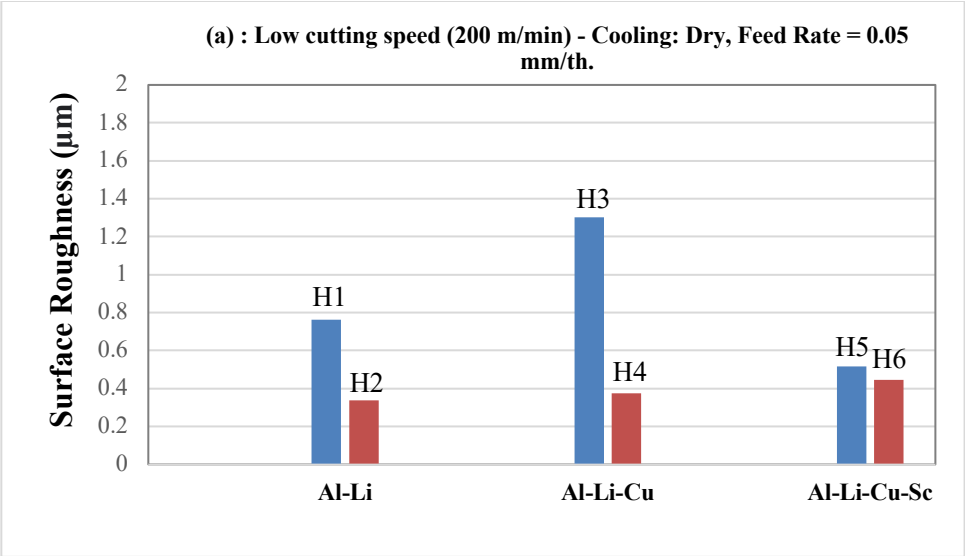
(a) : Low cutting speed (200 m/min) - Cooling: Dry, Feed Rate = 0.05 mm/th.
Surface Roughness (µm)
2
1.8
1.6
1.4
1.2
1
0.8
0.6
0.4
0.2
0
H1
H2
H3
H4
H5
H6
Al-Li
Al-Li-Cu
Al-Li-Cu-Sc

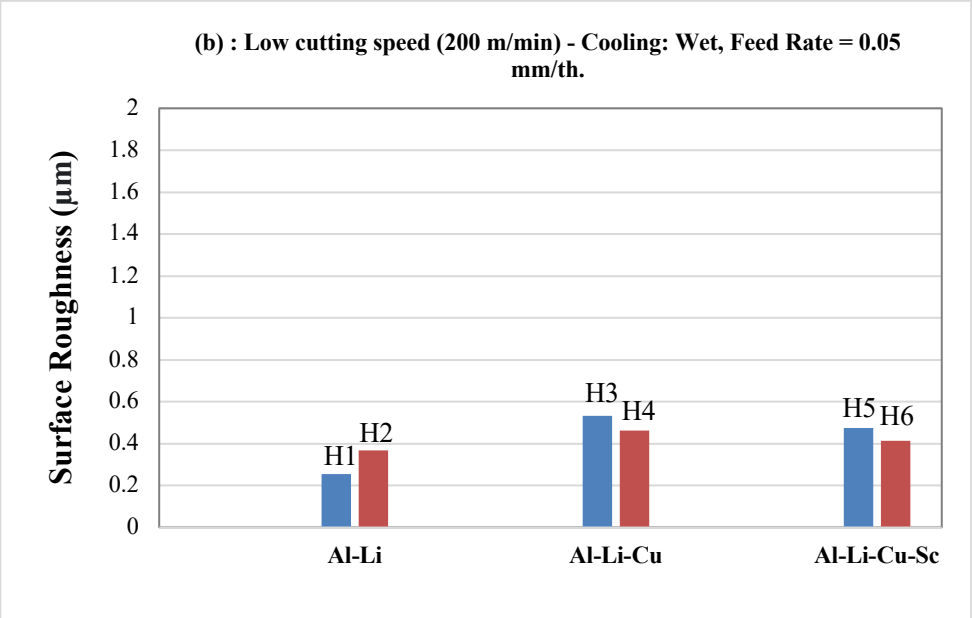
(b) : Low cutting speed (200 m/min) - Cooling: Wet, Feed Rate = 0.05 mm/th.
Surface Roughness (µm)
2
1.8
1.6
1.4
1.2
1
0.8
0.6
0.4
0.2
0
H1
H2
H3
H4
H5
H6
Al-Li
Al-Li-Cu
Al-Li-Cu-Sc

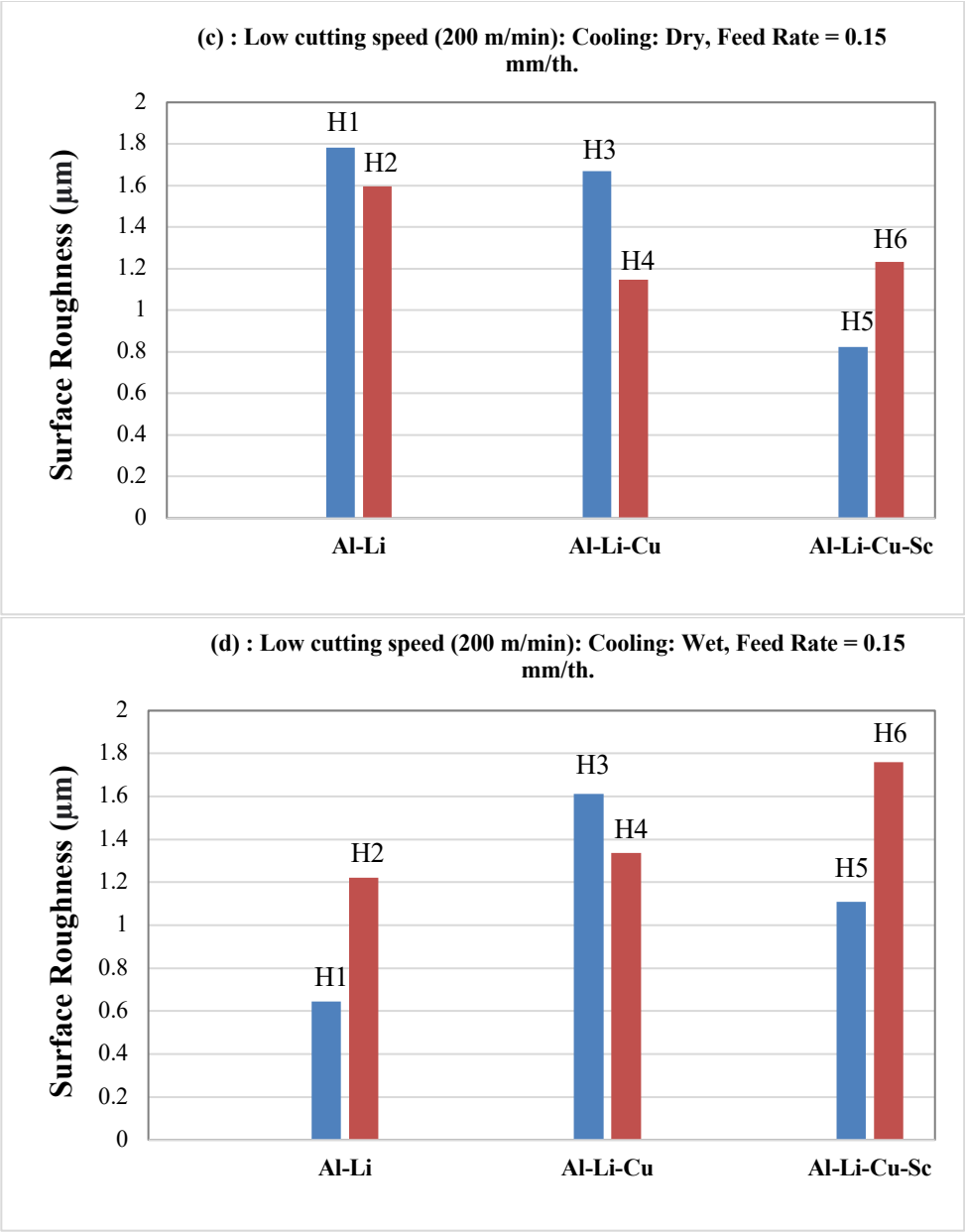


Figure 4.31 Behavior of the Al-Li, Al-Li-Cu and Al-Li-Cu-Sc alloys when using low cutting speed (200 m/min):
a) Cooling: Dry, Feed Rate = 0.05 mm/th,
b) Cooling: Wet, Feed Rate = 0.05 mm/th,
c) Cooling: Dry, Feed Rate = 0.15 mm/th,
d) Cooling: Wet, Feed Rate = 0.15 mm/th

Figure 4.32 depicts the behavior of the alloys at a high cutting speed of 600 m/min under various cooling and feed rate conditions. With dry cooling at a feed rate of 0.05 mm/th (Figure 4.32-a), Al-Li alloy exhibits low roughness, Al-Li-Cu alloy shows slightly higher roughness, and Al-Li-Cu-Sc alloy has the lowest roughness. When wet cooling is applied at the same feed rate (Figure 4.32-b), Al-Li alloy achieves the lowest roughness, Al-Li-Cu displays moderate roughness, and Al-Li-Cu-Sc presents low roughness. For a higher feed rate of 0.15 mm/th under dry cooling (Figure 4.32-c), Al-Li alloy shows moderate roughness, Al-Li-Cu has higher roughness, and Al-Li-Cu-Sc exhibits the lowest roughness. Wet cooling at this feed rate (Figure 4.32-d) results in low roughness for Al-Li, higher roughness for Al-Li-Cu, and low roughness for Al-Li-Cu-Sc.

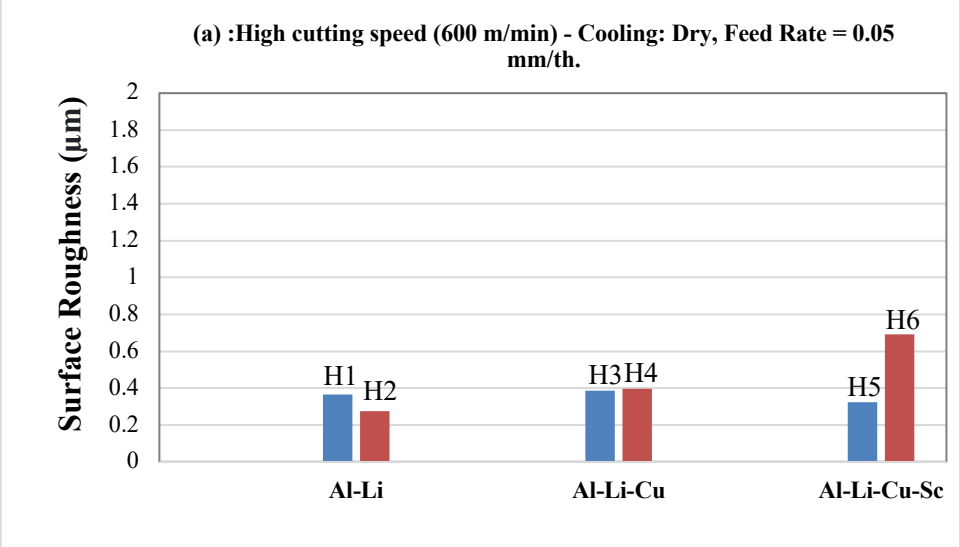
(a) :High cutting speed (600 m/min) - Cooling: Dry, Feed Rate = 0.05 mm/th.
Surface Roughness (µm)
2
1.8
1.6
1.4
1.2
1
0.8
0.6
0.4
0.2
0
H1
H2
H3
H4
H5
H6
Al-Li
Al-Li-Cu
Al-Li-Cu-Sc

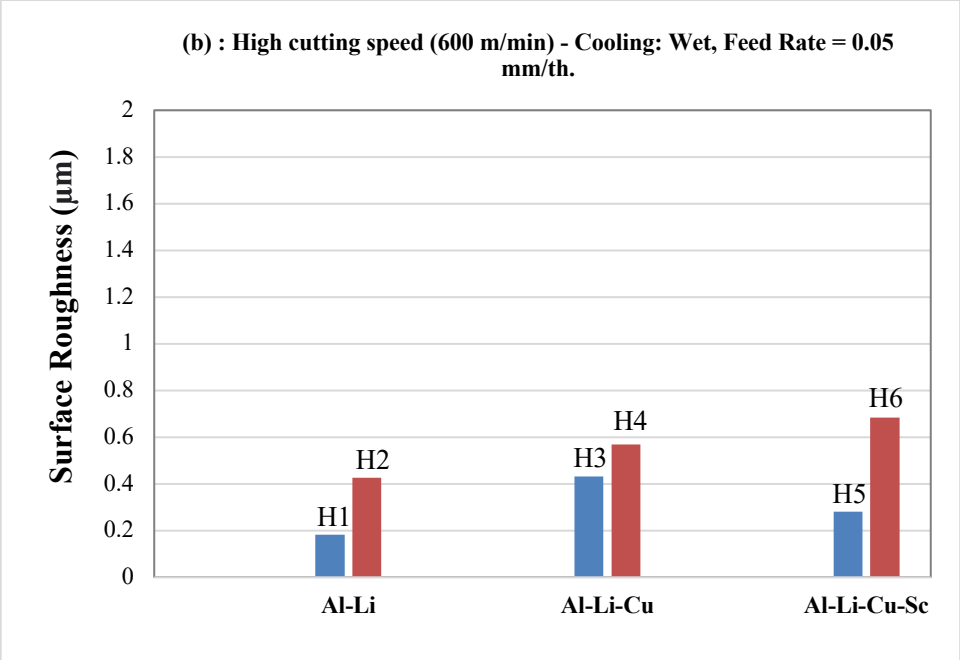
(b) : High cutting speed (600 m/min) - Cooling: Wet, Feed Rate = 0.05 mm/th.
Surface Roughness (µm)
2
1.8
1.6
1.4
1.2
1
0.8
0.6
0.4
0.2
0
H1
H2
H3
H4
H5
H6
Al-Li
Al-Li-Cu
Al-Li-Cu-Sc

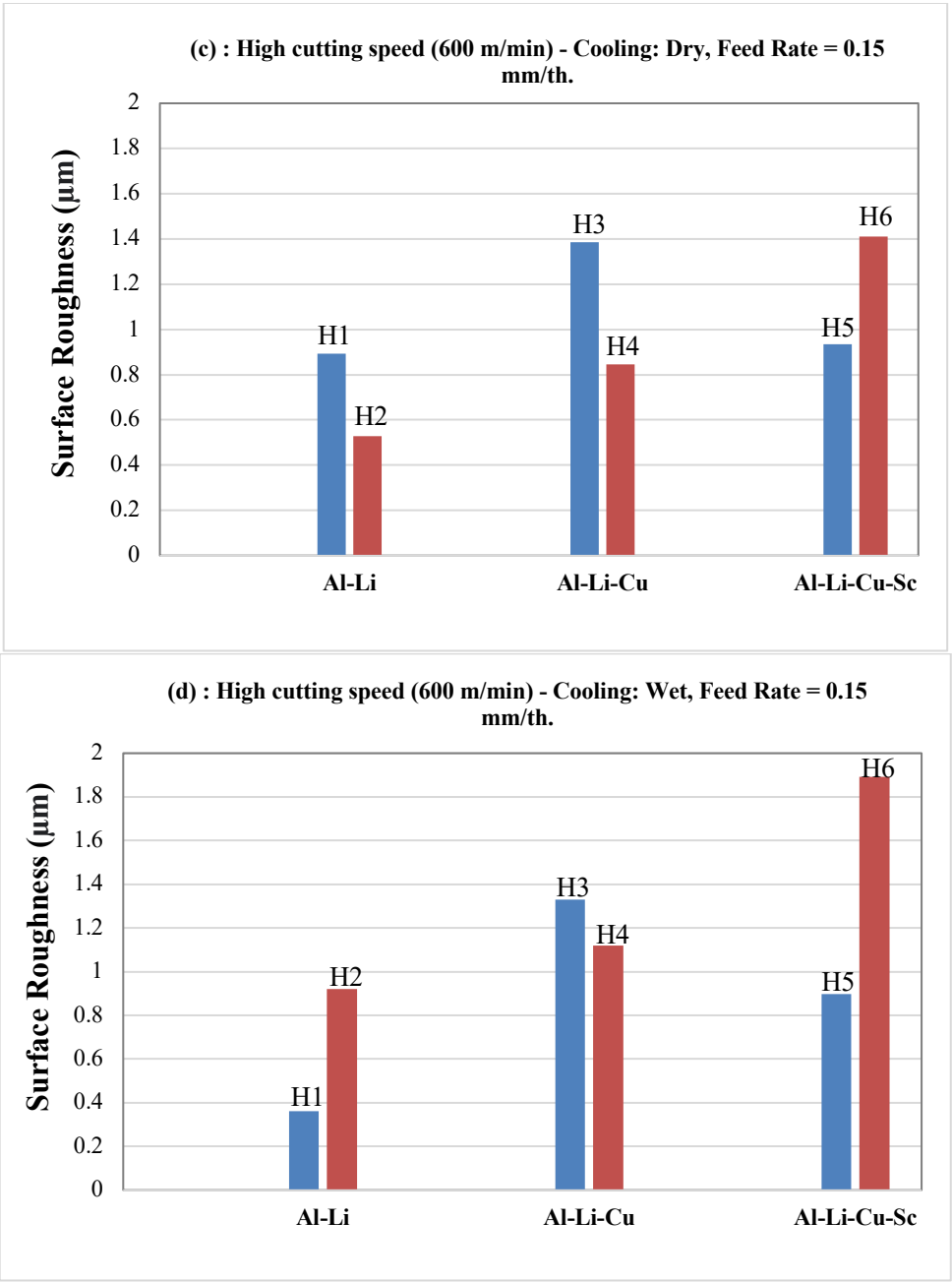


Figure 4.32 Behavior of the Al-Li, Al-Li-Cu and Al-Li-Cu-Sc alloys when using high cutting speed (600 m/min):

a) Cooling: Dry, Feed Rate = 0.05 mm/th,
b) Cooling: Wet, Feed Rate = 0.05 mm/th,
c) Cooling: Dry, Feed Rate = 0.15 mm/th,
d) Cooling: Wet, Feed Rate = 0.15 mm/th

The analysis indicates that Al-Li-Cu alloy generally shows higher surface roughness compared to Al-Li and Al-Li-Cu-Sc alloys under most conditions. Al-Li-Cu-Sc alloy often shows the lowest roughness, indicating better performance in terms of surface finish. The effect of cooling mode and feed rate varies, but wet cooling tends to reduce surface roughness compared to dry cooling across all alloys and conditions. The roughness also generally increases with feed rate, and the trends are consistent across both low and high cutting speeds.

## 4.5 Conclusions

Based on the analysis of the machining process for Al-Li, Al-Li-Cu, and Al-Li-Cu-Sc alloys, it is evident that several factors significantly influence surface roughness and quality. These factors include feed rate, cutting speed, hardness, and cooling mode.

Among the three, Al-Li alloy shows minimal impact of hardness (56 – 97 HV), with surface roughness largely unaffected by hardness variations and improved by increased cutting speed and wet cooling. Al-Li-Cu alloy demonstrates greater sensitivity to hardness, with higher hardness levels enhancing surface quality due to a stable microstructure. It achieves the best machining results overall, as higher cutting speeds and hardness improve surface roughness, while higher feed rates worsen it. In contrast, Al-Li-Cu-Sc alloy is the most complex to machine due to significant interactions between feed rate, cutting speed, and hardness. It achieves the smoothest surface (0.61 μm) at the highest hardness (182.7 HV) and cutting speed but exhibits higher roughness (1.20 μm) at the lowest hardness and cutting speed.

Overall, Al-Li alloy is the easiest to machine due to its straightforward response to machining parameters, while Al-Li-Cu alloy offers the best machinability and performance, combining smoother surfaces and better adaptability across varying conditions. Al-Li-Cu-Sc alloy, although more challenging to machine, highlights the importance of precise control over machining parameters to achieve optimal results.

# CHAPITRE 5

# RESULTS AND DISCUSSION OF CUTTING FORCE

## 5.1 Introduction

Cutting force analysis is a critical aspect of machining operations, providing valuable insights into the forces exerted during material removal processes. Understanding cutting forces and their impact is essential for improving machining performance, ensuring dimensional accuracy, and prolonging tool life. Cutting force analysis helps in assessing the efficiency and effectiveness of machining processes. It provides valuable information for selecting appropriate cutting tools, determining optimal cutting speeds and feed rates, and minimizing tool wear and breakage.

Various factors affect cutting forces, including material properties (such as hardness, ductility, and thermal conductivity), cutting tool geometry, cutting parameters (such as depth of cut, feed rate, and cutting speed), workpiece geometry, and machining conditions (such as temperature, lubrication, and vibration).

Cutting forces have a direct impact on tool wear, tool life, and machining accuracy. By choosing an appropriate cutting parameters to minimize cutting forces, manufacturers can improve tool life, reduce machining costs, and enhance overall process efficiency.

Cutting force analysis also plays a crucial role in predicting and preventing machining-related issues such as chatter, vibration, and tool deflection, which can compromise surface finish quality and dimensional accuracy (Childs 2000; Meng, Lin, and Mi 2021; Pathak, Sahoo, and Mishra 2013; Korkmaz et al. 2024).

In the following section, we will conduct a detailed statistical analysis of the cutting force outcomes. This analysis aims to investigate how workpiece characteristics, particularly microhardness, along with several process parameters including feed rate, cutting speed, and cooling mode, impact the overall machining conditions.

In the forthcoming section, we will conduct a statistical examination of the cutting force outcomes. This analysis aims to investigate how workpiece characteristics, particularly microhardness, and different machining parameters, including feed rate, cutting speed, and cooling method, affect machining conditions.

## 5.2 The Statistical Analysis of Cutting Force in Machining of Al-Li Alloy

An ANOVA analysis was performed on the cutting force data, aiming to explore the impacts of various independent variables such as feed rate, cutting speed, microhardness, and cooling mode on the cutting force during the milling process of Al-Li alloy.

The model successfully explains 88.95% of the variation in cutting force attributed to the mentioned factors. Further details of the ANOVA analysis are provided in Table AII.7.

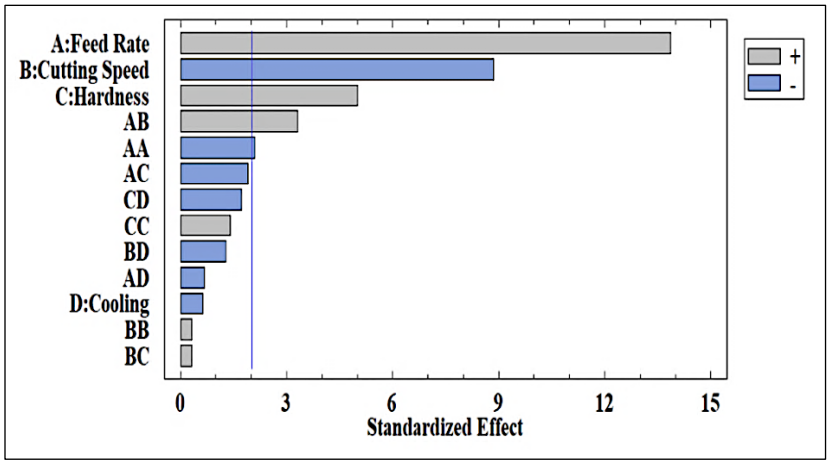


Figure 5.1 Pareto chart of cutting force for Al-Li alloy

Feed rate is the most influential parameter, with cutting force increasing by approximately 53.05 N as feed rate rises from 0.05 to 0.15 mm/th (Figures 5.1 and 5.2-a). This aligns with findings by Songmene et al. and Akram et al. (Songmene et al. 2011; Akram et al. 2015), where higher feed rates resulted in greater cutting forces due to the removal of thicker chips and

increased material volume. Higher feed rates also generate more heat from friction between the tool and workpiece, causing the material to soften and deform more easily. Consequently, thicker chips and elevated thermal effects collectively demand greater cutting force.

As cutting speed increases from 200 to 600 m/min, cutting force decreases from 145.08 N to 111.19 N (Figure 5.2-b). This reduction is attributed to thermal softening and thinner, more manageable chips at higher speeds, consistent with findings by Thi-Hoa et al. and Srivastava et al. (Thi-Hoa et al. 2018; Srivastava et al. 2021). These trends underscore the importance of cutting speed in reducing tool resistance and improving machining efficiency.

Alloy with higher hardness (97 HV) increases cutting force by 19.15 N compared to material with lower hardness (56 HV), as shown in Figure 5.2-c. Materials with higher hardness resist deformation more, requiring greater force for chip formation. This trend aligns with studies by Pathak et al. and Gökkaya (Pathak, Sahoo, and Mishra 2013; Gökkaya 2010), which report higher cutting forces in harder aluminum alloys due to increased material strength.

Cooling conditions (dry vs. wet) have negligible impact on cutting force, as shown in Figure 5.2-d and supported by 3D plots (Figures 5.4-a to 5.4-d). This contrasts with studies by Kishawy et al. (Kishawy et al. 2005), where wet cooling reduced cutting forces by lowering tool temperature. The unique properties of Al-Li alloy, which maintains consistent behavior regardless of cooling, explain this discrepancy.

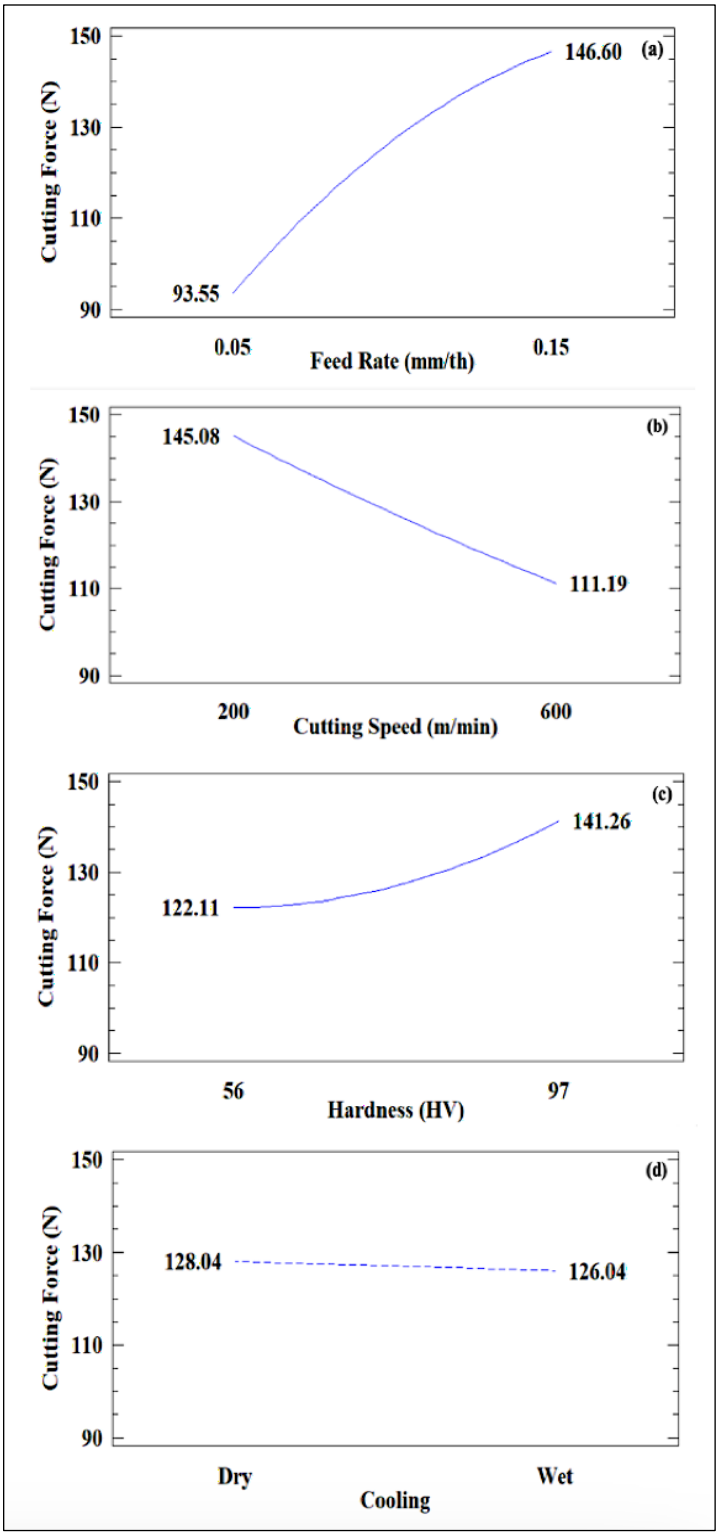


Figure 5.2 Main effects plot for cutting force in machining of Al-Li alloy

Feed rate and cutting speed interactions significantly affect cutting force. At higher speeds (600 m/min), cutting force is lower across feed rates, with a notable difference of 53 N at lower feed rates (0.05 mm/th), diminishing to 20 N at higher feed rates (0.15 mm/th) (Figure 5.3-a). Similarly, hardness and feed rate interactions show increased cutting force for harder materials, though differences diminish slightly at higher feed rates (Figure 5.3-b).

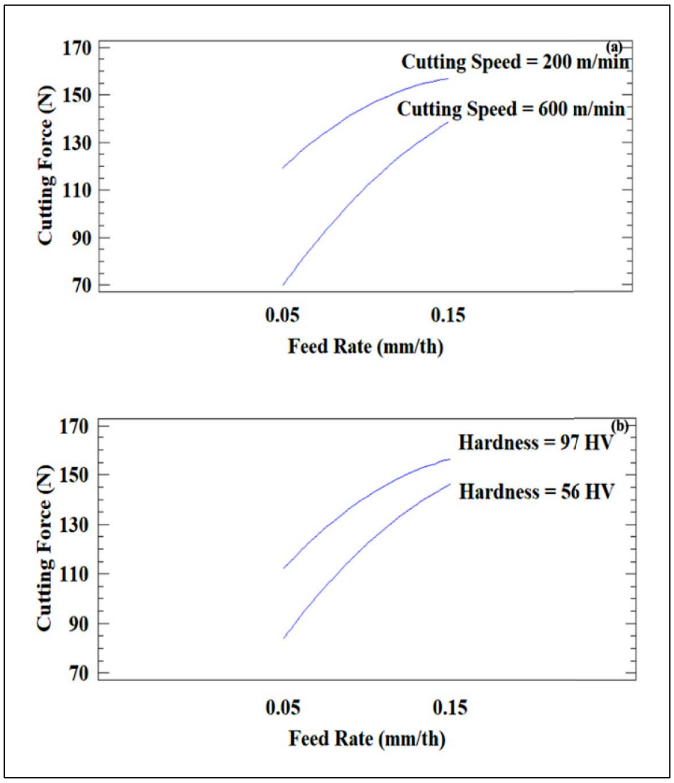


Figure 5.3 Interaction plot for cutting force in Al-Li alloy machining

As illustrated by the Pareto chart (Figure 5.1), cooling does not exert a significant influence on cutting force. Transitioning from dry to wet conditions results in the cutting force remaining nearly constant, as observed in 3D plots (Figures 5.4-a and 5.4-b). This trend persists even at higher hardness levels, as depicted in Figures 5.4-c and 5.4-d.

With an increase in hardness, a slight but noticeable change occurs, which is more pronounced in dry conditions and at lower feed rates (0.05 mm/th) and higher cutting speeds (600 m/min).

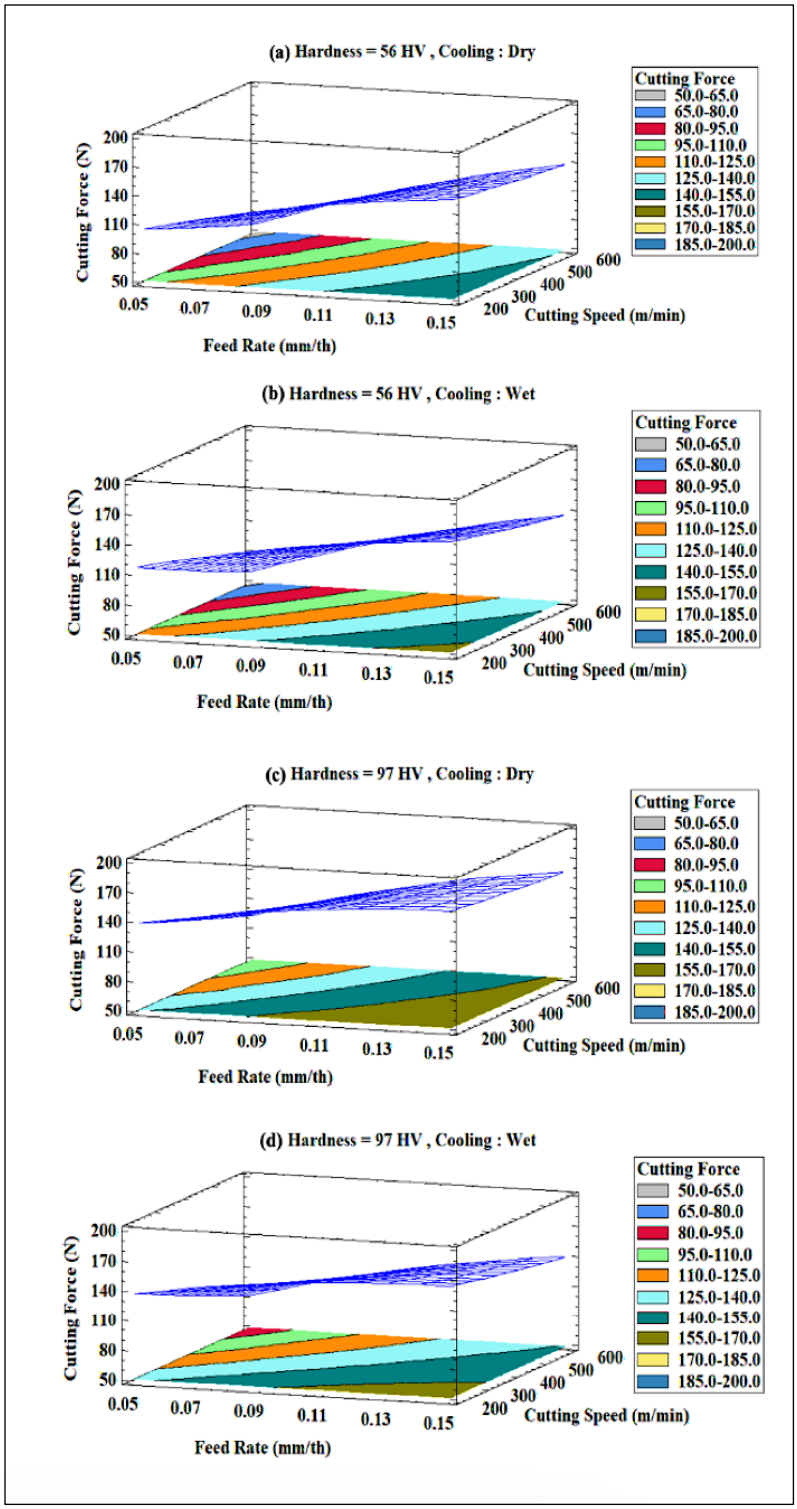


Figure 5.4 3D surface plots of cutting force in different hardness and cooling mode for Al-Li alloy

## 5.3 The Statistical Analysis of Cutting Force in Machining of Al-Li-Cu Alloy

The cutting force outcomes derived from Al-Li-Cu alloy machining are outlined in Table AI.8. The statistical analysis conducted on the cutting force results yields an R-squared value of 93.18%, indicating that the model accounts for nearly 93% of the variability in cutting force based on the analyzed variables. The ANOVA details can be found in Table AII.8.

In the context of Al-Li-Cu machining, the most influential factor impacting cutting force is the feed rate, as highlighted in the Pareto chart (Figure 5.5). Following the feed rate in terms of significance are hardness, the interaction between feed rate and hardness, and cooling mode.

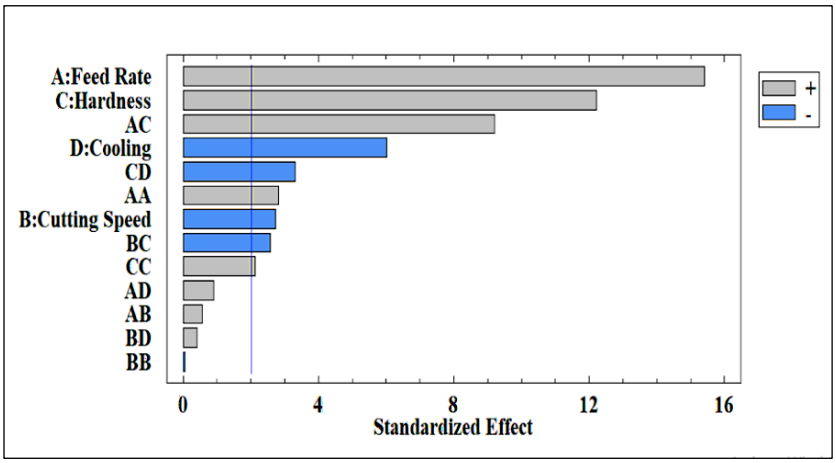


Figure 5.5 Pareto chart of cutting force for Al-Li-Cu alloy

As feed rate increases from 0.05 to 0.15 mm/th, cutting force rises by approximately 34.83 N (Figure 5.6-a). This increase aligns with studies by Kiswanto et al. and Gökkaya (Kiswanto, Zariatin, and Ko 2014; Gökkaya 2010), which link higher feed rates to greater material removal per unit time and larger chip formation. The additional material volume and chip load necessitate more force to shear and remove material. This behavior is consistent across aluminum alloys, as confirmed by Venkatesan et al. and Srivastava et al. (Venkatesan et al. 2014; Srivastava et al. 2021). For the Al-Li-Cu alloy, this trend is particularly pronounced due to its relatively high strength and ductility, requiring careful optimization of feed rate to balance productivity and tool wear.

The variation in cutting speed (200–600 m/min) resulted in a slight reduction in cutting force (approximately 5.15 N or 2–3%), as shown in Figure 5.6-b. This minor decrease can be attributed to thermal softening and more efficient chip removal at higher speeds, trends observed in studies by Campos et al. and Duan et al. (Campos, Mougo, and Araujo 2017; Duan, Li, et al. 2021). Although less impactful than feed rate, cutting speed remains a critical parameter for managing heat generation and reducing tool resistance. The reduced cutting force at higher speeds aligns with broader trends in aluminum alloys, reinforcing cutting speed's role in enhancing machining efficiency.

Hardness significantly affects cutting force, with alloys with higher hardness (164 HV) requiring 27.66 N more force than ones with lower hardness (129 HV) (Figure 5.6-c). This correlation is supported by El-Kady et al. and Kaya et al. (El-Kady et al. 2015; Kaya et al. 2012), who found that increased hardness in aluminum alloys and composites raises cutting resistance due to greater material strength. For Al-Li-Cu, the presence of copper-rich precipitates (e.g., θ' or T1 phases) further contributes to increased cutting forces, as these precipitates enhance alloy strength by impeding dislocation movement, making the material more resistant to shearing (Figure 3.3-a).

Wet cooling reduces cutting force by approximately 11 N compared to dry machining (Figure 5.6-d). This reduction is attributed to improved lubrication and chip evacuation, as well as stabilized thermal gradients that prevent localized softening of the workpiece. These findings align with studies by Namlu et al. and Kouam et al. (Namlu et al. 2019; Kouam et al. 2012), which demonstrated that wet machining lowers cutting forces through effective cooling and lubrication. The effect is more pronounced for alloys with higher hardness, as shown in Figure 5.7-b, where cutting force under dry conditions is 20 N higher for the alloy with higher hardness (164 HV) than in wet conditions. Cooling mitigates thermal degradation of precipitates, preserving hardness and minimizing cutting resistance.

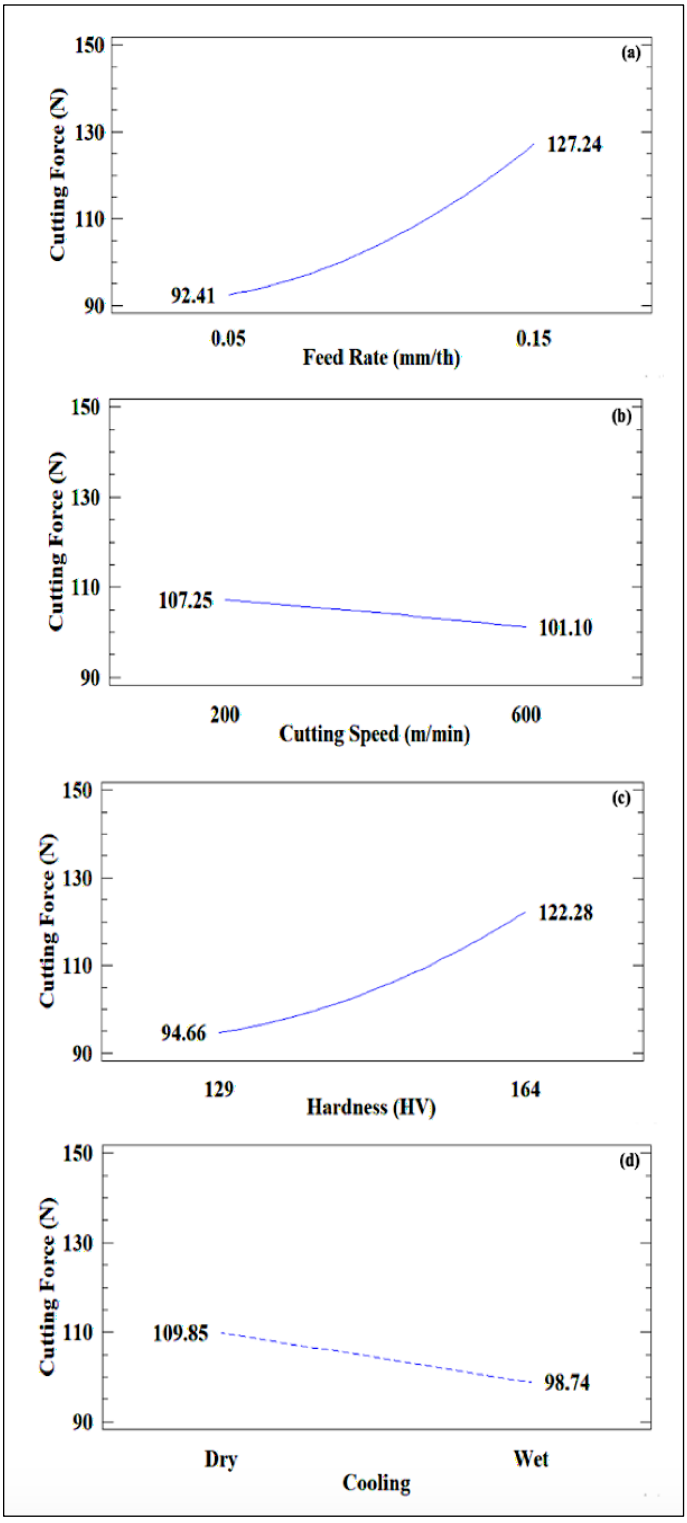


Figure 5.6 Main effects plot for cutting force in machining of Al-Li-Cu alloy

The interplay between feed rate and hardness significantly impacts cutting force. At low feed rates (0.05 mm/th), both alloys with higher and lower hardness require approximately 95 N of force. However, at high feed rates (0.15 mm/th), the alloy with higher hardness requires over 60 N more force than the alloy with lower hardness (Figure 5.7-a). This is due to the harder material's greater resistance to deformation, amplified by the increased chip load at higher feed rates.

Cooling mode interacts similarly with hardness, as the cutting force disparity between dry and wet conditions is negligible for the alloy with lower hardness but substantial (20 N) for the alloy with higher hardness (Figure 5.7-b). This difference highlights cooling's role in stabilizing microstructural phases under high thermal conditions, which is crucial for alloys with higher hardness prone to localized thermal degradation during dry machining.

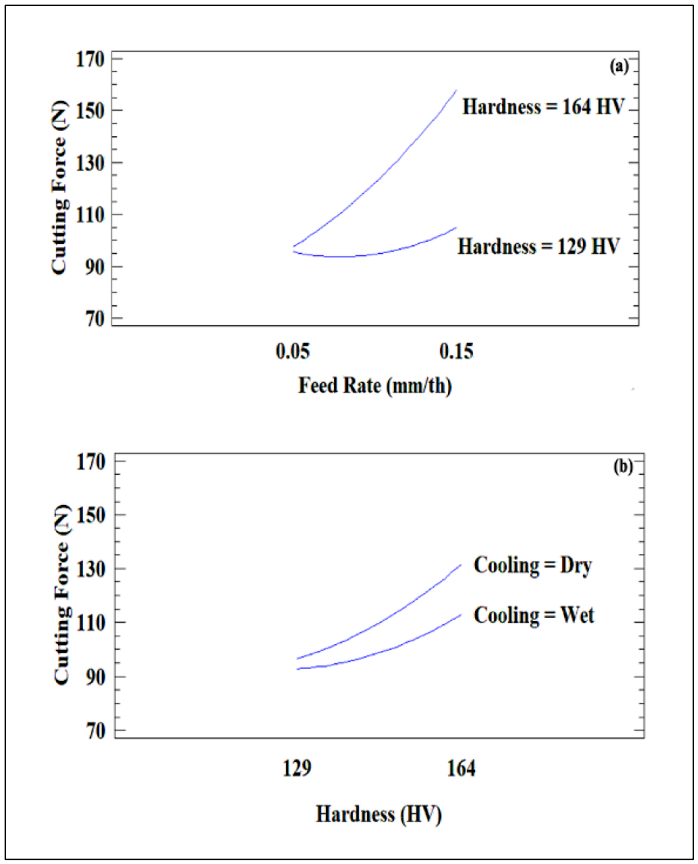


Figure 5.7 Interaction plot for cutting force in Al-Li-Cu alloy

The 3D plots (Figure 5.8) reveal that increased hardness significantly raises cutting forces, particularly at higher feed rates (0.15 mm/th). Wet cooling reduces cutting force for the alloy with higher hardness (164 HV), stabilizing the material's hardness by maintaining consistent temperatures. However, for the alloy with lower hardness (129 HV), the impact of cooling is minimal, as its microstructure remains less sensitive to thermal fluctuations.

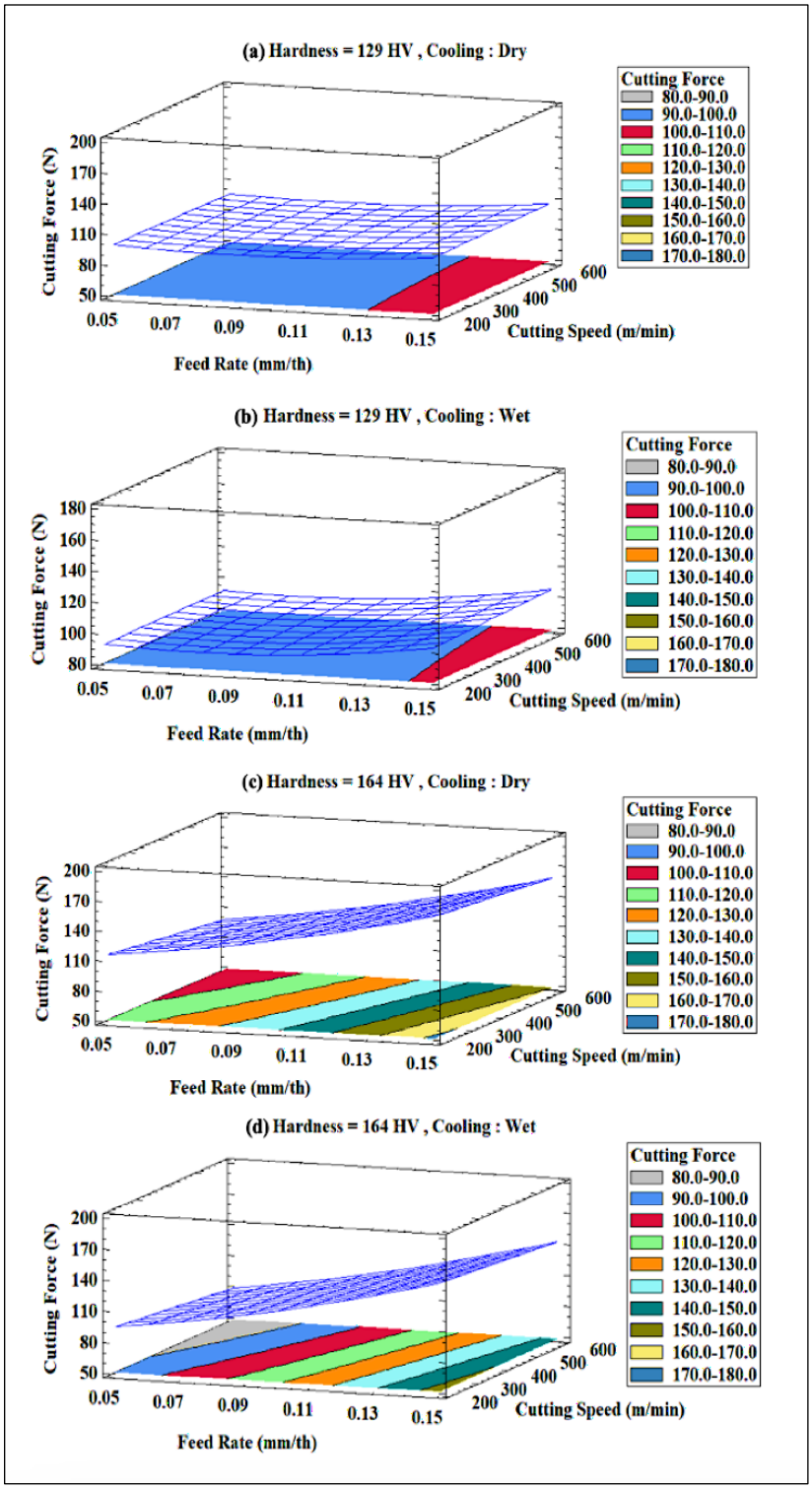


Figure 5.8 3D Surface plots of cutting force in different hardness and cooling mode for Al-Li-Cu alloy

## 5.4 The Statistical Analysis of Cutting Force in Machining of Al-Li-Cu-Sc Alloy

The machining process of the Al-Li-Cu-Sc alloy demonstrates a notable sensitivity to variations in cutting parameters. Specifically, the developed model effectively accounts for 96.27 % of the observed variability in cutting force, indicating a clear correlation between the selected cutting parameters and the resulting cutting force.

The ANOVA table for the statistical analysis of the Al-Li-Cu-Sc alloy is provided in Table AII.9. In the Pareto chart (Figure 5.9), which illustrates all independent variables and their interactions, all parameters are exceed the threshold indicated by the blue line.

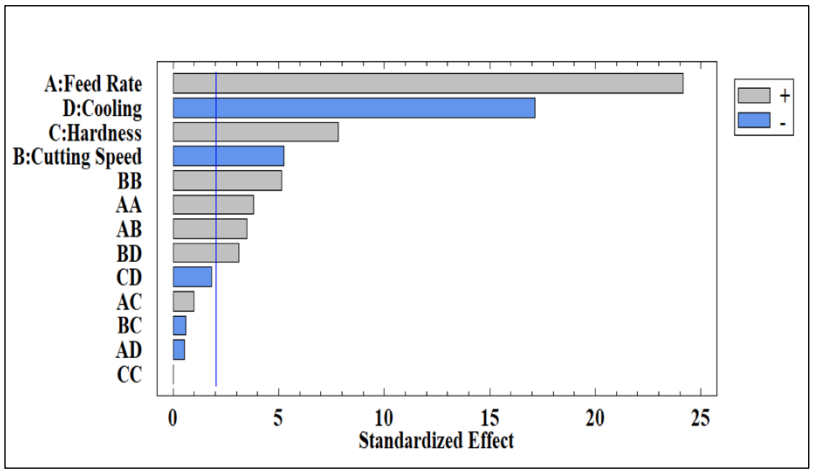


Figure 5.9 Pareto chart of cutting force for Al-Li-Cu-Sc alloy

Feed rate is the most influential parameter, with cutting force increasing from 95.54 N at a low feed rate (0.05 mm/th) to 158.09 N at a high feed rate (0.15 mm/th), an increase of 63 N (Figure 5.10-a). This aligns with Zha et al. and Wang et al. (Zha et al. 2024; Wang et al. 2016), who found that higher feed rates in titanium and aluminum alloys result in greater chip loads, requiring more force for material removal. Similarly, Sequeira et al. (Sequeira et al. 2012) observed increased cutting forces at higher feed rates in aluminum components due to thicker chips. For Al-Li-Cu-Sc alloy, feed rate directly impacts cutting force, emphasizing the need for optimal parameter selection to balance efficiency and tool wear.

Increasing cutting speed from 200 to 600 m/min reduces cutting force from 136.58 N to 122.95 N, a modest decrease (Figure 5.10-b). This reduction stems from thermal softening of the material, improved chip formation, and reduced friction, as supported by studies by Kumar et al. and Giasin et al. (Kumar, Mahapatra, and Jha 2014; Giasin et al. 2016). While the decrease is less pronounced in Al-Li-Cu-Sc, optimizing cutting speed is crucial to manage cutting forces and enhance machining efficiency.

Hardness significantly affects cutting force, materials with higher hardness (182.7 HV) requiring 128.45 N compared to 108.15 N for materials with lower hardness (144.6 HV) (Figure 5.10-c). The increase in cutting force is due to the greater resistance of materials with higher hardness to deformation, as highlighted by Kaya et al. and Tash et al. (Kaya et al. 2012; Tash et al. 2007). Hardness changes caused by heat treatments alter the alloy's microstructure, increasing cutting forces. For Al-Li-Cu-Sc, the presence of fine scandium precipitates further enhances hardness, increasing resistance to cutting forces during machining.

Wet machining significantly reduces cutting force, from 100.11 N in dry conditions to 36.38 N under wet conditions (Figure 5.10-d). Cooling fluids lower cutting forces by reducing friction, heat generation, and tool wear, consistent with studies by Boswell et al. and Jebaraj et al. (Boswell et al. 2017; Jebaraj and Pradeep Kumar 2019). For Al-Li-Cu-Sc alloys, cooling stabilizes the microstructure by preventing thermal degradation, maintaining material integrity, and reducing cutting force variability.

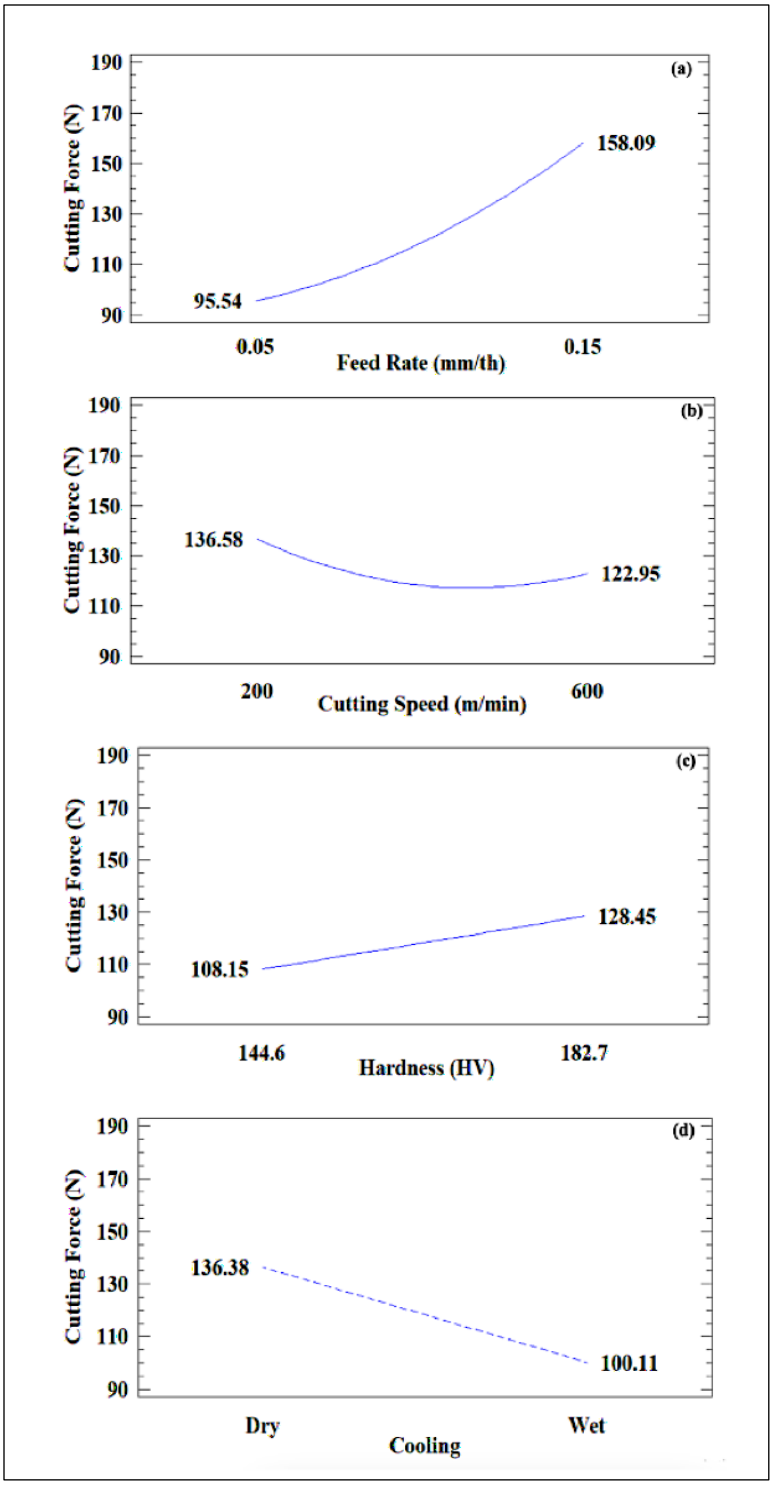


Figure 5.10 Main effects plot for cutting force in machining of Al-Li-Cu-Sc

Feed rate and cutting speed interactions significantly influence cutting force. At low feed rates (0.05 mm/th), higher cutting speeds (600 m/min) reduce cutting force by 25 N compared to 200 m/min (Figure 5.11-a). Similarly, wet cooling mitigates cutting force at all cutting speeds, with the relative reduction remaining constant across conditions (Figure 5.11-b).

Hardness and feed rate interactions show a more substantial cutting force difference at higher feed rates (0.15 mm/th), particularly under dry conditions, where thermal effects amplify resistance (Figures 5.12-a and 5.12-c). Wet machining reduces this disparity, stabilizing cutting forces for both alloys with higher and lower hardness, especially at lower feed rates (Figures 5.12-b and 5.12-d).

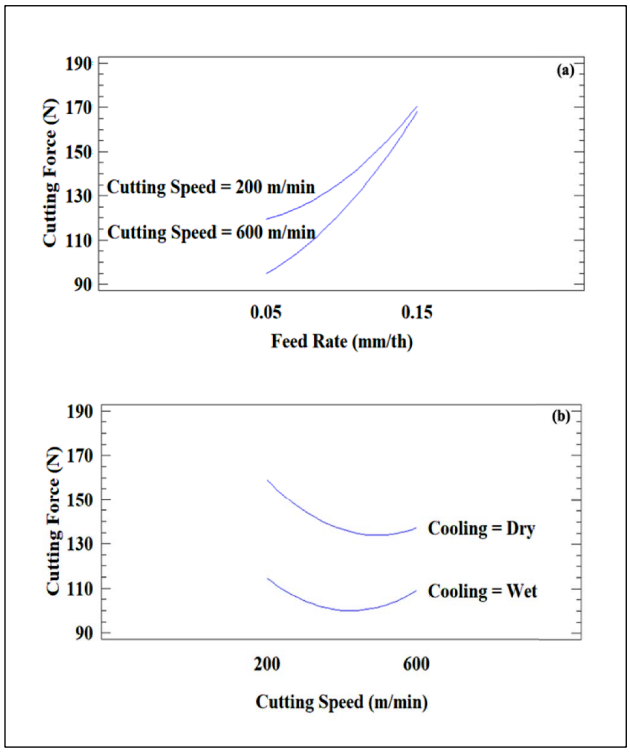


Figure 5.11 Interaction plot for cutting force in Al-Li-Cu-Sc alloy

The 3D plots (Figure 5.12) confirm that increased hardness and feed rate significantly raise cutting force, particularly under dry conditions. Wet cooling moderates these effects, maintaining nearly constant cutting forces for alloys with lower hardness and mitigating increases for alloys with higher hardness, particularly at low feed rates.

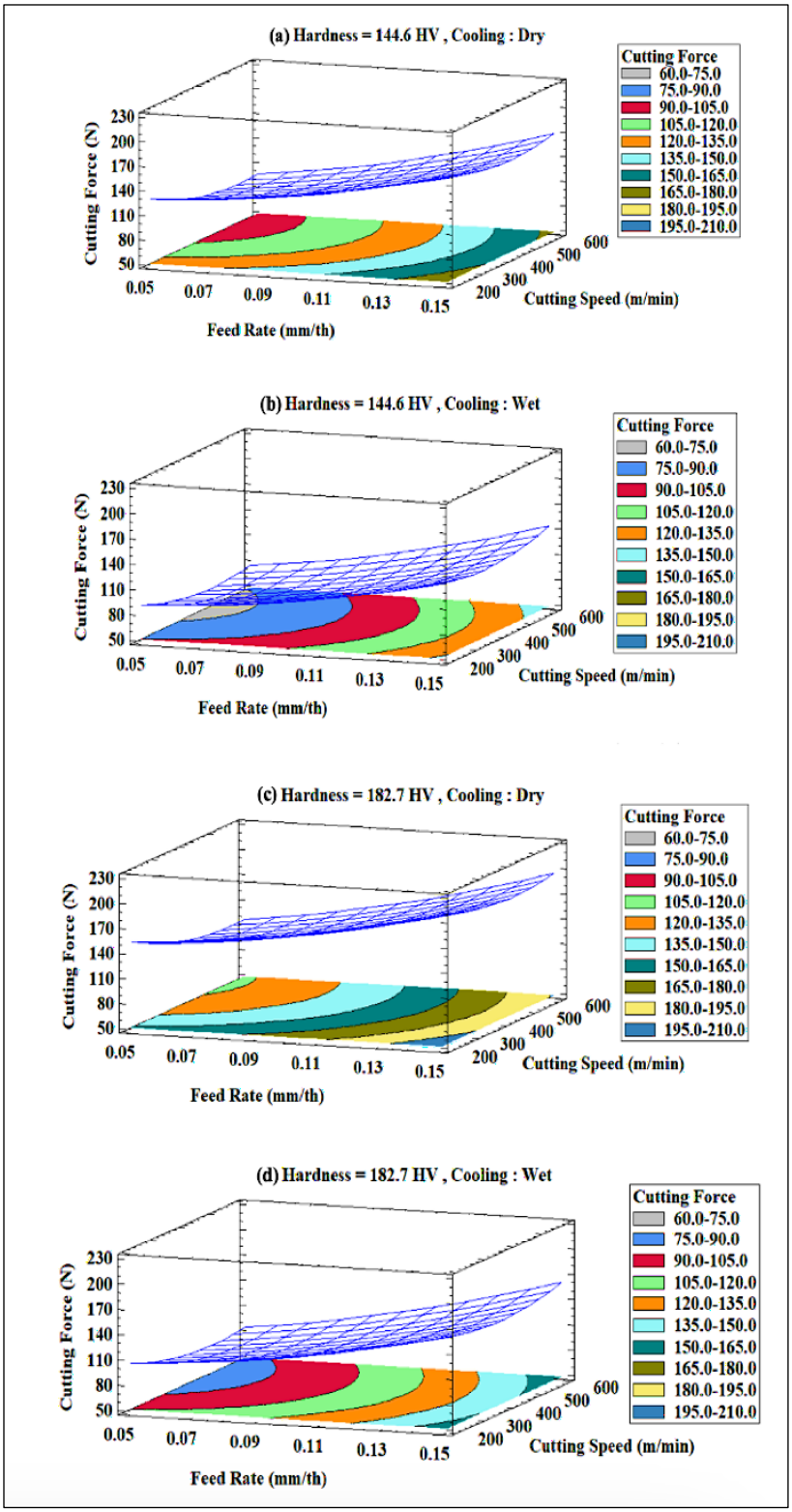


Figure 5.12 3D Surface plots of cutting force in different hardness and cooling mode for Al-Li-Cu-Sc alloy

## 5.5 Summary of Cutting Force Statistical Analysis for Al-Li, Al-Li-Cu and Al-Li-Cu-Sc alloys

The cutting forces for three different alloys Al-Li, Al-Li-Cu, and Al-Li-Cu-Sc under various conditions are presented in Figures 5.13 to 5.16. These figures explore the effects of cutting speed, cooling mode, feed rate, and alloy hardness on cutting force.

Figure 5.13 examines the cutting force at a low cutting speed of 200 m/min. Under dry cooling with a feed rate of 0.05 mm/th, Al-Li-Cu-Sc exhibits the highest cutting force, followed by Al-Li and Al-Li-Cu. When wet cooling is applied at the same feed rate, the cutting forces for Al-Li and Al-Li-Cu are significantly lower compared to Al-Li-Cu-Sc. Increasing the feed rate to 0.15 mm/th under dry cooling conditions still results in Al-Li-Cu-Sc showing the highest cutting force, with Al-Li and Al-Li-Cu having lower values. Under wet cooling with the same feed rate, the cutting forces are generally lower than in dry conditions, but Al-Li-Cu-Sc continues to lead, followed by Al-Li and Al-Li-Cu.

H1, H2, H3 and H4 are different heat treatments which are described in table 5.2.

Table 5.1 Description of different heat treatments

| Alloy | Heat Treatment | | Hardness (HV) |
|---|---|---|---|
| Al-Li | 580 °C/1 h + 130 °C /1 h | H1 | 56 |
| Al-Li | 580 °C/1 h + 150 °C / 45 h | H2 | 97 |
| Al-Li-Cu | 505 °C/5 h + 200 °C / 25 h | H3 | 129 |
| Al-Li-Cu | 505 °C/5 h + 180 °C / 20 h | H4 | 164 |
| Al-Li-Cu-Sc | 505 °C/5 h + 200 °C / 25 h | H5 | 144.6 |
| Al-Li-Cu-Sc | 505 °C/5 h + 180 °C / 20 h | H6 | 182.7 |

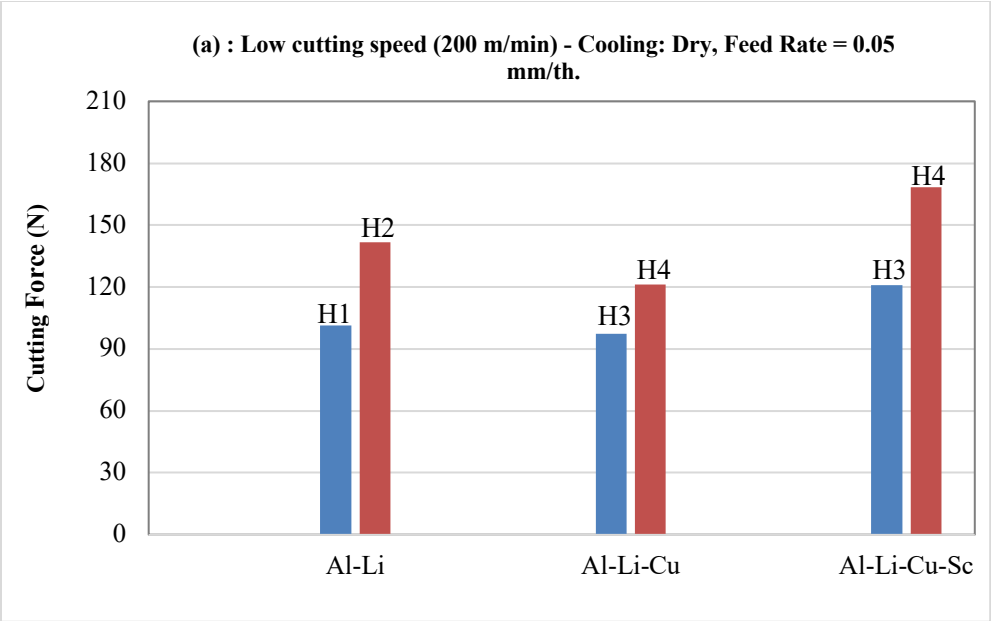
(a) : Low cutting speed (200 m/min) - Cooling: Dry, Feed Rate = 0.05 mm/th.
Cutting Force (N)
210
180
150
120
90
60
30
0
H1
H2
H3
H4
H3
H4
Al-Li
Al-Li-Cu
Al-Li-Cu-Sc

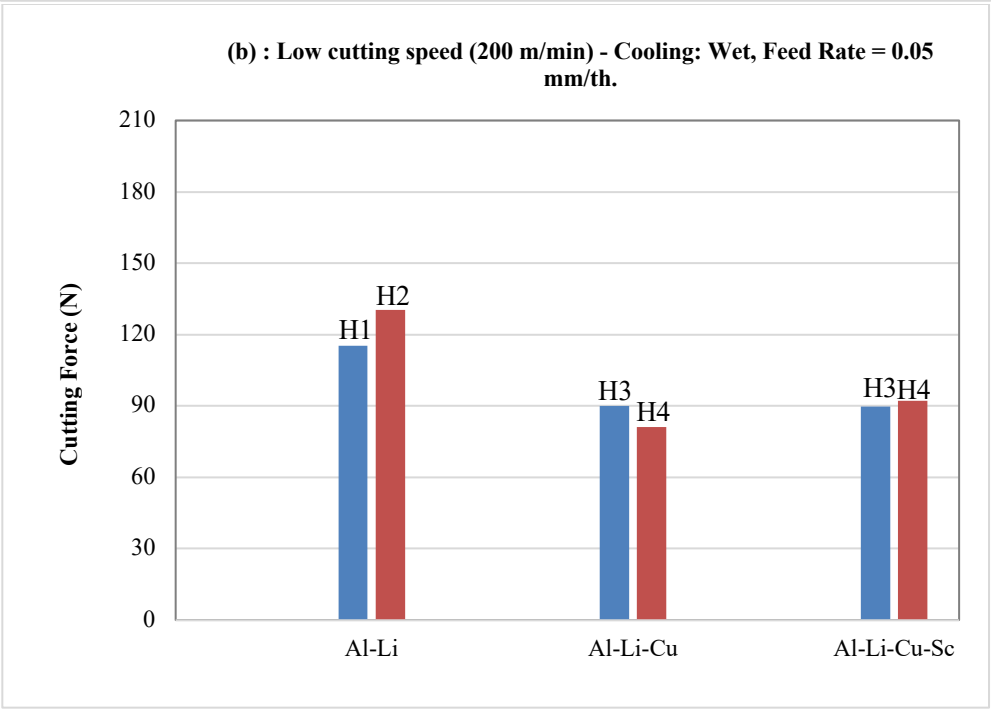
(b) : Low cutting speed (200 m/min) - Cooling: Wet, Feed Rate = 0.05 mm/th.
Cutting Force (N)
210
180
150
120
90
60
30
0
H1
H2
H3
H4
H3H4
Al-Li
Al-Li-Cu
Al-Li-Cu-Sc

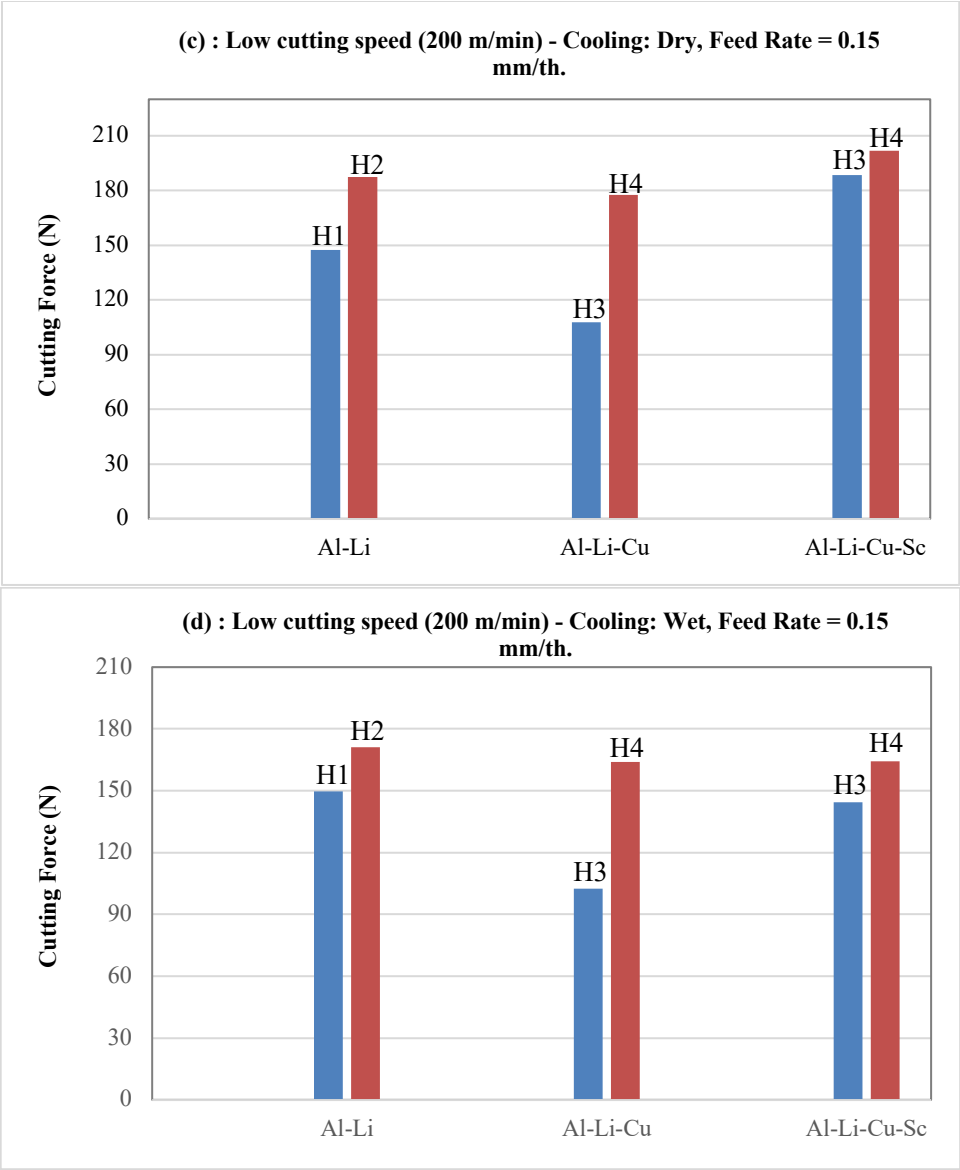


Figure 5.13 Cutting force of the Al-Li, Al-Li-Cu and Al-Li-Cu-Sc alloys when using low cutting speed (200 m/min):

a) Cooling: Dry, Feed Rate = 0.05 mm/th,
b) Cooling: Wet, Feed Rate = 0.05 mm/th,
c) Cooling: Dry, Feed Rate = 0.15 mm/th,
d) Cooling: Wet, Feed Rate = 0.15 mm/th

In Figure 5.14, the cutting forces are compared at a higher cutting speed of 600 m/min. For dry cooling with a feed rate of 0.05 mm/th, the cutting forces for all alloys are lower than those at

low speed, with Al-Li-Cu-Sc still having the highest force. Under wet cooling at the same feed rate, Al-Li-Cu shows the highest cutting force, with Al-Li-Cu-Sc and Al-Li having lower values. Increasing the feed rate to 0.15 mm/th under dry cooling conditions results in relatively higher cutting forces, with Al-Li-Cu-Sc again showing the highest value. In wet cooling with the same feed rate, Al-Li-Cu-Sc maintains the highest cutting force, followed by Al-Li and Al-Li-Cu.

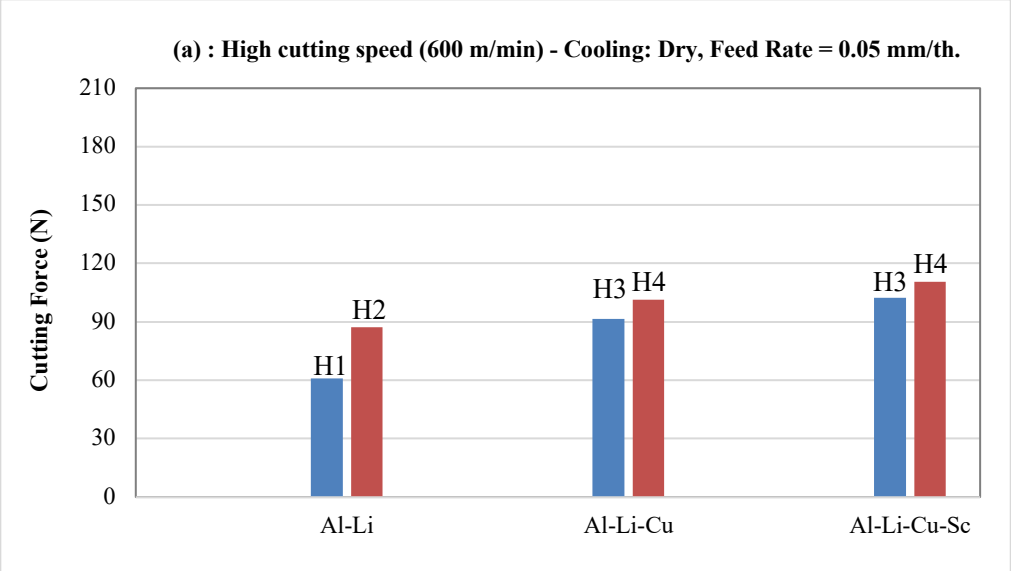


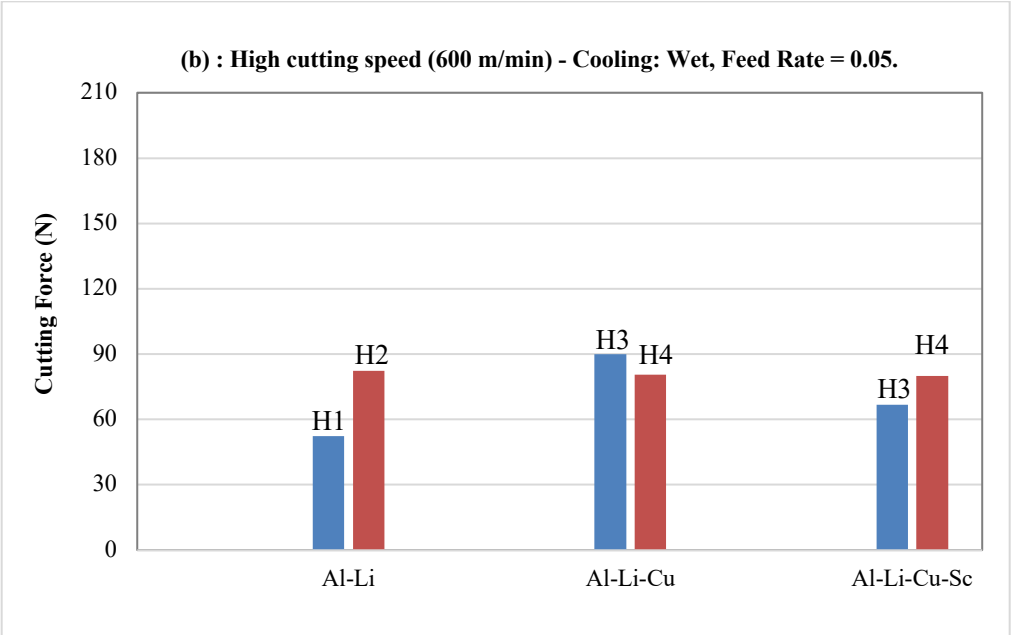

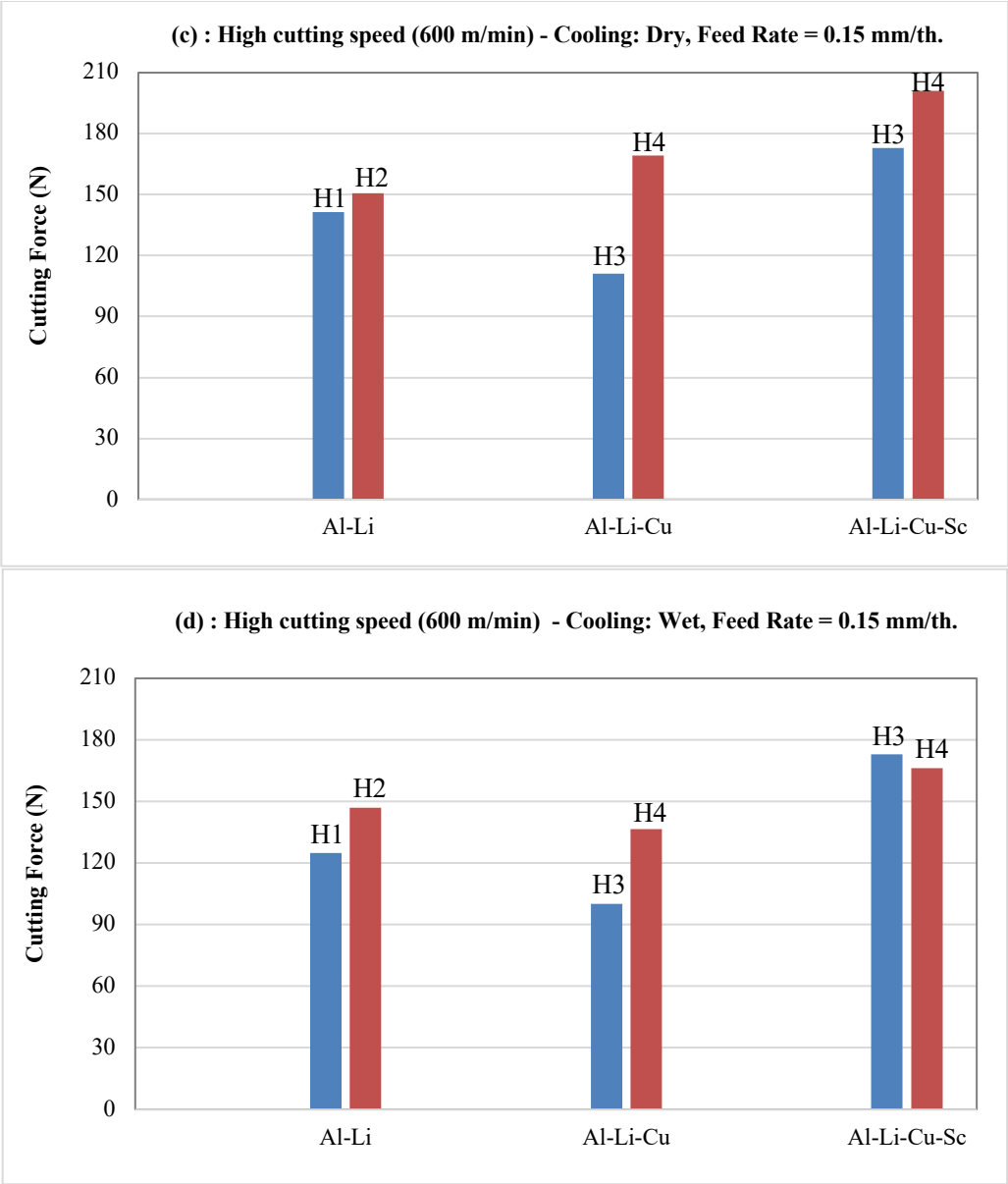


Figure 5.14 Cutting force of the Al-Li, Al-Li-Cu and Al-Li-Cu-Sc alloys when using high cutting speed (600 m/min):

a) Cooling: Dry, Feed Rate = 0.05 mm/th,
b) Cooling: Wet, Feed Rate = 0.05 mm/th,
c) Cooling: Dry, Feed Rate = 0.15 mm/th,
d) Cooling: Wet, Feed Rate = 0.15 mm/th

Across all figures, Al-Li-Cu-Sc alloy generally exhibits the highest cutting force, particularly in dry cooling conditions and at higher feed rates. The cutting force for all alloys tends to increase with feed rate and hardness. However, high cutting speeds generally reduce the cutting force across all alloys. Wet cooling conditions often result in lower cutting forces compared to dry conditions, highlighting the cooling mode's significant impact on cutting performance.

## 5.6 Conclusions

Based on the analysis of the machining process for Al-Li, Al-Li-Cu, and Al-Li-Cu-Sc alloys, it is evident that several factors significantly influence cutting force. These factors include feed rate, cutting speed, hardness, and cooling mode.

At the highest hardness (182.7 HV), the Al-Li-Cu-Sc alloy requires a cutting force of 128.45 N, which is lower than the corresponding values for Al-Li-Cu (164 HV needing 27.66 N more) and Al-Li (97 HV needing 19.15 N more). At its lowest hardness (144.6 HV), the Al-Li-Cu-Sc alloy also outperforms, requiring only 108.15 N of cutting force. The interaction between hardness and feed rate significantly influences cutting force in the Al-Li-Cu-Sc alloy, making it more sensitive to hardness changes. Despite this sensitivity, the alloy maintains consistent performance under different machining conditions, highlighting its adaptability and ease of machining.

The Al-Li-Cu-Sc alloy shows a notable reduction in cutting force with increasing cutting speed, a trend less pronounced in Al-Li and Al-Li-Cu alloys. High cutting speeds (600 m/min) and low feed rates (0.05 mm/th) consistently result in lower cutting forces and better surface quality across all alloys, with the Al-Li-Cu-Sc alloy benefiting the most. Wet machining significantly reduces cutting force, the Al-Li-Cu-Sc alloy showing the greatest improvements. Cooling methods stabilize microstructural properties, particularly in the presence of scandium, reducing tool wear and ensuring predictable machining outcomes.

Scandium in the Al-Li-Cu-Sc alloy refines the grain structure and forms stable precipitates (e.g., $\delta'$ and T1), improving hardness and mechanical properties while maintaining excellent machinability.

The statistical model for the Al-Li-Cu-Sc alloy explains a high percentage of variability in cutting force (92.52%), ensuring reliable and predictable machining performance. Optimal machining conditions, including high cutting speeds and wet machining, provide the best results for all alloys, with Al-Li-Cu-Sc benefiting the most. A low feed rate (0.05 mm/th) consistently minimizes cutting forces and surface roughness, while higher hardness alloys, particularly Al-Li-Cu-Sc, perform best at higher cutting speeds due to their enhanced microstructural stability.

# CHAPITRE 6

# RESULTS AND DISCUSSION OF PARTICLE EMISSION

## 6.1 Introduction

Mass concentration, a crucial parameter in machining, measures the amount of airborne particulate matter generated during cutting. It is vital for worker health and safety, regulatory compliance, and environmental protection. The successful machining of aluminum alloys involves a delicate balance of machining parameters and cooling methods to obtain quality part at acceptable cycle times while maintaining the metallic particle emission low.

By finding appropriate cutting speeds, feed rates, hardness and cooling strategies, industries can achieve high productivity and quality while ensuring a safe and clean working environment. The insights from recent studies underline the importance of continued research and innovation in machining practices to further enhance the machinability of aluminum alloys and control particle emissions.

In this study, the effects of feed rate, cutting speed, and hardness were evaluated on the milling of Al-Li, Al-Li-Cu, and Al-Li-Cu-Sc alloys under both wet and dry conditions.

## 6.2 The ANOVA Results for Fine Metallic Particles and Aerosols Emissions During Dry Machining of Al-Li, Al-Li-Cu and Al-Li-Cu-Sc Alloys

Tables 6.1 to 6.3 present the ANOVA results for particle emissions (mass concentration) during the dry machining of Al-Li, Al-Li-Cu, and Al-Li-Cu-Sc alloys. These tables highlight the significance of various factors, including feed rate, cutting speed, and hardness, as well as their interactions, in influencing particle emissions.

The Pareto chart (Figure 6.1) visualizes the relative importance of these factors and their interactions, using the data from Tables 6.1 to 6.3. The chart ranks factors in descending order of influence, with a significance threshold indicated by a blue line. The data in Tables 6.1 to 6.3 directly supports the construction of the Pareto chart by ranking factors based on their F-Ratios and p-values. Cutting speed (B) consistently holds the highest F-Ratio in all three alloys, underscoring its dominant influence, followed by hardness and feed rate. This systematic approach, reflected in the visual representation of the Pareto chart, effectively synthesizes the statistical insights into a clear depiction of the key factors impacting particle emissions during machining. These findings emphasize both universal trends, such as the significant role of cutting speed, and unique alloy-specific behaviors driven by microstructural variations.

Table 6.1 The Al-Li alloy ANOVA table for Particle Emission (mass concentration) Dry Condition

| Source | Sum of Squares | Df | Mean Square | F-Ratio | P-Value |
|---|---|---|---|---|---|
| A: Feed Rate | 0.159236 | 1 | 0.159236 | 11.71 | 0.0032 |
| B: Cutting Speed | 1.4827 | 1 | 1.4827 | 109.06 | 0.0000 |
| C: Hardness | 0.491734 | 1 | 0.491734 | 36.17 | 0.0000 |
| AA | 0.00908445 | 1 | 0.00908445 | 0.67 | 0.4250 |
| AB | 0.0957653 | 1 | 0.0957653 | 7.04 | 0.0167 |
| AC | 0.0336021 | 1 | 0.0336021 | 2.47 | 0.1343 |
| BB | 0.151252 | 1 | 0.151252 | 11.13 | 0.0039 |
| BC | 0.130813 | 1 | 0.130813 | 9.62 | 0.0065 |
| CC | 0.653642 | 1 | 0.653642 | 48.08 | 0.0000 |
| Total error | 0.231117 | 17 | 0.0135951 | | |
| Total (corr.) | 3.43895 | 26 | | | |

Table 6.2 The Al-Li-Cu alloy ANOVA table for Particle Emission (mass concentration) Dry Condition

| Source | Sum of Squares | Df | Mean Square | F-Ratio | P-Value |
|---|---|---|---|---|---|
| A: Feed Rate | 15.0938 | 1 | 15.0938 | 19.96 | 0.0003 |
| B: Cutting Speed | 116.205 | 1 | 116.205 | 153.68 | 0.0000 |
| C: Hardness | 59.7507 | 1 | 59.7507 | 79.02 | 0.0000 |
| AA | 0.0313445 | 1 | 0.0313445 | 0.04 | 0.8411 |
| AB | 0.125461 | 1 | 0.125461 | 0.17 | 0.6888 |
| AC | 1.924 | 1 | 1.924 | 2.54 | 0.1291 |
| BB | 0.4365 | 1 | 0.4365 | 0.58 | 0.4578 |
| BC | 11.2617 | 1 | 11.2617 | 14.89 | 0.0013 |
| CC | 0.219013 | 1 | 0.219013 | 0.29 | 0.5974 |
| Total error | 12.8548 | 17 | 0.756163 | | |
| Total (corr.) | 217.902 | 26 | | | |

Table 6.3 The Al-Li-Cu-Sc alloy ANOVA table for Particle Emission (mass concentration) Dry Condition

| Source | Sum of Squares | Df | Mean Square | F-Ratio | P-Value |
|---|---|---|---|---|---|
| A: Feed Rate | 1.35521 | 1 | 1.35521 | 20.66 | 0.0003 |
| B: Cutting Speed | 8.89857 | 1 | 8.89857 | 135.63 | 0.0000 |
| C: Hardness | 2.57948 | 1 | 2.57948 | 39.32 | 0.0000 |
| AA | 0.0165375 | 1 | 0.0165375 | 0.25 | 0.6221 |
| AB | 0.0726963 | 1 | 0.0726963 | 1.11 | 0.3072 |
| AC | 0.110208 | 1 | 0.110208 | 1.68 | 0.2123 |
| BB | 0.281667 | 1 | 0.281667 | 4.29 | 0.0538 |
| BC | 0.196096 | 1 | 0.196096 | 2.99 | 0.1020 |
| CC | 0.291281 | 1 | 0.291281 | 4.44 | 0.0503 |
| Total error | 1.11534 | 17 | 0.065608 | | |
| Total (corr.) | 14.9171 | 26 | | | |

## 6.3 The Pareto Charts and Analysis of Effective Factors on Mass Concentration of Al-Li, Al-Li-Cu and Al-Li-Cu-Sc Alloys

The machining process of Al-Li, Al-Li-Cu, and Al-Li-Cu-Sc alloys in dry condition demonstrates notable sensitivity to variations in mass concentration. Specifically, the developed model accounts for 93.28 %, 94.10 %, and 92.52 % of the variation in mass concentration for Al-Li, Al-Li-Cu, and Al-Li-Cu-Sc alloys, respectively. This indicates a clear correlation between the selected cutting parameters and the resulting mass concentration.

In the Pareto chart (Figure 6.1), which illustrates all independent variables and their interactions, all parameters are exceed the threshold indicated by the blue line. As depicted in the Pareto charts (Figure 6.1), cutting speed, hardness, and feed rate have notable impacts on the mass concentration of particle emissions across all three alloys. Interestingly, in the Al-Li-Cu alloy, the effect of hardness on particle emission deviates from the other two alloys.

Here, increasing hardness results in decreased particle emissions, contrary to the expected trend. This anomaly can be attributed to microstructural effects, as explained in Chapter 3 on heat treatment. Copper atoms in aluminum alloys tend to segregate to grain boundaries, acting as a grain refiner in aluminum-lithium alloys. However, in Figure 3.3(a), the grains grow unexpectedly large. The presence of copper at the grain boundaries may hinder grain boundary mobility and promote grain growth, leading to larger grain sizes compared to pure aluminum-lithium alloy.

Zhao et al. (Zhao et al. 2023) found that higher cutting speeds and feed rates increase particle emissions, with harder materials generating more particles due to increased brittleness and fragmentation. Khettabi et al. (Khettabi, Songmene, and Masounave 2010) identified cutting speed as the most influential factor, followed by feed rate, with hardness increasing emissions due to more significant chip fragmentation. Niknam et al. (Niknam, Kouam, and Songmene 2016), in their study on milling 6061-T6 aluminum alloy, showed that increased cutting speed and feed rate lead to higher emissions, and harder materials generally produce more particles. Djebara et al. (Djebara, Jomaa, et al. 2013) investigated dust emissions in dry machining of

aeronautic aluminum alloys and found that dust emissions increase significantly with cutting speed, with hardness contributing to greater particle emissions due to increased brittleness. Khettabi et al. (Khettabi et al. 2017) in another study demonstrated that dry machining generally produces higher particle emissions compared to MQL, with cutting speed and feed rate being critical factors.

Our results for Al-Li and Al-Li-Cu-Sc alloys align with these findings, showing increased emissions with higher speeds and feeds. However, the unique behavior observed in the Al-Li-Cu alloy suggests that microstructural characteristics, particularly copper segregation, play a significant role in altering the expected emission patterns.

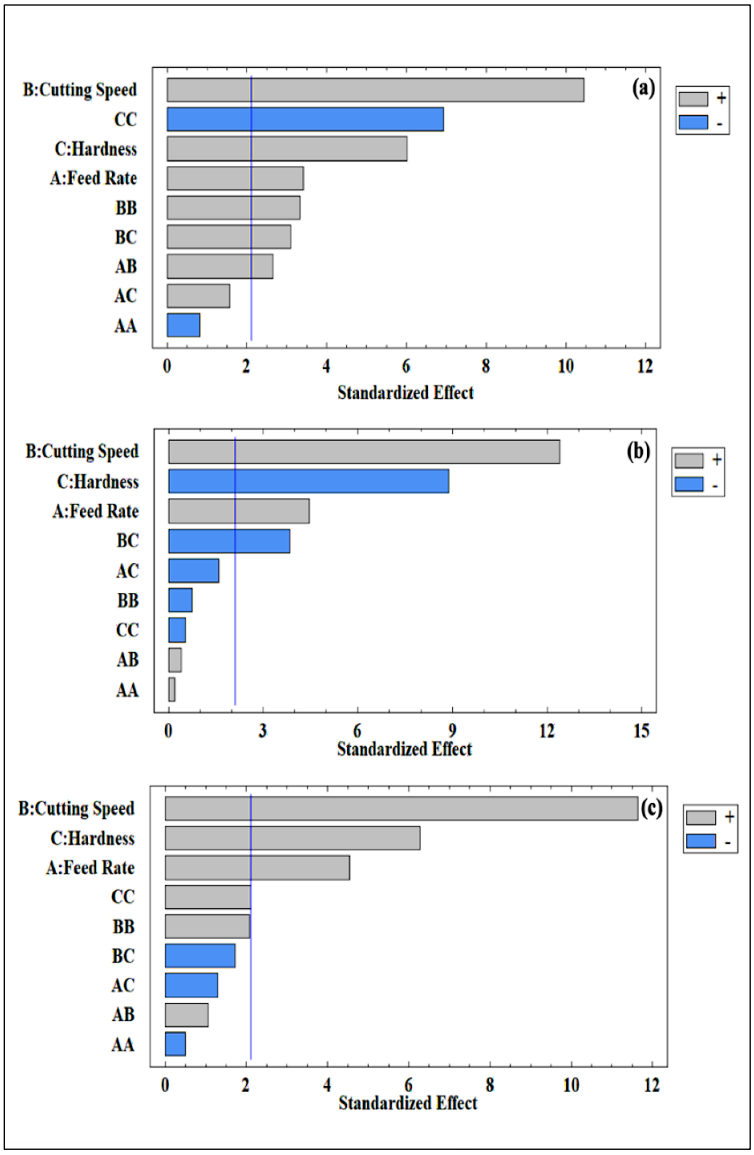


Figure 6.1 Pareto charts of mass concentration for (a) Al-Li Alloy, (b) Al-Li-Cu Alloy, (c) Al-Li-Cu-Sc Alloy in dry condition

Cutting speed is the most significant factor impacting mass concentration across all three alloys (Figures 6.2–6.4). Higher cutting speeds increase material removal rates and intensify chip fragmentation, leading to more airborne particles. This trend aligns with findings by Khettabi et al. and Djebara et al. (Khettabi, Songmene, and Masounave 2010; Djebara, Jomaa, et al. 2013), who reported that increased speeds amplify emissions in aluminum alloys due to higher brittleness and chip fragmentation. For Al-Li-Cu and Al-Li-Cu-Sc alloys, the effect is

particularly pronounced due to their complex microstructures, which influence chip formation mechanisms.

Feed rate has a secondary but noticeable impact on mass concentration. As feed rate increases, particle emissions also rise (Figures 6.2-b, 6.3-b, and 6.4-b), attributed to greater material engagement and higher chip load. Zhao et al. (Zhao et al. 2023) observed similar trends in aluminum machining, where increased feed rates generated more fine particles. However, the effect is less significant than cutting speed, suggesting that feed rate primarily affects the volume of material removed rather than particle size distribution.

Hardness exhibits varying effects across the alloys. In Al-Li alloy Higher hardness increases particle emissions due to increased brittleness and enhanced chip fragmentation (Figure 6.2-c). This aligns with studies by Niknam et al. and Djebara et al. (Niknam, Kouam, and Songmene 2016; Djebara, Jomaa, et al. 2013), which reported that harder materials tend to produce more particles. Contrary to expectations, in Al-Li-Cu alloy, increased hardness reduces mass concentration. This anomaly stems from copper segregation to grain boundaries, resulting in larger grains and reduced chip fragmentation (Figure 6.3-c). This behavior highlights the role of microstructural properties in emission patterns, as noted by Songmene et al. (Songmene et al. 2011). In Al-Li-Cu-Sc alloy, similar to Al-Li, hardness increases mass concentration, consistent with the brittleness and fragmentation observed in harder materials (Figure 6.4-c).

The deviation in hardness effects for Al-Li-Cu alloy underscores the influence of copper-induced grain coarsening. Coarse grains reduce grain boundary mobility and alter fracture mechanisms, resulting in fewer fine particles during machining. This finding is consistent with Zhao et al. (Zhao et al. 2023), who emphasize the role of material composition in emission patterns, but highlights the distinct behavior of alloys with grain boundary modifications.

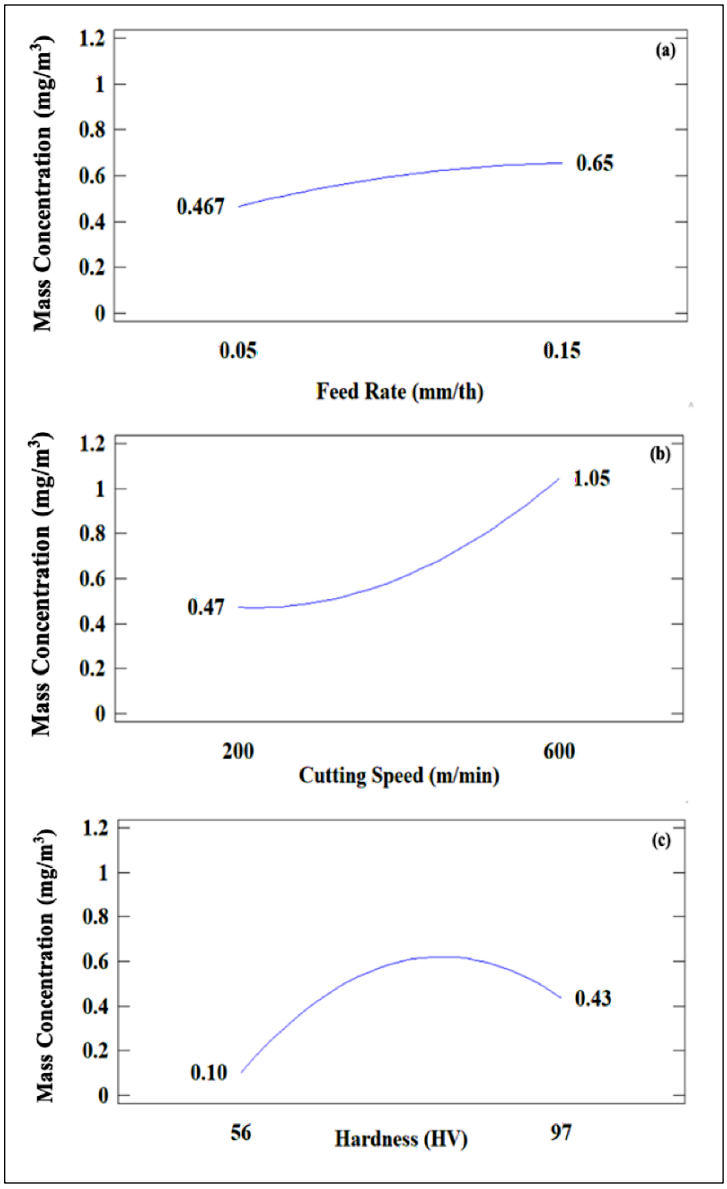


Figure 6.2 Main effects plot for mass concentration in dry machining of Al-Li alloy

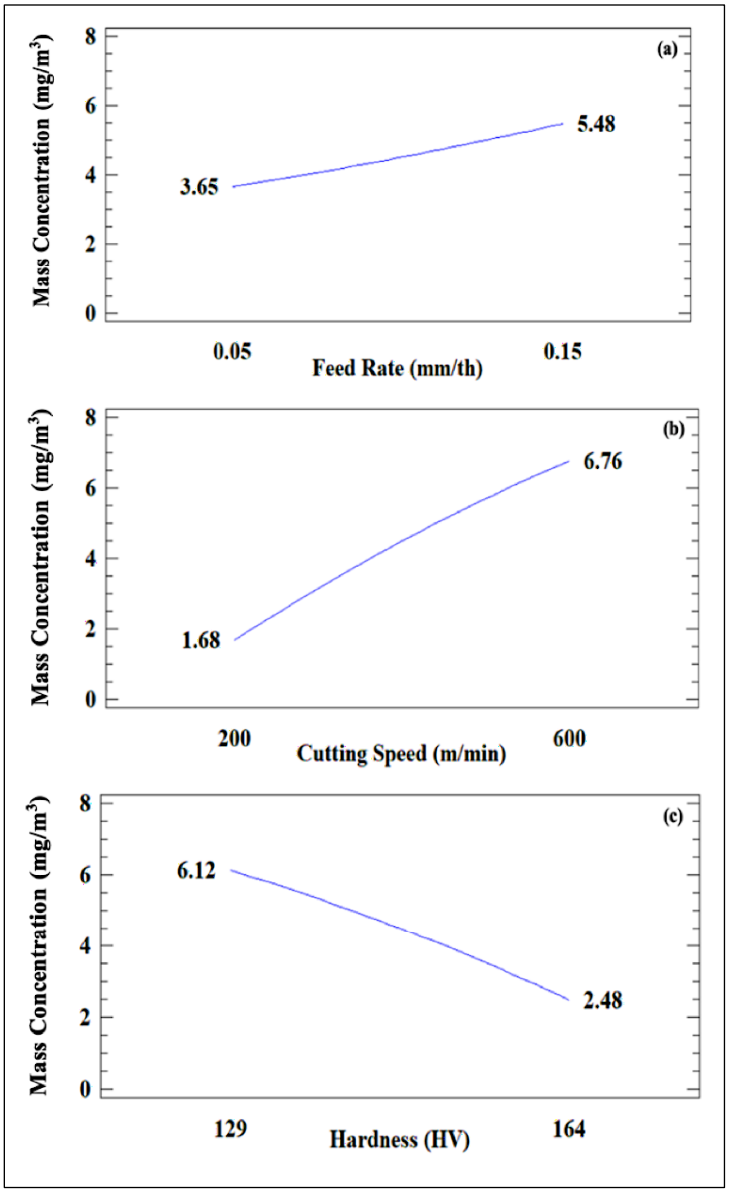


Figure 6.3 Main effects plot for mass concentration in dry machining of Al-Li-Cu alloy

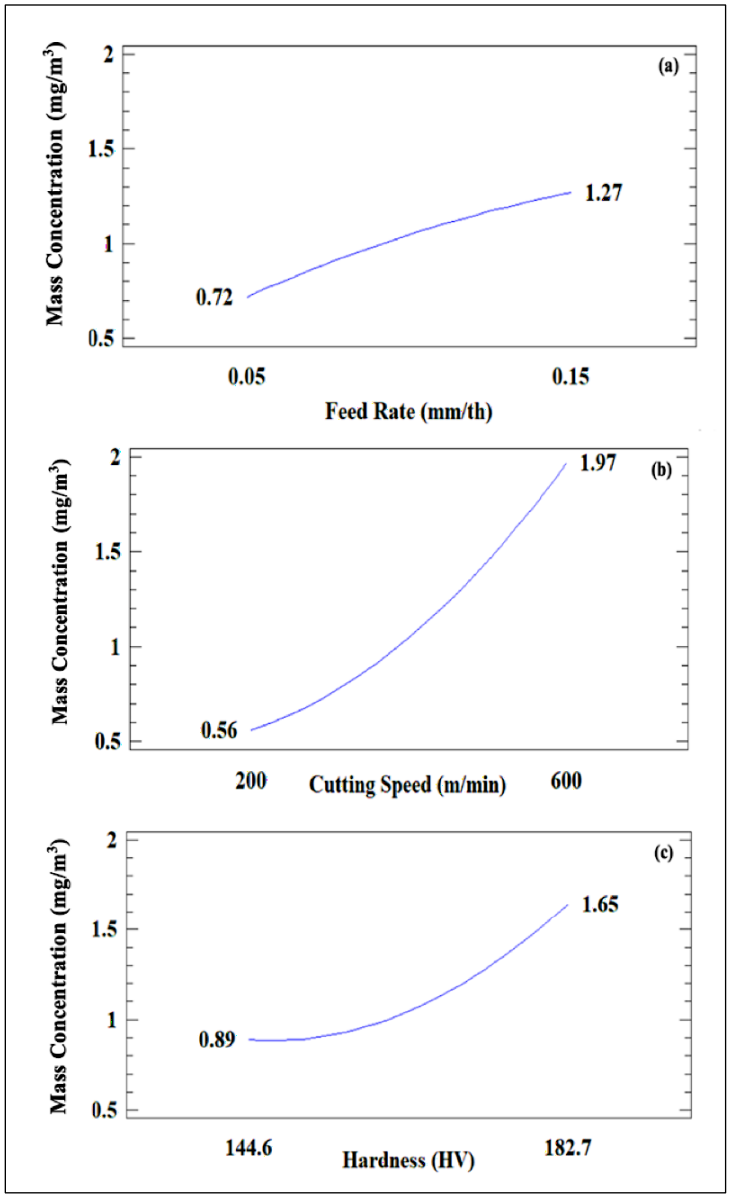


Figure 6.4 Main effects plot for mass concentration in dry machining of Al-Li-Cu-Sc alloy

## 6.4 The Interaction Plots for Mass Concentration of Al-Li, Al-Li-Cu and Al-Li-Cu-Sc Alloys

Interaction plots (Figures 6.5 and 6.6) reveal that cutting speed and hardness interactions significantly impact emissions. For Al-Li and Al-Li-Cu-Sc alloys, the difference in mass

concentration between soft and hard materials becomes more pronounced at higher speeds, reflecting the increased fragmentation of harder materials. For Al-Li-Cu alloy, the interaction shows that higher cutting speeds amplify emissions for softer materials but mitigate them for harder materials, likely due to altered chip formation dynamics.

Higher feed rates also exacerbate the effect of cutting speed on emissions, with the largest differences observed at high feed rates and cutting speeds. This interaction suggests that the combined effects of thermal and mechanical loads on chip fragmentation intensify particle emissions.

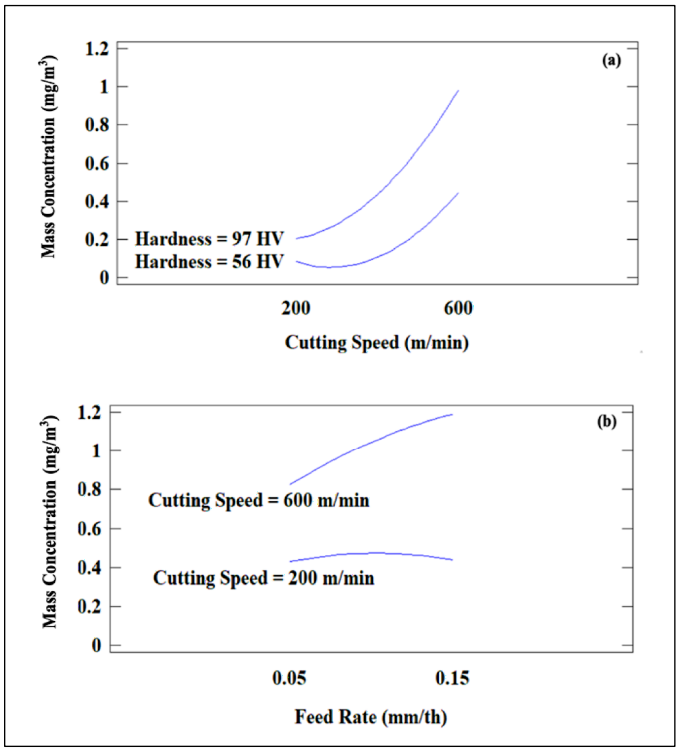


Figure 6.5 Interaction plots for mass concentration for Al-Li alloy in dry condition

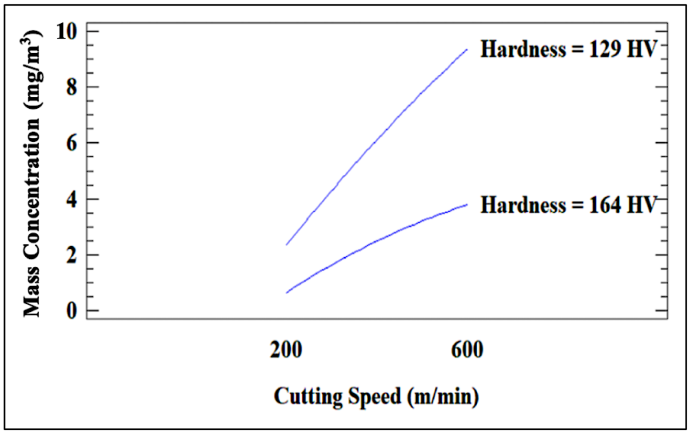


Figure 6.6 Interaction plots for mass concentration for Al-Li-Cu alloy in a dry condition

The wet machining process for Al-Li, Al-Li-Cu, and Al-Li-Cu-Sc alloys is detailed in APPENDIX AI and APPENDIX AII, specifically in Tables AI-10 to AI-18, and the ANOVA analyses provided in Tables II-10, II.12, and II.14. The results indicate significantly higher mass concentrations during wet machining. This increase is attributed to the combined presence of solid particles and liquid aerosols in the machining environment.

Table 6.4 Comparative analysis of particle emissions in dry and wet machining of Aluminum alloys

| **Study** | **Material** | **Machining Condition** | **Key Findings** |
|---|---|---|---|
| Our Study | Al-Li, Al-Li-Cu, Al-Li-Cu-Sc | Dry | Emissions increase with speed and feed; Al-Li-Cu shows decreased emissions with hardness |
| Zhao et al. (Zhao et al. 2023) | Various Al Alloys | Dry | Higher speeds and feeds increase emissions; microstructure affects emissions |
| Khettabi et al. (Khettabi, Songmene, and Masounave 2010) | Al Alloys | Dry | Cutting speed was found as most influential, followed by feed rate |

| Study | Material | Machining Condition | Key Findings |
|---|---|---|---|
| Niknam et al. (Niknam, Kouam, and Songmene 2016) | 6061-T6 Alloy | Dry | Higher speeds and feeds increase emissions |
| Djebara et al. (Djebara, Jomaa, et al. 2013) | Aeronautic Al-Alloys | Dry | Dust emissions decrease with speed; wet conditions not studied |
| Pattnaik et al. (Pattnaik et al. 2018) | Various Al - Alloys | Dry | Tool performance and wear impact particle emissions; higher emissions with increased tool wear |
| Songmene et al. (Songmene, Balout, and Masounave 2008) | Al - Alloys | Dry | Emissions increase associated with hardness; influence of microstructure noted |
| Djebara et al. (Djebara and Songmene 2012) | Al - Alloys | Dry | Increased dust emissions with speed; consistent findings with other studies |
| Arumugam et al. (Arumugam et al. 2003) | Al-Si Alloy | Dry | High particle emissions at higher speeds; focus on tool coatings |
| Zaghbani et al. (2009) | 6061-T6 Al-Alloy | Dry | Characterization of fine and ultrafine particles; emissions decrease with speed |
| Djebara et al. (Djebara, Zedan, et al. 2013) | Al-7Si-Mg Cast Alloys | Dry | Heat treatment effects on dust emissions; increased emissions with speed |
| Songmene & Doko (Songmene and Njoya Doko 2015) | Al Alloys and MMCs | Dry | Fine metallic particle emissions; focus on milling of alloys and composites |
| Dasch et al. (Dasch et al. 2005) | Automotive Al - Alloys | Dry | Characterization of fine particles; emissions increase with speed |
| Balout et al. (Balout, Songmene, and Masounave 2007) | Various Al - Alloys | Dry | Study of dust generation during dry drilling; pre-cooled and pre-heated workpieces analyzed |
| Marani et al. (Marani et al. 2018) | Al-20Mg2Si-2Cu MMC | Dry | Effects of modifier elements on significant dust emission during milling |

| Study | Material | Machining Condition | Key Findings |
|---|---|---|---|
| Özsoy et al. (Özsoy and Ozsoy 2019) | 6082-T6 Al-Alloy | Dry, Wet | Surface roughness and particle emissions; wet machining reduces emissions |
| Dhanalakshmi et al. (Dhanalakshmi and Rameshbabu 2021) | LM 25 Al - Alloy | Dry, Wet | Comparative study: wet machining shows lower emissions compared to dry |
| Yoshimura et al. (Yoshimura et al. 2006) | Various Al - Alloys | Near Dry | Near dry machining techniques reduce emissions compared to fully dry machining |
| Hadzley et al. (Hadzley et al. 2018) | Al - Alloys | Dry, Wet | Surface integrity and material side flow; wet machining reduces emissions |
| Kouam et al. (Kouam et al. 2015) | 7075-T6 Al - Alloy | MQL | MQL conditions significantly reduce particle emissions compared to dry machining |
| Kouam et al. (Kouam et al. 2012) | 6061-T6 Aluminum Alloy | Dry, Semi-dry, Wet | Comparative study: wet and semi-dry machining show lower emissions compared to dry |
| Khettabi et al. (Khettabi et al. 2017) | Al - Alloys | Dry, MQL | Dry machining produces higher emissions compared to MQL. |

## 6.5 Conclusions

Based on the analysis of the machining process for Al-Li, Al-Li-Cu, and Al-Li-Cu-Sc alloys, it is evident that several factors significantly influence metallic particles and wet aerosols emissions. These factors include feed rate, cutting speed, hardness, and cooling mode.

1. Considering the balance between machinability and particle emissions, Al-Li-Cu-Sc alloy demonstrates the best overall performance. It provides a good balance of

mechanical properties and machinability while maintaining manageable levels of particle emissions under specific cutting conditions.

2. Al-Li-Cu alloy presents unique advantages due to its microstructural characteristics, but the unexpected behavior in particle emissions requires careful consideration during machining. The generated metallic particles emissions were much higher for this alloy compared to the two other alloys (Al-Li and Al-Li-Cu-Sc).
3. There are several similarities between the findings in the particle emission chapter and those in the surface roughness, cutting force, and heat treatment chapters:
    - Higher feed rates significantly increase surface roughness, and this is mirrored in the cutting force chapter, where increased feed rates result in higher cutting forces due to larger chip volumes and higher material removal rates. Similarly, the particle emission chapter indicates that higher feed rates lead to an increase in particle emissions, likely due to greater material removal and higher energy inputs generating more particulate matter.
    - Additionally, higher cutting speeds generally result in smoother surface finishes by reducing tool-workpiece interaction time. This trend is also observed in the cutting force, where higher cutting speeds reduce cutting forces due to better chip formation and material softening from heat.
    - The use of cutting fluid also shows consistent effects across chapters. Wet machining conditions improve surface quality and significantly reduce cutting forces by lowering the temperature and improving lubrication.
    - In the surface roughness part, hardness does not significantly impact surface roughness for Al-Li alloy, but it does for other aluminum alloys due to changes in material microstructure. Conversely, in the cutting force chapter, harder materials re higher cutting forces due to increased resistance to deformation.

# GENERAL CONCLUSION

This study investigated the impact of alloy composition, heat treatment processes, and machining parameters on the machinability and mechanical performance of aluminum-lithium based alloys (8xxx group), including Al-Li, Al-Li-Cu, and Al-Li-Cu-Sc. The results demonstrated the critical role of adding elements such as copper (Cu) and scandium (Sc), combined with optimized heat treatments, in tailoring the properties of these alloys for high-performance applications.

Key findings highlighted that optimized heat treatment conditions significantly improved hardness, with increases of 73.2% in Al-Li, 26.9% in Al-Li-Cu, and 26.34% in Al-Li-Cu-Sc. Specific heat treatments, such as solution treatment at 580 °C for 1 hour followed by artificial aging at 150 °C for 45 hours (for Al-Li), and solution treatment at 505 °C for 5 hours followed by artificial aging at 180 °C for 20 hours (for Al-Li-Cu and Al-Li-Cu-Sc), were effective in enhancing machinability without compromising mechanical strength.

Machining trials revealed that Al-Li alloy required the least machining force (52.3 N) compared to Al-Li-Cu (90 N) and Al-Li-Cu-Sc (67 N). The use of cutting fluid reduced cutting forces for Al-Li-Cu-Sc (by 26.6%) and improved surface finish for Al-Li (by 32.2%) when machined at a low cutting speed (200 m/min), but did increase significantly the emission of wet aerosols in the machining environement.

Validation of machining outcomes, such as surface roughness and cutting forces, aligned closely with established studies, confirming consistency with known Al-Li alloy behaviors. Furthermore, cutting speed was identified as the most critical factor influencing fine metallic particle emission during machining, followed by alloy hardness and feed rate. For similar hardness, Al-Li-Cu generated more fine metallic particle emission than the Al-Li-Cu-Sc at all the three cutting speeds and feed rates tested. The Al-Li-Cu-Sc was found to perform better in terms of during the heat treatment and the machining. This alloy could be hardness 11% better than the Al-Li-Cu and 88% better than the Al-Li but the Al-Li-Cu-Sn generated 54% less metallic particles than the Al-Li-Cu alloy.

In conclusion, this study demonstrated that the integration of alloying elements like Cu and Sc, optimized heat treatments, and precisely controlled machining parameters can significantly enhance the machinability and mechanical performance of Al-Li based alloys. These findings provide critical insights for industries such as aerospace, where advanced materials with high strength, excellent machinability, and reliable performance are essential.

## RECOMMENDATIONS

Further research is necessary to build upon the findings of this study and address any remaining gaps in knowledge. Specific areas for future research include:

- Investigating the effects of advanced cooling techniques, such as cryogenic cooling, minimum quantity lubrication (MQL), or hybrid cooling methods, on the machinability of aluminum-lithium based alloys. These methods could potentially offer better temperature control, reduce thermal stresses, and improve surface finish and tool life.

- Exploring the performance of different cutting tool materials and advanced tool coatings to determine their effectiveness in machining these alloys. Different tool materials and coatings can significantly affect wear resistance, heat dissipation, and overall machining performance.

- Conducting detailed microstructural analysis of machined surfaces to understand the effects of various machining parameters on the material's microstructure. This could provide insights into phenomena such as work hardening, phase transformations, or grain refinement, which influence the mechanical properties and fatigue life of the components.

- Assessing the environmental and health impacts of machining aluminum-lithium based alloys, particularly in terms of particle emissions and coolant disposal. Research in this area can lead to the development of safer and more sustainable machining practices.

- Developing and validating computational models to simulate the machining process of these alloys. Such models can help predict outcomes like surface roughness, tool wear, and cutting forces, reducing the need for extensive experimental trials.

- Conducting long-term performance studies of machined components in actual aerospace applications. This research would involve testing the components under real-world conditions to assess their durability, reliability, and performance, providing a direct link between machining practices and operational success.

## APPENDIX I

## MACHINING DATA RESULTS

Table AI.1 Surface roughness (Ra) results of Al-Li alloy dependence on cutting speed and feed rate

| Test Number | Cutting Speed (m/mm) | Feed Rate (mm/tooth) | Ra (μm) | | | | | |
|---|---|---|---|---|---|---|---|---|
| | | | Lower Hardness (HV) 56 | | Medium Hardness (HV) 76.5 | | Higher Hardness (HV) 97 | |
| | | | Dry | Wet | Dry | Wet | Dry | Wet |
| 1 | 200 | 0.05 | 0.7620 | 0.2560 | 0.4485 | 0.3065 | 0.3385 | 0.3670 |
| 2 | | 0.1 | 1.0420 | 0.4550 | 1.4675 | 0.8275 | 0.9470 | 0.3800 |
| 3 | | 0.15 | 1.7815 | 0.6440 | 1.7635 | 1.1475 | 1.5970 | 1.2205 |
| 4 | 400 | 0.05 | 0.3980 | 0.2705 | 0.2560 | 0.3610 | 0.5635 | 0.3270 |
| 5 | | 0.1 | 0.9790 | 0.4735 | 0.6675 | 0.9105 | 0.7425 | 0.3875 |
| 6 | | 0.15 | 1.4640 | 0.5525 | 1.1105 | 1.1090 | 0.8180 | 0.7650 |
| 7 | 600 | 0.05 | 0.3645 | 0.1825 | 0.4425 | 0.3060 | 0.2765 | 0.4250 |
| 8 | | 0.1 | 0.6585 | 0.2530 | 0.7440 | 0.5050 | 0.4815 | 0.4275 |
| 9 | | 0.15 | 0.8930 | 0.3630 | 0.7970 | 0.6455 | 0.5280 | 0.9200 |

Table AI.2 Surface roughness (Rt) results of Al-Li alloy dependence on cutting speed and feed rate

| Test Number | Cutting Speed (m/mm) | Feed Rate (mm/tooth) | Rt (μm) | | | | | |
|---|---|---|---|---|---|---|---|---|
| | | | Lower Hardness (HV) 56 | | Medium Hardness (HV) 76.5 | | Higher Hardness (HV) 97 | |
| | | | Dry | Wet | Dry | Wet | Dry | Wet |
| 1 | 200 | 0.05 | 7.3880 | 6.0450 | 6.4550 | 6.1650 | 6.2475 | 6.2145 |
| 2 | | 0.1 | 9.0800 | 6.7381 | 10.2080 | 7.3215 | 8.3205 | 6.6760 |
| 3 | | 0.15 | 11.9755 | 7.3031 | 11.1295 | 9.2075 | 10.5960 | 9.2475 |
| 4 | 400 | 0.05 | 7.6445 | 6.1883 | 6.4640 | 6.4675 | 7.0140 | 6.4510 |
| 5 | | 0.1 | 11.3485 | 6.8527 | 7.3790 | 8.2996 | 7.6420 | 6.7991 |
| 6 | | 0.15 | 12.1420 | 7.1288 | 8.9845 | 8.8642 | 8.0140 | 7.8245 |
| 7 | 600 | 0.05 | 6.2580 | 5.2930 | 6.6902 | 6.2700 | 6.4910 | 6.6045 |
| 8 | | 0.1 | 7.4025 | 6.2676 | 7.6871 | 6.8902 | 6.9270 | 7.2760 |
| 9 | | 0.15 | 8.1798 | 6.8440 | 7.8624 | 7.3753 | 7.0902 | 8.2125 |

Table AI.3 Surface roughness (Ra) results of Al-Li-Cu alloy dependence on cutting speed and feed rate

| Test Number | Cutting Speed (m/mm) | Feed Rate (mm/tooth) | Ra (μm) | | | | | |
|---|---|---|---|---|---|---|---|---|
| | | | Lower Hardness (HV) 129 | | Medium Hardness (HV) 146.7 | | Higher Hardness (HV) 164 | |
| | | | Dry | Wet | Dry | Wet | Dry | Wet |
| 1 | 200 | 0.05 | 1.3025 | 0.5340 | 0.4780 | 0.4655 | 0.3765 | 0.4630 |
| 2 | | 0.1 | 1.3365 | 0.6010 | 1.3435 | 1.4075 | 0.4460 | 0.8340 |
| 3 | | 0.15 | 1.6680 | 1.6135 | 1.4825 | 1.4200 | 1.1480 | 1.3375 |
| 4 | 400 | 0.05 | 0.4325 | 0.4685 | 0.4235 | 0.7600 | 0.3620 | 0.3605 |
| 5 | | 0.1 | 1.1010 | 0.6345 | 1.4320 | 1.5550 | 0.4715 | 0.7535 |
| 6 | | 0.15 | 1.1515 | 1.1180 | 1.6885 | 1.9070 | 1.0495 | 1.2635 |
| 7 | 600 | 0.05 | 0.3850 | 0.4330 | 0.3405 | 0.7680 | 0.3975 | 0.5690 |
| 8 | | 0.1 | 0.6565 | 0.8015 | 0.7485 | 1.1805 | 0.4535 | 0.7655 |
| 9 | | 0.15 | 1.3865 | 1.3300 | 0.8345 | 1.5435 | 0.8460 | 1.1185 |

Table AI.4 Surface roughness (Rt) results of Al-Li-Cu alloy dependence on cutting speed and feed rate

| Test Number | Cutting Speed (m/mm) | Feed Rate (mm/tooth) | Rt (μm) | | | | | |
|---|---|---|---|---|---|---|---|---|
| | | | Lower Hardness (HV) 129 | | Medium Hardness (HV) 146.7 | | Higher Hardness (HV) 164 | |
| | | | Dry | Wet | Dry | Wet | Dry | Wet |
| 1 | 200 | 0.05 | 8.6353 | 6.5865 | 6.3140 | 6.2495 | 5.6910 | 6.1832 |
| 2 | | 0.1 | 8.7365 | 6.6555 | 8.1085 | 8.9639 | 6.6680 | 7.2754 |
| 3 | | 0.15 | 9.7237 | 9.6031 | 9.6410 | 9.0381 | 7.5350 | 9.1020 |
| 4 | 400 | 0.05 | 6.6795 | 6.1085 | 6.4910 | 7.0453 | 5.8845 | 5.8327 |
| 5 | | 0.1 | 8.6580 | 6.8945 | 9.4010 | 9.4050 | 6.1824 | 7.1084 |
| 6 | | 0.15 | 9.2865 | 8.0840 | 9.7907 | 10.5091 | 7.8521 | 8.6242 |
| 7 | 600 | 0.05 | 5.9362 | 6.0523 | 5.7540 | 7.0528 | 6.1675 | 6.7840 |
| 8 | | 0.1 | 6.8374 | 7.1732 | 6.9628 | 8.3706 | 6.2740 | 7.0299 |
| 9 | | 0.15 | 9.3525 | 8.7176 | 7.3090 | 9.4087 | 7.2848 | 8.1301 |

Table AI.5 Surface roughness (Ra) results of Al-Li-Cu-Sc alloy dependence on cutting speed and feed rate

| Test Number | Cutting Speed (m/mm) | Feed Rate (mm/tooth) | Ra (μm) | | | | | |
|---|---|---|---|---|---|---|---|---|
| | | | Lower Hardness (HV) 144.6 | | Medium Hardness (HV) 163.4 | | Higher Hardness (HV) 182.7 | |
| | | | Dry | Wet | Dry | Wet | Dry | Wet |
| 1 | 200 | 0.05 | 0.5160 | 0.4740 | 0.3420 | 0.3545 | 0.4450 | 0.4140 |
| 2 | | 0.1 | 0.7760 | 0.8790 | 0.4080 | 1.1040 | 0.9415 | 0.6370 |
| 3 | | 0.15 | 0.8235 | 1.1095 | 0.9800 | 1.5035 | 1.2320 | 1.7610 |
| 4 | 400 | 0.05 | 0.5620 | 0.3550 | 0.2955 | 1.0125 | 0.4030 | 0.4350 |
| 5 | | 0.1 | 0.7920 | 0.5710 | 0.3200 | 1.1540 | 0.9045 | 1.3610 |
| 6 | | 0.15 | 1.1500 | 1.5430 | 1.0560 | 1.5210 | 1.0165 | 1.6683 |
| 7 | 600 | 0.05 | 0.3225 | 0.2820 | 0.7560 | 0.8285 | 0.6920 | 0.6830 |
| 8 | | 0.1 | 0.6340 | 0.4140 | 0.9900 | 0.8840 | 1.2885 | 1.0620 |
| 9 | | 0.15 | 0.9345 | 0.8970 | 1.1320 | 1.5190 | 1.4120 | 1.8915 |

Table AI.6 Surface roughness (Rt) results of Al-Li-Cu-Sc alloy dependence on cutting speed and feed rate

| Test Number | Cutting Speed (m/mm) | Feed Rate (mm/tooth) | Rt (μm) | | | | | |
|---|---|---|---|---|---|---|---|---|
| | | | Lower Hardness (HV) 144.6 | | Medium Hardness (HV) 163.4 | | Higher Hardness (HV) 182.7 | |
| | | | Dry | Wet | Dry | Wet | Dry | Wet |
| 1 | 200 | 0.05 | 6.3570 | 6.3102 | 5.8810 | 6.1930 | 6.8585 | 6.0756 |
| 2 | | 0.1 | 7.1766 | 7.5795 | 6.4100 | 8.3751 | 7.7269 | 6.8264 |
| 3 | | 0.15 | 7.3264 | 8.8075 | 7.8376 | 9.5074 | 8.7408 | 11.1950 |
| 4 | 400 | 0.05 | 6.6703 | 6.0140 | 5.6710 | 7.9552 | 5.9965 | 7.9425 |
| 5 | | 0.1 | 7.2570 | 7.0480 | 5.9560 | 8.4793 | 7.5612 | 9.5885 |
| 6 | | 0.15 | 8.4024 | 9.5960 | 8.8600 | 9.5486 | 7.9375 | 10.0495 |
| 7 | 600 | 0.05 | 5.5295 | 5.6142 | 7.1049 | 7.5920 | 7.1365 | 6.8648 |
| 8 | | 0.1 | 6.8505 | 6.0702 | 7.8585 | 8.0688 | 8.9234 | 8.0972 |
| 9 | | 0.15 | 7.7205 | 7.5580 | 8.4180 | 9.4859 | 9.4615 | 10.7333 |

Table AI.7 Cutting force results of Al-Li alloy dependence on cutting speed and feed rate

| Test Number | Cutting Speed (m/mm) | Feed Rate (mm/tooth) | Cutting Force (N) AL-Li | | | | | |
|---|---|---|---|---|---|---|---|---|
| | | | Lower Hardness (HV) 56 | | Medium Hardness (HV) 76.5 | | Higher Hardness (HV) 97 | |
| | | | Dry | Wet | Dry | Wet | Dry | Wet |
| 1 | 200 | 0.05 | 101.4 | 115.3 | 124.5 | 121.7 | 141.7 | 130.3 |
| 2 | | 0.1 | 133.4 | 190.5 | 137 | 131.9 | 149.4 | 141.6 |
| 3 | | 0.15 | 147.3 | 149.6 | 158.3 | 151.1 | 187.5 | 171 |
| 4 | 400 | 0.05 | 61.8 | 79.9 | 98.3 | 92.4 | 129 | 125.4 |
| 5 | | 0.1 | 122.5 | 132 | 130.4 | 115.2 | 139.9 | 136.7 |
| 6 | | 0.15 | 146 | 143.9 | 148.7 | 143.4 | 158.4 | 155 |
| 7 | 600 | 0.05 | 60.9 | 52.3 | 77 | 71.1 | 87.2 | 82.5 |
| 8 | | 0.1 | 117.8 | 106.4 | 119.7 | 112.5 | 120.7 | 118 |
| 9 | | 0.15 | 141.5 | 125 | 143.9 | 139.2 | 150.8 | 147.1 |

Table AI.8 Cutting force results of Al-Li-Cu alloy dependence on cutting speed and feed rate

| Test Number | Cutting Speed (m/mm) | Feed Rate (mm/tooth) | Cutting Force (N) Al-Li-Cu | | | | | |
|---|---|---|---|---|---|---|---|---|
| | | | Lower Hardness (HV) 129 | | Medium Hardness (HV) 146.7 | | Higher Hardness (HV) 164 | |
| | | | Dry | Wet | Dry | Wet | Dry | Wet |
| 1 | 200 | 0.05 | 97.4 | 90.1 | 103.3 | 89 | 121.2 | 81.2 |
| 2 | | 0.1 | 100.3 | 95.5 | 110.2 | 107.5 | 141.7 | 116.1 |
| 3 | | 0.15 | 107.9 | 102.4 | 129.8 | 112 | 177.5 | 163.9 |
| 4 | 400 | 0.05 | 95.6 | 92.1 | 99.7 | 91.1 | 110.2 | 89 |
| 5 | | 0.1 | 99.9 | 97.3 | 106.8 | 104.3 | 132.2 | 112.4 |
| 6 | | 0.15 | 106.1 | 101.6 | 121.3 | 118.9 | 151.8 | 163.5 |
| 7 | 600 | 0.05 | 91.5 | 89.9 | 96.6 | 92.2 | 101.4 | 80.6 |
| 8 | | 0.1 | 96.7 | 93.1 | 104.4 | 90.1 | 117.4 | 100.1 |
| 9 | | 0.15 | 111.3 | 100.2 | 137.2 | 127.9 | 169.1 | 136.6 |

Table AI.9 Cutting force results of Al-Li-Cu-Sc alloy dependence on cutting speed and feed rate

| Test Number | Cutting Speed (m/mm) | Feed Rate (mm/tooth) | Cutting Force (N) Al-Li-Cu-Sc | | | | | |
|---|---|---|---|---|---|---|---|---|
| | | | Lower Hardness (HV) 144.6 | | Medium Hardness (HV) 163.4 | | Higher Hardness (HV) 182.7 | |
| | | | Dry | Wet | Dry | Wet | Dry | Wet |
| 1 | 200 | 0.05 | 121.1 | 89.7 | 143.3 | 90.7 | 168.4 | 92.2 |
| 2 | | 0.1 | 134.6 | 106.9 | 151.9 | 115.5 | 171.2 | 126.6 |
| 3 | | 0.15 | 188.4 | 144.3 | 197 | 153.9 | 201.8 | 164.4 |
| 4 | 400 | 0.05 | 113.6 | 81.5 | 117.9 | 84.4 | 121.7 | 88.7 |
| 5 | | 0.1 | 120.7 | 90.2 | 132.4 | 100.5 | 148.9 | 119.9 |
| 6 | | 0.15 | 163.2 | 121.7 | 177.5 | 128.3 | 189 | 131.8 |
| 7 | 600 | 0.05 | 102.3 | 66.9 | 104.9 | 80.9 | 110.5 | 79.9 |
| 8 | | 0.1 | 120 | 109.6 | 133.3 | 114.2 | 149.4 | 121.5 |
| 9 | | 0.15 | 172.9 | 140.2 | 187.9 | 155 | 201.1 | 166.2 |

Table AI.10 Particle emission (Surface) results of Al-Li alloy

| Test Number | Cutting Speed (m/mm) | Feed Rate (mm/ tooth) | Surface (µm²/cm³) | | | | | |
|---|---|---|---|---|---|---|---|---|
| | | | Lower Hardness (HV) 56 | | Medium Hardness (HV) 76.5 | | Higher Hardness (HV) 97 | |
| | | | Dry | Wet | Dry | Wet | Dry | Wet |
| 1 | 200 | 0.05 | 18.5 | 1.29E+04 | 371.4 | 1.30E+04 | 192.8 | 8.27E+03 |
| 2 | | 0.1 | 46.2 | 1.41E+04 | 261.1 | 1.20E+04 | 209.5 | 9.71E+03 |
| 3 | | 0.15 | 76.4 | 2.49E+04 | 338.8 | 1.10E+04 | 210.7 | 8.47E+03 |
| 4 | 400 | 0.05 | 23 | 2.55E+04 | 344.9 | 1.85E+04 | 157.8 | 1.60E+04 |
| 5 | | 0.1 | 91.9 | 2.46E+04 | 351.8 | 2.67E+04 | 227.9 | 1.86E+04 |
| 6 | | 0.15 | 149.2 | 5.06E+04 | 625.2 | 2.77E+04 | 352.4 | 2.09E+04 |
| 7 | 600 | 0.05 | 188.1 | 6.01E+04 | 601.8 | 4.86E+04 | 536 | 4.35E+04 |
| 8 | | 0.1 | 316.1 | 5.76E+04 | 767 | 5.61E+04 | 928.7 | 4.67E+04 |
| 9 | | 0.15 | 18.5 | 9.73E+04 | 722.6 | 6.02E+04 | 1.11E+03 | 5.38E+04 |

Table AI.11 Particle emission (mass concentration) results of Al-Li alloy

| Test Number | Cutting Speed (m/mm) | Feed Rate (mm/tooth) | Mass (mg/m³) | | | | | |
|---|---|---|---|---|---|---|---|---|
| | | | Lower Hardness (HV) 56 | | Medium Hardness (HV) 76.5 | | Higher Hardness (HV) 97 | |
| | | | Dry | Wet | Dry | Wet | Dry | Wet |
| 1 | 200 | 0.05 | 2.74E-02 | 21.3 | 0.486 | 22.3 | 0.237 | 13.8 |
| 2 | | 0.1 | 0.0532 | 23 | 0.372 | 20.5 | 0.253 | 17.1 |
| 3 | | 0.15 | 9.52E-02 | 40.5 | 0.447 | 18.9 | 0.238 | 14.6 |
| 4 | 400 | 0.05 | 2.25E-02 | 42.5 | 0.413 | 31.6 | 0.184 | 27.5 |
| 5 | | 0.1 | 0.11 | 40.8 | 0.419 | 45.5 | 0.261 | 31.6 |
| 6 | | 0.15 | 0.17 | 79.2 | 0.778 | 46.9 | 0.407 | 35.9 |
| 7 | 600 | 0.05 | 0.219 | 93.4 | 0.713 | 77.3 | 0.622 | 70.8 |
| 8 | | 0.1 | 0.454 | 89.2 | 0.951 | 90.3 | 1.12 | 76.4 |
| 9 | | 0.15 | 2.74E-02 | 175.2 | 0.932 | 98.3 | 1.32 | 87.9 |

Table AI.12 Particle emission (number) results of Al-Li alloy

| Test Number | Cutting Speed (m/mm) | Feed Rate (mm/tooth) | Number (#/cm³) | | | | | |
|---|---|---|---|---|---|---|---|---|
| | | | Lower Hardness (HV) 56 | | Medium Hardness (HV) 76.5 | | Higher Hardness (HV) 97 | |
| | | | Dry | Wet | Dry | Wet | Dry | Wet |
| 1 | 200 | 0.05 | 0.876 | 502.4 | 17.8 | 477.9 | 17.9 | 333.3 |
| 2 | | 0.1 | 2.425 | 551.3 | 26.9 | 439.8 | 18.3 | 340.2 |
| 3 | | 0.15 | 6.53 | 1.03E+03 | 29.1 | 414.9 | 19.3 | 315.3 |
| 4 | 400 | 0.05 | 4.84 | 996.7 | 31.6 | 673.8 | 15.7 | 596.1 |
| 5 | | 0.1 | 13.1 | 970.2 | 51.3 | 977.2 | 23.3 | 691.7 |
| 6 | | 0.15 | 18.4 | 2.43E+03 | 52.1 | 998.1 | 32.8 | 751.1 |
| 7 | 600 | 0.05 | 22.4 | 2.86E+03 | 63 | 2.14E+03 | 46.8 | 1.88E+03 |
| 8 | | 0.1 | 26.8 | 2.92E+03 | 58.3 | 2.57E+03 | 70.9 | 2.09E+03 |
| 9 | | 0.15 | 30.9 | 3.29E+03 | 64.6 | 2.72E+03 | 85.1 | 2.39E+03 |

Table AI.13 Particle emission (Surface) results of Al-Li-Cu alloy

| Test Number | Cutting Speed (m/mm) | Feed Rate (mm/ tooth) | Surface (µm²/cm³) | | | | | |
|---|---|---|---|---|---|---|---|---|
| | | | Lower Hardness (HV) 129 | | Medium Hardness (HV) 146.7 | | Higher Hardness (HV) 164 | |
| | | | Dry | Wet | Dry | Wet | Dry | Wet |
| 1 | 200 | 0.05 | 205.7 | 7.51E+03 | 1.37E+03 | 9.44E+03 | 510.1 | 6.29E+03 |
| 2 | | 0.1 | 2.11E+03 | 5.43E+03 | 182.4 | 8.22E+03 | 769.8 | 5.06E+03 |
| 3 | | 0.15 | 3.41E+03 | 5.42E+03 | 885.1 | 8.39E+03 | 1.10E+03 | 5.34E+03 |
| 4 | 400 | 0.05 | 3.53E+03 | 1.42E+04 | 2.40E+03 | 1.52E+04 | 1.19E+03 | 1.39E+04 |
| 5 | | 0.1 | 5.27E+03 | 1.46E+04 | 3.28E+03 | 2.10E+04 | 1.89E+03 | 2.01E+04 |
| 6 | | 0.15 | 5.47E+03 | 2.01E+04 | 3.94E+03 | 2.25E+04 | 2.37E+03 | 1.97E+04 |
| 7 | 600 | 0.05 | 6.07E+03 | 3.41E+04 | 4.56E+03 | 3.50E+04 | 2.30E+03 | 3.12E+04 |
| 8 | | 0.1 | 6.97E+03 | 4.30E+04 | 4.87E+03 | 4.05E+04 | 2.71E+03 | 3.54E+04 |
| 9 | | 0.15 | 7.34E+03 | 3.88E+04 | 6.80E+03 | 4.48E+04 | 3.12E+03 | 3.81E+04 |

Table AI.14 Particle emission (mass concentration) results of Al-Li-Cu alloy

| Test Number | Cutting Speed (m/mm) | Feed Rate (mm/tooth) | Mass (mg/m³) | | | | | |
|---|---|---|---|---|---|---|---|---|
| | | | Lower Hardness (HV) 129 | | Medium Hardness (HV) 146.7 | | Higher Hardness (HV) 164 | |
| | | | Dry | Wet | Dry | Wet | Dry | Wet |
| 1 | 200 | 0.05 | 0.266 | 12.5 | 1.84 | 15.5 | 0.691 | 10.4 |
| 2 | | 0.1 | 2.85 | 9.26 | 0.278 | 14.2 | 1.05 | 8.72 |
| 3 | | 0.15 | 4.69 | 9.1 | 1.27 | 14.3 | 1.5 | 9.18 |
| 4 | 400 | 0.05 | 4.94 | 24 | 3.38 | 25.8 | 1.56 | 23.5 |
| 5 | | 0.1 | 6.95 | 24.5 | 4.63 | 35.3 | 2.46 | 34.5 |
| 6 | | 0.15 | 7.27 | 33.4 | 5.44 | 38.3 | 3.1 | 33.6 |
| 7 | 600 | 0.05 | 8.15 | 54.3 | 6.24 | 56.4 | 3.02 | 50 |
| 8 | | 0.1 | 9.16 | 68.2 | 6.67 | 65.6 | 3.63 | 58 |
| 9 | | 0.15 | 9.66 | 62.2 | 9.51 | 71.9 | 4.13 | 62 |

Table AI.15 Particle emission (number) results of Al-Li-Cu alloy

| Test Number | Cutting Speed (m/mm) | Feed Rate (mm/tooth) | Number (#/cm³) | | | | | |
|---|---|---|---|---|---|---|---|---|
| | | | Lower Hardness (HV) 129 | | Medium Hardness (HV) 146.7 | | Higher Hardness (HV) 164 | |
| | | | Dry | Wet | Dry | Wet | Dry | Wet |
| 1 | 200 | 0.05 | 17.1 | 314 | 85.3 | 410.3 | 30.6 | 268 |
| 2 | | 0.1 | 139.2 | 218.8 | 8.64 | 314.6 | 45.5 | 201.7 |
| 3 | | 0.15 | 206.3 | 221.9 | 46.5 | 340.8 | 65.3 | 217.7 |
| 4 | 400 | 0.05 | 213.9 | 560.5 | 135.7 | 606.2 | 74.1 | 547 |
| 5 | | 0.1 | 338.3 | 574.6 | 183.7 | 841.4 | 121.6 | 761 |
| 6 | | 0.15 | 347.4 | 819.7 | 227.7 | 875.9 | 153.3 | 757.6 |
| 7 | 600 | 0.05 | 380.5 | 1.63E+03 | 276.7 | 1.70E+03 | 148.9 | 1.55E+03 |
| 8 | | 0.1 | 458.2 | 1.90E+03 | 289.7 | 1.92E+03 | 172.6 | 1.70E+03 |
| 9 | | 0.15 | 481.2 | 2.13E+03 | 393.9 | 2.16E+03 | 203.6 | 1.87E+03 |

Table AI.16 Particle emission (Surface) results of Al-Li-Cu-Sc alloy

| Test Number | Cutting Speed (m/mm) | Feed Rate (mm/ tooth) | Surface (µm²/cm³) | | | | | |
|---|---|---|---|---|---|---|---|---|
| | | | Lower Hardness (HV) 144.6 | | Medium Hardness (HV) 163.4 | | Higher Hardness (HV) 182.7 | |
| | | | Dry | Wet | Dry | Wet | Dry | Wet |
| 1 | 200 | 0.05 | 43.5 | 1.90E+04 | 204.1 | 1.10E+04 | 852.2 | 1.17E+04 |
| 2 | | 0.1 | 151.4 | 1.20E+04 | 644 | 1.01E+04 | 604.6 | 7.82E+03 |
| 3 | | 0.15 | 236 | 1.32E+04 | 796.4 | 9.43E+03 | 959.6 | 8.42E+03 |
| 4 | 400 | 0.05 | 238.5 | 2.42E+04 | 634 | 1.96E+04 | 1.08E+03 | 1.99E+04 |
| 5 | | 0.1 | 584.8 | 2.72E+04 | 877.4 | 2.44E+04 | 1.41E+03 | 2.61E+04 |
| 6 | | 0.15 | 876.4 | 2.97E+04 | 1.08E+03 | 2.36E+04 | 1.47E+03 | 3.18E+04 |
| 7 | 600 | 0.05 | 1.10E+03 | 4.90E+04 | 1.21E+03 | 8.19E+04 | 1.60E+03 | 5.12E+04 |
| 8 | | 0.1 | 1.68E+03 | 1.11E+05 | 1.37E+03 | 8.63E+04 | 2.01E+03 | 5.59E+04 |
| 9 | | 0.15 | 1.91E+03 | 1.11E+05 | 1.52E+03 | 9.62E+04 | 2.05E+03 | 5.77E+04 |

Table AI.17 Particle emission (mass concentration) results of Al-Li-Cu-Sc alloy

| Test Number | Cutting Speed (m/mm) | Feed Rate (mm/tooth) | Mass (mg/m³) | | | | | |
|---|---|---|---|---|---|---|---|---|
| | | | Lower Hardness (HV) 144.6 | | Medium Hardness (HV) 163.4 | | Higher Hardness (HV) 182.7 | |
| | | | Dry | Wet | Dry | Wet | Dry | Wet |
| 1 | 200 | 0.05 | 5.93E-02 | 30.5 | 0.239 | 18.7 | 1.22 | 18.7 |
| 2 | | 0.1 | 0.183 | 20 | 0.849 | 17.4 | 0.8 | 12.8 |
| 3 | | 0.15 | 0.354 | 22.3 | 1.05 | 16.5 | 1.27 | 13.8 |
| 4 | 400 | 0.05 | 0.295 | 41.1 | 0.782 | 33.9 | 1.43 | 32.6 |
| 5 | | 0.1 | 0.725 | 47.5 | 1.1 | 42.4 | 1.84 | 41.8 |
| 6 | | 0.15 | 1.08 | 51.9 | 1.33 | 40.7 | 1.85 | 51.9 |
| 7 | 600 | 0.05 | 1.45 | 82 | 1.54 | 126.8 | 2.06 | 79.8 |
| 8 | | 0.1 | 2.2 | 172.2 | 1.67 | 134.1 | 2.68 | 88 |
| 9 | | 0.15 | 2.61 | 175.6 | 1.85 | 149.9 | 2.65 | 90.4 |

Table AI.18 Particle emission (number) results of Al-Li-Cu-Sc alloy

| Test Number | Cutting Speed (m/mm) | Feed Rate (mm/tooth) | Number (#/cm³) | | | | | |
|---|---|---|---|---|---|---|---|---|
| | | | Lower Hardness (HV) 144.6 | | Medium Hardness (HV) 163.4 | | Higher Hardness (HV) 182.7 | |
| | | | Dry | Wet | Dry | Wet | Dry | Wet |
| 1 | 200 | 0.05 | 4.1 | 794.3 | 15 | 411.8 | 43.4 | 475.9 |
| 2 | | 0.1 | 69.5 | 459.8 | 37.9 | 380 | 35.9 | 316 |
| 3 | | 0.15 | 15.1 | 507.1 | 47.3 | 344.4 | 56.1 | 346.4 |
| 4 | 400 | 0.05 | 17.1 | 894.7 | 42.5 | 718.1 | 66.9 | 784.7 |
| 5 | | 0.1 | 42.4 | 941.8 | 55.4 | 893.1 | 88.8 | 1.09E+03 |
| 6 | | 0.15 | 62.5 | 1.04E+03 | 71.6 | 884.8 | 95.2 | 1.27E+03 |
| 7 | 600 | 0.05 | 69.5 | 2.08E+03 | 77 | 3.75E+03 | 101.6 | 2.46E+03 |
| 8 | | 0.1 | 105.9 | 5.22E+03 | 94.2 | 3.97E+03 | 126.5 | 2.62E+03 |
| 9 | | 0.15 | 117.3 | 5.11E+03 | 106.8 | 4.42E+03 | 134.2 | 2.75E+03 |

## APPENDIX II

## ANOVA TABLES

Table AII.1 The Al-Li alloy ANOVA table for Ra

| Source | Sum of Squares | Df | Mean Square | F-Ratio | P-Value |
|---|---|---|---|---|---|
| A: Cutting Speed | 3.653 | 1 | 3.653 | 127.95 | 0.000 |
| B: Feed Rate | 1.187 | 1 | 1.187 | 41.59 | 0.000 |
| C: Hardness | 0.002 | 1 | 0.002 | 0.08 | 0.783 |
| D: Cooling mode | 1.053 | 1 | 1.053 | 36.91 | 0.000 |
| AA | 0.000 | 1 | 0.000 | 0.00 | 0.967 |
| AB | 0.518 | 1 | 0.519 | 18.14 | 0.000 |
| AC | 0.000 | 1 | 0.000 | 0.01 | 0.917 |
| AD | 0.151 | 1 | 0.152 | 5.31 | 0.026 |
| BB | 0.003 | 1 | 0.003 | 0.14 | 0.712 |
| BC | 0.008 | 1 | 0.008 | 0.28 | 0.603 |
| BD | 0.318 | 1 | 0.318 | 11.15 | 0.002 |
| CC | 0.173 | 1 | 0.173 | 6.07 | 0.018 |
| CD | 0.405 | 1 | 0.405 | 14.19 | 0.000 |
| Total error | 1.142 | 40 | 0.028 | | |
| Total (corr.) | 8.618 | 53 | | | |

Table AII.2 The Al-Li alloy ANOVA table for Rt

| Source | Sum of Squares | Df | Mean Square | F-Ratio | P-Value |
|---|---|---|---|---|---|
| A: Cutting Speed | 48.141 | 1 | 48.141 | 85.28 | 0.000 |
| B: Feed Rate | 11.899 | 1 | 11.898 | 21.08 | 0.000 |
| C: Hardness | 1.149 | 1 | 1.149 | 2.04 | 0.161 |
| D: Cooling mode | 18.719 | 1 | 18.719 | 33.16 | 0.000 |
| AA | 0.141 | 1 | 0.140 | 0.25 | 0.620 |
| AB | 7.027 | 1 | 7.027 | 12.45 | 0.001 |
| AC | 0.325 | 1 | 0.325 | 0.58 | 0.452 |
| AD | 2.256 | 1 | 2.256 | 4.00 | 0.052 |
| BB | 1.136 | 1 | 1.136 | 2.01 | 0.164 |
| BC | 0.535 | 1 | 0.535 | 0.95 | 0.336 |
| BD | 4.641 | 1 | 4.641 | 8.22 | 0.007 |
| CC | 0.302 | 1 | 0.302 | 0.54 | 0.468 |
| CD | 10.803 | 1 | 10.803 | 19.14 | 0.000 |
| Total error | 22.580 | 40 | 0.564 | | |
| Total (corr.) | 129.658 | 53 | | | |

Table AII.3 The Al-Li-Cu alloy ANOVA table for Ra

| Source | Sum of Squares | Df | Mean Square | F-Ratio | P-Value |
|---|---|---|---|---|---|
| A: Feed Rate | 5.910 | 1 | 5.910 | 115.38 | 0.000 |
| B: Cutting Speed | 0.380 | 1 | 0.380 | 7.42 | 0.009 |
| C: Hardness | 0.431 | 1 | 0.430 | 8.41 | 0.006 |
| D: Cooling | 0.095 | 1 | 0.094 | 1.85 | 0.181 |
| AA | 0.000 | 1 | 0.000 | 0.01 | 0.939 |
| AB | 0.032 | 1 | 0.032 | 0.64 | 0.430 |
| AC | 0.009 | 1 | 0.009 | 0.19 | 0.669 |
| AD | 0.032 | 1 | 0.031 | 0.62 | 0.434 |
| BB | 0.010 | 1 | 0.010 | 0.20 | 0.658 |
| BC | 0.108 | 1 | 0.107 | 2.10 | 0.155 |
| BD | 0.315 | 1 | 0.314 | 6.15 | 0.017 |
| CC | 0.851 | 1 | 0.851 | 16.61 | 0.000 |
| CD | 0.401 | 1 | 0.401 | 7.83 | 0.008 |
| Total error | 2.050 | 40 | 0.051 | | |
| Total (corr.) | 10.625 | 53 | | | |

Table AII.4 The Al-Li-Cu alloy ANOVA table for Rt

| Source | Sum of Squares | Df | Mean Square | F-Ratio | P-Value |
|---|---|---|---|---|---|
| A: Feed Rate | 52.670 | 1 | 52.669 | 121.74 | 0.000 |
| B: Cutting Speed | 2.841 | 1 | 2.840 | 6.57 | 0.014 |
| C: Hardness | 5.531 | 1 | 5.531 | 12.79 | 0.001 |
| D: Cooling | 0.432 | 1 | 0.432 | 1.00 | 0.323 |
| AA | 0.009 | 1 | 0.009 | 0.02 | 0.881 |
| AB | 0.266 | 1 | 0.266 | 0.62 | 0.437 |
| AC | 0.323 | 1 | 0.322 | 0.75 | 0.393 |
| AD | 0.267 | 1 | 0.266 | 0.62 | 0.437 |
| BB | 0.648 | 1 | 0.648 | 1.50 | 0.228 |
| BC | 1.078 | 1 | 1.078 | 2.49 | 0.122 |
| BD | 1.884 | 1 | 1.884 | 4.36 | 0.043 |
| CC | 6.404 | 1 | 6.404 | 14.80 | 0.000 |
| CD | 5.841 | 1 | 5.841 | 13.50 | 0.001 |
| Total error | 17.305 | 40 | 0.432 | | |
| Total (corr.) | 95.502 | 53 | | | |

Table AII.5 The Al-Li-Cu-Sc alloy ANOVA table for Ra

| Source | Sum of Squares | Df | Mean Square | F-Ratio | P-Value |
|---|---|---|---|---|---|
| A: Feed Rate | 5.427 | 1 | 5.427 | 123.89 | 0.000 |
| B: Cutting Speed | 0.103 | 1 | 0.102 | 2.34 | 0.134 |
| C: Hardness | 0.755 | 1 | 0.754 | 17.23 | 0.000 |
| D: Cooling | 0.499 | 1 | 0.499 | 11.40 | 0.002 |
| AA | 0.040 | 1 | 0.0401 | 0.92 | 0.344 |
| AB | 0.017 | 1 | 0.017 | 0.39 | 0.535 |
| AC | 0.160 | 1 | 0.160 | 3.67 | 0.063 |
| AD | 0.279 | 1 | 0.279 | 6.38 | 0.016 |
| BB | 0.008 | 1 | 0.007 | 0.18 | 0.675 |
| BC | 0.302 | 1 | 0.302 | 6.90 | 0.012 |
| BD | 0.060 | 1 | 0.060 | 1.38 | 0.248 |
| CC | 0.009 | 1 | 0.009 | 0.23 | 0.636 |
| CD | 0.068 | 1 | 0.067 | 1.55 | 0.220 |
| Total error | 1.752 | 40 | 0.043 | | |
| Total (corr.) | 9.481 | 53 | | | |

Table AII.6 The Al-Li-Cu-Sc alloy ANOVA table for Rt

| Source | Sum of Squares | Df | Mean Square | F-Ratio | P-Value |
|---|---|---|---|---|---|
| A: Feed Rate | 52.367 | 1 | 52.367 | 106.75 | 0.000 |
| B: Cutting Speed | 0.423 | 1 | 0.423 | 0.86 | 0.358 |
| C: Hardness | 10.921 | 1 | 10.920 | 22.26 | 0.000 |
| D: Cooling | 7.075 | 1 | 7.074 | 14.42 | 0.001 |
| AA | 0.486 | 1 | 0.486 | 0.99 | 0.325 |
| AB | 0.202 | 1 | 0.202 | 0.41 | 0.524 |
| AC | 0.780 | 1 | 0.780 | 1.59 | 0.214 |
| AD | 1.969 | 1 | 1.969 | 4.01 | 0.052 |
| BB | 0.427 | 1 | 0.427 | 0.87 | 0.356 |
| BC | 2.672 | 1 | 2.671 | 5.45 | 0.025 |
| BD | 0.832 | 1 | 0.832 | 1.70 | 0.200 |
| CC | 0.073 | 1 | 0.072 | 0.15 | 0.702 |
| CD | 0.909 | 1 | 0.909 | 1.85 | 0.181 |
| Total error | 19.622 | 40 | 0.490 | | |
| Total (corr.) | 98.760 | 53 | | | |

Table AII.7 The Al-Li ANOVA table for Cutting force

| Source | Sum of Squares | Df | Mean Square | F-Ratio | P-Value |
|---|---|---|---|---|---|
| A: Feed Rate | 25334.0 | 1 | 25334.0 | 192.05 | 0.000 |
| B: Cutting Speed | 10332.7 | 1 | 10332.7 | 78.33 | 0.000 |
| C: Hardness | 3300.5 | 1 | 3300.5 | 25.02 | 0.000 |
| D: Cooling | 54.0 | 1 | 54.0 | 0.41 | 0.526 |
| AA | 582.413 | 1 | 582.413 | 4.42 | 0.042 |
| AB | 1450.82 | 1 | 1450.82 | 11.00 | 0.002 |
| AC | 486.0 | 1 | 486.0 | 3.68 | 0.0621 |
| AD | 59.29 | 1 | 59.29 | 0.45 | 0.506 |
| BB | 14.301 | 1 | 14.301 | 0.11 | 0.744 |
| BC | 14.107 | 1 | 14.107 | 0.11 | 0.745 |
| BD | 214.623 | 1 | 214.623 | 1.63 | 0.209 |
| CC | 258.541 | 1 | 258.541 | 1.96 | 0.169 |
| CD | 395.347 | 1 | 395.347 | 3.00 | 0.091 |
| Total error | 5276.56 | 40 | 131.914 | | |
| Total (corr.) | 47773.3 | 53 | | | |

Table AII.8 The Al-Li-Cu ANOVA table for Cutting force

| Source | Sum of Squares | Df | Mean Square | F-Ratio | P-Value |
|---|---|---|---|---|---|
| A: Feed Rate | 10916.8 | 1 | 10916.8 | 237.78 | 0.000 |
| B: Cutting Speed | 340.403 | 1 | 340.403 | 7.41 | 0.009 |
| C: Hardness | 6861.36 | 1 | 6861.36 | 149.45 | 0.000 |
| D: Cooling | 1665.56 | 1 | 1665.56 | 36.28 | 0.000 |
| AA | 367.045 | 1 | 367.045 | 7.99 | 0.007 |
| AB | 14.727 | 1 | 14.7267 | 0.32 | 0.574 |
| AC | 3898.95 | 1 | 3898.95 | 84.92 | 0.000 |
| AD | 37.414 | 1 | 37.414 | 0.81 | 0.372 |
| BB | 0.1712 | 1 | 0.171 | 0.00 | 0.952 |
| BC | 304.594 | 1 | 304.594 | 6.63 | 0.014 |
| BD | 7.7469 | 1 | 7.747 | 0.17 | 0.683 |
| CC | 208.889 | 1 | 208.889 | 4.55 | 0.039 |
| CD | 503.254 | 1 | 503.254 | 10.96 | 0.002 |
| Total error | 1836.44 | 40 | 45.911 | | |
| Total (corr.) | 26963.3 | 53 | | | |

Table AII.9 The Al-Li-Cu-Sc ANOVA table for Cutting force

| Source | Sum of Squares | Df | Mean Square | F-Ratio | P-Value |
|---|---|---|---|---|---|
| A: Feed Rate | 35218.8 | 1 | 35218.8 | 582.65 | 0.000 |
| B: Cutting Speed | 1670.08 | 1 | 1670.08 | 27.63 | 0.000 |
| C: Hardness | 3708.81 | 1 | 3708.81 | 61.36 | 0.000 |
| D: Cooling | 17759.8 | 1 | 17759.8 | 293.81 | 0.000 |
| AA | 881.796 | 1 | 881.796 | 14.59 | 0.001 |
| AB | 742.594 | 1 | 742.594 | 12.29 | 0.00 |
| AC | 57.970 | 1 | 57.970 | 0.96 | 0.333 |
| AD | 16.268 | 1 | 16.268 | 0.27 | 0.607 |
| BB | 1593.14 | 1 | 1593.14 | 26.36 | 0.000 |
| BC | 21.850 | 1 | 21.850 | 0.36 | 0.551 |
| BD | 588.871 | 1 | 588.871 | 9.74 | 0.003 |
| CC | 0.0370 | 1 | 0.0370 | 0.00 | 0.980 |
| CD | 200.694 | 1 | 200.694 | 3.32 | 0.076 |
| Total error | 2417.84 | 40 | 60.446 | | |
| Total (corr.) | 64878.5 | 53 | | | |

Table AII.10 The Al-Li alloy ANOVA table for Particle Emission (mass concentration) wet condition

| Source | Sum of Squares | Df | Mean Square | F-Ratio | P-Value |
|---|---|---|---|---|---|
| A: Feed Rate | 2153.87 | 1 | 2153.87 | 16.84 | 0.0007 |
| B: Cutting Speed | 24701.2 | 1 | 24701.2 | 193.16 | 0.0000 |
| C: Hardness | 2926.13 | 1 | 2926.13 | 22.88 | 0.0002 |
| AA | 308.645 | 1 | 308.645 | 2.41 | 0.1387 |
| AB | 889.241 | 1 | 889.241 | 6.95 | 0.0173 |
| AC | 1034.16 | 1 | 1034.16 | 8.09 | 0.0112 |
| BB | 1533.87 | 1 | 1533.87 | 11.99 | 0.0030 |
| BC | 579.63 | 1 | 579.63 | 4.53 | 0.0482 |
| CC | 111.227 | 1 | 111.227 | 0.87 | 0.3641 |
| Total error | 2173.93 | 17 | 127.878 | | |
| Total (corr.) | 36411.9 | 26 | | | |

Table AII.11 The Al-Li alloy ANOVA table for Particle Emission (mass concentration) Dry Condition

| Source | Sum of Squares | Df | Mean Square | F-Ratio | P-Value |
|---|---|---|---|---|---|
| A: Feed Rate | 0.159236 | 1 | 0.159236 | 11.71 | 0.0032 |
| B: Cutting Speed | 1.4827 | 1 | 1.4827 | 109.06 | 0.0000 |
| C: Hardness | 0.491734 | 1 | 0.491734 | 36.17 | 0.0000 |
| AA | 0.00908445 | 1 | 0.00908445 | 0.67 | 0.4250 |
| AB | 0.0957653 | 1 | 0.0957653 | 7.04 | 0.0167 |
| AC | 0.0336021 | 1 | 0.0336021 | 2.47 | 0.1343 |
| BB | 0.151252 | 1 | 0.151252 | 11.13 | 0.0039 |
| BC | 0.130813 | 1 | 0.130813 | 9.62 | 0.0065 |
| CC | 0.653642 | 1 | 0.653642 | 48.08 | 0.0000 |
| Total error | 0.231117 | 17 | 0.0135951 | | |
| Total (corr.) | 3.43895 | 26 | | | |

Table AII.12 The Al-Li-Cu alloy ANOVA table for Particle Emission (mass concentration) wet condition

| Source | Sum of Squares | Df | Mean Square | F-Ratio | P-Value |
|---|---|---|---|---|---|
| A: Feed Rate | 210.672 | 1 | 210.672 | 19.37 | 0.0004 |
| B: Cutting Speed | 11023.2 | 1 | 11023.2 | 1013.68 | 0.0000 |
| C: Hardness | 3.1752 | 1 | 3.1752 | 0.29 | 0.5960 |
| AA | 16.8673 | 1 | 16.8673 | 1.55 | 0.2299 |
| AB | 141.591 | 1 | 141.591 | 13.02 | 0.0022 |
| AC | 4.06003 | 1 | 4.06003 | 0.37 | 0.5493 |
| BB | 207.917 | 1 | 207.917 | 19.12 | 0.0004 |
| BC | 12.2816 | 1 | 12.2816 | 1.13 | 0.3028 |
| CC | 140.941 | 1 | 140.941 | 12.96 | 0.0022 |
| Total error | 184.865 | 17 | 10.8744 | | |
| Total (corr.) | 11945.5 | 26 | | | |

Table AII.13 The Al-Li-Cu alloy ANOVA table for Particle Emission (mass concentration) Dry Condition

| Source | Sum of Squares | Df | Mean Square | F-Ratio | P-Value |
|---|---|---|---|---|---|
| A: Feed Rate | 15.0938 | 1 | 15.0938 | 19.96 | 0.0003 |
| B: Cutting Speed | 116.205 | 1 | 116.205 | 153.68 | 0.0000 |
| C: Hardness | 59.7507 | 1 | 59.7507 | 79.02 | 0.0000 |
| AA | 0.0313445 | 1 | 0.0313445 | 0.04 | 0.8411 |
| AB | 0.125461 | 1 | 0.125461 | 0.17 | 0.6888 |
| AC | 1.924 | 1 | 1.924 | 2.54 | 0.1291 |
| BB | 0.4365 | 1 | 0.4365 | 0.58 | 0.4578 |
| BC | 11.2617 | 1 | 11.2617 | 14.89 | 0.0013 |
| CC | 0.219013 | 1 | 0.219013 | 0.29 | 0.5974 |
| Total error | 12.8548 | 17 | 0.756163 | | |
| Total (corr.) | 217.902 | 26 | | | |

Table AII.14 The Al-Li-Cu-Sc alloy ANOVA table for Particle Emission (mass concentration) wet condition

| Source | Sum of Squares | Df | Mean Square | F-Ratio | P-Value |
|---|---|---|---|---|---|
| A: Feed Rate | 1231.73 | 1 | 1231.73 | 4.53 | 0.0482 |
| B: Cutting Speed | 47853.9 | 1 | 47853.9 | 176.12 | 0.0000 |
| C: Hardness | 2527.61 | 1 | 2527.61 | 9.30 | 0.0072 |
| AA | 105.002 | 1 | 105.002 | 0.39 | 0.5424 |
| AB | 1694.56 | 1 | 1694.56 | 6.24 | 0.0231 |
| AC | 422.453 | 1 | 422.453 | 1.55 | 0.2293 |
| BB | 4664.88 | 1 | 4664.88 | 17.17 | 0.0007 |
| BC | 1730.4 | 1 | 1730.4 | 6.37 | 0.0219 |
| CC | 143.082 | 1 | 143.082 | 0.53 | 0.4779 |
| Total error | 4619.15 | 17 | 271.715 | | |
| Total (corr.) | 64992.7 | 26 | | | |

Table AII.15 The Al-Li-Cu-Sc alloy ANOVA table for Particle Emission (mass concentration) Dry Condition

| Source | Sum of Squares | Df | Mean Square | F-Ratio | P-Value |
|---|---|---|---|---|---|
| A: Feed Rate | 1.35521 | 1 | 1.35521 | 20.66 | 0.0003 |
| B: Cutting Speed | 8.89857 | 1 | 8.89857 | 135.63 | 0.0000 |
| C: Hardness | 2.57948 | 1 | 2.57948 | 39.32 | 0.0000 |
| AA | 0.0165375 | 1 | 0.0165375 | 0.25 | 0.6221 |
| AB | 0.0726963 | 1 | 0.0726963 | 1.11 | 0.3072 |
| AC | 0.110208 | 1 | 0.110208 | 1.68 | 0.2123 |
| BB | 0.281667 | 1 | 0.281667 | 4.29 | 0.0538 |
| BC | 0.196096 | 1 | 0.196096 | 2.99 | 0.1020 |
| CC | 0.291281 | 1 | 0.291281 | 4.44 | 0.0503 |
| Total error | 1.11534 | 17 | 0.065608 | | |
| Total (corr.) | 14.9171 | 26 | | | |

## BIBLIOGRAPHY


Aamir, Muhammad, Khaled Giasin, Majid Tolouei-Rad, and Ana Vafadar. 2020. 'A review: Drilling performance and hole quality of aluminium alloys for aerospace applications', *Journal of Materials Research and Technology*, 9: 12484-500.

Abdelaziz, M. H., A. M. Samuel, H. W. Doty, and F. H. Samuel. 2020. 'Effect of Extended Thermal Exposure and Alloying Elements on the Morphology of Eutectic Si in Al–Si Cast Alloys', *International Journal of Metalcasting*, 14: 1013-24.

Akkurt, Adnan, Mustafa Kemal Kulekci, Ulvi Seker, and Fevzi Ercan. 2004. 'Effect of feed rate on surface roughness in abrasive waterjet cutting applications', *Journal of Materials Processing Technology*, 147: 389-96.

Akram, Sohail, Syed Husain Imran Jaffery, Mushtaq Khan, Aamir Mubashar, and Liaqat Ali. 2015. 'A numerical investigation of effects of cutting velocity and feed rate on residual stresses in aluminum alloy Al-6061', *Int J Mater Mech Manuf*, 3: 26-30.

Arumugam, Prabhu U, Ajay P Malshe, Stephen A Batzer, and Deepak G Bhat. 2003. 'Study of airborne dust emission and process performance during dry machining of aluminum-silicon alloy with PCD and CVD diamond-coated tools', *Journal of Manufacturing Processes*, 5: 163-69.

Ashton, RF, DS Thompson, and FW Gayle. 1986. 'The effect of processing on the properties of Al-Li alloys', *Aluminum alloys-their physical and mechanical properties. EMAS, Warley, England*: 403-17.

Bagali, Anoop, Bose JS, and Gnyaneshwar Nayak. 2023. 'Analysis of Al-Li Alloy Machinability Characteristics for Better Surface Smoothness using the Taguchi Method', *Journal of Mines, Metals & Fuels*, 71.

Balout, B, Victor Songmene, and Jacques Masounave. 2007. 'An experimental study of dust generation during dry drilling of pre-cooled and pre-heated workpiece materials', *Journal of Manufacturing Processes*, 9: 23-34.

Benardos, P. G., and G. C. Vosniakos. 2003. 'Predicting surface roughness in machining: a review', *International journal of machine tools and manufacture*, 43: 833-44.

Bhushan, Rajesh Kumar, Sudhir Kumar, and S Das. 2010. 'Effect of machining parameters on surface roughness and tool wear for 7075 Al alloy SiC composite', *The International Journal of Advanced Manufacturing Technology*, 50: 459-69.

Biermann, Dirk, and Markus Heilmann. 2010. 'Improvement of workpiece quality in face milling of aluminum alloys', *Journal of Materials Processing Technology*, 210: 1968-75.

Boswell, Brian, Mohammad Nazrul Islam, Ian J Davies, and Alokesh Pramanik. 2017. 'Effect of machining parameters on the surface finish of a metal matrix composite under dry cutting conditions', *Proceedings of the Institution of Mechanical Engineers, Part B: Journal of engineering manufacture*, 231: 913-23.

Bull, MJ, and DJ Lloyd. 1986. 'Textures developed in Al-Li-Cu-Mg alloy', *Aluminium-lithium alloys III*: 402-10.

Campos, Fabio de Oliveira, Adriane Lopes Mougo, and Anna Carla Araujo. 2017. 'Study of the cutting forces on micromilling of an aluminum alloy', *Journal of the Brazilian Society of Mechanical Sciences and Engineering*, 39: 1289-96.

Carvalho, Paulo Paiva, Gustavo HN Fernandes, Lucas MQ Barbosa, Felipe CR de Souza, José AG de Sousa, Paulo S Martins, Elhadji HT Ba, and Álisson R Machado. 2021. 'Study About Minimum Quantity Lubrification in Bearing Holes Bored with Pcd Tools in Aluminum Alloy', DOI: https://doi.org/10.21203/rs.3.rs-972806/v1.

Chen, Xiaoxue, Xinwu Ma, Huakun Xi, Guoqun Zhao, Yongxiao Wang, and Xiao Xu. 2020. 'Effects of heat treatment on the microstructure and mechanical properties of extruded 2196 Al-Cu-Li alloy', *Materials & Design*, 192: 108746.

Childs, Thomas HC. 2000. *Metal machining: theory and applications* (Butterworth-Heinemann).

Committee, ASM Handbook. 1990. 'Properties and selection: nonferrous alloys and special-purpose materials. In.: ASM international.

Dasch, Jean, James D'Arcy, Aaron Gundrum, John Sutherland, John Johnson, and David Carlson. 2005. 'Characterization of fine particles from machining in automotive plants', *Journal of occupational and environmental hygiene*, 2: 609-25.

De Jong, HF. 1984. 'Aluminium-Lithium Alloys: The answer of the aluminium industry to the threat of advanced fibre-reinforced materials', *Delft University of Technology, Department of Aerospace Engineering, Report LR-406*.

Deschamps, Alexis, Benjamin Decreus, Frederic De Geuser, Thomas Dorin, and Matthew Weyland. 2013. 'The influence of precipitation on plastic deformation of Al–Cu–Li alloys', *Acta materialia*, 61: 4010-21.

Dhanalakshmi, S, and T Rameshbabu. 2021. 'Comparative study of parametric influence on wet and dry machining of LM 25 aluminium alloy', *Materials Today: Proceedings*, 39: 48-53.

Djebara, A, Walid Jomaa, A Bahloul, and V Songmene. 2013. 'Dust emission during dry machining of Aeronautic Aluminum Alloys.' In Proceedings of 1st International Conference on Aeronautics Sciences (Oran, Algeria) ICAS.

Djebara, A, and V Songmene. 2012. 'Dry machining of aluminum alloys and air quality.' In *Proceedings of the 37th International MATADOR Conference*, 135. Springer Science & Business Media.

Djebara, A, Y Zedan, Jules Kouam, and Victor Songmene. 2013. 'The effect of the heat treatment on the dust emission during machining of an Al-7Si-Mg cast alloys', *Journal of materials engineering and performance*, 22: 3840-53.

Duan, Shu-Wei, Kenji Matsuda, Tao Wang, and Yong Zou. 2021. 'Microstructures and mechanical properties of a cast Al–Cu–Li alloy during heat treatment procedure', *Rare Metals*, 40: 1897-906.

Duan, Zhenjing, Changhe Li, Wenfeng Ding, Yanbin Zhang, Min Yang, Teng Gao, Huajun Cao, Xuefeng Xu, Dazhong Wang, and Cong Mao. 2021. 'Milling force model for aviation aluminum alloy: academic insight and perspective analysis', *Chinese journal of mechanical engineering*, 34: 1-35.

Dursun, Tolga, and Costas Soutis. 2014. 'Recent developments in advanced aircraft aluminium alloys', *Materials & Design (1980-2015)*, 56: 862-71.

Ekvall, JC, JE Rhodes, and GG Wald. 1982. 'Methodology for evaluating weight savings from basic material properties.' in, *Design of fatigue and fracture resistant structures* (ASTM international).

El-Kady, EY, AM Gaafer, MHG Ghaith, T Khalil, and AA Mostafa. 2015. 'The effect of machining parameters on the cutting forces, tool wear, and machined surface roughness of metal matrix nano composite material', *Advances in Materials*, 4: 43-50.

Fridlyander, IN, NI Kolobnev, AL Berezina, and KV Chuistov. 1992. 'The effect of scandium on decomposition kinetics in aluminium-lithium alloys', *Aluminium—lithium alloys VI, Deutsche Gesellschaft für Metallkunde, Frankfurt, Germany*: 107-12.

Garza Elizondo, Guillermo Hernan. 2010. 'Machinability of Al-(7-11%) Si casting alloys: role of free-cutting elements', M. Eng. Thesis, Université du Québec à Chicoutimi, Quebec, Canada.

Giasin, Khaled, Alma Hodzic, Vaibhav Phadnis, and Sabino Ayvar-Soberanis. 2016. 'Assessment of cutting forces and hole quality in drilling Al2024 aluminium alloy: experimental and finite element study', *The International Journal of Advanced Manufacturing Technology*, 87: 2041-61.

Gökkaya, Hasan. 2010. 'The Effects of Machining Parameters on Cutting Forces, Surface Roughness, Built-Up Edge (BUE) and Built-Up Layer (BUL) During Machining AA2014 (T4) Alloy', *Journal of Mechanical Engineering/Strojniški Vestnik*, 56.

Gonçalves, Ricardo Augusto, and Márcio Bacci da Silva. 2015. 'Influence of copper content on 6351 aluminum alloy machinability', *Procedia Manufacturing*, 1: 683-95.

Gregson, PJ, and HM Flower. 1984. 'δ′ precipitation in Al-Li-Mg-Cu-Zr alloys', *Journal of materials science letters*, 3: 829-34.

Guo, Huairui, and Adamantios Mettas. 2010. 'Design of experiments and data analysis', In *2012 Annual Reliability and Maintainability Symposium*.

Hadzley, AB, AA Anis, MN Farizan, MH Osman, T Norfauzi, and S Noorazizi. 2018. 'Analysis of surface integrity and formation of material side flow in dry and wet machining of aluminum alloy', *Journal of Advanced Manufacturing Technology (JAMT)*, 12: 501-12.

Huang, Kai, Qin Feng, Wenbiao Zhou, Yuelu Ren, Liang Huang, Jing Xiang, Hongqun Tang, Yutao Zhu, and Yuezhou Wei. 2021. 'Enhancement of strength mechanical and corrosion resistance of 7055 alloy with minor Sc and Y addition', *Materials Research Express*, 8: 016524.

Hyde, KB, AF Norman, and PB Prangnell. 2001. 'The effect of cooling rate on the morphology of primary Al3Sc intermetallic particles in Al–Sc alloys', *Acta materialia*, 49: 1327-37.

Jebaraj, M, and M Pradeep Kumar. 2019. 'Effect of cryogenic CO2 and LN2 coolants in milling of aluminum alloy', *Materials and Manufacturing Processes*, 34: 511-20.

Jiang, Feng, Jianfeng Li, Lan Yan, Jie Sun, and Song Zhang. 2010. 'Optimizing end-milling parameters for surface roughness under different cooling/lubrication conditions', *The International Journal of Advanced Manufacturing Technology*, 51: 841-51.

Jiang, Shengqiang, Chao Tang, Xu Li, Yuanqiang Tan, Ruitao Peng, Dongmin Yang, and Sisi Liu. 2020. 'Discrete element modeling of the machining processes of brittle materials: Recent development and future prospective', *The International Journal of Advanced Manufacturing Technology*, 109: 2795-829.

Joshi, Amit. 2005. 'Lithium aluminium alloys–the new generation aerospace alloys', *Indian Institute of Technology Bombay*.

Karkalos, Nikolaos E, Panagiotis Karmiris-Obratański, Szymon Kurpiel, Krzysztof Zagórski, and Angelos P Markopoulos. 2021. 'Investigation on the surface quality obtained during trochoidal milling of 6082 aluminum alloy', *Machines*, 9: 75.

Kaya, Hasan, Mehmet Uçar, Abdulkadir Cengiz, Dursun Özyürek, AHMET Çalışkan, and Emre Ergün. 2012. 'The effect of aging on the machinability of AA7075 aluminium alloy', *Scientific Research and Essays*, 7.

Khettabi, Riad, Mourad Nouioua, Abdelhakim Djebara, and Victor Songmene. 2017. 'Effect of MQL and dry processes on the particle emission and part quality during milling of aluminum alloys', *The International Journal of Advanced Manufacturing Technology*, 92: 2593-98.

Khettabi, Riad, Victor Songmene, and Jacques Masounave. 2010. 'Effects of speeds, materials, and tool rake angles on metallic particle emission during orthogonal cutting', *Journal of materials engineering and performance*, 19: 767-75.

Khettabi, Riad, Imed Zaghbani, Abdelhakim Djebara, Jules Kouam, and Victor Songmene. 2011. 'A new sustainability model for machining processes', *International Journal of Business Continuity and Risk Management*, 2: 187-202.

Kishawy, HA, M Dumitrescu, E-G Ng, and MA Elbestawi. 2005. 'Effect of coolant strategy on tool performance, chip morphology and surface quality during high-speed machining of A356 aluminum alloy', *International journal of machine tools and manufacture*, 45: 219-27.

Kiswanto, Gandjar, DL Zariatin, and TJ Ko. 2014. 'The effect of spindle speed, feed-rate and machining time to the surface roughness and burr formation of Aluminum Alloy 1100 in micro-milling operation', *Journal of Manufacturing Processes*, 16: 435-50.

Klobes, Benedikt, Danny Petschke, Frank Lotter, Vasily Potapkin, and Torsten EM Staab. 2022. 'The Li stance on precipitation in Al–Li-based alloys: An investigation by X-ray Raman spectroscopy', *Journal of Materials Science*, 57: 6157-66.

Kolobnev, NI. 2002. 'Aluminum-lithium alloys with scandium', *Metal science and heat treatment*, 44: 297-99.

Korkmaz, Mehmet Erdi, Munish Kumar Gupta, Murat Sarikaya, Mustafa Günay, Mehmet Boy, Nafiz Yaşar, Recep Demirsöz, and Fatih Pehlivan. 2024. 'Analytical Modeling Methods in Machining: A State of the Art on Application, Recent Challenges, and Future Trends', *Arabian Journal for Science and Engineering*.

Kouam, J, V Songmene, M Balazinski, and P Hendrick. 2012. 'Dry, semi-dry and wet machining of 6061-T6 aluminium alloy', *Dry, Aluminium Alloys–New Trends in Fabrication and Applications*: 199-221.

Kouam, Jules, Victor Songmene, Marek Balazinski, and Patrick Hendrick. 2015. 'Effects of minimum quantity lubricating (MQL) conditions on machining of 7075-T6 aluminum alloy', *The International Journal of Advanced Manufacturing Technology*, 79: 1325-34.

Kumar, Anand, MM Mahapatra, and Pradeep Kumar Jha. 2014. 'Effect of machining parameters on cutting force and surface roughness of in situ Al–4.5% Cu/TiC metal matrix composites', *Measurement*, 48: 325-32.

Kumar, M Bhuvanesh, R Parameshwaran, K Deepandurai, and SM Senthil. 2020. 'Influence of Milling Parameters on Surface Roughness of Al–SiC–B 4 C Composites', *Transactions of the Indian Institute of Metals*, 73: 1171-83.

Kuttolamadom, Mathew, Sina Hamzehlouia, and Laine Mears. 2010. 'Effect of machining feed on surface roughness in cutting 6061 aluminum', *SAE International journal of materials and manufacturing*, 3: 108-19.

Lee, Dong-Hyeok, and Nahm-Gyoo Cho. 2012. 'Assessment of surface profile data acquired by a stylus profilometer', *Measurement science and technology*, 23: 105601.

Li, C, Yi Wan, RR Zhang, and Zhan Qiang Liu. 2012. 'Effect of Milling Speed and Feed on Surface Residual Stress of 7050-T7451 Aluminum Alloy', *Key Engineering Materials*, 499: 217-22.

Li, Hu Zeng, Yi Wang, Nai Xiong Zhu, Rao Bo Hu, Chong Zhang, and Fang Bao Wang. 2012. 'Measurement and Analysis of Cutting Force and Optimization of Cutting Parameters by High Speed Milling', *Applied Mechanics and Materials*, 141: 344-49.

Li, JH, M Wiessner, Mihaela Albu, S Wurster, B Sartory, Ferdinand Hofer, and P Schumacher. 2015. 'Correlative characterization of primary Al3 (Sc, Zr) phase in an Al–Zn–Mg based alloy', *Materials Characterization*, 102: 62-70.

Li, Jin-feng, Ping-li Liu, Yong-lai Chen, Xu-hu Zhang, and Zi-qiao Zheng. 2015. 'Microstructure and mechanical properties of Mg, Ag and Zn multi-microalloyed Al–(3.2–3.8) Cu–(1.0–1.4) Li alloys', *Transactions of Nonferrous Metals Society of China*, 25: 2103-12.

Lin, Yi, Chengyang Wei, and Ziqiao Zheng. 2018. 'Effect of aging treatment on microstructures, tensile properties and intergranular corrosion behavior of Al–Cu–Li alloy', *Materials Characterization*, 141: 163-68.

Liu, Li, Ying-Ying Jia, Jian-Tang Jiang, Bo Zhang, Guo-Ai Li, Wen-Zhu Shao, and Liang Zhen. 2019. 'The effect of Cu and Sc on the localized corrosion resistance of Al-Zn-Mg-X alloys', *Journal of Alloys and Compounds*, 799: 1-14.

Liu, Qibing, Genlian Fan, Zhanqiu Tan, Zhiqiang Li, Di Zhang, Jia Wang, and Hao Zhang. 2021. 'Precipitation of Al3Zr by two-step homogenization and its effect on the recrystallization and mechanical property in 2195 Al–Cu–Li alloys', *Materials Science and Engineering: A*, 821: 141637.

Ma, Juan, Desheng Yan, Lijian Rong, and Yiyi Li. 2014. 'Effect of Sc addition on microstructure and mechanical properties of 1460 alloy', *Progress in Natural Science: Materials International*, 24: 13-18.

Kevin Anderson, John Weritz and J. Gilbert Kaufman (eds.). 2018. 'Machining and Mechanical Finishing' , *Aluminum Science and Technology* (ASM International).

Mahalingam, K, BP Gu, GL Liedl, and TH Sanders Jr. 1987. 'Coarsening of δ′(Al3Li) precipitates in binary al-li alloys', *Acta Metallurgica*, 35: 483-98.

Marakini, Vikas, Srinivasa P Pai, Udaya K Bhat, DineshSingh Thakur, and Bhaskara Achar. 2024. 'Surface integrity investigation and VIKOR optimisation during the milling of aluminium–lithium alloy using uncoated and PVD-coated carbide tools', *Canadian Metallurgical Quarterly*, 63: 767-78.

Marani, Mohsen, Victor Songmene, Jules Kouam, and Yasser Zedan. 2018. 'Experimental investigation on microstructure, mechanical properties and dust emission when milling Al-20 Mg 2 Si-2Cu metal matrix composite with modifier elements', *The International Journal of Advanced Manufacturing Technology*, 99: 789-802.

Matras, Andrzej. 2019. 'Research and optimization of surface roughness in milling of SLM semi-finished parts manufactured by using the different laser scanning speed', *Materials*, 13: 9.

McDonald, Russell J. 2009. '*Characterization of delamination in 2099-T861 Aluminum-Lithium'*, Ph. D. Thesis, University of Illinois at Urbana-Champaign.

Meng, Xinxin, Youxi Lin, and Shaowei Mi. 2021. 'The research of tool wear mechanism for high-speed milling ADC12 aluminum alloy considering the cutting force effect', *Materials*, 14: 1054.

Montgomery, Douglas C. 2017. *Design and analysis of experiments* (John wiley & sons).

Moradi, Hadi. 2014. 'Optimization of cutting parameters for pocket milling on the skin plate in Al and Al-Li materials', *M. A.Sc thesis, Polytechnique Montreal, Qc, Canada*.

Mou, Haikuo, Xinda Huang, Xiaoming Zhang, and Han Ding. 2013. 'Experimental Study of Surface Integrity of Aluminum Lithium Alloy by Face Milling.' In *Intelligent Robotics and Applications: 6th International Conference, ICIRA 2013, Busan, South Korea, September 25-28, 2013, Proceedings, Part II 6*, 491-502. Springer.

Murray, J, A Peruzzi, and JP Abriata. 1992. 'The Al-Zr (aluminum-zirconium) system', *Journal of phase equilibria*, 13: 277-91.

Murray, JL. 1998. 'The Al-Sc (aluminum-scandium) system', *Journal of Phase Equilibria and Diffusion*, 19: 380.

Namlu, RH, OD Yılmaz, SE Kilic, and B Cetin. 2019. 'Investigating the effect of cutting conditions on machining performance of Al 6061-T6 alloy', *10th Int. Congr. Machining, Antalya, Turkey*: 293-304.

Nikitin, SL, OE Osintsev, and S Ya Betsofen. 2010. 'Effect of heat treatment conditions on the structure and mechanical properties of a cast Al-Li-Cu aluminum alloy', *Russian Metallurgy (Metally)*, 2010: 1041-45.

Niknam, Seyed Ali, Jules Kouam, and Victor Songmene. 2016. 'Experimental investigation on part quality and metallic particle emission when milling 6061-T6 aluminium alloy', *International Journal of Machining and Machinability of Materials*, 18: 120-37.

Noble, B, and SE Bray. 1998. 'On the α (Al)/δ′(Al3Li) metastable solvus in aluminium–lithium alloys', *Acta materialia*, 46: 6163-71.

Noble, B, and AJ Trowsdale. 1995. 'Precipitation in an aluminium-14at.% lithium alloy', *Philosophical Magazine A*, 71: 1345-62.

Norman, AF, PB Prangnell, and RS McEwen. 1998. 'The solidification behaviour of dilute aluminium–scandium alloys', *Acta materialia*, 46: 5715-32.

Özsoy, Neslihan. 2019. 'Experimental investigation of surface roughness of cutting parameters in T6 aluminum alloy milling process', *International Journal of Computational and Experimental Science and Engineering*, 5: 105-11.

Özsoy, Neslihan, and Murat Ozsoy. 2019. 'Influence of dry-wet machining conditions on surface roughness of 6082-T6 aluminum alloy in milling process', *Academic Platform-Journal of Engineering and Science*, 8: 222-29.

Palmer, IG, WS Miller, DJ Lloyd, and MJ Bull. 1986. 'Effect of grain structure and texture on mechanical properties of Al-Li base alloys', *Aluminium-lithium alloys III*: 565-75.

Patel, Kandarp, Ajay Batish, and Anirban Bhattacharya. 2009. 'Optimization of surface roughness in an end-milling operation using nested experimental design', *Production Engineering*, 3: 361-73.

Pathak, B. N., K. L. Sahoo, and Madhawanand Mishra. 2013. 'Effect of Machining Parameters on Cutting Forces and Surface Roughness in Al-(1-2) Fe-1V-1Si Alloys', *Materials and Manufacturing Processes*, 28: 463-69.

Pattnaik, Sisira Kanta, Neeraj Kumar Bhoi, Sachidananda Padhi, and Saroj Kumar Sarangi. 2018. 'Dry machining of aluminum for proper selection of cutting tool: tool performance and tool wear', *The International Journal of Advanced Manufacturing Technology*, 98: 55-65.

Perez, I, A Madariaga, M Cuesta, A Garay, PJ Arrazola, JJ Ruiz, FJ Rubio, and R Sanchez. 2018. 'Effect of cutting speed on the surface integrity of face milled 7050-T7451 aluminium workpieces', *Procedia Cirp*, 71: 460-65.

Pérez-Landazábal, JI, ML Nó, G Madariaga, V Recarte, and J San Juan. 2000. 'Quantitative analysis of δ′ precipitation kinetics in Al–Li alloys', *Acta materialia*, 48: 1283-96.

Pham, Thi-Hoa, Duc-Toan Nguyen, Tien-Long Banh, and Van-Canh Tong. 2020. 'Experimental study on the chip morphology, tool–chip contact length, workpiece vibration, and surface roughness during high-speed face milling of A6061 aluminum alloy', *Proceedings of the Institution of Mechanical Engineers, Part B: Journal of engineering manufacture*, 234: 610-20.

Prasad, K Satya, N Eswara Prasad, and Amol A Gokhale. 2014. 'Microstructure and precipitate characteristics of aluminum–lithium alloys', *Aluminum-lithium Alloys*: 99-137.

Prasad, N Eswara, AA Gokhale, and P Rama Rao. 2003. 'Mechanical behaviour of aluminium-lithium alloys', *Sadhana*, 28: 209-46.

Rioja, R, C Giummarra, and S Cheong. 2008. 'The role of crystallographic texture on the performance of flat rolled aluminum products for aerospace applications. In *Light Metals-Warrendale-Proceeding*, 1065. TMS.

Rioja, Roberto J, and John Liu. 2012. 'The evolution of Al-Li base products for aerospace and space applications', *Metallurgical and Materials Transactions A*, 43: 3325-37.

Sadiq, Taoheed Olohunde, Baloch Abdul Hameed, Jamaliah Idris, Olusegun Olaoye, Siti Nursyaza, Zul Hairi Samsudin, and Mohamad Imran Hasnan. 2019. 'Effect of different machining parameters on surface roughness of aluminium alloys based on Si and Mg content', *Journal of the Brazilian Society of Mechanical Sciences and Engineering*, 41: 1-11.

Salem Mohamed, Serageldin. 2018. 'Effects of Metallurgical Parameters on the Development of Residual Stresses in Al-Si Alloys Used in Engine Block Manufacturing', *Ph. D. Thesis, Université du Québec à Chicoutimi*.

Santos, Mário C, Alisson R Machado, Wisley F Sales, Marcos AS Barrozo, and Emmanuel O Ezugwu. 2016. 'Machining of aluminum alloys: a review', *The International Journal of Advanced Manufacturing Technology*, 86: 3067-80.

Sequeira, Anil Antony, Ravikantha Prabhu, NS Sriram, and Thirumaleshwara Bhat. 2012. 'Effect of cutting parameters on cutting force and surface roughness of aluminium components using face milling process-a Taguchi Approach', *IOSR Journal of Mechanical and Civil Engineering*, 3: 7-13.

Singh, Kamaljeet, Anoop Kumar Singh, and KD Chattopadhyay. 2020. 'Selection of optimal cutting conditions and coolant flow rate (CFR) for enhancing surface finish in milling of aluminium alloy', *Materials Today: Proceedings*, 21: 1520-24.

Singh, Sunpreet, Chander Prakash, Parvesh Antil, Rupinder Singh, Grzegorz Królczyk, and Catalin I Pruncu. 2019. 'Dimensionless analysis for investigating the quality characteristics of aluminium matrix composites prepared through fused deposition modelling assisted investment casting', *Materials*, 12: 1907.

Sogorovic, Danijel, and Anica Knezevic. 2019. 'Testing of the surface roughness parameters of aluminium-lithium parts machined by milling.' In *Proceedings of the 30th DAAAM International Symposium*, 0148-54.

Solutions, Helical. 2024. '3 Flute, Square - 35° Helix End Mill for Aluminum - 3/16" Dia', Helical Accessed 5 August 2024. https://www.helicaltool.com/products-en-ca/en-ca-tool-details-48235.

Songmene, V, and OA Olufayo. 2020. 'Advances in Fine and Ultrafine Particles Emission and Dispersion in Machining: cases of metals and granite.' In *2020 IEEE 11th International Conference on Mechanical and Intelligent Manufacturing Technologies (ICMIMT)*, 36-45. IEEE.

Songmene, Victor, B and Balout, and Jacques Masounave. 2008. 'Clean machining: Experimental investigation on dust formation-part I: Influence of machining parameters and chip formation', *International Journal of Environmentally Conscious Design & Manufacturing*, 14: 1-16.

Songmene, Victor, R Khettabi, I Zaghbani, J Kouam, and A Djebara. 2011. 'Machining and machinability of aluminum alloys', *Alum. Alloys Theory Appl*, 377: 400.

Songmene, Victor, Riad Khettabi, Martin Viens, Jules Kouam, Stéphane Hallé, François Morency, Jacques Masounave, and Abdelhakim Djebara. 2015. 'Nanoparticle measurement, control and characterization: Procedure applied to machining processes and mechanical friction'.

Songmene, Victor, and R Njoya Doko. 2015. 'Fine metallic particle emission when milling aluminium alloys and aluminium metal matrix composites.' In *Materials Science Forum*, 381-88. Trans Tech Publ.

Srivastava, Vishal Shankar, Tarun Kumar Gupta, Ashish Kumar Srivastava, Sandeep Chauhan, and Pankaj Kumar Chauhan. 2021. 'Effects of cutting parameters on aluminium alloys-A review', *Materials Today: Proceedings*, 47: 3823-27.

Starink, MJ, P Wang, I Sinclair, and PJ Gregson. 1999a. 'Microstrucure and strengthening of Al–Li–Cu–Mg alloys and mmcs: I. Analysis and modelling of microstructural changes', *Acta materialia*, 47: 3841-53.

Starink, MJ. 1999b. 'Microstrucure and strengthening of Al–Li–Cu–Mg alloys and MMCs: II. Modelling of yield strength', *Acta materialia*, 47: 3855-68.

Starke, EA, TH Sanders, and IG Palmer. 1981. 'New approaches to alloy development in the Al-Li system', *JOM*, 33: 24-33.

Starke Jr, Edgar A. 2014. 'Historical development and present status of aluminum–lithium alloys.' in, *Aluminum-lithium Alloys* (Elsevier).

Stephenson, David A, and John S Agapiou. 2018. *Metal cutting theory and practice* (CRC press).

Suresh, M, A Sharma, AM More, N Nayan, and S Suwas. 2018. 'Effect of Scandium addition on evolution of microstructure, texture and mechanical properties of thermo-mechanically processed Al-Li alloy AA2195', *Journal of Alloys and Compounds*, 740: 364-74.

Tao, Jiashen, Liang Zhang, Guohua Wu, Antao Chen, Xiaolong Zhang, and Chunchang Shi. 2018. 'Effect of heat treatment on the microstructure and mechanical properties of extruded Al–4Cu–1Li–0.4 Mg–0.4 Ag–0.18 Zr Alloy', *Materials Science and Engineering: A*, 717: 11-19.

Tash, M, FH Samuel, F Mucciardi, and HW Doty. 2007. 'Effect of metallurgical parameters on the hardness and microstructural characterization of as-cast and heat-treated 356 and 319 aluminum alloys', *Materials Science and Engineering: A*, 443: 185-201.

Tash, M, FH Samuel, F Mucciardi, HW Doty, and S Valtierra. 2006. 'Effect of metallurgical parameters on the machinability of heat-treated 356 and 319 aluminum alloys', *Materials Science and Engineering: A*, 434: 207-17.

Teng, GB, CY Liu, ZY Ma, WB Zhou, LL Wei, Y Chen, J Li, and YF Mo. 2018. 'Effects of minor Sc addition on the microstructure and mechanical properties of 7055 Al alloy during aging', *Materials Science and Engineering: A*, 713: 61-66.

Thi-Hoa, Pham, Mac Thi-Bich, Tong Van-Canh, Banh Tien-Long, and Nguyen Duc-Toan. 2018. 'A study on the cutting force and chip shrinkage coefficient in high-speed milling of A6061 aluminum alloy', *The International Journal of Advanced Manufacturing Technology*, 98: 177-88.

Toenshoff, Hans Kurt, and Berend Denkena. 2013. 'Basics of cutting and abrasive processes'.

Tosun, Nihat, and Mesut Huseyinoglu. 2010. 'Effect of MQL on surface roughness in milling of AA7075-T6', *Materials and Manufacturing Processes*, 25: 793-98.

Trent, Edward M, and Paul K Wright. 2000. *Metal cutting* (Butterworth-Heinemann).

Vakondios, Dimitrios, Panagiotis Kyratsis, Suleyman Yaldiz, and Aristomenis Antoniadis. 2012. 'Influence of milling strategy on the surface roughness in ball end milling of the aluminum alloy Al7075-T6', *Measurement*, 45: 1480-88.

Venkatesan, K, R Ramanujam, J Joel, P Jeyapandiarajan, M Vignesh, Darsh Jiten Tolia, and R Venkata Krishna. 2014. 'Study of cutting force and surface roughness in machining of Al alloy hybrid composite and optimized using response surface methodology', *Procedia Engineering*, 97: 677-86.

Wang, Bing, Zhanqiang Liu, Qinghua Song, Yi Wan, and Zhenyu Shi. 2016. 'Proper selection of cutting parameters and cutting tool angle to lower the specific cutting energy during high speed machining of 7050-T7451 aluminum alloy', *Journal of Cleaner Production*, 129: 292-304.

Wang, Hongtao, Shaolin Zhang, and Guangxi Li. 2022. 'Experimental study on ultrasonic-assisted end milling forces in 2195 aluminum-lithium alloy', *Materials*, 15: 2508.

Wang, SC, and MJ Starink. 2005. 'Precipitates and intermetallic phases in precipitation hardening Al–Cu–Mg–(Li) based alloys', *International Materials Reviews*, 50: 193-215.

Wang, SJ, X Chen, Suet To, XB Ouyang, Q Liu, JW Liu, and Wing Bun Lee. 2015. 'Effect of cutting parameters on heat generation in ultra-precision milling of aluminum alloy 6061', *The International Journal of Advanced Manufacturing Technology*, 80: 1265-75.

Wang, ZM, and RN Shenoy. 1998. 'Microstructural characterization of aluminum-lithium alloys 1460 and 2195.' National Aeronautics and Space Administration.

Wu, Guohua, Xiaolong Zhang, Liang Zhang, Yixiao Wang, Chunchang Shi, Peisen Li, Guangxiao Ren, and Wenjiang Ding. 2021. 'An insight into the precipitate evolution and mechanical properties of a novel high-performance cast Al-Li-Cu-Mg-X alloy', *Journal of Alloys and Compounds*, 875: 159996.

Wu, Xijia, Philippe Kanz, Hassan Mahmoud, Jason Millar, Peyman Shabani, and Jose Martinez Torres. 2021. 'Characterization of the microstructure and surface roughness effects on fatigue life using the Tanaka–Mura–Wu model', *Applied Sciences*, 11: 9955.

Wu, Yi-ping, Ling-ying Ye, Yu-zhen Jia, LIU Ling, and Xin-ming Zhang. 2014. 'Precipitation kinetics of 2519A aluminum alloy based on aging curves and DSC analysis', *Transactions of Nonferrous Metals Society of China*, 24: 3076-83.

Xie, Bingxin, Liang Huang, Jiahui Xu, Hongliang Su, Huiping Zhang, Yike Xu, Jianjun Li, and Yu Wang. 2022. 'Effect of the aging process and pre-deformation on the precipitated phase and mechanical properties of 2195 Al–Li alloy', *Materials Science and Engineering: A*, 832: 142394.

Xiuli, Fu, Pan Yongzhi, Wan Yi, and Ai Xing. 2010. 'Research on predictive model surface roughness in high speed milling for aluminum alloy 7050-T7451.' In *2010 International Conference on Computing, Control and Industrial Engineering*, 186-89. IEEE.

Yoshimura, Hiromi, Toshimichi Moriwaki, Nobuo Ohmae, Tetsuo Nakai, Toshiro Shibasaka, Hiroshi Kinoshita, Makoto Matsui, and Manabu Shimizu. 2006. 'Study on near dry machining of aluminum alloys', *JSME International Journal Series C Mechanical Systems, Machine Elements and Manufacturing*, 49: 83-89.

YUAN, Zhi-shan, LU Zheng, You-hua XIE, Sheng-long DAI, and Chang-sheng LIU. 2007. 'Effects of RRA treatments on microstructures and properties of a new high-strength aluminum-lithium alloy-2A97', *Chinese Journal of Aeronautics*, 20: 187-92.

Yue, Haitao, Chenguang Guo, Qiang Li, Lijuan Zhao, and Guangbo Hao. 2020. 'Milling Parameters Optimization of Al-Li Alloy Thin-Wall Workpieces Using Response Surface Methodology and Particle Swarm Optimization', *Computer Modeling in Engineering & Sciences*, 124: 937-52.

Zaghbani, Imed, Victor Songmene, and Riad Khettabi. 2009. 'Fine and ultrafine particle characterization and modeling in high-speed milling of 6061-T6 aluminum alloy', *Journal of materials engineering and performance*, 18: 38-48.

Zedan, Y, and S Alkahtani. 2013. 'Influence of the microstructure on the machinability of heat-treated Al–10.8% Si cast alloys: Role of copper-rich intermetallics', *Journal of Materials Processing Technology*, 213: 167-79.

Zha, Xuming, Hao Qin, Zhi Yuan, Linqing Xi, Tao Zhang, and Feng Jiang. 2024. 'Effect of cutting feed rate on machining performance and surface integrity in cutting process of Ti-6Al-4V alloy', *The International Journal of Advanced Manufacturing Technology*, 131: 2791-809.

Zhang, S. J., S. To, S. J. Wang, and Z. W. Zhu. 2015. 'A review of surface roughness generation in ultra-precision machining', *International journal of machine tools and manufacture*, 91: 76-95.

Zhao, Jinfu, Zhanqiang Liu, Bing Wang, Qinghua Song, Yukui Cai, Aqib Mashood Khan, Yi Wan, and Xiaoping Ren. 2023. 'A comprehensive review of generating, monitoring, evaluating, and controlling particle emissions during machining process', *Journal of Manufacturing Systems*, 70: 395-416.

Žist, Sandi, Matej Steinacher, Tonica Bončina, Mihaela Albu, Jaka Burja, Maja Vončina, and Franc Zupanič. 2022. 'The Effect of Scandium on the Microstructure of the Aluminium Alloy AA 6086', *Crystals*, 12: 973.